

**The sediment record of Lake Ohrid (Albania/Macedonia) –  
new methodological approaches, tephrostratigraphy,  
chronology, and inferences of past climatic and  
environmental changes**

**Inaugural-Dissertation  
zur  
Erlangung des Doktorgrades  
der Mathematisch-Naturwissenschaftlichen Fakultät  
der Universität zu Köln**

**vorgelegt von**

**Hendrik Vogel  
aus Braunschweig**

**Köln 2009**

**Berichtersteller: Prof. Dr. Martin Melles  
Prof. Dr. Thomas Wagner  
Dr. Bernd Wagner**

**Tag der mündlichen Prüfung: 14. Oktober 2009**

# Abstract

This thesis had two primary objectives: One objective was to explore and develop applications of Fourier transform infrared spectroscopy (FTIRS) for the quantification of biogeochemical properties in lake sediment; the other objective was to assess the Lake Ohrid (Albania/Macedonia) sediment record with an emphasis on tephrostratigraphy and inferences of climatic and environmental changes using a 15 m long sediment succession (core Co1202) from the north-eastern part of the lake. Studies presented in this thesis were conducted within the scope of an envisaged deep drilling campaign at Lake Ohrid and therefore represent important preliminary studies.

FTIR spectra of lacustrine sediment samples were calibrated to infer concentrations of total organic carbon (TOC), total inorganic carbon (TIC), total nitrogen (TN), and biogenic silica (BSi). To test the applicability of the FTIRS technique, site-specific FTIRS calibrations and FTIRS calibrations based on a surface sediment dataset from 94 northern Swedish lakes were constructed. Both approaches demonstrated significant correlations between FTIRS-inferred and conventionally assessed biogeochemical property concentrations, ranging between  $R^2 = 0.79 - 0.99$  for TOC,  $R^2 = 0.85 - 0.99$  for TIC,  $R^2 = 0.62 - 0.84$  for TN, and  $R^2 = 0.68 - 0.94$  for BSi. These results, in combination with the small amount of sample material (0.01 g) required, negligible sample pre-treatments, and low costs of analysis, show that FTIRS is a promising analytical alternative to infer biogeochemical properties, especially when large sample quantities need to be analysed.

The finding of ten tephra and cryptotephra layers throughout the Co1202 sediment succession and their correlation with explosive eruptions of Italian volcanoes provided new data on the dispersal of ash originating from these eruptions. The relatively well-known ages of these tephra and cryptotephra layers combined with seven radiocarbon dates, enabled a chronological framework for core Co1202 to be established. Based on these chronological constrains, the Co1202 succession covers the last glacial-interglacial cycle back to 136 ka, except for a hiatus between 97.6 and 81.7 ka. Assessment of climatic and environmental changes using lithological, sedimentological, geochemical, and physical indicators revealed that Lake Ohrid's sediments sensitively recorded both long- and short-term climatic fluctuations over the past 136 kyrs. Despite some minor discrepancies, the climate fluctuations documented in the Lake Ohrid sediment record are well correlated with other climate records in the wider Mediterranean region. These studies emphasise the potential of Lake Ohrid as a valuable archive of dispersed volcanic products from Italian volcanoes and for climatic and environmental changes in the northern-central Mediterranean region.

# Kurzfassung

Die vorliegende Arbeit hatte zwei Hauptzielsetzungen: Die erste befasste sich mit der Untersuchung und Entwicklung von Anwendungen, basierend auf der Fourier-Transformation Infrarot Spektroskopie (FTIRS) zur Quantifizierung von biogeochemischen Bestandteilen in Seesedimenten. Die zweite Zielsetzung befasste sich mit den Sedimenten des Ohridsees (Albanien/Mazedonien). Der Schwerpunkt lag hierbei auf der Tephrostratigraphie und Abschätzungen bezüglich der Klima und Umweltgeschichte unter Zuhilfenahme einer ca. 15 m langen Sedimentsequenz aus dem nordöstlichen Bereich des Sees. Die in der Arbeit vorgestellten Untersuchungen dienen als wichtige Vorstudie für eine vorgesehene Tiefbohrung am Ohridsee.

FTIR Spektreninformationen von Seesedimentproben wurden für die Messung von organischem Gesamtkohlenstoff (TOC), anorganischem Gesamtkohlenstoff (TIC), Gesamtstickstoff (TN) und biogenem Silikat (BSi) kalibriert. Für eine kritische Abschätzung der Anwendbarkeit von FTIRS wurden standortspezifische FTIRS Kalibrierungen und FTIRS Kalibrierungen die auf einem Oberflächensedimentprobensatz von 94 nordschwedischen Seen basieren, entwickelt und erprobt. Beide Ansätze lieferten überzeugende Korrelationen zwischen FTIRS und konventionell gemessenen Konzentrationen mit Schwankungsbreiten von  $R^2 = 0.79 - 0.99$  für TOC,  $R^2 = 0.85 - 0.99$  für TIC,  $R^2 = 0.62 - 0.84$  für TN, and  $R^2 = 0.68 - 0.94$  für BSi. Diese Ergebnisse, in Kombination mit der geringen Menge an benötigtem Probenmaterial (0,01 g), sowie dem geringen Bedarf an Probenaufbereitung und den geringen Kosten, zeigen, dass FTIRS eine vielversprechende analytische Alternative darstellt, um biogeochemische Bestandteile in Seesedimenten zu quantifizieren, im Speziellen, wenn eine große Probenanzahl analysiert werden muss.

Das Auffinden von zehn Tephra- und Kryptotephralagen in der Co1202 Sedimentsequenz, sowie die erfolgreiche Korrelation dieser Lagen mit explosiven Eruptionen italienischer Vulkane, lieferte neue Erkenntnisse über die Verteilung der von diesen Eruptionen ausgehenden Aschen. Aufgrund der relativ gut bekannten Alter der Tephra- und Kryptotephralagen sowie sieben zusätzlicher Radiokarbondatierungen, konnte ein chronologischer Rahmen für den Kern Co1202 erstellt werden. Auf der Basis dieser chronologischen Überlegungen ergab sich, dass die Co1202 Sequenz, mit Ausnahme eines Hiatus zwischen 97.6 und 81.7 ka, den letzten Glazial-Interglazial Zyklus zurück bis 136 ka umfasst. Untersuchungen zu Klima- und Umweltveränderungen unter Zuhilfenahme von lithologischen, sedimentologischen, geochemischen und physikalischen Indikatoren ergaben, dass die Sedimente des Ohridsees lang- und kurzfristige Klimaschwankungen während der letzten 136 kyrs aufgezeichnet haben. Die lang- und kurzfristigen Klimaschwankungen, abgeleitet aus den Sedimenten des Ohridsees, zeigen, abgesehen von einigen geringfügigen Abweichungen, eine gute Übereinstimmung mit anderen Klimarekonstruktionen aus dem Mittelmeerraum. Diese Untersuchungen betonen das Potential des Ohridsees als wertvolles Archiv für die Verteilung von vulkanischem Material italienischer Vulkane, sowie auch für Klima und Umweltveränderungen im zentralen Bereich des nördlichen Mittelmeerraums.

# Acknowledgements

The outcome of this thesis work benefited greatly from many fruitful discussions with numerous colleagues. Especially, I would like to thank my supervisors Bernd Wagner, Peter Rosén, and Martin Melles who introduced me to this exciting field in geosciences and provided advice, support, and motivation throughout the past three years. Bernd Wagner designed the main body of the project, which was due to his diligent preliminary work, granted by the Deutsche Forschungsgemeinschaft (DFG). Peter Rosén pioneered in applications of FTIRS on lake sediment samples without which the outcome of an important part of this thesis would have been unthinkable. Martin Melles heads the working group at the University of Cologne, where I was part of during the last three years, and provided access to coring equipment and analytical devices without which essential parts of this thesis work would not have been accomplishable.

Giovanni Zanchetta and Roberto Sulpizio are greatly acknowledged for hosting me during a short stay at the University of Pisa and for giving me a quick introduction in tephra analyses. Per Persson is thanked for providing access to his state of the art FTIRS laboratory at the Umeå University and for sharing his expert knowledge on FTIR spectra interpretation. Laura Cunningham is thanked for help with FTIRS analyses, for checking English spelling in this thesis work, and many fruitful discussions. Goce Kostoski, Sasho Trajanoski, and Zoran Brdaroski are greatly acknowledged for their logistic support during the 2007 field campaign. Ariane Liermann, Jens Aubel, and Michael Fritz completed the 2007 field team and greatly contributed to the success of the coring campaign. Nicole Mantke and Florian Boxberg are thanked for their enduring help in the laboratory at the University of Cologne. Norbert Nowaczyk is thanked for providing access to his magnetic susceptibility device at the Geoforschungszentrum Potsdam (GFZ).

Moreover I would like to thank my colleagues Sonja Berg, Jan Bohaty, Hanna Cyszieński, Peter Hofmann, Olaf Juschus, Martin Klug, Christel Krings, Sabrina Ortlepp, Friederike Schürhoff-Goeters, Steffi Schmidt, Armine Shahnazarian, Ellen Stefan, Eliza Stehr, Oliver Stock, Finn Viehberg, and Volker Wennrich, at the University of Cologne for creating a peaceful and stimulating working atmosphere.

# Contents

<b>Chapter I: Introduction</b> .....	1
1.1. General introduction .....	2
1.2. Background and detailed objectives .....	6
1.2.1. Part I: Applications of Fourier transform infrared spectroscopy (FTIRS) as fast and cost efficient alternative for the quantification of biogeochemical properties .....	6
1.2.2. Part II: Lake Ohrid's sediment record for the last glacial-interglacial cycle: tephrostratigraphy, chronology, and inferences of climatic and environmental change .....	9
1.3. Chapter contributions .....	12
<b>Chapter II: Fourier transform infrared spectroscopy, a new cost-effective tool for quantitative analysis of biogeochemical properties in long sediment records</b> .....	14
2.1. Introduction .....	15
2.2. Study sites .....	16
2.3. Material and methods .....	17
2.3.1. Core recovery and composition .....	17
2.3.2. Biogeochemistry (conventional methods) .....	18
2.3.3. FTIRS .....	18
2.3.4. Numerical analysis .....	19
2.4. Results and discussion .....	21
2.4.1. Spectral information .....	21
2.4.2. Model development .....	22
2.4.3. Relationships between FTIRS models and biogeochemical properties .....	23
2.4.4. Predictions .....	26
2.4.5. Advantages of FTIRS compared to conventional analytical techniques .....	29
2.5. Conclusions .....	30
<b>Chapter III: Fourier transform infrared spectroscopy, a new method for rapid determination of total organic and inorganic carbon and biogenic silica concentration in lake sediments</b> .....	31
3.1. Introduction .....	32
3.2. Materials and methods .....	33
3.2.1. Study area .....	33
3.2.2. Field and laboratory methods .....	35
3.2.3. Numerical analyses .....	36
3.3. Results and discussion .....	37
3.3.1. Statistical performance and spectral information for the FTIRS/LOI550°C model .....	37

3.3.2.	Model performance and spectral information for the FTIRS-TIC model .....	40
3.3.3.	Model performance and spectral information for the FTIRS-BSi model .....	41
3.3.4.	Application of the FTIRS models to Swedish, Siberian and Albanian/Macedonian sediments .....	43
3.4.	Conclusions and future possibilities and limitations of the FTIRS technique .....	46
<b>Chapter IV:</b>	<b>A tephrostratigraphic record for the last glacial-interglacial cycle from Lake Ohrid, Albania and Macedonia .....</b>	<b>47</b>
4.1.	Introduction .....	48
4.2.	Site description .....	49
4.3.	Materials and methods .....	51
4.4.	Results and discussion .....	53
4.4.1.	Lithology .....	53
4.4.2.	Magnetic susceptibility and X-ray fluorescence analysis .....	55
4.4.3.	Radiocarbon dating .....	56
4.4.4.	Tephrostratigraphy .....	57
4.4.5.	Core chronology and interpretation .....	74
4.5.	Conclusions .....	77
<b>Chapter V:</b>	<b>A paleoclimate record with tephrochronological age control for the last glacial-interglacial cycle from Lake Ohrid, Albania and Macedonia .....</b>	<b>78</b>
5.1.	Introduction .....	79
5.2.	Site description .....	81
5.3.	Materials and methods .....	84
5.3.1.	Core recovery .....	84
5.3.2.	Analytical work .....	84
5.4.	Results and discussion .....	87
5.4.1.	Lithology and lithofacies classification .....	87
5.4.2.	Chronology of core Co1202 .....	90
5.4.3.	Indicators for environmental and climatic change .....	91
5.5.	Interpretation .....	96
5.5.1.	The penultimate glacial and transition II (c. 135.9 – 127.3 ka) .....	96
5.5.2.	The last interglacial complex (c. 127.3 – 97.6 ka) .....	98
5.5.3.	The last glacial (c. 81.7 – 15 ka) .....	101
5.5.4.	Transition I and the Holocene (c. 15 ka – present) .....	103
5.6.	Conclusions .....	108
<b>Chapter VI:</b>	<b>Summary, critical review, and outlook .....</b>	<b>110</b>
6.1.	Part I: Fourier transform infrared spectroscopy (FTIRS) .....	111
6.2.	Part II: Lake Ohrid's sediment record .....	113
<b>References</b>	.....	<b>119</b>

# **Chapter I**

## **Introduction**

## 1.1. General introduction

Large ancient lakes contain valuable archives for the investigation of past climatic, environmental, tectonic, volcanic, and evolutionary changes over long time scales in the terrestrial realm. Therefore these lakes have become one of the main targets within the scope of the International Continental Scientific Drilling Program (ICDP). Over the last decade numerous sedimentary records, up to several hundred meters long, from ancient lakes including Lake Baikal (e.g. Colman et al. 1998), Qinghai (e.g. An Zhisheng et al., 2006), Bosumtwi (e.g. Koeberl et al. 2005), Malawi (e.g. Scholz et al. 2006), Peten Itza (e.g. Hodell et al. 2006), Titicaca (e.g. Fritz et al. 2007), Potrok Aike (e.g. Zolitschka et al. 2006), and most recently El'gygytgyn (e.g. Brigham-Grette et al. 2009) have been recovered under the umbrella of ICDP (Fig. 1-1). Forthcoming ICDP deep drilling sites are situated in the densely populated, climate sensitive, tectonically, and volcanically active Mediterranean region and encompass Lake Van in Turkey (e.g. Litt et al. 2009), the Dead Sea in Israel, and Lake Ohrid in Albania/Macedonia (Fig. 1-1).

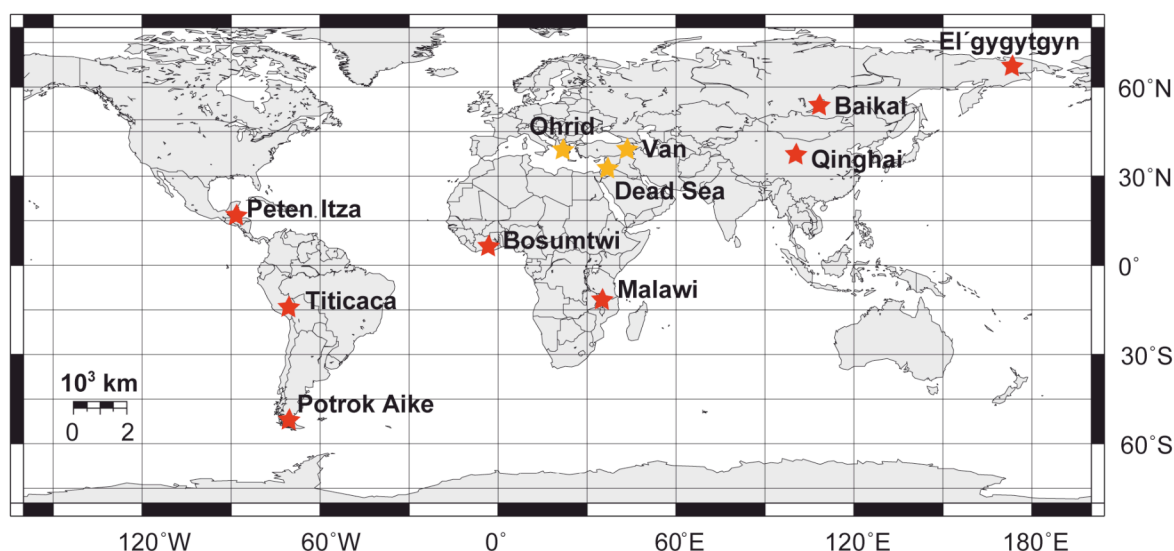


Fig. 1-1. Map showing the location of ICDP lake sites referred to in the text. Already drilled sites are indicated by red asterisks and future sites are indicated by orange asterisks.

The UNESCO world heritage site Lake Ohrid is a transboundary lake shared by the Republics of Albania and Macedonia. It is situated within an active subsidence zone and is believed to have formed five to two million years ago. Due to its likely Pliocene origin and assumed continuous existence since, Lake Ohrid is amongst the few existing lakes in the world, and potentially the only lake in Europe, which provides a sedimentary record that reaches so far back in time. Exact information on the age and origin of Lake Ohrid is, however, still lacking.

Not only its age and proposed continuous existence since the Pliocene but also its geographic setting in the central/northern Mediterranean emphasize Lake Ohrid's role as an invaluable archive to record climatic and environmental changes in this climate sensitive region. Owing to its location at the boundary of the large scale atmospheric Hadley and Mid-latitude cells, and a climate influenced by the westerlies as well as maritime and continental factors, Lake Ohrid is particularly valuable for investigations focusing on reconstructions of the variability of these major components of the Mediterranean climate system. Although a globally unprecedented wealth of paleoenvironmental information has already been gathered from the Mediterranean region, most of this information is restricted to the late last glacial and the Holocene (e.g. Sadori and Narcisi 2001; Wick et al. 2003; Bordon et al. 2008; Kotthoff et al. 2008; Magny et al. 2009; Fig. 1-2). Information which continuously covers at least the last glacial-interglacial cycle or more is relatively sparse from the marine realm (e.g. Martrat et al. 2004; Schmiedl et al. 1998; Fig. 1-2) and even sparser from the terrestrial realm (e.g. Bar-Matthews et al. 2000; Tzedakis et al. 2006; Brauer et al. 2007; Fig. 1-2). The sediment record of Lake Ohrid can thus yield important information required for a better

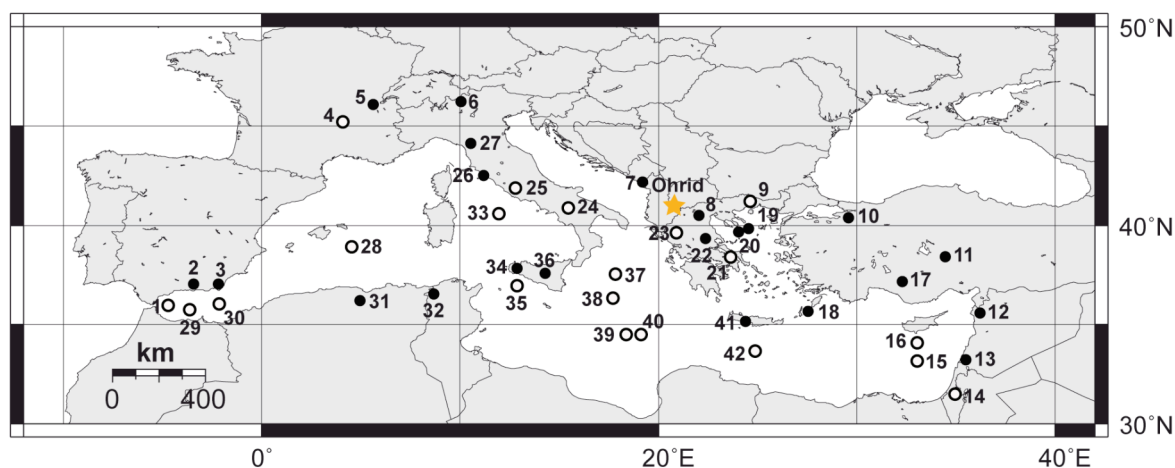


Fig. 1-2. Map showing the location of a subset of important paleorecords in the Mediterranean. Black dots indicate records covering short time windows during the Pleistocene including the late last glacial and/or the Holocene. Open circles indicate paleorecords covering longer time scales such as the last glacial-interglacial cycle or more. 1. ODP 976 (Comas et al. 1996); 2. Padul (Pons and Reille 1988); 3. San Rafael (Pantaléon-Cano et al. 2003); 4. Ribains/Lac du Bouchet (Reille et al. 1998); 5. Les Echets (Wohlfarth et al. 2008); 6. Lefte (Ravazzi and Rossignol-Strick 1995); 7. Shkodra (Van Welden et al. 2008); 8. Nisi Fen (Lawson et al. 2005); 9. Tenaghi Philippon (Tzedakis et al. 2006); 10. Iznik (Franz et al. 2006); 11. Nar Gölü (Jones et al. 2006); 12. Ghab (Meadows et al. 2005); 13. Huleh (Meadows et al. 2005); 14. Soreq (Bar-Matthews et al. 1999); 15. ODP 965, 966 (Comas et al. 1996); 16. ODP 967, 968 (Comas et al. 1996); 17. Konya basin (Roberts et al. 1999); 18. SL123 (Ehrmann et al. 2007); 19. SL152 (Kotthoff et al. 2008); 20. SL148 (Ehrmann et al. 2007); 21. Kopais (Tzedakis 1999); 22. Xinas (Digerfeld et al. 2000); 23. Ioannina (Tzedakis et al. 2003); 24. Monticchio (Brauer et al. 2007); 25. Valle di Castiglione (Follieri et al. 1988); 26. Argentarola Cave (Bard et al. 2002); 27. Corchia Cave (Drysdale et al. 2005); 28. ODP 975 (Comas et al. 1996); 29. ODP 979 (Comas et al. 1996); 30. ODP 977, 978 (Comas et al. 1996; Martrat et al. 2004); 31. La Châtaigneraie (Salamani 1993); 32. Dar Fatma (Ben Tiba and Reille 1982); 33. ODP 974 (Comas et al. 1996); 34. Gorgo Basso (Tinner et al. 2009); 35. ODP 963 (Comas et al. 1996); 36. Pergusa (Sadori and Narcisi 2001); 37. M25/4-KL13 (Schmiedl et al. 1998); 38. ODP 964 (Comas et al. 1996); 39. ODP 973 (Comas et al. 1996); 40. ODP 972 (Comas et al. 1996); 41. Delphinos (Bottema and Sarpaki 2003); 42. ODP 969, 970, 971 (Comas et al. 1996).

understanding of climate variability over several glacial-interglacial cycles and furthermore on the imprint of major climate perturbations associated with the Pliocene/Pleistocene and the Mid-Pleistocene transitions in the Mediterranean realm.

Situated within the Albanian mountain chain, which is part of the tectonically active Afro-European Convergence Zone, Lake Ohrid and its sediment record have great potential as archive for studies aiming to reconstruct paleoseismicity and neotectonic movements. Several features related to ongoing tectonic activity, including active faults and mass movement deposits, have been identified in Lake Ohrid, particularly in the lateral parts of the lake basin (Wagner et al. 2008a; S. Krastel-Gudegast personal communication). Especially the occurrence of mass movement deposits at the same stratigraphic level on opposing slopes of the lake points to an isochronous triggering mechanism, such as seismic shaking and thus potentially serves as proxy for paleoseismicity. However, in order to obtain absolute ages for these earthquake related events adequate drilling and powerful dating techniques are required.

Perpetual explosive volcanic activity in the course of the Quaternary led to frequent and widespread dispersal of pyroclastic material (tephra) in the Mediterranean region (e.g. Peccerillo 2005). Due to its location downwind of most of the Italian volcanoes active during this period, Lake Ohrid is particularly important as archive for tephra originating from these sources. Because pyroclastic deposits in close proximity to the volcanic source are often subject to erosion and thus commonly have a relatively short retention time, distal marine and lacustrine archives become exceedingly important for investigations of volcanic activity in the past. Distal tephra occurrences can, for instance, yield important information for improving volume estimations of an eruption (e.g. Sulpizio 2005), the energy released during an eruption, the eruptive budget of a volcano (Buttner et al. 2006) and for refining volcanic stratigraphy. Owing to the almost synchronous deposition on land, lakes, and oceans, tephra furthermore provide excellent marker horizons to link different spatially distributed sedimentary successions. Ar/Ar and K/Ar dating of mineral phases occurring in volcanic material can additionally provide radiometric controlled ages and thus a crucial “absolute” dating tool necessary for the establishment of independent chronologies beyond the limit of radiocarbon dating.

Assessments of the fauna and flora of Lake Ohrid revealed that the lake harbours an outstanding degree of biodiversity (e.g. Stankovic 1960). With 212 endemic species described and a relatively small surface area Lake Ohrid is by far the lake with the highest endemic diversity in the world. It therefore represents an extant hot spot of evolution and a potential evolutionary reservoir, which facilitated the survival of relict species. Evolutionary data gathered since 2003 revealed concurrent genetic breaks in several invertebrate groups, indicating that major geological and/or environmental events must have shaped the

evolutionary history of endemic faunal elements in Lake Ohrid (Albrecht and Wilke 2008). Hence, Lake Ohrid is a unique site to investigate the impact of major geological, climatic, and environmental events on general evolutionary patterns.

A deep drilling program, within the scope of the ICDP, at Lake Ohrid will thus help to: (i) obtain more precise information about the age and origin of the lake, (ii) unravel the seismotectonic history of the lake area including effects of major earthquakes and associated mass wasting events, (iii) obtain a long and continuous record for the assessment of volcanic activities and climate changes in the Mediterranean region, and (iv) better understand the impact of major geological/environmental events on general evolutionary patterns and shaping an extraordinary degree of endemic biodiversity as a matter of global significance.

Prior to such a deep drilling campaign at Lake Ohrid, several preliminary studies are required. These comprise investigations of: (a) the tectonic framework of the surrounding area (N. Hoffmann in preparation), (b) the sediment architecture of the lake basin (K. Lindhorst in preparation), and (c) the upper sediment succession. The thesis work presented here has its focus on (c) the upper sediment succession of Lake Ohrid. Key objectives included new methodological approaches, evaluations of the sediment succession with respect to dating techniques, as well as its suitability as archive for tephra dispersal and climatic and environmental changes. A more detailed description of the key objectives dealt within chapters II-V and how these are addressed is given in the following section.

## **1.2. Background and detailed objectives**

Research presented in this thesis can be separated in two parts. Part I deals with the development of new methodological approaches. Part II deals with the evaluation of Lake Ohrid's sediment record with respect to tephrostratigraphy, chronology, and climatic and environmental change.

### **1.2.1. Part I: Applications of Fourier transform infrared spectroscopy (FTIRS) as fast and cost efficient alternative for the quantification of biogeochemical properties**

In chapters II and III new methodological approaches to infer biogeochemical properties such as: total organic carbon (TOC), total nitrogen (TN), total sulfur (TS), total inorganic carbon (TIC), and biogenic silica (BSi) based on Fourier transform infrared spectroscopy (FTIRS) are presented and evaluated using sediments from Lakes El'gygytgyn and Ohrid (Fig. 1-1) as well as 94 lakes from northernmost Sweden. The motivation to develop a new methodology capable of providing quantitative information on biogeochemical properties in a somewhat faster and more cost efficient way arose from the background of the forthcoming ICDP deep drilling at Lake El'gygytgyn back in 2006. In 2009 the successful deep drilling at Lake El'gygytgyn led to the recovery of more than 300 m of lacustrine sediments, which provide a unique record of climatic and environmental changes in the Arctic 3.6 million years back in time. The planned ICDP deep drilling at Lake Ohrid envisaged for 2011 will also provide several hundred meters of sediments and thus a paleorecord back to Pliocene times. In order to extract information on climatic and environmental change from these long records in high temporal resolution rapid, cost-efficient, and preferably non-destructive methods are required. X-ray fluorescence core scanners and multi sensor core loggers can provide crucial information on the inorganic geochemistry, magnetic properties, and bulk density of long sedimentary successions in a rapid, cost-efficient, and non-destructive way. Methods providing such quantitative information on biogeochemical properties have, however, not been available until present. One such method capable of providing this information is FTIRS. FTIRS is a rapid, cost-saving technique, which only requires small amounts (0.01g dry weight) of sample material and, most importantly, FTIR spectra provide information about a wide variety of mineralogical and organic substances.

### Theoretical background of the FTIRS technique

The basic principle of the FTIRS technique is that infrared radiation stimulates molecular vibrations, and as a consequence of quantum mechanical behavior, this radiation is absorbed at specific wavenumbers. Major changes of organic and inorganic properties present in sediment can therefore be qualitatively identified from the FTIR spectra (Fig. 1-3). For example, the band between 2850 and 2950  $\text{cm}^{-1}$  is due to C-H vibrations in  $-\text{CH}_3$ ,  $-\text{CH}_2$  and  $-\text{CH}$  groups of organic compounds (Fig. 1-3). Bands centred at 1715  $\text{cm}^{-1}$  are assigned to the stretching vibration of the  $-\text{C}=\text{O}$  group of fatty acids (Mecozzi and Pietrantonio 2006). Carbonate in calcite minerals has important C-O molecular vibrations around 710, 875, 1425, 1460, 1800 and 2500  $\text{cm}^{-1}$  (White 1974; Mecozzi and Pietrantonio 2006; Chapter II, III; Fig. 1-3) and SiO in biogenic silica has an important absorbance maxima at 1100  $\text{cm}^{-1}$  (Stehfest et al. 2005; Chapter II, III; Fig. 1-3). FTIRS can thus provide information on a large number of organic and mineralogical components. This information in combination with the fact that absorbance in FTIR spectra directly relates to the concentration of specific compounds forms the base for the quantification of biogeochemical properties in lacustrine sediment using FTIRS.

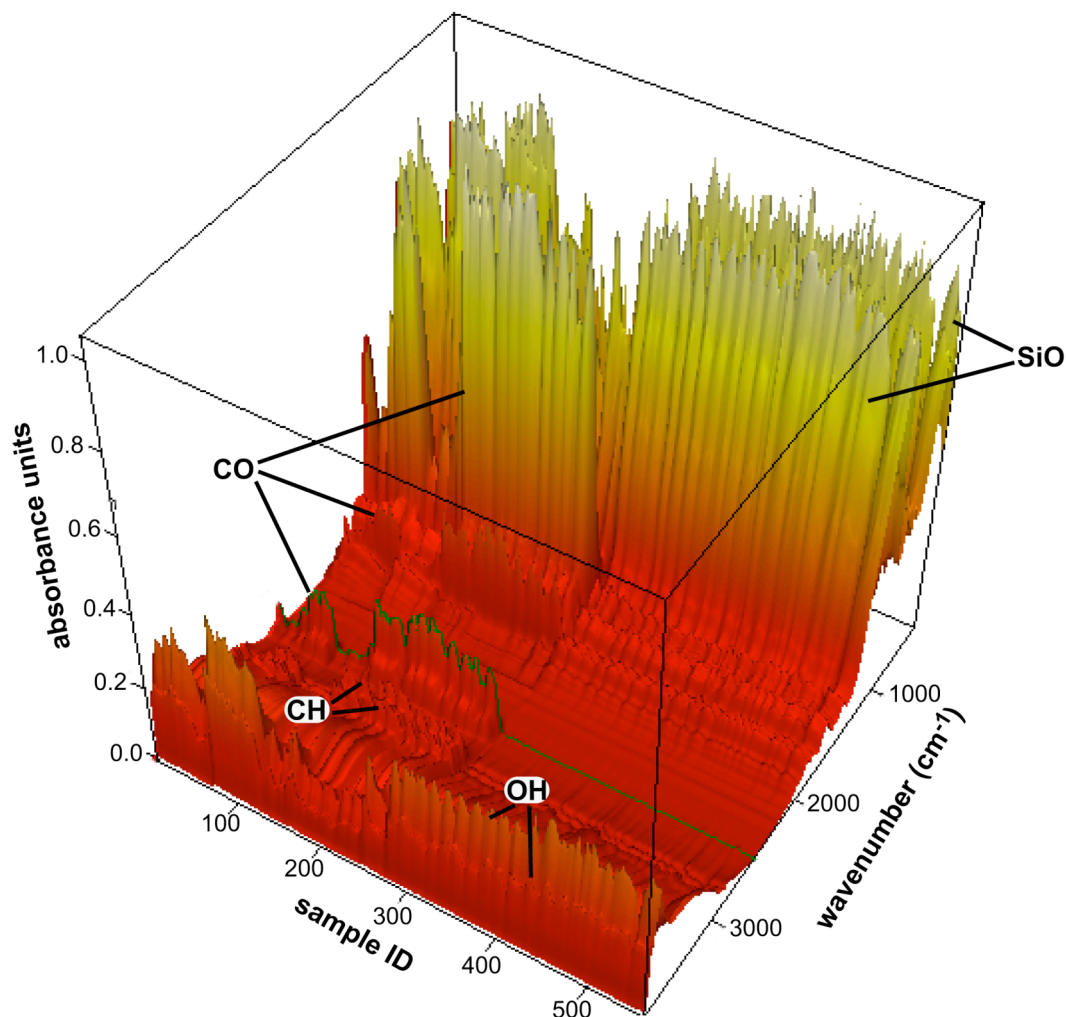


Fig. 1-3. 3D plot of FTIR spectra of core Lz1120 from Lake Ohrid (Wagner et al. 2008b, 2009; Chapter II, III). Wavenumbers are displayed on the x-, absorbance units on the y-, and sample ID's on the z-axis. Black lines indicate important spectral regions for OH, CH, CO, and SiO bonds.

Quantification of biogeochemical properties from lake sediment using FTIRS is, however, not straightforward. Due to the fact that lacustrine sediment is commonly a mixture of a large number of organic and minerogenic components and FTIR spectra display a sum of these, assignment of a compound specific absorbance maxima to its concentration is commonly confounded by other substances overlapping in the same region of the FTIR spectra. Therefore statistical methods need to be applied to extract quantitative information from infrared spectra. Statistical methods particularly capable of extracting quantitative information from FTIR spectra include multicomponent regressions. One particularly promising approach is partial least squares regression (PLSR) as proposed by Martens and Næs (1989). In PLSR concentrations of biogeochemical properties assessed by conventional methods are regressed against FTIR spectra. The resulting calibration model or transfer function can then be used to quantify biogeochemical property concentrations solely from FTIR spectra. PLSR loading plots can also be used to compare reference spectra of pure components to the wavenumbers used by the model, and thus give the opportunity to assure that the calibration model uses the correct wavenumbers from FTIR spectra (Chapters II and III).

#### Site specific applications of FTIRS

Chapter II assesses the performance of FTIRS analysis of long sedimentary successions, by testing the method on a c. 13 m long record from Lake El'gygytgyn (Fig. 1-1) and on a c. 10 m long record from Lake Ohrid (Fig. 1-1, 1-2). Due to the different character of sediment composition within each lake, two different approaches are used. For Lake El'gygytgyn, FTIRS calibrations for TOC, TN, TS, and BSi were based on the upper part of the sediment succession and applied downcore. This approach was not suitable for Lake Ohrid as the sediment composition vary significantly throughout the investigated succession. Thus, FTIRS calibrations for TOC, TIC, TN, TS, and BSi are based on a subset of samples spaced at wide intervals down the core and then applied to the intervening samples, which were not included in the subset. In order to validate the accuracy of the FTIRS inferred concentrations for TOC, TN, TS, and BSi, the results were compared with concentrations assessed using conventional methods.

#### Test of the general applicability of FTIRS

Every lake is different, and thus both sedimentation and sediment composition differ significantly between lakes. This indisputable fact raises the question of whether FTIRS can become a stand-alone analytical technique or if it necessarily requires calibration to site-

specific peculiarities. In order to assess the general applicability of FTIRS for the quantitative inference of TOC, TIC, and BSi in lake sediment, the method was applied to lakes from very different settings. Consequently, in Chapter III, calibration models based upon a surface sediment set from northern Sweden are applied to a 340 kyr record from Lake El'gygytygn, a 40 kyr record from Lake Ohrid, and Holocene records from northernmost Sweden. Concentrations inferred using FTIRS are validated by comparison with concentrations assessed using conventional methods.

### **1.2.2. Part II: Lake Ohrid's sediment record for the last glacial-interglacial cycle: tephrostratigraphy, chronology, and inferences of climatic and environmental change**

Chapters IV and V evaluate the suitability of the Lake Ohrid sediment record as archive for tephra dispersal, and climatic and environmental changes. Furthermore the practicality of radiocarbon dating and tephrochronology for the establishment of a chronological framework of sediments from Lake Ohrid are reviewed in Chapter IV. This part of my research ties in with previous investigations conducted by B. Wagner who investigated a number of sediment successions recovered from Lake Ohrid between in 2004 and 2005 with the longest extending 40 kyrs back in time (core Lz1120, Wagner et al. 2008a; 2008b; 2009). These studies shed significant light on recent and subrecent sedimentation (Wagner et al. 2008a), the viability of Lake Ohrids sediments as distal tephra archive (Wagner et al. 2008b), and as archive for climatic and environmental change (Wagner et al. 2009). Despite this important questions remained unanswered, including:

- (1) *Can the viability of Lake Ohrid as important distal tephra archive be confirmed for longer periods?*
- (2) *Can a chronological framework for sediments beyond the limit of radiocarbon dating be established using tephra?*
- (3) *Can the identification of cryptotephra in sediments of Lake Ohrid be accelerated and improved using magnetic susceptibility and X-ray fluorescence scanning?*
- (4) *What are the mechanisms controlling sedimentation in Lake Ohrid over a glacial-interglacial cycle and how does this relate to climatic and environmental change?*
- (5) *Did sedimentation during the last interglacial differ from the Holocene?*
- (6) *How is the transition from the last glacial to the Holocene imprinted in sediments of Lake Ohrid?*
- (7) *Is sedimentation in Lake Ohrid comparable between different sites in the lake basin or are there major differences?*

In order to address these questions additional sediment successions were recovered from Lake Ohrid during a field campaign in September-October 2007.

### The 2007 coring campaign

During the September-October 2007 field campaign three sediment successions were recovered from the north-eastern part of Lake Ohrid at c. 32, 55, and 145 m water depth, respectively (Fig. 1-4). The successions from 32 m (core Co1200) and 55 m (core Co1201)

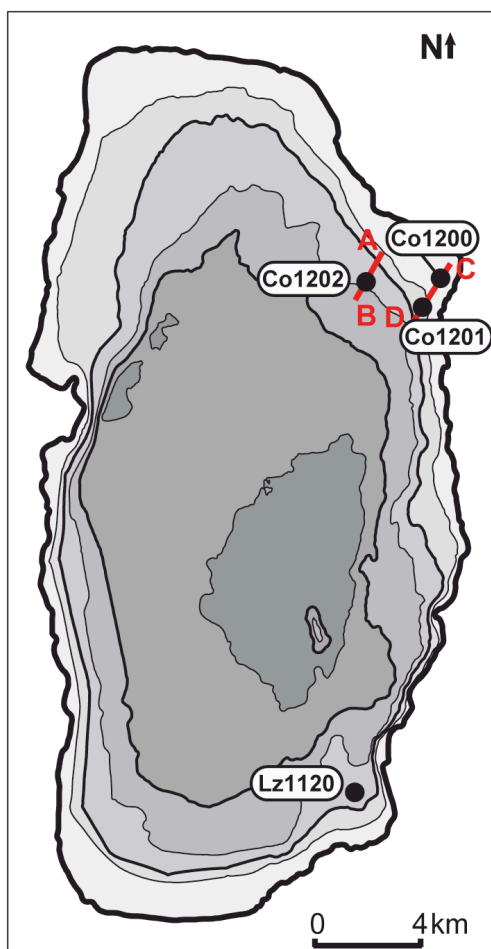


Fig. 1-4. Lake Ohrid with bathymetry in 50 m contour lines. Also shown are coring sites of the 2005 (Lz1120; Wagner et al. 2008b; 2009) and 2007 (Co1200, Co1201, Co1202) field campaigns and beginning (A; C) and end (B; D) of the hydroacoustic profiles shown in Fig. 1-5 and 6-4.

water depth were recovered from subaquatic terrace levels. The longest succession (core Co1202) was recovered from a slightly inclined slope c. 2.5 km offshore at 145 m water depth (Fig. 1-4, 1-5). Although situated on a slightly inclined slope, hydroacoustic data revealed clearly distinguishable parallel reflectors, which indicate that site Co1202 is generally undisturbed (Fig. 1-5).

With a length of c. 15 m core Co1202 represents the longest sediment succession recovered from Lake Ohrid to date. Therefore my research primarily focused on lithological, sedimentological, geochemical, and physical analyses of this sediment succession. Lithological, sedimentological, and geochemical analyses have also been conducted for cores Co1200 and Co1201. However, since both cores comprise discontinuous successions, which date well back beyond the limit of radiocarbon dating, other dating methods are to be tested and applied in order to provide a chronological framework. In addition to radiocarbon dating and tephrochronology, the dating methods included electron spin resonance (ESR) on calcareous shell fragments and infrared stimulated luminescence (IRSL) on silt to sand

sized quartz and feldspar. ESR and IRSL measurements were conducted in close cooperation with Dr. A. Hilgers, who heads the Geochronology Laboratory at the Geographical Institute of the University of Cologne. Due to the relocation of the Geochronology Laboratory in 2008 these measurements are still ongoing but will be available by the end of 2009.

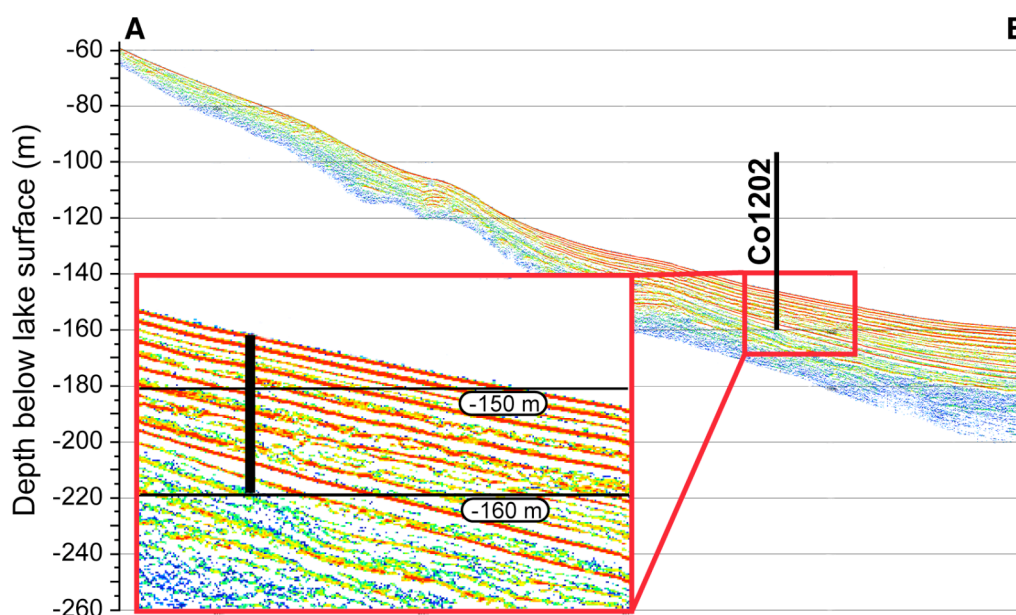


Fig. 1-5. NE-SW trending hydroacoustic profile crossing coring site Co1202. Bold letters (A) and (B) refer to the profile indicated in Fig. 1-4. The insert indicates the penetration depth of core Co1202 (black line) into widely undisturbed sediments.

#### Tephrostratigraphy and chronology of core Co1202

Chapter IV evaluates the potential of Lake Ohrid as an archive for the dispersal of tephra originating from the explosive activity of Italian volcanoes, using the c. 15 m long sediment succession of core Co1202 (Fig. 1-4, 1-5). In addition, the use of high-resolution XRF-scanning techniques as vehicle for the rapid identification of cryptotephra, i.e. small amounts of volcanic glass and micropumice admixed with lacustrine sediment, in lacustrine sediment successions is tested. Based on the morphology, chemistry, mineral phases, and stratigraphy of the glass shards and micropumices, the establishment of correlations with the explosive eruptions of Italian volcanoes is tested. This data is then used to (1) improve the knowledge about the dispersal of ash from Italian volcanoes in the central Mediterranean and its vicinity, and, in combination with radiocarbon dating, (2) establish a chronological framework for core Co1202.

#### Sedimentation and climatic and environmental inferences in course of the last glacial-interglacial cycle at Lake Ohrid deduced from lithological, sedimentological, geochemical, and physical properties of core Co1202

In Chapter V the lithological, sedimentological, geochemical, and physical properties of core 1202 are used to assess how climatic and environmental changes are imprinted in the sediment record of Lake Ohrid over the course of the last glacial-interglacial cycle. This data is compared to other records from Lake Ohrid and the wider Mediterranean region in order to evaluate if the Lake Ohrid sediment record is a valuable archive for paleoclimatic and paleoenvironmental studies over longer time periods.

### 1.3. Chapter contributions

#### **Chapter II: “Fourier transform infrared spectroscopy, a new cost-effective tool for quantitative analysis of biogeochemical properties in long sediment records”**

H. Vogel conducted all FTIRS analyses and statistical evaluation of the generated data. Concentrations for biogeochemical properties (TOC, TN, TIC, BSi) measured using conventional methods were provided by M. Melles and B. Wagner. H. Vogel evaluated and interpreted the data with contributing discussions from P. Rosén, B. Wagner, M. Melles, and P. Persson. H. Vogel wrote the text with contributions from P. Rosén, B. Wagner, M. Melles, and P. Persson. Overall H. Vogel contributed >80 % to Chapter II.

#### **Chapter III: “Fourier transform infrared spectroscopy, a new method for rapid determination of total organic and inorganic carbon and biogenic silica concentration in lake sediments”**

H. Vogel conducted FTIRS analyses for core Lz1024 (Lake El'gygytgyn) and core Lz1120 (Lake Ohrid). All other FTIRS analyses were conducted by P. Rosén and co-workers. Concentrations of biogeochemical properties (TOC, TIC, BSi), using conventional techniques, were provided by O. Juschus and B. Wagner for cores Lz1024 and Lz1120, respectively. Biogeochemical properties for lakes from N Sweden were measured by P. Rosén and co-workers. P. Rosén did all statistical analyses and data evaluation. H. Vogel and L. Cunningham contributed to the interpretation of the data. P. Rosén wrote the text with contributions from H. Vogel, L. Cunningham, D. Conley, and P. Persson. Overall H. Vogel's contribution to Chapter III was <30 %.

#### **Chapter IV: “A tephrostratigraphic record for the last glacial-interglacial cycle from Lake Ohrid, Albania and Macedonia”**

H. Vogel did the logistics for the 2007 field campaign and led the coring, resulting in the successful recovery of the 15 m long core Co1202 which is the major focus of this study. Core descriptions, XRF-scanning, magnetic susceptibility measurements, as well as subsampling of tephra and cryptotephra layers were all done by H. Vogel and student co-workers. R. Sulpizio and G. Zanchetta conducted geochemical analyses on volcanic glasses and micropumices at the University of Pisa. Interpretations of the sedimentology, lithology, XRF-, and MS-data as well as interpretation of radiocarbon measurements and the establishment of the chronology of core Co1202 were done by H. Vogel. Interpretation and

correlation of tephra and cryptotephra layers was primarily done by R. Sulpizio and G. Zanchetta with only a minor contribution from H. Vogel. H. Vogel wrote the main body of the text with contributions from B. Wagner, R. Sulpizio, and G. Zanchetta. The tephrostratigraphy forms one of the main parts of the chapter and was primarily written by R. Sulpizio and G. Zanchetta with only minor contribution from H. Vogel. Overall H. Vogel's contribution to Chapter IV exceeded 70 %.

**Chapter V: “A paleoclimate record with tephrochronological age control for the last glacial-interglacial cycle from Lake Ohrid, Albania and Macedonia”**

H. Vogel did the logistics for the 2007 field campaign and led the coring, which resulted in the successful recovery of the 15 m long core Co1202, which is the major focus of this study. H. Vogel and student co-workers conducted lithological, sedimentological, geochemical, and physical investigations on core Co1202. P. Rosén and co-workers did FTIRS measurements at the Umeå University, Sweden. Data interpretation was primarily done by H. Vogel but benefited greatly from discussions with B. Wagner. H. Vogel wrote the text almost independently, with only minor contributions from B. Wagner, P. Rosén, G. Zanchetta, and M. Melles. Overall H. Vogel's contribution to Chapter V was >90%.

# Chapter II

## **Fourier transform infrared spectroscopy, a new cost-effective tool for quantitative analysis of biogeochemical properties in long sediment records**

### **Abstract**

Measurements of Fourier transform infrared spectroscopy (FTIRS) in the mid-infrared (MIR) region were conducted on sedimentary records from Lake El'gygytgyn, NE Siberia, and Lake Ohrid, Albania/Macedonia. Calibration models relating FTIR spectral information to biogeochemical property concentrations were established using partial least squares regression (PLSR). They showed good statistical performance for total organic carbon (TOC), total nitrogen (TN), and biogenic silica (opal) in the sediment record from Lake El'gygytgyn, and for TOC, total inorganic carbon (TIC), TN, and opal in sediments from Lake Ohrid. In both cases, the calibration models were successfully applied for down-core analysis. The results, in combination with the small amount of sample material needed, negligible sample pre-treatments, and low costs of analysis, demonstrate that FTIRS is a promising, cost-effective tool that allows high-resolution paleolimnological studies.

## 2.1. Introduction

Lacustrine sedimentary records are valuable archives of past environmental changes. A few of these records, such as the well-known records from the lakes Baikal (e.g. Peck et al. 1994; Colman et al. 1995; Williams et al. 1997), Tanganyika (e.g. Cohen et al. 1993), Malawi (e.g. Tiercelin and Lezzar 2002), Biwa (e.g. Fuji 1988), and Bosumtwi (e.g. Grieve et al. 1995) cover more than one million years. Recent studies have also shown that the lakes Ohrid (Stankovic 1960; Watzin 2002) and El'gygytgyn (Layer 2000) probably have a sediment record more than 3 million years old.

The investigation of the sedimentary records of these ancient lakes requires several analytical methods, one of which comprises their biogeochemical properties. Analysis of biogeochemical properties in sedimentary records often involves intensive sample pre-treatment and incorporates several different analytical techniques, which makes the analytical process both time consuming and expensive. As one approach to develop a fast and cost-effective tool to obtain information of the biogeochemical properties and related climate changes, near infrared spectroscopy (NIRS) has been successfully applied to marine (e.g. Chang et al. 2005; Jarrard and Vanden Berg 2006) and lacustrine (Malley et al. 1999; 2000; Korsman et al. 2001; Rosén et al. 2000; Rosén 2005; Rosén and Hammarlund in press), sediments.

Fourier transform infrared spectroscopy (FTIRS) in the mid infrared region (MIR) is more sensitive to molecules present in minerogenic and organic material than NIRS (e.g. Farmer 1974; Colthup et al. 1990; Harris 1998; Kellner et al. 1998). FTIRS has been applied to sediments to quantitatively reconstruct lake water TOC (Rosén and Persson 2006), silicate minerals (Sifeddine et al. 1994; Bertaux et al. 1996; Wirrmann et al. 2001), carbonates (Mecozzi et al. 2001), and humic substances (Braguglia et al. 1995; Belzile et al. 1997; Calace et al. 1999; 2006). The potential to use FTIRS as a rapid and cost-effective tool for the analysis of biogeochemical properties on long lacustrine sediment records has yet to be tested.

Within the scope of this study, we aim (1) to test if calibration models for the determination of TOC, TIC, TN, total sulphur (TS), and opal concentrations in Lake El'gygytgyn and Lake Ohrid sediments can be established using FTIRS and (2) to test the calibration models on down-core sediment samples by comparing the results to measured concentrations of already established analytical methods.

## 2.2. Study sites

Lake El'gygytgyn (67°30'N, 172°05'E) is situated in north-eastern Siberia, in a 18 km wide crater, which was formed by a meteorite impact 3.6 Ma ago (Layer 2000). The bedrock of the crater is formed by felsic to intermediate igneous rocks of Late Cretaceous age (Ispolatov 2004). Where Tertiary or Quaternary sediments prevail in the vicinity of the lake, the continuous permafrost reaches depths between 100 - 300 m (Nolan and Brigham-Grette 2007). The lake is located in the south-eastern part of the crater and has a diameter of 12 km and a maximum depth of 175 m. The lake probably formed shortly after the meteorite impact and is believed to have never been inundated by quaternary ice sheets (Brigham-Grette et al. 2007; Glushkova and Smirnov 2007). Due to the harsh climate the lake remains ice covered for at least nine months of the year (Nolan and Brigham-Grette 2007). The catchment of the lake is restricted to the area formed by the crater rim and drained by 50 small ephemeral creeks during the short (2 - 3 month) summer period. The river Emnyaam forms the outlet of the lake in its south-eastern corner. The sparse vegetation in the Lake El'gygytgyn basin is dominated by lichen and herbaceous taxa, with rare occurrences of shrub forms of *Salix* and *Betula* in protected areas (Lozhkin et al. 2007).

Lake Ohrid (41°01'N, 20°43'E) is a transboundary lake located between the Republics of Albania and Macedonia. The lake is c. 30 km long, c. 15 km wide and has a maximum depth of c. 280 m. Lake Ohrid is believed to be 5-2 Ma old (Stankovic 1960; Watzin 2002). It contains more than 200 endemic species (Stankovic 1960; Watzin et al. 2002) and reacts sensitive to recent environmental change (Matzinger et al. 2006). The lake basin is located within an active tectonic graben system (Watzin et al. 2002) and surrounded by high mountain ranges reaching up to 2,300 m above sea level. Strongly karstified limestones and clastic sedimentary rocks of Mesozoic age as well as metamorphic rocks of Paleozoic age crop out in the watershed of Lake Ohrid (Robertson and Shallo 2000; Watzin et al. 2002). According to Matzinger et al. (2006), Lake Ohrid is fed by karst aquifers, surface runoff, and direct precipitation on the lake surface area. Surface outflow (60 %) to the River Crn Drim to the north and evaporation (40 %) are the main net outputs. Mediterranean vegetation with clear indications of anthropogenic degradation is characteristic for the Lake Ohrid region (Stankovic 1960).

Both Lake Ohrid and Lake El'gygytgyn are large, old, deep, and oligotrophic lakes. However, their geographic locations, hydrological regimes, catchment dynamics, tectonic frameworks, vegetation, and climatic conditions differ significantly, leading to considerably different sediment characteristics.

## 2.3. Materials and methods

### 2.3.1. Core recovery and composition

Core PG1351 from Lake El'gygytgyn was recovered during an expedition in 1998 from the lake ice in the central part of the lake, where a water depth of 175 m was measured. The sediment succession is 1,290 cm long and composed of a gravity core (Uwitec Ltd., Austria) from the uppermost sediments and several successive percussion piston cores (Uwitec Ltd., Austria) of up to 300 cm length from deeper sediments. The sediment consists of clastic mud with low but variable amounts of organic matter (Melles et al. 2007). Massive horizons of olive grey alternate with laminated horizons of brown and dark grey colors (Asikainen et al. 2007; Melles et al. 2007). Core PG1351 has already been investigated for lithology, sedimentology, physical properties, palynology and geochemistry to assess past climate changes in the region and changes in the catchment and water column using a multiproxy approach (Nowaczyk et al. 2002; Asikainen et al. 2007; Lozhkin et al. 2007; Melles et al. 2007; Minyuk et al. 2007). The biogeochemical properties are some of the most valuable proxies for reconstructing changes in regional temperature and humidity (Melles et al. 2007). The base of core PG1351 at 1,290 cm sediment depth is dated to 250 kyrs (Nowaczyk et al. 2007).

Sediment cores from Lake Ohrid were taken from a floating platform in 2005, in the southeastern part of the lake, where a water depth of 105 m was measured. A 1,075 cm long composite core (Lz1120) was sampled using the same coring equipment as described above. Core Lz1120 can be subdivided into two units with distinctly different sediment composition. The lower Unit I (1,075-552 cm) with a basal age of c. 40 kyrs consists of poorly sorted, massive, medium to coarse silt of greyish colour. Carbonates and plant macrofossils are typically absent, and organic material is sparse in Unit I. The upper Unit II (545-0 cm) consists of medium to coarse-grained silt, with finely dispersed organic material, and calcareous remains of fossil ostracode and mollusc valves. Colour changes repeatedly from light grey to brownish-black in Unit II (Wagner et al. 2008b; 2009). Variations of biogeochemical properties throughout this sedimentary succession clearly reflect climate-induced changes in the catchment and water column of Lake Ohrid (Wagner et al. 2008b; 2009).

### 2.3.2. Biogeochemistry (conventional methods)

Both cores PG1351 and Lz1120 were sub-sampled in 2 cm intervals. The samples were freeze-dried and ground to a particle size below 63  $\mu\text{m}$  using a planetary mill. Concentrations of total carbon (TC), TN, and TS were measured with a combustion CNS elemental analyzer (VARIO Co. and EuroVector Co.). Samples for TOC analysis were pre-treated with HCl (10%) at a temperature of 80°C to remove carbonates and then analyzed using a Metalyt-CS-1000-S (ELTRA Corp.). TIC was calculated by subtracting TOC from TC. Opal measurements were conducted using the leaching method described by Müller and Schneider (1993).

### 2.3.3. FTIRS

The basic principle of the FTIRS technique is that vibrations in molecules containing polar bonds are excited by infrared (IR) radiation. The wavelengths at which molecules are excited are dependent on the structural and atomic composition of the molecule leading to the absorbance of IR radiation at molecule specific wavelengths (e.g. Colthup et al. 1990; Kellner et al. 1998).

FTIRS measurements were performed on a subset of 161 samples collected at 6 cm intervals from core PG1351 (Lake El'gygytgyn), and 505 samples at 2 cm intervals from core Lz1120 (Lake Ohrid). To avoid variations in measurement conditions caused by temperature, all samples were placed in the same thermostated laboratory ( $25 \pm 0.2^\circ\text{C}$ ) as the FTIRS device for at least 5 hours immediately prior to analysis, in order to adapt to the same temperature as the FTIRS device. For FTIRS analysis 0.5 g potassium bromide (KBr) (Uvasol®, Merck, Germany) was mixed with 0.011 g freeze-dried and ground sample material using a mortar and pestle. The mixing of KBr and sample material was performed without any safety precautions since KBr is rated as a non-toxic substance. KBr is transparent in the IR region and is used as a diluting substance to avoid distortions that are caused by optical effects (Griffiths and De Haseth 1986). The processed, powdered samples were placed into a sample cup and analyzed by means of the diffuse reflectance FTIRS technique using a Bruker IFS 66v/S FTIR spectrometer (Bruker Optik GmbH, Germany) equipped with a diffuse reflectance accessory (Harrick Inc., USA). For each sample, data were collected at 4 mbar vacuum conditions for wavelengths between 2,666 and 25,000 nm, or 3,750 and 400  $\text{cm}^{-1}$  expressed by means of wavenumbers, with an analysis each 2  $\text{cm}^{-1}$ , yielding 1,737 data points per sample.

### 2.3.4. Numerical analysis

FTIR spectra were normalized using baseline correction and multiple scatter correction (MSC). Internal variations of the FTIRS device during analysis can cause baseline-shifts and tilting between the sample spectra. In order to get the same baseline for all spectra, independent on measurement conditions, baseline correction performs a linear correction of the spectra, by setting two points (3,750 and 2,210 - 2,200  $\text{cm}^{-1}$ ) to zero. Since this correction is done for two points of the spectra it corrects for both baseline-shifts and tilting. MSC removes spectral variation arising from varying effective path lengths between the sample surface and the detector and particle size (Geladi et al. 1985, Martens and Næs 1989, Geladi and Dåbakk 1999). The aim of this method is to remove variation in spectra caused by between-sample scatter variation. Thus, MSC linearizes the spectra and eliminates variation caused by noise. The remaining variation is supposed to relate solely to the chemistry of the sample. Using spectral data from many samples enables the distinction between absorption and scatter. The scatter for each sample is estimated relative to that of an “ideal” sample, taken as the mean spectrum of all sample spectra. Each sample spectrum is then corrected to the same scatter level as the “ideal” sample. SIMCA-P (Umetrics AB, SE 901-91 Umeå, Sweden) software was used for all statistical analysis.

On core PG1351 calibration models for TOC and TN are based on 96 out of 100 samples and for opal on 64 out of 100 samples from the topmost 764 cm, respectively (Table 2-1). TIC was absent in core PG1351. For core Lz1120 calibration models were constructed in a different way since the sediment characteristics of units I and II are distinctively different. Hence, a calibration model built upon samples from unit II cannot be applied for unit I and vice versa. Thus on core Lz1120 calibration models for TOC, TIC, TN, and TS are based on 102 samples in 10 cm intervals and for opal on 58 samples in c. 20 cm intervals throughout the core. Partial least squares regression (PLSR) (e.g. Martens and Næs 1989 and references therein) was used to establish calibration models between FTIR-spectra of sediment samples and corresponding conventionally measured biogeochemical property concentrations. Quantitative validation of the internal statistical performance of the calibration models was carried out using cross validation (CV). In CV 90% of the conventionally measured dataset with biogeochemical property concentrations and their corresponding sample spectra are used for the calibration model. The model is then used to predict biogeochemical property concentrations of the remaining 10% of the sample set by solely using their recorded FTIR-spectra. Root mean square error of cross validation (RMSECV) and the cross-validated coefficient of determination  $R^2_{CV}$  were used to describe the best fit for internal model predictions. RMSECV was calculated according to equation (1):

$$RMSECV = \frac{1}{n} \sqrt{\frac{\sum_{i=1}^n (y_i - x_i)^2}{\sum_{i=1}^n (y_i - \bar{y})^2}} \quad (1)$$

With  $n$  the number of samples,  $y_i$  the conventionally measured property concentration for sample  $i$ ,  $x_i$  the FTIRS-inferred property concentration for sample  $i$ , and  $\bar{y}$  the mean conventionally measured property concentration for all samples.

Adjacent to CV, in a second validation procedure FTIRS calibration models were used to assess the concentrations of biogeochemical properties on sediment samples not included in the model and compared with measurements using conventional methods. To verify the robustness of the calibration models, 61 FTIRS-inferred concentrations for each property were compared to conventionally measured concentrations in the section between 1,290 and 772 cm of core PG1351. For this purpose, 60 samples with conventional TOC and TN measurements and 18 samples with conventional opal measurements were available.

Calibration models for TOC, TIC, TN, and TS were verified on 403 interspersed samples with conventional measurements available for core Lz1120. Since only 119 conventionally measured opal concentrations were available throughout core Lz1120 the calibration model for opal built upon 58 samples was verified on the remaining 61 conventional measured samples. Then, the opal model was applied to infer opal concentrations in the sample set not conventionally measured.

The coefficient of determination ( $R^2$ ) between the conventionally measured and the FTIRS-inferred property concentrations, as well as the standard error of estimate of  $y$  on  $x$  ( $SE_{y,x}$ ), were calculated to get a quantitative estimate about how the calibration model performs if the property concentrations in the samples are derived from FTIR spectra. The  $SE_{y,x}$  was calculated according to equation (2):

$$SE_{y,x} = \sqrt{\frac{\sum (y - x)^2}{n}} \quad (2)$$

with  $n$  the number of samples,  $y$  the primary biogeochemical property concentration, and  $x$  the FTIRS-inferred biogeochemical property concentration. Loadings or weight vector ( $w^*c$ ) values of the PLS component 1 (PLSC1), the most important principal component equivalent in PLSR, which explains most of the correlation between the sample spectra and the concentration of the regarded biogeochemical property, were plotted against wavenumbers to identify the spectral region contributing most to the calibration models.

## 2.4. Results and discussion

### 2.4.1. Spectral information

#### Lake El'gygytgyn

The FTIR spectra of the MIR-region from Lake El'gygytgyn sediments show only little variation and generally the highest absorbance at wavenumbers between 1,000 - 1,150  $\text{cm}^{-1}$  (Fig. 2-1a). This region of the spectrum as well as regions between 400 - 650  $\text{cm}^{-1}$  and centred at 800  $\text{cm}^{-1}$  can be attributed to absorbance caused by SiO (Farmer 1974) or organic material (Colthup et al. 1990). In Lake El'gygytgyn organic compounds are only minor constituents of the sediment (<2.5% TOC) (Melles et al. 2007) whilst minerogenic material containing SiO such as chlorite, smectite, illite (Asikainen et al. 2007), kaolinite, quartz, feldspar (Dehnert 2004), and opal (Melles et al. 2007) is dominant. Hydroxyl ions are major constituents of clay minerals, opal, and of organic substances present in lake sediments. Within the recorded spectra of Lake El'gygytgyn the absorbance maximum centred around 3,600  $\text{cm}^{-1}$  and further absorbance between 3,000 - 3,750  $\text{cm}^{-1}$  can be mostly attributed to hydroxyl vibrations (Farmer 1974, Kellner et al. 1998). Molecules present in organic substances show absorbance in a large part of the whole MIR-region. Carbon hydrogen bonds show absorbance between 2,850 - 3,000  $\text{cm}^{-1}$  (Colthup et al. 1990) (Fig. 2-1a). Absorbance in the 1,600 - 1,800  $\text{cm}^{-1}$  region is characteristic for CO bonds, such as those originating from carbonates (Mecozzi et al. 2001) or carboxyl-groups of humic substances (Calace et al. 1999). Since carbonates are almost absent in Lake El'gygytgyn (Melles et al. 2007) absorbance in the 1,600 - 1,800  $\text{cm}^{-1}$  region is probably related to the occurrence of

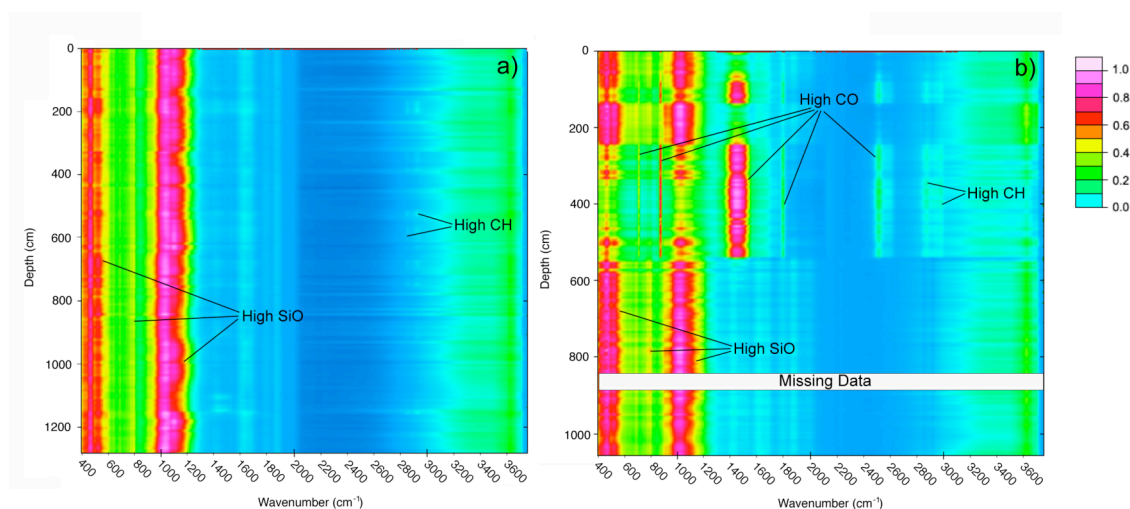


Fig. 2-1. 2D plot of FTIR spectra from cores a) PG1351 and b) Lz1120. Wavenumbers are displayed on the x-axis, sediment depths are shown on the y-axis, and absorbance is indicated by a color chart with red/violet indicating highest and blue indicating lowest absorbance. SiO equals silicon oxygen bond, CO equals carbon oxygen bond, and CH equals carbon hydrogen bond.

humic substances. Further determination of chemical bonds present in organic substances is difficult in Lake El'gygytgyn, as the high concentration of minerogenic components leads to overlapping spectra in regions where organic substances absorb.

### Lake Ohrid

FTIR spectra from Lake Ohrid generally show the highest absorbance in the  $1,450\text{ cm}^{-1}$  region for the uppermost 550 cm sediment depth (Fig. 2-1b). This spectral region ( $1,450\text{ cm}^{-1}$ ) as well as absorbance centred at 710, 880, 1,800, and  $2,520\text{ cm}^{-1}$  (Fig. 2-1b) can be attributed to CO vibrations of calcite (White 1974). Calcite is one major component of Lake Ohrid sediments within the uppermost 550 cm, reaching concentrations of up to 80wt% (Wagner et al. 2009). The region between  $1,000 - 1,050\text{ cm}^{-1}$  (Fig. 2-1b) shows highest absorbance from 1,075 - 550 cm sediment depth. This spectral region as well as absorbance maxima at 800, and between  $400 - 650\text{ cm}^{-1}$  (Fig. 2-1b) are related to SiO vibrations mainly derived by quartz, feldspars, clay minerals, and opal. Absorbance between  $3,000 - 3,750\text{ cm}^{-1}$  with a characteristic maximum at  $3,600\text{ cm}^{-1}$  (Fig. 2-1b) is due to OH vibrations and shows the highest absorbance values in samples with low carbonate content and correspondingly high amounts of silicate minerals. Absorbance in the  $2,850 - 3,000\text{ cm}^{-1}$  region, in particular visible in the uppermost 550 cm of core Lz1120 (Fig. 2-1b), can be attributed to CH vibrations.

### **2.4.2. Model development**

The statistical performance for the calibration models by means of the root mean square error of cross-validation (RMSECV), RMSECV as percentage of the calibration set gradient (the gradient is the difference between minimum and maximum concentrations of the regarded property within the sample set used for the calibration model),  $R^2_{CV}$ , and the number of PLS components is presented in Table 2-1 for both lakes.

### Lake Elgygytgyn

For Lake El'gygytgyn, the correlation is high between the FTIRS inferred and conventionally measured TOC ( $R^2_{CV} = 0.96$ ), TN ( $R^2_{CV} = 0.68$ ), and opal ( $R^2_{CV} = 0.75$ ) concentrations. Correspondingly the RMSECV is low for TOC (0.07%, 3.79% of the gradient), TN (0.017%, 10.45% of the gradient), and opal (1.76%, 10.66% of the gradient). Model performance for TS ( $R^2_{CV} = 0.11$ ) was low so a correlation was not performed.

Lake Ohrid

The statistical performance of the calibration models for Lake Ohrid is high for TOC ( $R^2_{cv} = 0.81$ ), TIC ( $R^2_{cv} = 0.96$ ), TN ( $R^2_{cv} = 0.69$ ), and opal ( $R^2_{cv} = 0.63$ ). Correspondingly the RMSECV is low for TOC (0.25%, 13.15% of the gradient), TIC (0.69%, 7.11% of the gradient), TN (0.022%, 9.21% of the gradient), and opal (1.02%, 13.22% of the gradient). The statistical performance of the TS model ( $R^2_{cv} = 0.26$ ) is poor and the FTIRS model is therefore not good enough for quantitative estimations of TS in the sediment from Lake Ohrid.

Table 2-1. Descriptive statistics for calibration models for the estimation of biogeochemical properties of core PG1351 (PG) and Lz1120 (Lz) from FTIR-spectra.

Statistic	TOC		TIC		TN		TS		Opal	
	PG	Lz	PG	Lz	PG	Lz	PG	Lz	PG	Lz
PLS components	6	1	-	1	5	2	-	2	4	1
samples (n)	96	102	-	102	96	102	-	102	64	58
min (%)	0.12	0.48	-	0.00	0.00	0.07	-	0.02	6.22	0.10
max (%)	1.94	2.40	-	9.64	0.17	0.31	-	0.36	22.72	7.84
gradient (%)	1.82	1.92	-	9.64	0.167	0.240	-	0.340	16.50	7.74
mean (%)	0.54	1.19	-	2.85	0.067	0.160	-	0.090	13.07	3.39
RMSECV (%)	0.07	0.25	-	0.69	0.017	0.022	-	0.047	1.76	1.02
RMSECV (% gradient)	3.79	13.15	-	7.11	10.45	9.21	-	13.91	10.66	13.22
$R^2_{cv}$	0.96	0.81	-	0.96	0.68	0.69	-	0.26	0.75	0.63

#### 2.4.3. Relationships between FTIRS models and biogeochemical properties

Lake El'gygytgyn

Since the FTIRS model uses similar wavenumbers for TOC and TN these elements can probably not be assessed independently. Especially the regions around 500, 850 - 1,000, 1,400 - 1,800, 2,850 - 3,000, and 3,600  $\text{cm}^{-1}$  are important for the PLSR models (Fig. 2-2). The regions between 1,400 - 1,800 and between 2,850 - 3,000  $\text{cm}^{-1}$  are sensitive to molecules present in organic substances. This indicates that the models are partly based on a direct relationship between spectral variation and organic matter content. In contrast, spectral regions at around 500 and between 850 - 1,000  $\text{cm}^{-1}$  are indicative for absorbance mainly caused by SiO, and absorbance in the 3,600  $\text{cm}^{-1}$  region is mainly caused by OH vibrations. This indicates that indirect relationships are also important for the calibration models. Spectral bands between 600 - 800 and 1,040 - 1,240  $\text{cm}^{-1}$  are anti-correlated to the TOC and TN concentrations (Fig. 2-2). Absorbance in these spectral regions is mainly due to SiO groups in silicate minerals.

Within the calibration model for opal, spectra between  $1,050 - 1,350 \text{ cm}^{-1}$  (Fig. 2-2), explain most of the variation, however the region between  $3,000 - 3,500 \text{ cm}^{-1}$  and the small

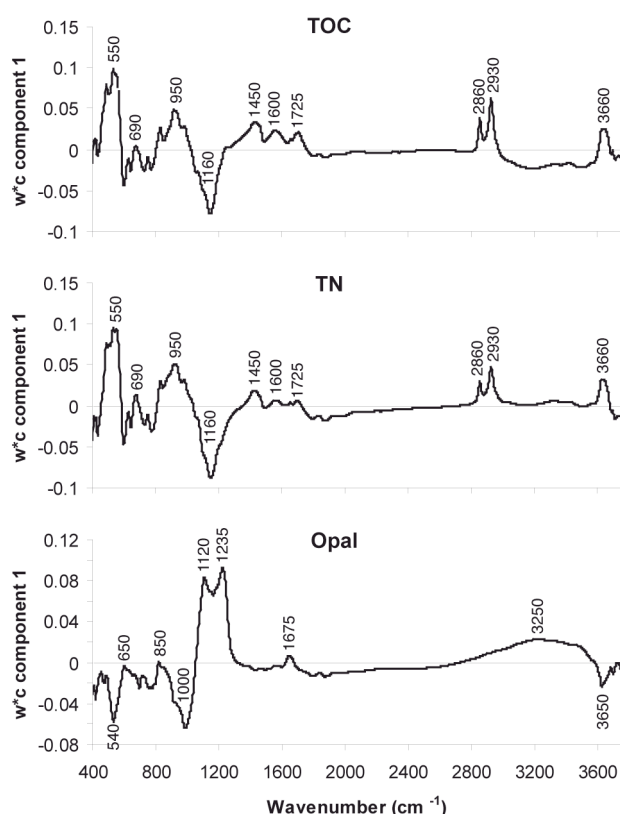


Fig. 2-2. Loadings expressed by weight vectors ( $w^*c$ ) of the PLSC1 (y-axis) for the FTIRS-inferred properties of sediment from core PG1351. The figure shows the spectral regions important for the predictive models. Positive loadings indicate wavenumbers positively correlated to the property of interest and negative loadings indicate wavenumbers negatively correlated to the property.

peak centred around  $1,675 \text{ cm}^{-1}$  (Fig. 2-2) also contribute to the correlation. Opal shows characteristic SiO absorbance maxima at 480, 790, and in particular at  $1,100 \text{ cm}^{-1}$  (Moenke 1974, Gendron-Badou et al. 2003). The absorbance around  $1,100 \text{ cm}^{-1}$  is probably the most important region for the FTIRS opal model. The absorbance between  $3,000 - 3,500 \text{ cm}^{-1}$  can be linked to OH molecular vibrations (Moenke 1974), which are also important constituents of opal. Thus it can be assumed that the model is predominantly based on a direct relationship between opal concentration and spectral variation. The regions between  $400 - 1,000 \text{ cm}^{-1}$  and at  $3,600 \text{ cm}^{-1}$  are anti-correlated to the concentration of opal (Fig. 2-2). Even though the  $400 - 1,000 \text{ cm}^{-1}$  region is also indicative for SiO it is difficult to define specific silicate minerals causing

absorbance in this region. Absorbance at  $3,600 \text{ cm}^{-1}$  is due to OH and in this particular region it is negatively correlated to opal concentrations.

Even though the variation observed in the raw spectra is very little the models for TOC and TN on the one hand and the model for opal are clearly distinguishable regarding the wavenumbers used by the models. This shows that spectral variation even if it is not clearly visible to the human eye can contain important information on the concentration of the regarded biogeochemical properties.

### Lake Ohrid

The FTIRS models for TOC, TIC, TN, TS, and opal use similar wavenumbers (Fig. 2-3), which indicates that these models may not be independent of each other. In particular the wavenumbers indicative for carbonate at 710, 880, 1,450, 1,800, and  $2,520 \text{ cm}^{-1}$  (White

1974, Gaffey 1986) are clearly the most important wavenumbers for all calibration models (Fig. 2-3). Whereas TOC, TIC, and TN are positively correlated, opal is negatively correlated to these wavenumbers. This is probably due to the dominance of calcium carbonate in the uppermost 550 cm of the Lz1120 record (Wagner et al. 2009) and changes in TIC concentration have a large impact on the relative concentration of other compounds.

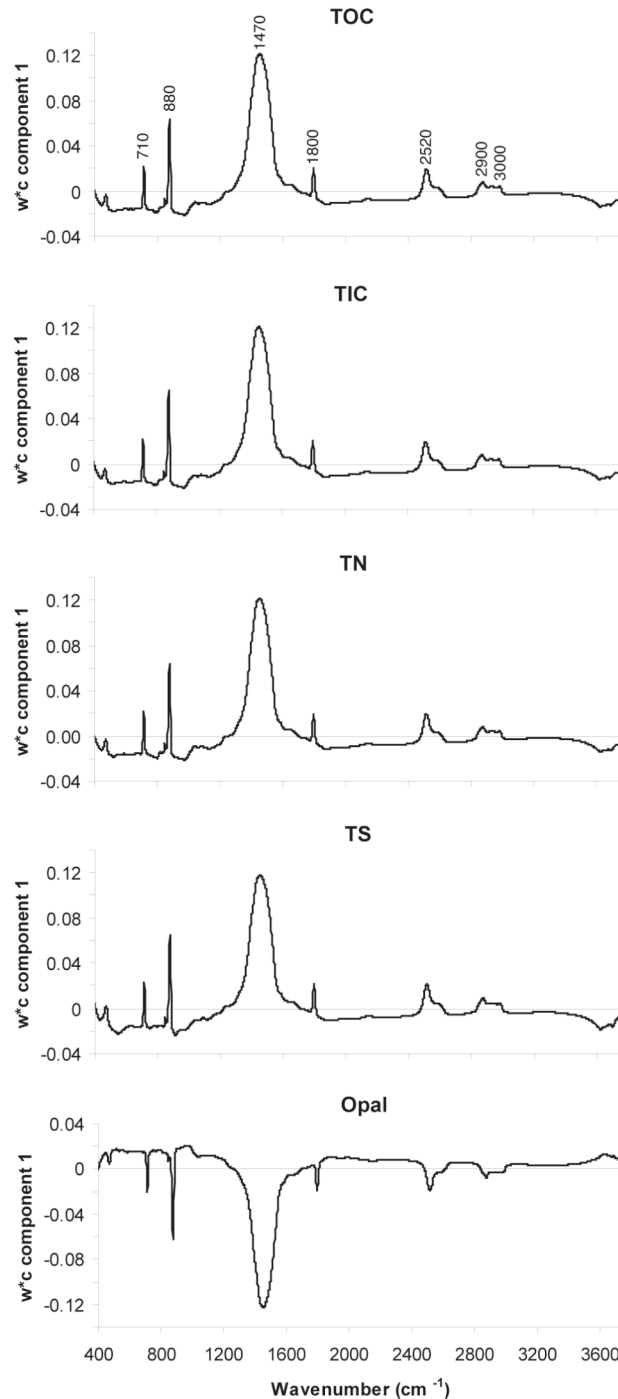


Fig. 2-3. Loadings expressed by weight vectors ( $w^*c$ ) of the PLSC1 (y-axis) for the FTIRS-inferred properties of sediment from core Lz1120. The figure shows the spectral regions important for the predictive models. Positive loadings indicate wavenumbers positively correlated to the property of interest and negative loadings indicate wavenumbers negatively correlated to the property.

#### 2.4.4. Predictions

The results for the predictions of biogeochemical properties solely using FTIR spectral information is displayed by means of the SE  $y,x$ , the SE  $y,x$  as percentage of the prediction set gradient (the gradient is the difference between minimum and maximum concentrations of the regarded property within the prediction set) and the  $R^2$  between FTIRS-inferred and conventionally measured property concentrations in Table 2-2.

Table 2-2. Descriptive statistics for the prediction of biogeochemical properties estimated by applying calibration models to samples not included in the calibration models for core PG1351 and core Lz1120.

Statistic	TOC		TIC		TN		TS		Opal	
	PG	Lz	PG	Lz	PG	Lz	PG	Lz	PG	Lz
samples (n)	60	403	-	403	60	403	-	403	18	61
min	0.16	0.48	-	0.00	0.03	0.07	-	0.01	4.71	0.68
max	1.66	2.85	-	9.72	0.11	0.30	-	1.39	21.15	6.74
gradient	1.50	2.37	-	9.72	0.084	0.230	-	1.380	16.44	5.79
mean	0.39	1.20	-	2.75	0.07	0.16	-	0.10	10.72	3.18
SE $y,x$	0.12	0.25	-	0.48	0.010	0.020	-	0.090	2.17	0.68
SE $y,x$ (% gradient)	8.28	10.48	-	4.96	12.46	8.63	-	6.50	13.22	8.78
$R^2$	0.79	0.84	-	0.98	0.62	0.84	-	0.21	0.76	0.78

#### Lake El'gygytgyn

The FTIRS calibration models for TOC ( $R^2 = 0.79$ ), TN ( $R^2 = 0.62$ ), and opal ( $R^2 = 0.76$ ) show good statistical performance and can be used to reproduce general trends in down-core analysis (Fig. 2-4, 2-5). The SE  $y,x$  is low for TOC (0.12%, 8.28% of the gradient), TN (0.010%, 12.46% of the gradient), and opal (2.17%, 13.22% of the gradient), showing that the reproducibility in respect of absolute values is good. The statistical performance for TOC calibration models decreases substantially with a difference of 0.17 (TOC) between the  $R^2_{CV}$  (0.96) of the calibration model and the  $R^2$  (0.79) in down-core predictions (Fig. 2-5), due to 7 outliers between 1,089 and 1,144 cm sediment depth (Fig. 2-4). By removing these 7 outliers, the difference is reversed and the  $R^2$  (0.96) in down-core predictions equals the  $R^2_{CV}$  (0.96) of the internal calibration model validation. Since the gradient as well as maximum and minimum concentrations are covered by the calibration model, the discrepancy between FTIRS-inferred and conventionally measured concentrations might be due to inconsistency in the conventionally measured TOC concentrations. Another possibility could derive from low quality FTIRS data for this sediment sequence. However, no peculiarities were observed during analysis and among the collected spectra, further predictions for TN and opal within the same sediment sequence do not show similar discrepancies.

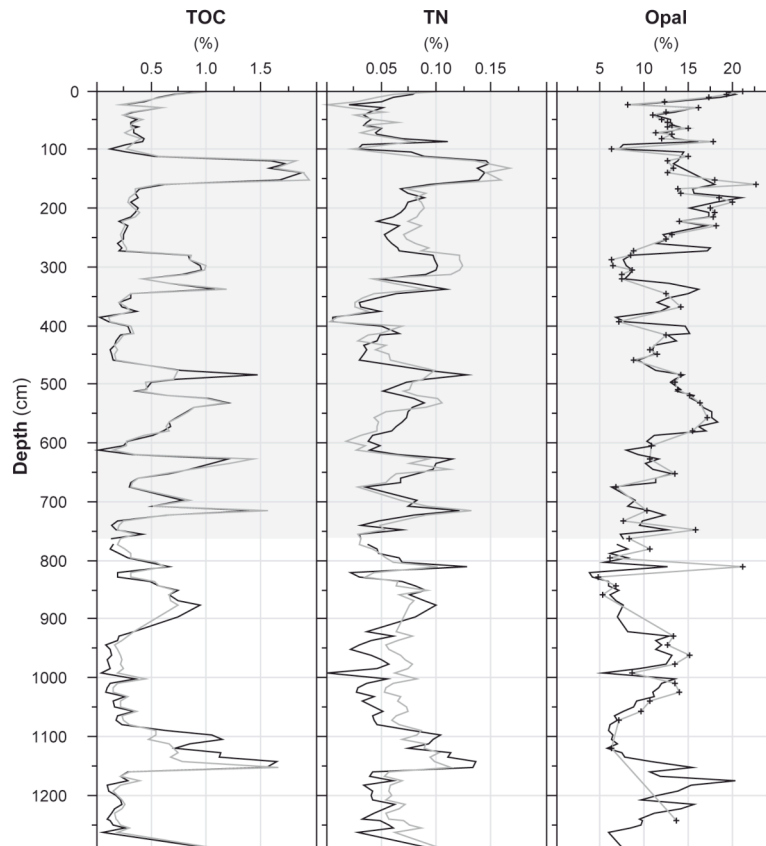


Fig. 2-4. Down-core plot of biogeochemical properties measured with conventional techniques (grey line) and inferred using FTIRS (black line) of core PG1351. The interval on which the calibration model has been built is indicated by the grey background for the uppermost 764 cm. Due to the few samples analyzed by conventional methods, opal concentrations measured by conventional method are indicated by crosses.

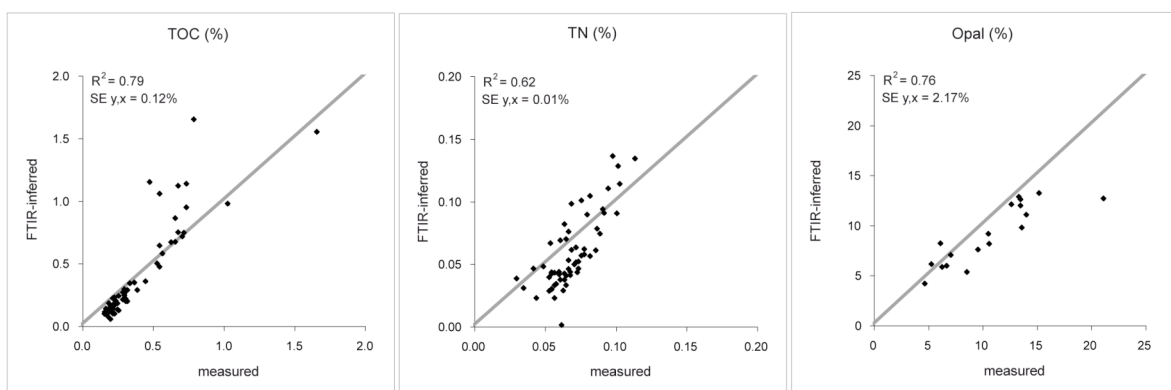


Fig. 2-5. Scatter plots of conventionally measured (x-axis) versus FTIR-inferred (y-axis) TOC, TIC, TN, TS, and opal concentrations for core PG1351.

Lake Ohrid

The FTIRS calibration models for TOC ( $R^2 = 0.84$ ), TIC ( $R^2 = 0.98$ ), TN ( $R^2 = 0.84$ ), and opal ( $R^2 = 0.78$ ) show good statistical performance (Fig. 2-6, 2-7). Correspondingly, the SE  $y,x$  is low for TOC (0.25%, 10.48% of the gradient), TN (0.020%, 8.63% of the gradient), opal (0.68%, 8.78% of the gradient), and especially low for FTIRS inferred TIC (0.48%, 4.96% of the gradient) concentrations. The small difference between conventional measured property concentrations and FTIRS-inferred concentrations for TOC, TN, and opal is probably related to the indirect relationship established by the models. The carbonates show strong absorbance in the MIR region and the concentration is highly variable in Lake Ohrid. Therefore it can be difficult to make independent models for TOC, TN, and opal from the Lz1120 core. The detection limit for FTIRS-inferred opal as seen in Fig. 2-7 is likely due to the dependency of the model to the carbonate concentration. The TS calibration model ( $R^2 = 0.21$ ) shows rather poor statistical performance and can thus not be used for predictions. Possible reasons for the poor predictability of TS is its low concentration in most samples, the large gradient combined with only very few high values (Fig. 2-6, 2-7), and the indirect relationships based on the carbonate specific wavenumbers used by the model.

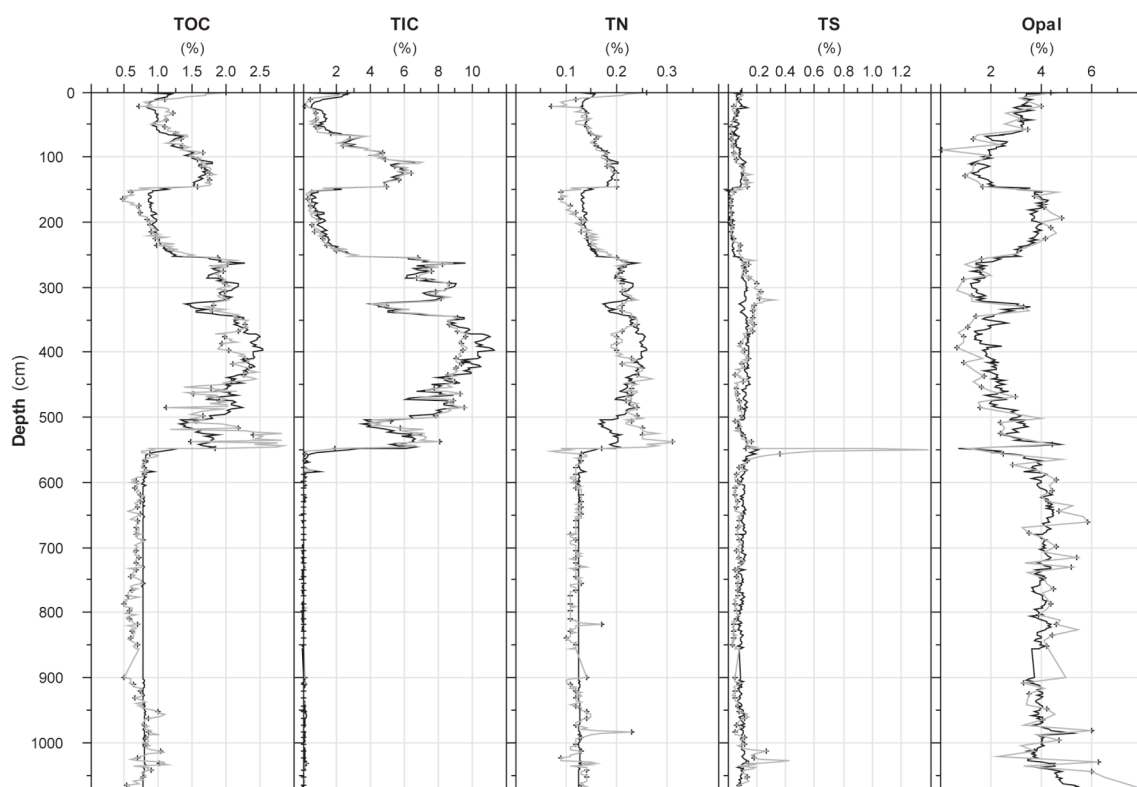


Fig. 2-6. Down-core plot of biogeochemical properties measured with conventional techniques (grey line) and inferred using FTIRS (black line) of core Lz1120. Black crosses indicate the samples used for the calibration models.

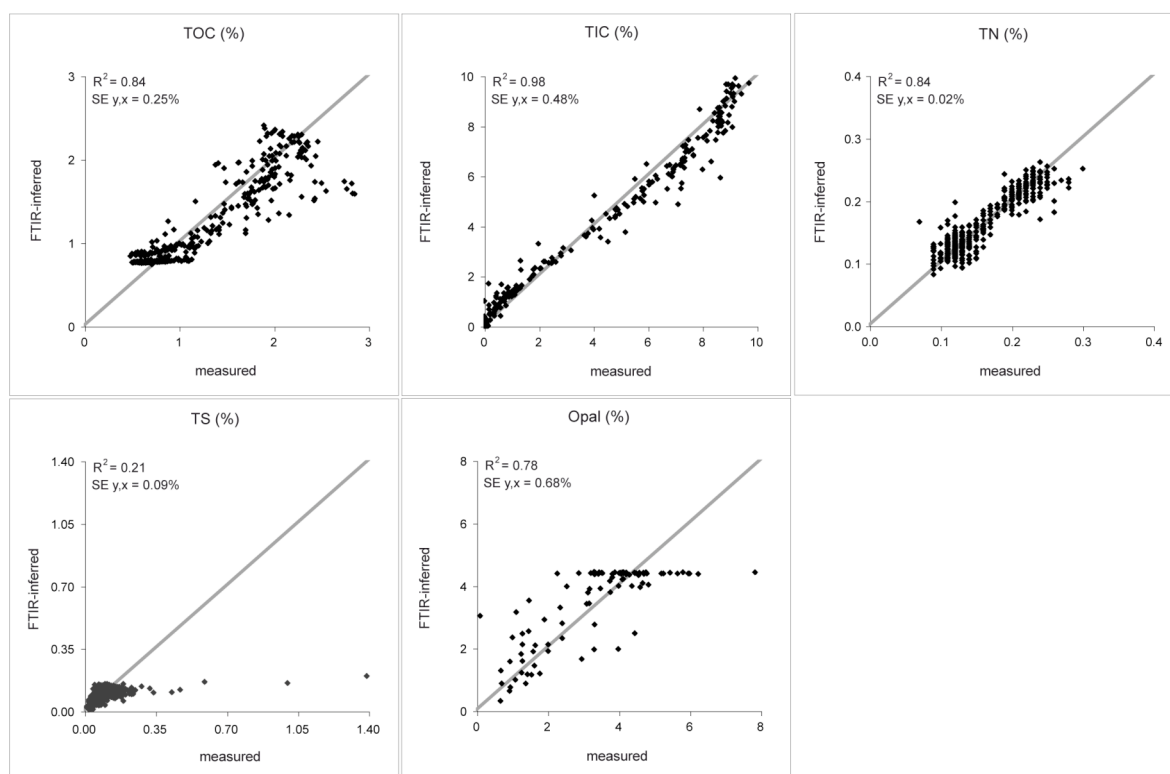


Fig. 2-7. Scatter plots of conventionally measured (x-axis) versus FTIRS-inferred (y-axis) TOC, TIC, TN, TS, and opal concentrations for core Lz1120.

#### 2.4.5. Advantages of FTIRS compared to conventional analytical techniques

This study demonstrates that reliable FTIRS calibrations for TOC, TIC, TN, and opal can be established and might be applied in high-resolution studies of lake sediments. FTIRS calibrations for TS could not be established due to the low concentrations of this property for cores from Lakes El'gygytyn and Ohrid, However the establishment of TS FTIRS calibrations might be possible for sediment sequences containing higher amounts of TS.

Due to simultaneous analysis of several biogeochemical properties and negligible sample pre-treatments, FTIRS is approximately three times faster and costs are about one third less compared to conventional methods. A limiting factor of the method is that FTIRS calibration models need to cover the whole gradient of the regarded property concentration. Thus calibration models developed for a certain sediment sequence can only be applied to sediment sequences, where the composition of the regarded properties is within the same range.

FTIR spectra contain information on minerals and thus calibration models relating the spectral information and absolute concentrations of minerals can also be established and applied as a tool for quantitative analysis. The approach of using FTIR spectra for the quantitative determination of crystallized and amorphous silicate (Bertaux et al. 1996,

Wirrman et al. 2001) as well as carbonate minerals (Mecozzi et al. 2001) has been demonstrated in earlier studies.

A significant advantage of FTIRS compared to conventional analytical methods is the fact that FTIRS provides information on mineralogical as well as organic components in lake sediments, which enables fast overviews of sediment composition without incorporating numerous analytical techniques and sample pre-treatments. Given the current knowledge about FTIRS, low-resolution data from conventional analytical methods should always be used to verify the FTIRS inferred results. Future research will include a large number of lakes with varying sediment properties to make more specific models with selected wavenumbers for different sediment properties.

## 2.5. Conclusions

This study demonstrates that FTIR-spectra in the MIR region can be used to quantitatively reconstruct TOC, TIC, TN, and opal in sediments from lakes El'gygytgyn and Ohrid. Calibration models relating FTIR spectra to the concentrations of TOC, TN, and opal in sediments from Lake El'gygytgyn showed good statistical performance. The most important wavenumbers used by the calibration model correspond well to known molecular vibrations of molecules indicative for the predicted biogeochemical properties. In sediments from Lake Ohrid, calibration models relating FTIR spectra to the concentrations of TOC, TIC, TN, and opal show good statistical performance, however the models for Lake Ohrid are predominantly dependent on the carbonate concentrations since all calibration models are based on known absorbance bands for carbonate. Statistical performances for TS calibration models could not reproduce results from conventional methods.

Furthermore it was demonstrated that FTIR spectra contain information on mineralogical as well as organic constituents in lake sediments. FTIRS is faster and costs are lower compared to conventional analytical methods, particularly when multiple sediment compounds need to be determined quantitatively. The amount of sample material needed for FTIRS is small (0.01g). Therefore FTIRS can be applied in high-resolution studies of sediments or as pre-screening tool enabling a rapid determination of important sediment components. However, since calibration to the regional peculiarities and verification with conventional methods is still required at present, FTIRS cannot yet entirely replace conventional analytical tools in paleolimnology.

## **Chapter III**

### **Fourier transform infrared spectroscopy, a new method for rapid determination of total organic and inorganic carbon and biogenic silica concentration in lake sediments**

#### **Abstract**

We demonstrate the use of Fourier transform infrared spectroscopy (FTIRS) to quantitatively assess total organic carbon (TOC), total inorganic carbon (TIC) and biogenic silica (BSi) concentrations in sediment. FTIRS is a fast and cost-effective technique, which only requires small amounts of sediment (0.01 g). Statistically significant models were developed using sediment from northern Sweden and applied to sedimentary records from Sweden, north east Siberia and Albania/Macedonia. The correlation between FTIRS-inferred values and conventionally assessed biogeochemical properties varied between  $R = 0.84 - 0.99$  for TOC,  $R = 0.85 - 0.99$  for TIC and  $R = 0.68 - 0.94$  for BSi. Since FTIR spectra contain information on a large number of both inorganic and organic components, there is great potential for FTIRS to become an important tool in paleolimnology.

### 3.1. Introduction

Lake sediments are useful archives for studies of past climatic and environmental changes (Battarbee 2000). For a robust interpretation of paleolimnological data it is important to use a multiproxy approach because each technique has advantages and limitations. Some analyses require large sample sizes, which can make multiproxy investigations difficult, especially high-resolution studies in which only small amounts of sediment are available. Furthermore, some lakes contain several hundred meters of sediment, including Lake Baikal (Peck et al. 1994; Colman et al. 1995; Williams et al. 1997), Lake Tanganyika (Cohen et al. 1993), Lake Biwa (Fuji 1988), Lake El'gygytgyn (Niessen et al. 2007; Gebhardt et al. 2006), and Lake Ohrid (Krastel personal communication), which would require analysis of very large numbers of individual samples. As a consequence, multiproxy studies in paleolimnology can be both time consuming and expensive.

Fourier transform infrared spectroscopy (FTIRS) allows detailed structural and compositional analysis of both organic and inorganic compounds using only small samples (0.01 g). The basic principle of the FTIRS technique is that infrared radiation excites vibrations in molecules and as a consequence of the quantum mechanical behaviour this radiation is absorbed at specific wavelengths. Because molecules and minerals have unique chemical compositions and structures, they display unique infrared spectra. FTIR spectra of sediment consist of spectral signatures from all the sediment compounds and are the sum of the characteristic infrared (IR) "fingerprints" of each compound present. FTIRS has been applied to sediment for analysis of silica and other minerals (Sifeddine et al. 1994; Bertaux et al. 1996; Wirrmann and Bertaux 2001; Mecozzi et al. 2001) and for assessment of tree-line changes and TOC in lake water (Rosén and Persson 2006). FTIRS has also been used to characterize humic materials (Braguglia et al. 1995; Belzile et al. 1997; Calace et al. 1999; Mecozzi and Pietrantonio 2006), and for the quantitative determination of sodium carbonate ( $\text{Na}_2\text{CO}_3$ ). Vogel et al. (2008) demonstrated the potential to use FTIRS to assess quantitatively the TOC, TIC, TON and BSi content in long sediment records from Lake El'gygytgyn (Siberia) and Lake Ohrid (Albania/Macedonia), using internal calibration sets. However, these models were only applied to these specific lakes.

The aim of this study is to assess the generality of FTIRS models to assess quantitatively total organic carbon (TOC), total inorganic carbon (TIC) and biogenic silica (BSi) in sediment from lakes in very different settings. Calibration sets from northern Sweden are applied to a 350-kyr sediment sequence from Lake El'gygytgyn, and to a 40-kyr sediment sequence from Lake Ohrid, as well as to more recent records from northern Sweden. To validate the FTIRS method, results are compared to concentrations measured by previously established traditional methods.

## 3.2. Materials and methods

### 3.2.1. Study area

A calibration set of 94 lakes from northern Sweden (67°07'–68°48'N, 17°31'–20°36'E; Table 3-1) was used to assess the correlation between FTIR spectra of lake sediment and total organic matter (LOI<sub>550°C</sub>) and biogenic silica (BSi) concentration of lake sediments. The surface sediment from the calibration set has LOI<sub>550°C</sub> values between 3 and 87% and BSi concentrations varying between 2 and 61% of dry weight (dw). The range in altitude is from 170 to 1,180 m above sea level (a.s.l.), annual precipitation varies from 300 to 1,900 mm/year, and mean July air temperatures vary from 7°C to 14.7°C (Bigler and Hall 2002). Correlation between the LOI<sub>550°C</sub> and BSi is  $r = 0.32$  for the surface sediment calibration set. The lakes are mainly small (<20 ha) headwater lakes situated on similar bedrock (mainly granite and gneiss), with maximum depths ranging from 1.5 to 16 m (Table 3-1). All lakes are from an area with low human impact.

Due to low content of TIC in the 94-lake calibration set, 55 Holocene sediment samples from Lake Badsjön, northern Sweden were used to assess the relationship between FTIR spectra and LOI<sub>950°C</sub>, from which TIC was calculated. Lake Badsjön is situated in the sub-alpine birch forest, 400 m a.s.l., with a maximum depth of 2.3 m (Table 3-1). To compare the LOI<sub>950°C</sub> values with measured TIC from downcore samples, all LOI<sub>950°C</sub> values were transformed to TIC using equation (1):

$$\text{TIC (\%)} = \text{LOI}_{950^{\circ}\text{C}} \cdot (60/44) \cdot (12/60) \quad (1)$$

where 44 is the molecular weight for the carbon dioxide coming from carbonate, and 12 is the atomic weight for C (Bengtsson and Enell 1986; Heiri et al. 2001). The TIC concentration of Lake Badsjön's sediment varies between 0 and 11% of dry weight.

To test the FTIRS models, sediment archives from the Swedish lakes Sotaure, Lundsjön, Seukokjaure, Vuolep Njakajaure, Makkasjön and Inre Harrsjön (unofficial names) were used (Table 3-1). To test if the FTIRS models also are applicable to large lakes outside the region of the calibration set, sediment from Lake El'gygytgyn (NE Siberia) and Lake Ohrid (Albania/Macedonia) were used. A lake from the calibration set Lake C57 (unofficial name) was used to show FTIR spectra from sediment without diatoms preserved. The Swedish test lakes were all small headwater lakes (2–13 ha) situated in the same region as the calibration set, with a maximum lake water depth of 4.5–15 m. Lake El'gygytgyn is 175 m deep and 29,300 ha in size and Lake Ohrid is 280 m deep and 35,800 ha in size. For further details about Sotaure, Lundsjön and Makkasjön see Rosén and Hammarlund (2007), for Seukokjaure see Rosén and Persson (2006), for Vuolep Njakajaure see Barnekow (2000), for Lake Inre Harrsjön see Karlsson et al. (submitted) and for Lake El'gygytgyn and Lake Ohrid see Vogel et al. (2008).

Table 3-1. Location and environmental characteristics of the study lakes

Variables	94-lake cal. set	Sweden							Siberia	Albania/ Macedonia
		Badsjön	Sotaure	Lundsjön	Seukok- jaure	Vuolep Njakajaure	Makkasjön	Inre Harrsjön		
Latitude (°N)	67°07'–68°48'	68°20'	66°43'	66°42'	67°46'	68°20'	66°43'	68°21'	67°30'	41°01'
Longitude (°E)	23°52'–17°48'	18°45'	20°36'	20°36'	17°31'	18°45'	20°35'	19°03'	172°05'	20°43'
Altitude (m a.s.l.)	170-1180	400	425	425	670	408	415	351	492	693
Lake area (ha)	<20	0.4	2	3	11	13	3	2	29 300	35 800
Catchment vegetation	Boreal to alpine	Subalpine birch forest	Boreal forest	Boreal forest	Alpine	Subalpine birch forest	Boreal forest	Permafrost mire Subarctic	Arctic Alpine Permafrost	Mediterranean Anthropogenic
Bedrock	Plutonites, Metamorphites	Metasediment, Dolomite	Granite	Granite	Granite, Syenite	Metasediment, Dolomite	Granite	Dolomite Sandstone	Volcanites	Limestone Metasediment Ultramafite
Max. depth (m)	<16	2.3	9	8	6.1	13.7	15	5	175	280
Core length (m)	Surface sed.	3.5	0.7	1.2	1.8	3.2	1.2	0.25	16.5	10.8
Sampling year	1997-98	2006	2003	2003	2006	2005	1995	2005	2003	2005

### 3.2.2. Field and laboratory methods

Surface sediment samples (0–1 cm) from 94 lakes were sampled during the summers in 1997–1998 from the deepest part of the lakes using a gravity corer (Renberg 1991). Sediment cores from Swedish lakes were taken from the deepest part of the lakes (Table 3-1) using a Russian peat corer. Surface sediment cores were taken using a gravity corer or a freeze corer (Inre Harrsjön). The sediments from Lake El'gygytgyn and Lake Ohrid were taken using a gravity corer (Uwitec Ltd., Austria) for the uppermost sediments and several successive percussion piston cores (Uwitec Ltd., Austria) of up to 3 m length for the deeper sediments.

Prior to FTIRS analysis, all calibration samples and samples used to test the models were freeze-dried, ground and mixed with oven dried (80°C) potassium bromide (KBr), which is transparent in the IR region. All samples from Sweden were ground by hand. The samples from Lake El'gygytgyn and Lake Ohrid were ground to a particle size <63  $\mu\text{m}$  using a planetary mill. The weight ratio between sediment and KBr (0.02) was chosen to avoid very high absorbances (>2), which results in low intensities of IR light reaching the detector, and thus produces noisy data and possibly spectral distortions (Herbert et al. 1992). Samples were analyzed by diffuse reflectance FTIRS under vacuum (4 mbar) conditions, using an FTIR spectrometer (Bruker IFS 66v/S) equipped with a diffuse reflectance accessory (Harrick Inc.). Each sample was scanned 64 times at a resolution of 2  $\text{cm}^{-1}$  for wavelengths between 2,666 and 25,000 nm, or from 3,750 and 400  $\text{cm}^{-1}$  (reciprocal centimetres) yielding 1,735 data points per sample. To avoid variations in measurement conditions caused by temperature, all samples were placed in the same temperature-controlled laboratory ( $25 \pm 0.2^\circ\text{C}$ ) as the FTIRS device for at least 5 h prior to analysis.

For comparative purposes, reference spectra of biogenic silica were also obtained by FTIR microspectroscopy on single diatom frustules in sediment samples from Lake El'gygytgyn and a lake (Lake C98-57, unofficial name) in the 94-lake calibration set. These spectra were recorded on a Bruker Equinox 55 spectrometer equipped with a microscopy accessory and a 64 x 64 focal plane array (FPA) detector (Hyperion 3000), providing a maximum spatial resolution of approximately 5  $\mu\text{m}$  at about 4,000  $\text{cm}^{-1}$ . Visual photographs for spectral overlay were snapshots of live images taken with a Sony Exwave HAD color digital video camera mounted on the top of the microscope. The sample tray was boxed and the chamber was continuously purged with dry air. The samples were applied onto polished rectangular  $\text{BaF}_2$  windows. Spectra were recorded in transmission mode over the range of 850 to 3,850  $\text{cm}^{-1}$  with a spectral resolution of 4  $\text{cm}^{-1}$ . The detector system has a cut-off at 850  $\text{cm}^{-1}$ ; hence the spectra quality from the microscopy technique is low below 1,000  $\text{cm}^{-1}$  and should not be interpreted. Also, the quality above 3,000  $\text{cm}^{-1}$  is comparatively poor and

of limited value. For each image, 100 interferograms were co-added to obtain high signal to noise ratios. Background spectra were recorded for each sample at a nearby empty spot on the BaF<sub>2</sub> crystal, prior to sample measurement, with the same number of scans.

TOC and TIC were analysed by LOI<sub>550°C</sub> and LOI<sub>950°C</sub>, respectively, using standard methods (Heiri et al. 2001). For Makkasjön, total carbon (TC) content was measured using a Costech Instruments ECS 4010 elemental analyzer (Rosén and Hammarlund 2007). As the lake is situated on granite and has a pH of ~6, we assumed that the sediment does not contain carbonates and that the TC results from Makkasjön reflect TOC. The accuracy is within ± 5% of the reported values based on replicate analyses of standard material. The FTIRS-inferred LOI<sub>550°C</sub> values for Makkasjön were transformed to TOC using equation (2):

$$\text{TOC (\%)} = \text{LOI}_{550^\circ\text{C}} * 12/30 \quad (2)$$

assuming an average atomic ratio of CH<sub>2</sub>O for the sediment organic matter. The atomic weight for carbon is 12 and the molecular weight for CH<sub>2</sub>O is 30. For Lake El'gygytgyn and Lake Ohrid, concentrations of TC were measured with a combustion CNS elemental analyzer (VARIO Co. and EuroVector Co.). Samples for TOC analysis were pre-treated with HCl (10%) at a temperature of 80°C to remove carbonates and then analyzed using a Metalyt-CS-1000-S (ELTRA Corp.). TIC was calculated by subtracting TOC from TC. BSi in N Sweden samples (surface and long core) was measured using Na<sub>2</sub>CO<sub>3</sub> according to the DeMaster (1981) method, as modified by Conley and Schelske (2001). BSi from Lake Ohrid and Lake El'gygytgyn was digested using NaOH according to the method described by Müller and Schneider (1993). Comparable BSi concentrations are obtained using the different methods (Conley 1998). Unfortunately we do not have a quantitative estimate of the relative abundance of diatoms and other contributors to BSi such as sponge spicules, but our experience is that diatoms generally form the major part of BSi visible in microscope slides from the study region (Wagner et al. 2008; unpublished data).

### 3.2.3. Numerical analyses

FTIR spectra were normalized using baseline correction and multiple scatter correction (MSC) to get the same baseline for all spectra, independent of measurement conditions. Baseline correction performs a linear correction of the spectra so that two points (3,750 and 2,210–2,200 cm<sup>-1</sup>) equal zero. MSC removes spectral variation arising from different effective path lengths and particle sizes (Geladi et al. 1985; Martens and Næs 1989; Geladi and Dåbakk 1999). The aim of the method is to remove variation in spectra caused by between-

sample variations to linearize spectra and eliminate variation caused by noise. Remaining variation should contain solely chemical information about the samples.

Partial least square regression (PLS) (e.g. Martens and Næs 1989) was used to develop a transfer function between FTIRS spectra of the sediment and measured values of LOI<sub>550°C</sub>, LOI<sub>950°C</sub> and BSi. To normalize the data, all LOI<sub>950°C</sub> values were square root-transformed and all BSi values were log10-transformed prior to analysis. The number of significant components in PLS was assessed by cross-validation (CV) with ten groups, e.g. 10% of the calibration lakes were used as a prediction set and the model was built on the remaining 90% of the lakes. This was repeated a total of 10 times as each group, in turn, was set aside. Root mean squared error of cross validation (RMSECV) was used as an estimate of prediction error. RMSECV was calculated according to equation (3):

$$RMSECV = \frac{1}{n} \sqrt{\frac{\sum_{i=1}^n (y_i - x_i)^2}{\sum_{i=1}^n (y_i - \bar{y})^2}} \quad (3)$$

where  $n$  is the number of lakes,  $y_i$  is the measured TOC for lake  $i$ ,  $\bar{y}$  is the mean TOC for all lakes and  $x_i$  is the predicted TOC. SIMCA-P 10.0 (Umetrics AB, SE-907 19 Umeå, Sweden) was used for all multivariate data analysis.

### 3.3. Results and discussion

The results clearly show that FTIR-spectra contain information on TOC (LOI<sub>550°C</sub>), TIC (LOI<sub>950°C</sub>), and BSi concentrations and can be used to determine the quantitative concentrations of these compounds in lake sediment.

#### 3.3.1. Statistical performance and spectral information for the FTIRS/LOI<sub>550°C</sub> model

The 94-lake calibration set shows a statistically significant correlation between FTIRS and the corresponding LOI<sub>550°C</sub> values of lake sediment. A 4-component PLS model gives an  $R^2_{cv} = 0.83$  and a RMSECV of 6.5% (Table 3-2). The PLS component 1 (PLSC1) model shows strong positive loading values in the region 1,050–1,750, 2,800–3,000  $\text{cm}^{-1}$  indicating a positive correlation with LOI<sub>550°C</sub>. The spectral regions between 400–1,000 and 3,500–3,700  $\text{cm}^{-1}$  showed strong negative loading values, indicating negative correlation with LOI<sub>550°C</sub> (Fig. 3-1b).

The results are supported by spectra from sediment with high organic carbon concentration, which also shows high absorbance values between 1,050–1,750 and 2,800–3,000  $\text{cm}^{-1}$  and low absorbance between 3,500–3,700 and 500–1,000  $\text{cm}^{-1}$  (Fig. 3-1a) as well as loading values reported by Vogel et al. (2008). These findings also correspond well with known absorption bands for organic compounds. For example, peaks centred around 1,125  $\text{cm}^{-1}$  may originate from  $\text{C-O-C}$  vibrations of complex carbohydrates and the spectral band centred around 1,250  $\text{cm}^{-1}$  may arise from  $\text{C-O}$  stretching modes (Mecozzi and Pietrantonio 2006). Proteins display strong bands in the region 1,500–1,700  $\text{cm}^{-1}$ , the so-called amide I and amide II vibrations, and these partly overlap with peaks around 1,650  $\text{cm}^{-1}$  originating from  $\text{C-O}$  stretching vibrations in carboxyl groups common in humic substances (Calace et al. 1999; Mecozzi and Pietrantonio 2006). Bands centred on 1,715  $\text{cm}^{-1}$  are assigned to the stretching vibration of the  $\text{C=O}$  group of fatty acids (Mecozzi and Pietrantonio 2006). Carbonates can also absorb in the 1,600–1,800  $\text{cm}^{-1}$  region, but because carbonates are almost totally absent in the 94-lake calibration set, we assume that humic compounds are more important. The band between 2,850 and 2,950  $\text{cm}^{-1}$  is due to  $\text{C-H}$  vibrations in  $\text{-CH}_3$ ,  $\text{-CH}_2$  and  $\text{-CH}$  groups of organic compounds. The regions 400–1,000 and 3,500–3,700  $\text{cm}^{-1}$ , which exhibit negative correlation with  $\text{LOI}_{550^\circ\text{C}}$ , correspond well with  $\text{SiO}$  and  $\text{-OH}$  molecular vibrations in silicates (Farmer 1974; Kellner et al. 1998). Because the  $\text{LOI}_{550^\circ\text{C}}$  contains information on the relative proportions of organic and minerogenic matter in the sediment, the model should perform best if spectral bands for both organic and minerogenic compounds are included. However, due to strong absorption bands for  $\text{CaCO}_3$  in the FTIR spectra, these bands need to be excluded when the FTIR/ $\text{LOI}_{550^\circ\text{C}}$  model is applied to carbonate-rich sediment. The statistical performance of the FTIRS/ $\text{LOI}_{550^\circ\text{C}}$  model, excluding carbonate-specific wavenumbers was still good, showing an  $R^2_{\text{cv}} = 0.71$  and a RMSECV of 11% (Table 3-2). This specific model exhibits slightly reduced statistical performance than the model including all wavenumbers. This is probably due to the fact that we excluded a wide range of wavenumbers around the  $\text{CaCO}_3$  peaks to make sure that no information on  $\text{CaCO}_3$  interferes with the FTIRS/ $\text{LOI}_{550^\circ\text{C}}$  model. This means that information on organic and inorganic compounds important for the FTIRS/ $\text{LOI}_{550^\circ\text{C}}$  also was excluded. For example, stretching vibration of the  $\text{C=O}$  group of fatty acids (1,715  $\text{cm}^{-1}$ ) absorbs in the same region as carbonates (1,800  $\text{cm}^{-1}$ ). The model, with the bands for carbonate excluded, should be used only when the FTIRS/ $\text{LOI}_{550^\circ\text{C}}$  model is applied to carbonate-rich sediment.

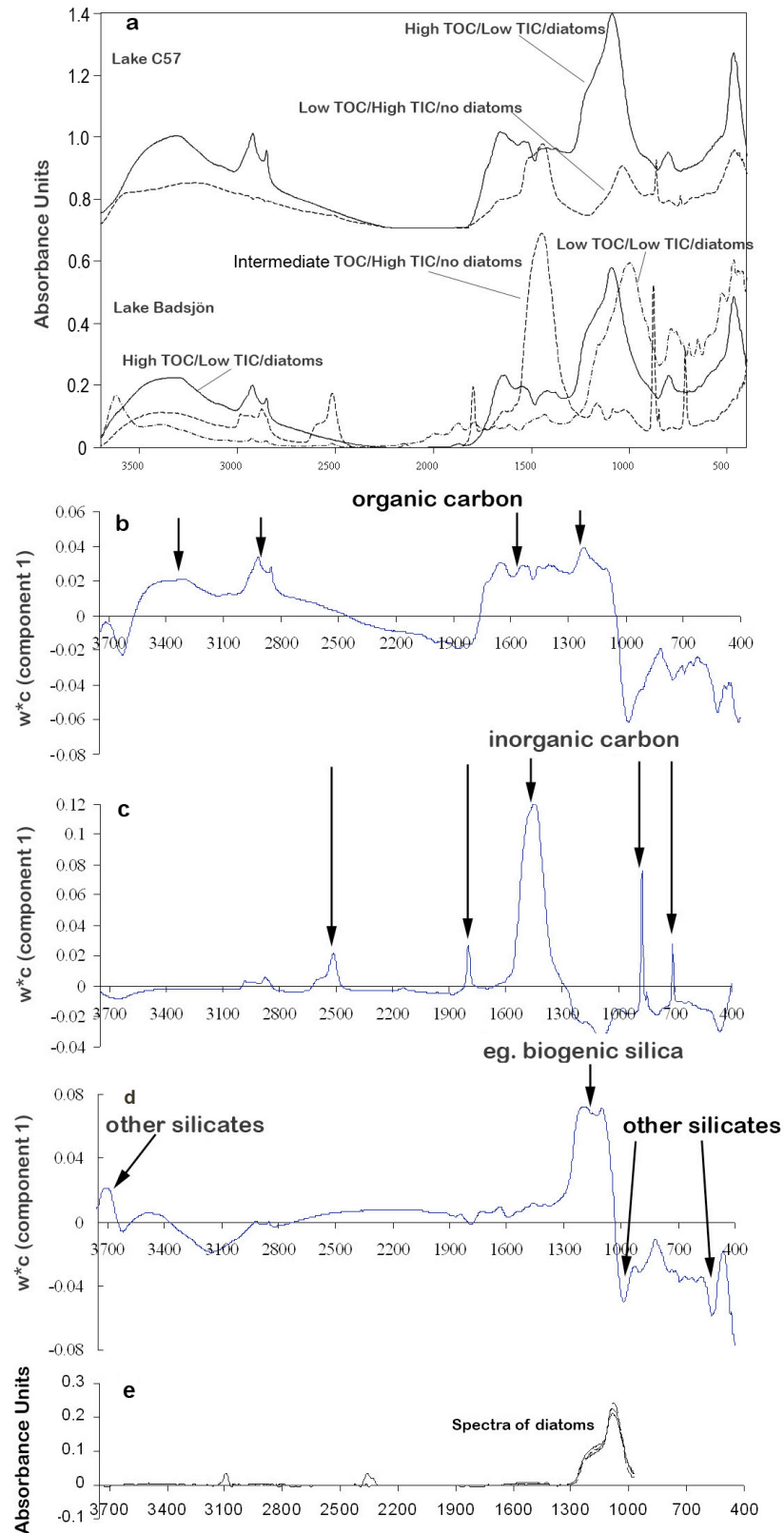


Fig. 3-1. (a) Examples of FTIR spectra from sediment samples with different concentrations of organic carbon, inorganic carbon and diatom BSi. Spectra are from Lake Badsjön and Lake C57. (b–d) Loading plots showing the FTIRS spectral regions contributing to the PLS regression model for total organic carbon (TOC), total inorganic carbon (TIC) and biogenic silica (BSi). Positive values indicate wavenumbers positively correlated to the Y variable and negative values indicate wavenumbers negatively correlated to the Y variable. Loadings refer to the weight vectors ( $w^*c$ ) in the PLS model (component 1) (y-axis) and the corresponding spectral region (x-axis). Arrows indicate important regions for organic carbon (b), inorganic carbon (c) and silicates (d). (e) FTIR spectra from both benthic and planktonic diatoms using the FTIRS microscope technique. The spectra come both from Lake El'gygytyn (NE Siberia) and Lake C98-54 (Sweden). The spectra quality from the microscope technique is poor below 1,000  $\text{cm}^{-1}$  and above 3,000  $\text{cm}^{-1}$  and should not be interpreted

### 3.3.2. Model performance and spectral information for the FTIRS-TIC model

To establish a FTIRS/TIC model, a Holocene sediment record from Lake Badsjön (Table 3-1), which contains sediment of both high and low carbonate content, was used. A 4-component PLS model showed a strong correlation between FTIR spectra and TIC concentration using all wavenumbers and 55 samples from Lake Badsjön. The statistical performance of the model had an  $R^2_{cv} = 0.96$  and RMSECV = 0.5% (Table 3-2). High absorbance values for carbonate-rich sediment were centred around 700–725; 860–890; 1,300–1,560; 1,780–1,810 and 2,460–2,640  $\text{cm}^{-1}$  (Fig. 3-1a), which corresponds well with strong positive loading values in the PLSC1 model for TIC (Fig. 3-1c) and the most important wavenumbers for carbonate in sediment reported by Vogel et al. (2008). Carbonate in calcite minerals has in previous investigations shown important C–O molecular vibrations around 710, 875, 1,425, 1,460, 1,800 and 2,500  $\text{cm}^{-1}$  (White 1974; Gaffey 1986; Mecozzi and Pietrantonio 2006). In a 4-component PLS model, in which only wavenumbers from calcite minerals were included, the statistical performance remained high, with  $R^2_{cv} = 0.95$  and RMSEP = 0.5% (Table 3-2).

Table 3-2. Statistical performance of the calibration models for Loss-on-ignition 550°C (LOI<sub>550°C</sub>), total inorganic carbon (TIC) and biogenic silica (BSi)

Statistics	LOI <sub>550°C</sub>		TIC (%)		BSi (%)	
	All WN	Sel. WN	All WN	4	All WN	Sel. WN
PLS components	4	1	4	4	3	1
Samples (n)	94	94	54	54	94	94
min	3	3	0	0	2	2
max	87	87	11	11	61	61
mean	42	42	3.0	3.0	23	23
RMSECV	6.5	8.9	0.5	0.5	7.1	7.9
RMSECV (% gradient)	7.7	11	5	5	12	13
$R^2_{cv}$	0.83	0.71	0.96	0.95	0.65	0.64
WN included ( $\text{cm}^{-1}$ )	400- 3750	400-680; 740-840; 900-1280; 1570-1770; 1830-2420; 2650-3750	400- 3750	700-725; 860-890; 1300-1560; 1780-1810; 2460-2640	400- 3750	1050-1250
Type of sediment	Surface sediment		Holocene core samples from Lake Badsjön		Surface sediment	
Transformation of sediment properties	no	no	log10(y)	log10(y)	Sqrt(y)	Sqrt(y)

### 3.3.3. Model performance and spectral information for the FTIRS-BSi model

The 94-lake calibration set shows a statistically significant correlation between BSi concentration of lake sediment and the corresponding FTIR spectra. A 3-component PLS model gives an  $R^2_{cv} = 0.65$  and RMSECV = 7.1 (dw %) (Table 3-2).

Strong positive loading values in the PLSC1 model are shown in the region 1,050–1,250  $\text{cm}^{-1}$  (Fig. 3-1d) and correspond well with the characteristic SiO absorbance maximum for BSi at 1,100  $\text{cm}^{-1}$  (Moenke 1974; Gendron-Badou et al. 2003; Stehfest et al. 2005), and with loading values reported by Vogel et al. (2008). Sediment with no diatoms preserved shows low absorbance values between 1,050 and 1,250  $\text{cm}^{-1}$ , while sediment with high diatom concentration shows high absorbance values in the same region (Fig. 3-1a). Further SiO molecular vibrations are responsible for most of the absorbance occurring between 400 and 1,000  $\text{cm}^{-1}$  with characteristic peaks centred around 480, 540, 600, 650, 800, 920  $\text{cm}^{-1}$ . Fossil marine diatom frustules have four characteristic bands. Two main bands at 1,100 and 471  $\text{cm}^{-1}$  are attributed to triply-degenerated, stretching and bending, vibration modes of the  $[\text{SiO}_4]$  tetrahedron, respectively (Gendron-Badou et al. 2003). The band at 800  $\text{cm}^{-1}$  corresponds to an inter-tetrahedral Si–O–Si bending vibration mode, and the band near 945  $\text{cm}^{-1}$  to a Si–OH mode present in marine-produced BSi (Rickert et al. 2002). However, strong negative loading values for all wavenumbers between 400 and 1,000  $\text{cm}^{-1}$  (Fig. 3-1d) indicate that these bands may not be specific to BSi produced in lakes, but also to other silicates. Other studies have used the bands around 470 and 3,615  $\text{cm}^{-1}$  as an estimate for BSi (Mecozzi and Pietrantonio 2006). Our study indicates that the region centred around 3,600  $\text{cm}^{-1}$  is not important for BSi because only moderate positive loading values were observed for that region and FTIR spectra from sediment with high contents of clastic matter show a clear absorbance peak centred on 3,600  $\text{cm}^{-1}$  even though the sample has low BSi concentration (Fig. 3-1a, 3-1d). The results indicate that the region near 3,600  $\text{cm}^{-1}$  should not be used to estimate BSi in lake sediment. This region is generally assigned to OH molecular vibrations (Farmer 1974; Kellner et al. 1998; Mecozzi and Pietrantonio 2006) and OH bonds are common not only in BSi but also in many other mineral phases.

Our measurements are supported by direct FTIRS measurements using the microspectroscopy technique on individual diatom valves, which clearly showed that diatoms (BSi) absorb in the region 1,050–1,250  $\text{cm}^{-1}$ . Spectra were very similar for both benthic (*Navicula sp.*) and planktonic species (*Cyclotella sp.*) (Fig. 3-1e). Based on these findings, a more specific FTIRS/BSi model was also developed in which only the band 1,050–1,250  $\text{cm}^{-1}$  was included. The model showed similar statistical performance and a 1-component PLS model gave an  $R^2_{cv} = 0.64$  and RMSECV = 7.9 (dw %) (Table 3-2). The reason why the statistical performance did not improve when only the 1,050–1,250  $\text{cm}^{-1}$  region was included

in the model is probably due to the fact that BSi values are expressed as percent of total sediment dry weight. Therefore the information about other organic and inorganic compounds in the sediment can contribute to the model. Also, other organic and inorganic compounds absorbing in other regions can be correlated to BSi and improve the model.

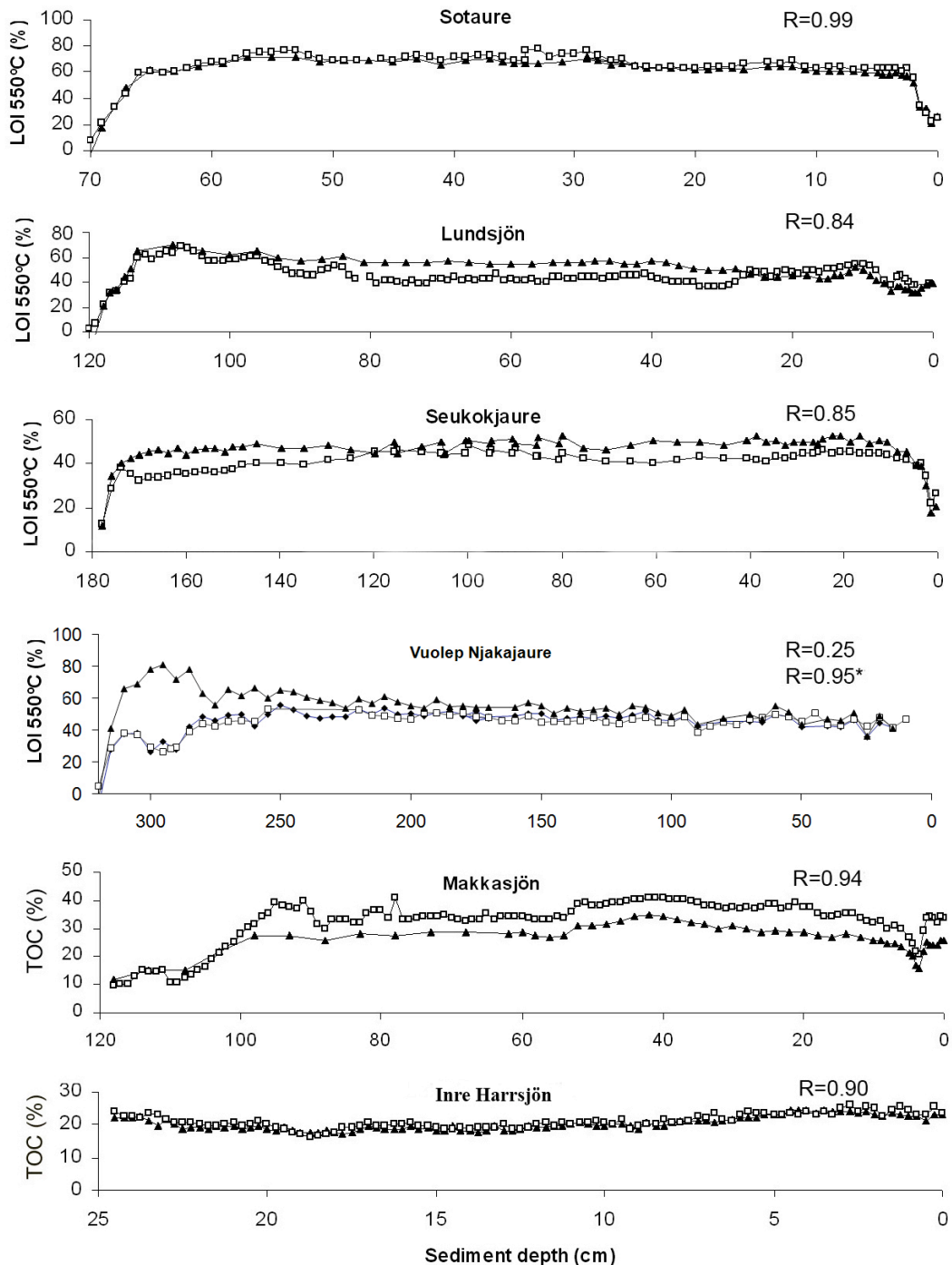


Fig. 3-2. Comparison between conventionally measured (rectangles) and FTIRS inferred LOI<sub>550°C</sub> and TOC (triangles) in five Holocene sediment cores and one core covering the last ~300 years (Inre Harrsjön). The sediment from Vuolep Njakajaure contains a large percentage of CaCO<sub>3</sub> and is therefore an outlier in the 94-lake calibration set. We therefore present results from two FTIRS-models including all wavenumbers (triangles) and a model excluding wavenumbers for CaCO<sub>3</sub> (diamonds). R is the correlation between conventionally measured TOC and the FTIRS-inferred values using a model including all wavenumbers and R\* the correlation to the FTIRS inferred values using a model excluding wavenumbers for CaCO<sub>3</sub>.

### 3.3.4. Application of the FTIRS models to Swedish, Siberian and Albanian/Macedonian lake sediments

The correlation between FTIRS-inferred  $\text{LOI}_{550^{\circ}\text{C}}$  and conventionally measured  $\text{LOI}_{550^{\circ}\text{C}}$  or TOC % varied between  $R = 0.84$  (Lundsjön) and  $R = 0.99$  (Inre Harrsjön) (Fig. 3-2). When the model was applied to marly sediment from Vuolep Njakajaure, the correlation was only  $R = 0.25$ . This is probably due to the fact that sediments from all calibration lakes have very low carbonate content. Carbonates show very distinct absorbance peaks in the mid-infrared region. Since  $\text{C-O}$  molecular vibration can occur in both organic and inorganic carbon, carbonate-specific wavenumbers should be excluded when TOC is inferred in carbonate-rich sediment. When the model that includes only carbonate-specific wavenumbers was applied to Vuolep Njakajaure, the correlation between FTIRS-inferred  $\text{LOI}_{550^{\circ}\text{C}}$  and conventionally measured  $\text{LOI}_{550^{\circ}\text{C}}$  increased from  $R = 0.25$  to  $R = 0.95$ . The FTIRS/ $\text{LOI}_{550^{\circ}\text{C}}$  model was not applicable to Lake El'gygytgyn and Lake Ohrid since their sediments contain very low amounts of TOC (mean 0.5–1.2%), with values plotting at the lower end of the calibration set gradient (TOC range 1.2–35%), thus the FTIRS/ $\text{LOI}_{550^{\circ}\text{C}}$  model was only tested on Swedish lakes. However, a previous study showed that an internal calibration model for TOC applied to Lake Ohrid and Lake El'gygytgyn performed well (Vogel et al. 2008). In all calibration work, it is beneficial to have analogues in the calibration set for accurate and reliable estimates of samples (Birks 1998).

The FTIRS/TIC model was applied to sediment cores from Lake Vuolep Njakajaure and Lake Ohrid. The correlation between FTIRS-inferred TIC and conventionally measured TIC values was  $R = 0.85$  for Vuolep Njakajaure and  $R = 0.99$  for Lake Ohrid when all wavenumbers were included (Fig. 3-3). When only wavenumbers indicative of  $\text{CaCO}_3$  were included in the model, the correlation was  $R = 0.83$  for Vuolep Njakajaure and  $R = 0.98$  for Lake Ohrid (Fig. 3-3). Vogel et al. (2008) presented an internal calibration for TIC from Lake Ohrid using FTIRS and the performance of their model was also very good, with an  $R = 0.99$  between FTIRS-inferred TIC and TIC measured with conventional techniques. Although a strong PLS calibration model was produced for TIC, there was still a significant difference between inferred and measured values for sediment samples with high carbonate concentration from Vuolep Njakajaure, and a general overestimation of low TIC values in Lake Ohrid. One possible explanation is that the sediment was heterogeneous during periods of rapid change in TIC concentration and that values for FTIRS and  $\text{LOI}_{950^{\circ}\text{C}}$  were not measured from the same sample. Another possible reason is that samples from Vuolep Njakajaure were ground by hand and that different particle sizes had an effect on the absorbance values in the mid-infrared region. The samples from Lake Ohrid were ground in a planetary mill to a particle size  $<63 \mu\text{m}$ , which might have yielded more consistent results.

Future improvement of the FTIRS/TIC model might be achieved by including a larger set of lakes that display a broader range of TIC concentration, and by using samples carefully ground in a planetary mill. The FTIRS/TIC model was not applied to the other lakes due to very low concentrations of TIC in their sediment and therefore TIC was not measured conventionally.

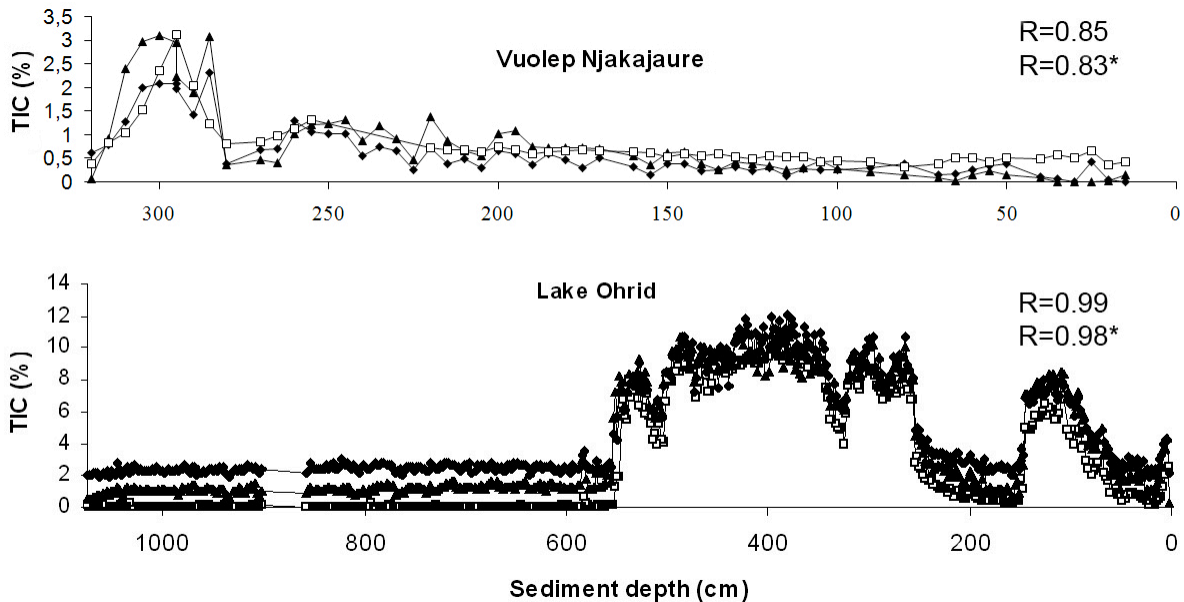


Fig. 3-3. Comparison between conventionally-measured (rectangles) and FTIRS-inferred TIC in a Holocene sediment core from Vuolep Njakajaure (Sweden) (9 kyrs) and Lake Ohrid (Albania/Macedonia) covering the last ~40 kyrs. Triangles represent FTIRS-inferred TIC including all wavenumbers and diamonds represent FTIRS-inferred TIC including only wavenumbers for  $\text{CaCO}_3$ . R is the correlation between conventionally-measured TIC and the FTIRS-inferred TIC using a model including all wavenumbers and R\* the correlation to the FTIRS-inferred TIC using a model including only wave numbers for  $\text{CaCO}_3$ .

The correlations between FTIRS-inferred BSi and conventionally measured BSi in down-core sediment samples from Sweden were  $R = 0.68$  (Seukokjaure) and  $R = 0.94$  (Inre Harrsjön) (Fig. 3-4). The FTIRS/BSi model also performed well for Lake Ohrid ( $R = 0.75$ ) and Lake El'gygytgyn ( $R = 0.86$ ) even though they are located far from the calibration lakes and are much larger and deeper (Table 3-1). The statistical performance of the results is very similar to the internal calibration models for Lake El'gygytgyn and Lake Ohrid presented by Vogel et al. (2008). They report an  $R = 0.87$  for Lake El'gygytgyn and an  $R = 0.79$  for Lake Ohrid between FTIRS-inferred BSi and BSi measured with conventional techniques. Although the patterns obtained between FTIRS and conventional measurements are very similar, the FTIRS modelled BSi is generally higher. Aquatic sediment and soils contain a broad range of material containing Si, which vary in their lability from readily dissolvable amorphous BSi to very stable, highly-ordered crystalline structures (Conley et al. 2006). Both the FTIRS estimates and the values obtained by traditional wet chemical digestion of BSi contain uncertainties. The FTIRS estimates can be confounded by organic components absorbing in the same region as BSi. Wet chemical digestion methods that use weak base

solutions to dissolve amorphous silica components of the sediment may fail to dissolve more refractory forms of amorphous silica (Saccone et al. 2007) that are detected by FTIRS.

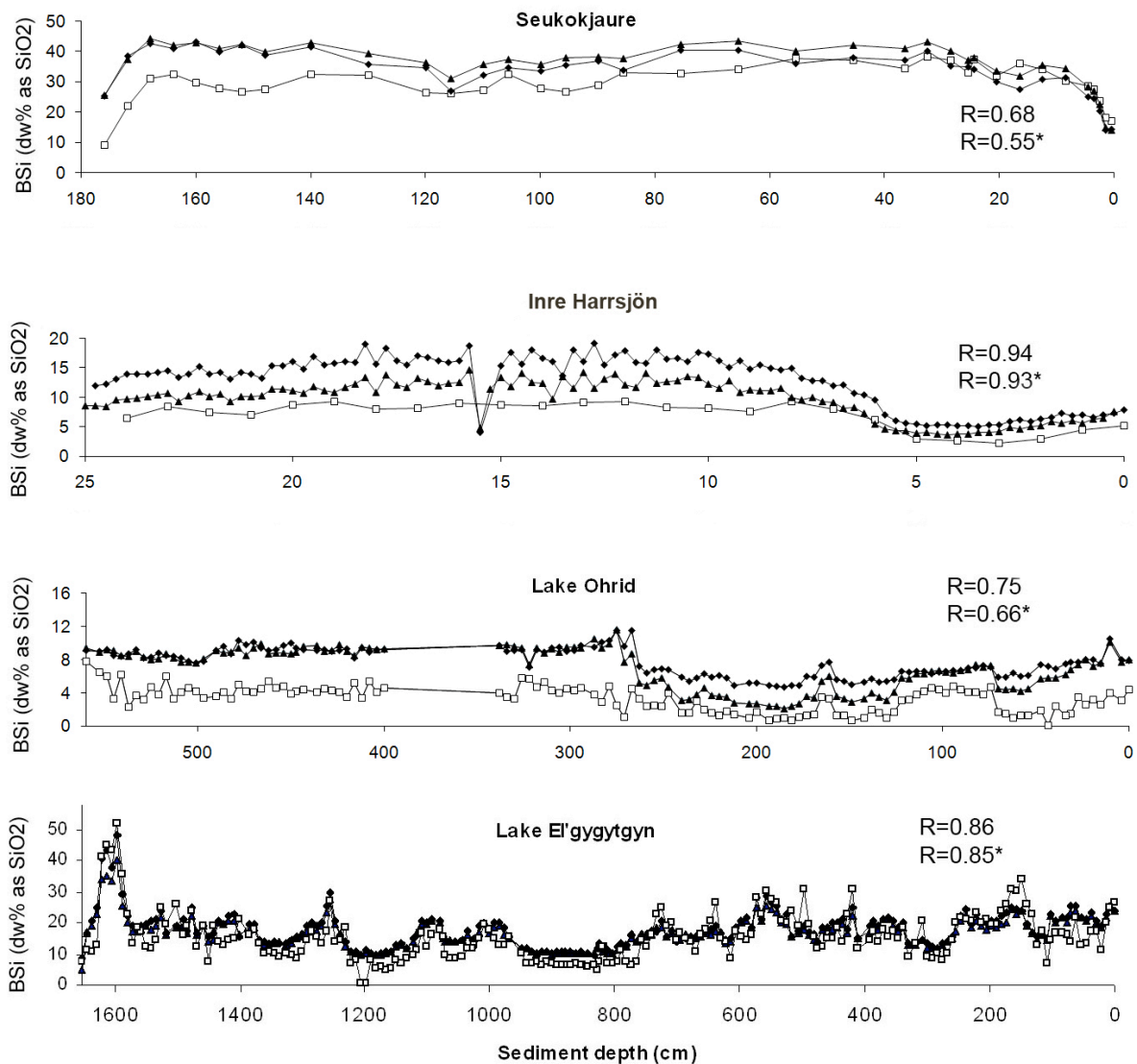


Fig. 3-4. Comparison between conventionally-measured (rectangles) and FTIRS-inferred BSi in a Holocene sediment core from Seukojaure (Sweden), a core covering the last ~300 years (Inre Harrsjön, Sweden), and Lake Ohrid (Albania/Macedonia) covering the last ~40 kyrs, and Lake El'gygytgyn (NE Siberia) covering the last ~350 kyrs. Triangles represent FTIRS-inferred BSi including all wavenumbers and diamonds represent FTIRS-inferred BSi including only wavenumbers for BSi (1,050–1,250  $\text{cm}^{-1}$ ). R is the correlation between conventionally-measured BSi and the FTIRS-inferred BSi using a model including all wavenumbers and R\* the correlation to the FTIRS-inferred BSi using a model including only wavenumbers for BSi.

### **3.4. Conclusions and future possibilities and limitations of the FTIRS technique**

This paper shows that FTIRS can be used to make quantitative assessments of organic and inorganic carbon and BSi in lake sediment. A major step forward compared to the study by Vogel et al. (2008) is that a calibration model from small lakes in Sweden was applied to much larger lakes in Macedonia and Siberia and still produced reasonable results. For accurate quantitative determination of different sediment constituents, we need to have detailed knowledge about their FTIR spectra. This will enable development of robust and specific models for the compounds of interest. Statistical models include correlations between the spectra and compounds, but some compounds can have overlapping spectra. As a result, model performance can vary among lakes, depending on the mixture of components in the sediment. We therefore advise that quantitative estimation using FTIRS should be verified with conventional methods. Alternatively, an internal calibration model for each lake could be developed in which a large number of samples is analysed by both FTIRS and conventional methods for the component of interest. If good models can be developed, they can then be used to assess the component of interest in a high-resolution, rapid and cost-efficient way. Internal calibration is probably the best choice when several hundred meters of sediment are to be analysed at high-resolution, such as the cases of Lakes El'gygytgyn and Ohrid (Vogel et al. 2008).

The FTIRS technique is used rarely in paleolimnological research. Results presented here and by Vogel et al. (2008), as well as the fact that the method is fast and cost-effective, requiring only small sediment samples, should encourage more paleolimnologists to use the method.

# Chapter IV

## **A tephrostratigraphic record for the last glacial-interglacial cycle from Lake Ohrid, Albania and Macedonia**

### **Abstract**

Here we present a 14.94 m long tephrostratigraphic record (core Co1202) recovered from the north-eastern part of Lake Ohrid (Republics of Macedonia and Albania). Overall ten horizons containing volcanic tephra have been recognized throughout core Co1202. Four tephra layers (OT0702-4, OT0702-6, OT0702-8, and OT0702-9) were visible at macroscopic inspection. Six additional cryptotephra (OT0702-1, OT0702-2, OT0702-3, OT0702-5, OT0702-7, and OT0702-10) were identified from peaks in K, Zr, and Sr, intensities, magnetic susceptibility measurements, and washing and sieving of the sediments. Glass shards of tephra layers and cryptotephra were analysed with respect to their major element composition, and correlated to explosive eruptions of Italian volcanoes. The stratigraphy and the major element composition allowed the correlation of OT0702-1 to AD 472 or AD 512 eruptions of Somma-Vesuvius, OT0702-2 to the FL eruption of Mount Etna, OT0702-3 to the Mercato eruption from Somma-Vesuvius, OT0702-4 to SMP1-e/Y-3 eruption from the Campi Flegrei caldera, OT0702-5 to the Codola eruption (Somma-Vesuvius or Campi Flegrei), OT0702-6 to the Campanian Ignimbrite/Y-5 from the Campi Flegrei caldera, OT0702-7 to the Green Tuff/Y-6 eruption from Pantelleria Island, OT0702-8 to the X-5 eruption probably originating from the Campi Flegrei caldera, OT0702-9 to the X-6 eruption of generic Campanian origin, and OT0702-10 to the P-11 eruption from Pantelleria Island. The fairly well known ages of these tephra layers and parent eruptions provides new data on the dispersal and deposition of these tephras and, furthermore, allow the establishment of a chronological framework for core Co1202 for a first interpretation of major sedimentological changes back to Marine Isotope Stage (MIS) 6.

## 4.1. Introduction

Lakes are known as valuable archives of past environmental and climatic variations within terrestrial settings. However, only few lake deposits covering the last glacial-interglacial cycle in the Mediterranean have been studied to date, such as those from Lago Grande di Monticchio (e.g. Allen et al. 1999; Brauer et al. 2000; Brauer et al. 2007), Tennaghi Phillipon (e.g. Tzedakis et al. 2003; 2006), Ioannina (e.g. Tzedakis et al. 2002), Kopais (e.g. Tzedakis 1999), Maars du Velay (de Beaulieu et al. 2001), and Valle di Castiglione (e.g. Follieri et al. 1989, Narcisi et al. 1992; Zanchetta et al. 1999). Among these sites, only records from Lago Grande di Monticchio have intensively been studied with respect to the occurrence of tephra layers as independent time markers (e.g. Wulf et al. 2004; 2008; Brauer et al. 2007).

The Mediterranean region is important for tephra studies, since it bears witness of frequent and intense Quaternary volcanic activity (e.g. Peccerillo 2005), which dispersed pyroclastic material (ash) over very large areas. In particular, tephra layers have become important time markers over the last 200 ka (Keller et al. 1978; Thunell et al. 1979; McCoy & Cornell 1990; Paterne et al. 1986; 1988; 1990; Calanchi et al. 1998; Narcisi and Vezzoli 1999; Siani et al. 2004). The widespread dispersal of these tephras allows the establishment of an independent event stratigraphy, and provides the framework for the spatial and temporal correlation of climatic and environmental changes in marine and terrestrial records. The importance of such an independent volcanic event stratigraphy is documented by the limitation and problematics of other common dating methods, such as radiocarbon dating, varve counting or orbital variations. For instance, the limit for radiocarbon dating is c. 50 kyrs, with uncertainties increasing towards higher ages. Furthermore, variable reservoir effects or contamination that are sometimes difficult to determine can affect both lacustrine and marine radiocarbon ages. Varve counting is often referred to as precise dating method (e.g. Hajdas et al. 1995; Brauer et al. 1999), but it requires continuously varved sediments, which only occur in very few lakes worldwide over long periods. The tuning of climate sensitive parameters to orbital parameters has become a common method to establish a chronological framework for long lacustrine sequences (e.g. Prokopenko et al. 2006; Tzedakis et al. 2006; Nowaczyk et al. 2007). Astronomical tuning of a proxy record, however, requires a direct response of the proxy to variation in the orbital parameters, which can be problematic and may cause discrepancies with respect to the timing of climatic events in different records.

Lake Ohrid, with its presumed Tertiary age (e.g. Cvijic 1911; Kossmat 1924; Nowack 1929; Stankovic 1960; Radoman 1985; Dumurdzanov et al. 2004) and its location downwind of most of the Italian volcanoes active during the Quaternary (e.g. Campanian volcanoes, Aeolian Islands, Mount Etna, Roman volcanoes, Pantelleria Island; Fig. 4-1), provides an important archive for studying the dispersal of tephras in the Mediterranean (e.g. Wagner et

al. 2008b). Therefore Lake Ohrid potentially provides an excellent tephrostratigraphic archive, and past climatic and environmental change recorded in its sedimentary succession can probably be linked with other marine and terrestrial records in the Mediterranean area over a long time scale.

Whilst distinct tephra layers can be generally identified macroscopically, the identification of cryptotephra, especially in minerogenic sediment successions, commonly requires several screening and preparation steps and thus is time-consuming and laborious. To speed up the process of identification, magnetic susceptibility measurements are commonly applied. However, cryptotephra in sediment sequences from Lake Ohrid cannot be identified by magnetic susceptibility measurements alone, since clastic sediments containing large amounts of magnetic mineral phases dominate (Wagner et al. 2008b). A promising approach for the identification of cryptotephra could be the use of XRF-scanning techniques, which provide semi-quantitative estimates on element concentrations in a very rapid and non-destructive way and in sub-millimetre resolution.

In this work, we evaluate the potential of Lake Ohrid as archive for the dispersal of tephra originating from the explosive activity of Italian volcanoes in a c. 15 m long sediment core (Co1202) from the northeastern part of the lake. Moreover, we test the use of high-resolution XRF-scanning techniques for the identification of finely dispersed cryptotephra. These data improve the knowledge about the dispersal of ash from Italian volcanoes in the central Mediterranean and its vicinity and help to assess a chronological and tephrostratigraphic frame for future studies on environmental changes deduced from sedimentary records in the northern Mediterranean region and from Lake Ohrid.

## 4.2. Site description

Lake Ohrid (41°01'N, 20°43'E; Fig. 4-1), a transboundary lake shared by the Republics of Albania and Macedonia, is situated at 693 m above sea level (a.s.l.) and surrounded by high mountain ranges reaching heights of up to 2,300 m a.s.l. It is ca. 30 km long, ca. 15 km wide and covers an area of 358 km<sup>2</sup>. The lake basin shows a relatively simple tub-shaped morphology with a maximum water depth of 289 m, an average water depth of 151 m, and a total volume of 50.7 km<sup>3</sup> (Popovska & Bonacci 2007; Fig 4-1c).

Lake Ohrid is mainly fed by inflow from karst springs (55 %), whilst the remaining 45 % of the hydrologic input include direct precipitation on the lake surface, river-, and direct surface runoff (Matzinger et al. 2006). The karst springs are depleted in minerogenic load and are supplied by water percolating through the karstified mountain ranges (50 %) and by water from Lake Prespa (50 %), which is located 10 km to the east of Lake Ohrid at an altitude of 848 m a.s.l. Including Lake Prespa, the watershed of Lake Ohrid comprises an

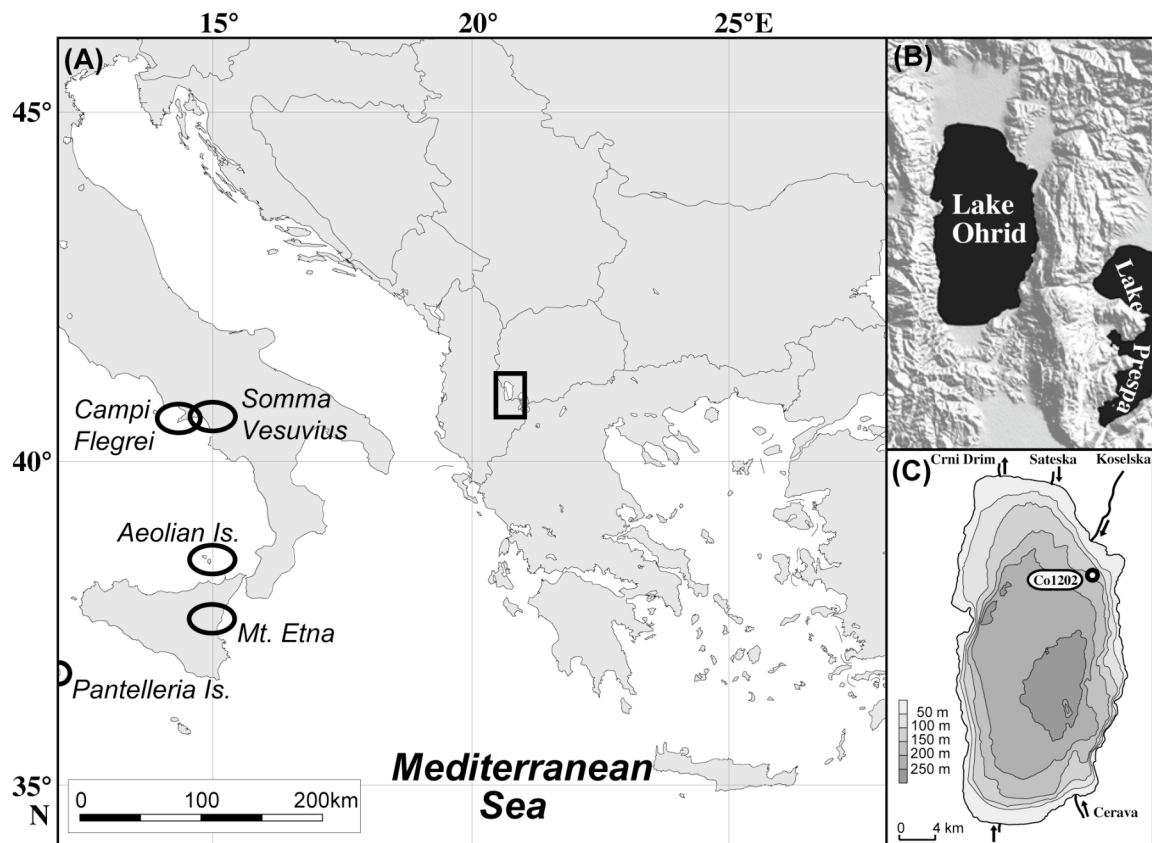


Fig. 4-1. Map showing the location of Lake Ohrid (black rectangle; A) in the Mediterranean and source areas of volcanic material from Italian volcanoes, basic morphological features including Lake Prespa in its vicinity (B), as well as the bathymetry with Co1202 coring site (C).

area of 2,393 km<sup>2</sup>. The direct watershed of Lake Ohrid covers an area of 1,002 km<sup>2</sup> (Popovska & Bonacci 2007). Surface outflow (60 %) through the River Crn Drim to the north and evaporation (40 %) are the main hydrologic outputs (Matzinger et al. 2006).

Due to its sheltered position by the surrounding mountain ranges and the proximity to the Adriatic Sea, the Lake Ohrid watershed shows Mediterranean climate with some continental influences (Watzin et al. 2002). The Lake Ohrid region belongs to the Mediterranean pluviometric regime, with highest amount of precipitation during winter and lowest during summer. The average annual precipitation on the Lake Ohrid watershed is 907 mm (Popovska & Bonacci 2007). Prevailing wind directions follow the N-S axis of the lake valley.

Lake Ohrid is located within an active tectonic graben system emplaced in the Western Macedonian geotectonic zone, which is part of the interior Dinaric Alps. Extensional tectonic movements initiated during the Miocene led to the subsidence of the Ohrid graben zone (Aliaj et al. 2001; Dumurdzanov et al. 2004). Metamorphic and magmatic rocks of Paleozoic age are exposed to the north and northeast of the valley. Strongly karstified limestones and clastic sedimentary rocks of Triassic age are exposed along the northwestern, eastern, and southeastern shorelines (Watzin et al. 2002). Partly serpentized

peridotites of Jurassic-Cretaceous age crop out along the southwestern and western shorelines (Dilek et al. 2007). Alluvial sediments of Pliocene age are exposed to the south and east of the lake. Quaternary lacustrine and fluvial deposits occupy the Struga and Ohrid plain to the north and northeast and the plain near Pogradec to the south (Watzin et al. 2002).

### 4.3. Materials and methods

Core Co1202 was recovered in autumn 2007 from the northeastern part of Lake Ohrid (Fig. 4-1c), where a shallow seismic survey indicated a water depth of 145 m and a widely undisturbed sediment succession with slightly inclined bedding and parallel reflectors. Coring was carried out from a floating platform, using a gravity corer and a 3 m long percussion piston corer (both UWITEC Co.). Core description and high-resolution colour scanning was carried out immediately after lengthwise opening of the cores in the laboratory, except for the interval between 910 and 895 cm depth (Fig. 4-2), which had to be sampled in the field due to heavy degassing and concomitant expansion of the sediment after recovery. A composite core of 14.94 m length was obtained by aligning optical, magnetic, and geochemical marker horizons of the recovered core segments.

One of the core halves was continuously sub-sampled at 2 cm intervals. The other core half was used for X-ray fluorescence (XRF) analysis and magnetic susceptibility (MS) measurements. XRF-analysis was carried out using an ITRAX core scanner (COX Ltd.), equipped with a Mo-tube set to 30 kV and 30 mA and a Si-drift chamber detector. Scanning was performed at 1 mm resolution and an analysis time of 20 s per measurement. The obtained count rates for K, Sr, and Zr can be used as estimates of the relative concentrations for these elements. MS measurements were performed at 1 mm resolution using a Bartington system equipped with a high-resolution MS2E sensor.

From horizons indicating conspicuousnesses in macroscopic grain size composition, colour, or element count rates derived from XRF scanning, about 1 cm<sup>3</sup> was washed and sieved. The > 40 µm fraction was embedded in epoxy resin and screened for glass shards and micro-pumice fragments using scanning electron microscopy (SEM). Energy-dispersive-spectrometry (EDS) analyses of glass shards and micro-pumice fragments were performed using an EDAX-DX micro-analyser mounted on a Philips SEM 515 (operating conditions: 20 kV acceleration voltage, 100 s live time counting, 200-500 nm beam diameter, 2,100-2,400 shots per second, ZAF correction). The ZAF correction procedure does not include natural or synthetic standards for reference, and requires the analyses normalization at a given value (which is chosen at 100 %). Analytical precision is of 0.5 % for abundances higher than 15 wt. %, 1 % for abundances around 5 wt. %, 5 % for abundances of 1 wt. %, and less than 20

% for abundances close to the detection limit (around 0.5 wt. %). Interlaboratory standards include ALV981R23 (basalt), CFA47 (trachyte), KE12 (pantellerite; Cioni et al. 1998; Table 4-1) samples, which have been recently augmented by the addition of SMP1-a (trachyte), Mercato (phonolite), and Aeolian (rhyolite) samples (Table 4-1). Accuracy of measurements is around 1 %, a value analogue to that obtained using wave dispersion spectroscopy (WDS), as tested by Cioni et al. (1998) and Marianelli and Sbrana (1998). Comparison of EDS and WDS micro-analyses carried out on the same samples has shown differences less than 1 % for abundances greater than 0.5 wt. % (e.g. Cioni et al. 1998). Some other comparisons of micro-analyses carried out with WDS microprobes at GeoForschungsZentrum (GFZ, Potsdam, Germany), at CAMPARIS service (CMP, Paris, France) and from Saclay (France; Cioni et al. 1998) on basalt to rhyolite glass shards are shown in Table 4-1, confirming the full comparability of EDS analyses from the Pisa laboratory and data from WDS microprobes.

Table 4-1. Comparison of the EDS device used in this study in comparison with WDS microprobes from GeoForschungsZentrum (GFZ, Potsdam, Germany), from CAMPARIS service (CMP, Paris, France) and from Saclay (France; Cioni et al. 1998). Reference material comprises volcanic glasses with a chemistry ranging from basalt to rhyolite. ALV981R23, CFA47, and KE12 samples from Cioni et al. (1998).

	ALV981R23 (basalt)				CFA 47 (trachyte)				KE 12 (pantellerite)			
	EDS		Sac-lay		EDS		Sac-lay		EDS		Sac-lay	
	n=12	sd	-	sd	n=12	sd	-	sd	n=10	sd	-	sd
SiO <sub>2</sub>	49.56	0.14	49.79	0.19	61.39	0.27	61.94	0.33	70.80	0.23	70.83	0.22
TiO <sub>2</sub>	1.3	0.07	1.28	0.05	0.48	0.09	0.42	0.05	0.31	0.06	0.28	0.02
Al <sub>2</sub> O <sub>3</sub>	16.57	0.13	16.67	0.08	18.61	0.11	18.62	0.16	7.92	0.16	7.82	0.03
FeO	8.44	0.22	8.46	0.09	2.76	0.12	2.66	0.15	8.41	0.06	8.67	0.20
MnO	0.22	0.03	0.14	0.06	0.24	0.13	0.18	0.04	0.38	0.07	0.29	0.03
MgO	8.82	0.16	8.73	0.11	0.58	0.08	0.42	0.02	0.10	0.04	0.00	0.00
CaO	11.84	0.25	11.87	0.11	1.83	0.08	1.85	0.06	0.36	0.07	0.35	0.01
Na <sub>2</sub> O	3	0.18	2.9	0.04	5.43	0.08	5.40	0.12	7.10	0.19	7.23	0.25
K <sub>2</sub> O	0.1	0.05	0.05	0.01	8.14	0.04	8.02	0.16	4.29	0.07	4.19	0.15
P <sub>2</sub> O <sub>5</sub>	-	-	-	-	-	-	-	-	-	-	-	-
Cl	-	-	-	-	-	-	-	-	-	-	-	-
S	0.14	0.04	0.12	0.00	0.54	0.08	0.49	0.01	0.32	0.08	0.33	0.00
	SMP1-a (trachyte)				Mercato (phonolite)				Aeolian rhyolite			
	EDS		GFZ		EDS		CMP		EDS		CMP	
	n=13	sd	n=12	sd	n=7	sd	n=9	sd	n=8	sd	n=11	sd
SiO <sub>2</sub>	60.29	0.16	60.17	0.17	58.48	0.25	58.89	0.30	74.58	0.25	74.93	0.63
TiO <sub>2</sub>	0.48	0.07	0.46	0.03	0.15	0.10	0.15	0.11	0.07	0.08	0.07	0.06
Al <sub>2</sub> O <sub>3</sub>	19.23	0.10	19.40	0.09	21.80	0.19	21.18	0.18	13.40	0.10	13.07	0.29
FeO	3.01	0.08	3.15	0.05	1.72	0.09	1.68	0.10	1.46	0.05	1.50	0.11
MnO	0.29	0.13	0.26	0.04	0.19	0.10	0.18	0.05	0.06	0.08	0.08	0.06
MgO	0.22	0.06	0.36	0.02	0.17	0.08	0.07	0.03	0.07	0.05	0.03	0.03
CaO	1.67	0.06	1.87	0.05	1.56	0.11	1.61	0.08	0.83	0.07	0.84	0.09
Na <sub>2</sub> O	6.65	0.23	6.34	0.17	8.78	0.26	8.90	0.24	3.95	0.09	3.90	0.33
K <sub>2</sub> O	7.23	0.21	7.10	0.08	6.65	0.19	6.64	0.14	5.28	0.11	5.15	0.38
P <sub>2</sub> O <sub>5</sub>	0.00	0.00	0.00	0.00	0.00	0.00	0.01	0.03	0.00	0.00	0.00	0.02
Cl	0.92	0.05	0.90	0.02	0.51	0.07	0.64	0.05	0.31	0.02	0.37	0.04
S	-	-	-	-	-	-	-	-	-	-	-	-

Radiocarbon dating was performed by accelerator mass spectrometry (AMS) at the Leibniz Laboratory for Radiometric Dating and Isotope Research in Kiel, Germany. Due to the absence of macrofossils, measurements were conducted for the alkali residue (AR) and the humic acid fraction (HA) on bulk organic carbon on seven samples throughout core Co1202 (Table 4-2). Radiocarbon ages for the AR and the HA of all samples were calibrated into calendar years before present (cal yrs BP) using CalPal-2007<sup>online</sup> and the CalPal2007\_HULU calibration curve (Danzeglocke et al. 2008).

Table 4-2. Radiocarbon measurements obtained on bulk organic carbon collected at seven different depths along core Co1202. Radiocarbon ages and calibrated (cal) ages, inferred using CalPal-2007<sup>online</sup> and the CalPal2007\_HULU calibration curve (Danzeglocke et al. 2008) are given for the alkali residue (AR), the humic acid fraction (HA), and/or the corrected (corr.) HA fraction.

Sample	Depth (cm)	<sup>14</sup> C age (yr BP) (AR)	cal age (AR cal yr BP)	<sup>14</sup> C age (yr BP) (HA)	corr. <sup>14</sup> C age (HA yr BP)	cal age (HA cal yr BP)
KIA35892	74	6,730 ± 50	7,600 ± 45	3,145 ± 35	1,581 ± 35	1,470 ± 45
KIA36600	217.5	7,425 ± 40	8,260 ± 50	7,860 ± 35	6,296 ± 35	7,225 ± 35
KIA35893	230	8,370 ± 30	9,400 ± 55	8,645 ± 45	7,081 ± 45	7,910 ± 40
KIA35894	242	10,730 ± 55	12,710 ± 50	10,880 ± 60	-	12,845 ± 85
KIA36601	400	27,890 ± 210	32,420 ± 310	21,170 ± 200	-	25,330 ± 400
KIA36602	500	22,540 +160/-150	27,260 ± 415	20,420 +170/-160	-	24,360 ± 340
KIA35895	617	28,040 +290/-280	32,510 ± 310	25,260 +210/-200	-	30,140 ± 280

## 4.4. Results and discussion

### 4.4.1. Lithology

Core Co1202 comprises two major lithofacies, differing distinctly in colour, sediment structure, grain size, carbonate and clastic detritus content.

Lithofacies 1 consists of poorly sorted sediments dominated by fine to medium sized silts and frequent occurrence of coarse sand to gravel sized grains (dropstones) and comprises the horizons between 1,494-1,439 cm, and 1,064-246 cm (Fig. 4-2). Microscope investigations of coarse-grained material revealed that they are commonly angular in shape. The occurrence of gravel and sand as well as their angular shape indicate short transportation and rapid deposition, as it could have occurred by ice floe transport. Sediment colours range from grey to dark-grey and black. Finely dispersed carbonates as well as carbonaceous and plant macrofossils do not occur. Scanning electron microprobe (SEM) investigations revealed that only few, poorly-preserved diatom frustules are present throughout Lithofacies 1. Based on changes in the structure of the sediments, Lithofacies 1 can be divided into two sub-lithofacies, with Lithofacies 1a being massive and bioturbated and occurring from 1,494 to 1,439 cm, from 949 to 825 cm, from 727 to 634 cm, and Lithofacies 1b showing irregular laminations and occurring from 1064 to 949 cm, from 825 to 727 cm, and from 634 to 246 cm (Fig. 4-2).

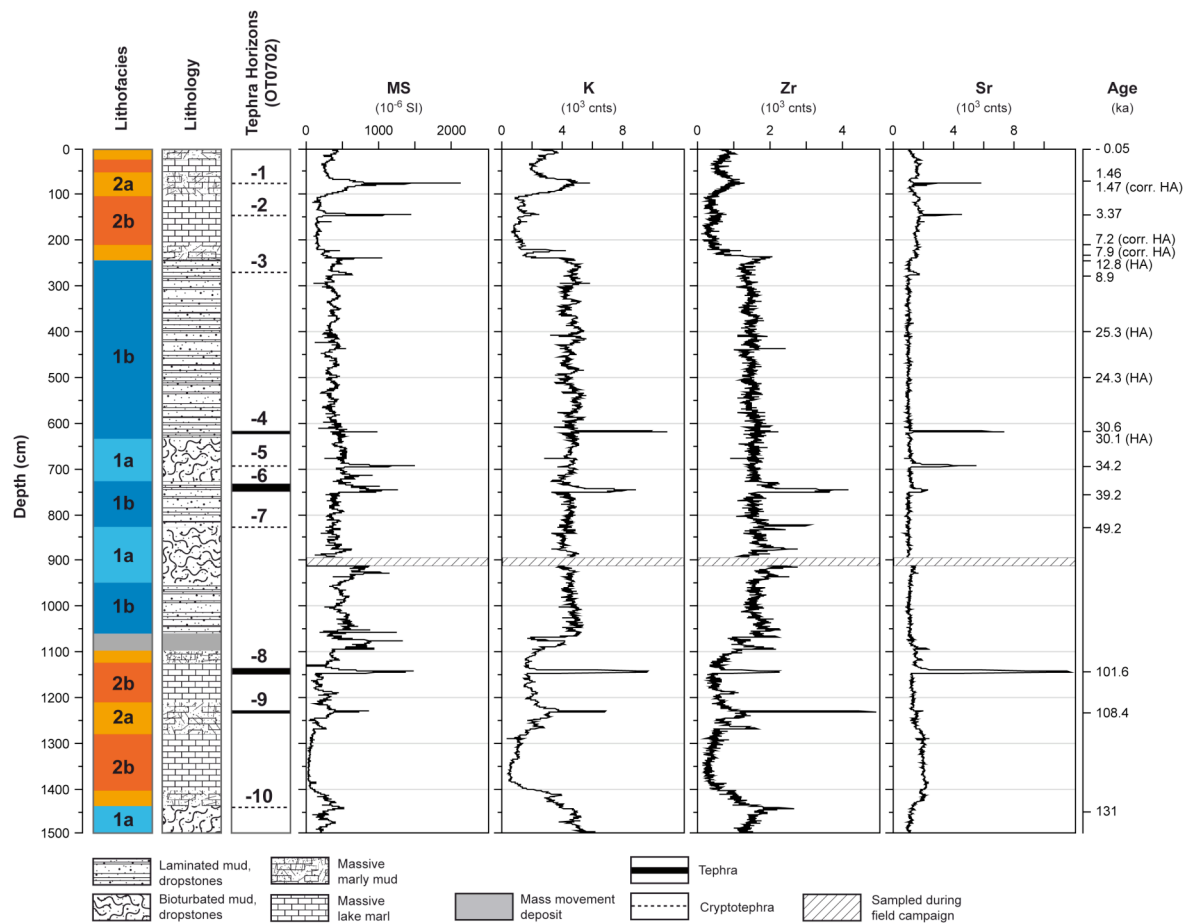


Fig. 4-2. Lithofacies, lithology, tephra and cryptotephra horizons, magnetic susceptibility (MS), and XRF measurements for core Co1202. Element intensities of K, Zr, and Sr are displayed as counts (cnts). The dashed box indicates the sediment interval already sampled during the field campaign. Ages are given as kiloyears (ka) for the identified tephra and cryptotephra and as calibrated ka before present (cal ka BP) for the corrected (corr. HA) and uncorrected (HA) radiocarbon ages obtained on the humic acid fraction (HA) of bulk organic carbon.

Lithofacies 2 is characterized by a clear dominance of fine to medium sized silt with single grains showing a rather spherical shape and absence of coarse sand to gravel sized clastics and covers the horizons between 1439 and 1097 cm, and from 246 cm to the top of the core (Fig. 4-2). Calcareous macrofossils (i.e. ostracods) and finely dispersed organic material are abundant, while plant macrofossils are absent. The content of finely dispersed carbonates and organic material is significantly increased if compared to Lithofacies 1. Lower carbonate contents, higher contents of detrital clastic material, and colours ranging from dark-brown to black in the intervals between 1,439-1402 cm, 1,271-1,209 cm, 1,122-1,095.5 cm, 246-222 cm, 106-52 cm, and 25 cm to the top of the core separate a Lithofacies 2a from a Lithofacies 2b, which is indicated by light-brown to light-grey colour, higher carbonate contents and lower contents of detrital clastic material and occurs between 1,402-1,271 cm, 1,209-1,122 cm, 222-106 cm, and 52-25 cm (Fig. 4-2). Despite these visible features, the

amount and preservation of diatom frustules as revealed by SEM investigations is higher and better, respectively, in Lithofacies 2b compared to Lithofacies 2a.

A sandy horizon with an erosive base separates Lithofacies 1 and 2 between 1,095.5-1,064 cm (Fig. 4-2). These characteristics imply that this horizon between 1095.5-1064 cm is formed by a mass-wasting event, which likely also caused an erosional hiatus in core Co1202. Mass wasting events triggered by earthquakes or lake level changes are common particularly in the lateral parts of the lake basin (Wagner et al. 2008a) and also might have affected core Co1202, which was recovered from a slightly inclined slope approximately 2.5 km offshore.

#### **4.4.2. Magnetic susceptibility and X-ray fluorescence analysis**

MS values differ slightly between Lithofacies 1 and 2, with Lithofacies 1 showing in general higher values than Lithofacies 2 (Fig. 4-2). The observed differences in MS values are likely due to the different amounts of clastic material and carbonate content. Whilst the MS values in Lithofacies 1 are rather uniform, with no appreciable differences for Lithofacies 1a and 1b, those in Lithofacies 2 differ significantly, with lower MS values in Lithofacies 2b (Fig. 4-2). The lower MS values of Lithofacies 2b are likely due to the higher carbonate content and lower amounts of clastic material. Besides these general patterns, MS maxima are centred around 1,229 cm, 1,143 cm, 927 cm, 746 cm, 693 cm, 619 cm, 275 cm, 240 cm, 145 cm, 76 cm (Fig. 4-2). Peak MS values at 1,095.5-1,064 cm are likely correlated to a mass-wasting deposit.

In correspondence to the MS values, K and Zr intensities show a fairly similar behaviour with higher values in Lithofacies 1 compared to Lithofacies 2 (Fig. 4-2). Whilst the differences between Lithofacies 1a and 1b are negligible, Lithofacies 2a shows higher K and Zr values compared with Lithofacies 2b, which is likely due to the higher amount of clastic material. High K intensities are centred on c. 1,229 cm, 1,143 cm, 746 cm, and 619 cm (Fig. 4-2). Zr peaks occur at 1,441 cm, 1,267 cm, 1,229 cm, 1,143 cm, 913 cm, 876 cm, 824 cm, and 746 cm.

Differently from MS, K, and Zr patterns, Sr values are slightly higher in Lithofacies 2 than in Lithofacies 1 (Fig. 4-2). This indicates that the variations of Sr intensities correlate with the carbonate content. Sr intensities are higher within Lithofacies 2b if compared to 2a, which is likely a result of differences in the contents of detrital clastic versus calcareous material of these sublithofacies. In addition, Sr peaks are centred on 1,143 cm, 746 cm, 693 cm, 619 cm, 275 cm, and 76 cm.

#### 4.4.3. Radiocarbon dating

Overall seven bulk organic matter samples from different depths along the Co1202 sediment sequence have been selected for radiocarbon dating by AMS (Table 4-2). Radiocarbon dating of bulk material from lake sediments with low organic carbon content taken from large hard water lakes with long water residence times as Lake Ohrid is in general susceptible to a large array of errors and quality insurance issues (e.g. Wohlfarth 1996; Lowe & Walker 1997; Cohen 2003 and references therein).

Since Lake Ohrid today is fed to an amount of c. 50 % by karstic spring water, which travels through karstified limestones of Triassic age (Popovska & Bonacci 2007), it can be assumed that the incorporation of old,  $^{14}\text{C}$  depleted carbon by photoautotrophic organisms living in the lake leads to a dilution of  $^{14}\text{C}$  levels of organic matter deposited at the lake floor. This so called “hard water effect” or “hard water error” may add as much as 1,200 years to the apparent age of in-situ produced organic material (e.g. Lowe & Walker 1997; Cohen 2003 and references therein). Moreover, Lake Ohrid has a relatively long calculated water residence time of 70 years and complete overturn of the water column only takes place sporadically once a decade (Matzinger et al. 2006). The long water residence time in combination with its meromictic character might result in an imperfect exchange of carbon with the atmosphere and thus to lower  $^{14}\text{C}$  levels in the water column of Lake Ohrid. Furthermore lake level changes, changing catchment dynamics, and changes of the hydrological and limnological settings in the past are likely to have been different from today (Wagner et al. 2009) and thus provide additional potential sources of error. An estimate of how strongly hard water, reservoir, and contamination effects bias the radiocarbon ages in Lake Ohrid is given in Wagner et al. (2008a), who quoted a radiocarbon age obtained on bulk material from a surface sediment sample from the central part of the lake basin of  $1,560 \pm 30$   $^{14}\text{C}$  yrs. BP. Taking all these sources of errors and quality insurance issues into account it seems obvious that radiocarbon ages obtained on bulk organic material from sediments of Lake Ohrid are most likely not adequate to establish a reliable chronology. The dates can, however, be used to establish a rough stratigraphic and chronological framework for the past c. 40 – 50 kyrs upon which a correlation of tephra and cryptotephra layers to volcanic eruptions or proximal deposits of known ages can be drawn.

The lowermost radiocarbon age obtained on sample KIA35895 at 617 cm depth within Lithofacies 1b indicates calibrated ages of  $32,510 \pm 310$  cal yrs BP for the AR and  $30,140 \pm 280$  cal yrs BP for the HA fraction (Table 4-2). These ages imply that the core Co1202 sediment sequence extends well back into the last glacial and furthermore that sample KIA35895 at 617 cm depth is situated close to the transition from marine isotopic stage (MIS) 3 to MIS 2. The assumption that Lithofacies 1b sediments upcore of KIA35895

can be placed into MIS 2 is confined by radiocarbon ages obtained on samples KIA36602 and KIA36601 at 500 and 400 cm, respectively. KIA36602 at 500 cm depth yielded ages of  $27,260 \pm 415$  cal yrs BP for the AR and  $24,360 \pm 340$  cal yrs BP for the HA (Table 4-2). KIA36601 at 400 cm depth yielded significantly older ages of  $32,420 \pm 310$  cal yrs BP for the AR and  $25,330 \pm 400$  cal yrs BP for the HA fraction (Table 4-2) if compared to sample KIA36602 at 500 cm depth. The large discrepancy between the ages of the AR and HA fraction of sample KIA36601 in combination with a significantly older age if compared to sample KIA36602 can probably be explained by a contamination of sample KIA36601 with old carbon. The process leading to this contamination remains, however, elusive since no observable change in sediment characteristics can be deduced from the lithological information of the respective sediment succession.

Sample KIA35894 at 242 cm yielded radiocarbon ages of  $12,710 \pm 50$  cal yrs BP for the AR and  $12,845 \pm 85$  cal yrs BP for the HA fraction (Table 4-2), which implies that the transition from the last glacial to the Holocene is close to 242 cm in core Co1202. KIA35893 at 230 cm yielded radiocarbon ages of  $9,400 \pm 55$  cal yrs BP for the AR and  $9,611 \pm 50$  cal yrs BP for the HA fraction (Table 4-2). KIA36600 at 217.5 cm yielded radiocarbon ages of  $8,262 \pm 52$  cal yrs BP for the AR and  $8,659 \pm 48$  cal yrs BP for the HA fraction (Table 4-2). KIA35892 at 74 cm yielded radiocarbon ages of  $7,599 \pm 43$  cal yrs BP for the AR and  $3382 \pm 30$  cal yrs BP for the HA fraction (Table 4-2). The ages assigned to KIA35893, KIA36600, and KIA35892 thus confirm the assumption that the sediment sequence upcore of 242 cm comprises sediments deposited during the Holocene in core Co1202.

#### 4.4.4. Tephrostratigraphy

Overall, four horizons containing glass shards and micropumice fragments were macroscopically identified at 1,232.5-1,229 cm (OT0702-9), 1,146.5-1,140 cm (OT0702-8), 752-743 cm (OT0702-6), and 620-617 cm (OT0702-4) depth. In addition, six horizons with peaks in XRF element intensities or MS values were recognised at 1,447-1,440 cm (OT0702-10), 825-822 cm (OT0702-7), 696-689 cm (OT0702-5), 277.5-269 cm (OT0702-3), 145.5-144 cm (OT0702-2), and 77.5-74.5 cm (OT0702-1) depth. They contain fine-grained glass shards dispersed in a silty-mud sediment, and were identified as cryptotephra.

Irrespective of the occurrence of volcanic material either as discrete horizon or as cryptotephra, the correlation of distal tephra layers with volcanic sources and proximal deposits (i.e. known eruptions) can be a somewhat complex exercise. This is particularly due to the large amount of tephra layers in the central Mediterranean area with relatively similar major element composition (e.g. Paterne et al. 1988; Giaccio et al. 2008a; Wulf et al. 2004). Therefore it is mandatory to include additional tephra characteristics, beside the major

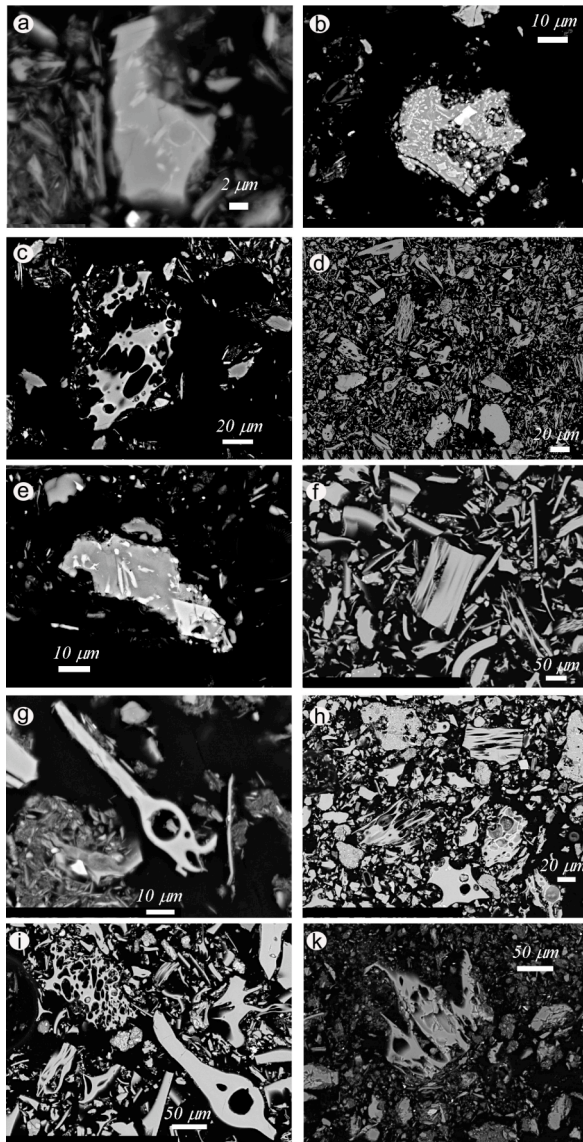


Fig. 4-3. Selected images of glass shards and micropumices of the studied tephras. a) glass shards of the OT0702-1 cryptotephra; b) porphyritic glass shard typical of the OT0702-2 cryptotephra; c) typical features of the OT0702-3 cryptotephra; d) wide view of the tephra OT0702-4; e) porphyritic glass shard of cryptotephra OT0702-5; f) general view of glass shards of OT0702-6 tephra; g) glass shard of the OT0702-7 cryptotephra; h) general view of glass shards from tephra OT0702-8; i) general view of glass shards from tephra OT0702-9; k) micropumices of cryptotephra OT0702-10.

element geochemistry, in the correlation procedure. These additional characteristics may include shape and colour of the volcanic fragments, mineral inclusions, vesicularity, and groundmass texture (e.g. Sulpizio et al. 2008; Cioni et al. 2008). Moreover, the relative stratigraphic positions as well as available ages from radiometric or other absolute dating methods are further important prerequisites to narrow the set of tephras for possible correlations. All these characteristics have been considered for correlating the tephra and cryptotephra layers recognised in core Co1202, while further support to the correlation has been derived from the comparison of data with tephra layers recognised in the nearby core Lz1120 from the south-eastern part of Lake Ohrid (Wagner et al. 2008b).

The OT0702-1 (77.5-74.5 cm) cryptotephra was identified from high MS and Sr values (Fig. 4-2). This cryptotephra comprises non-vesicular and blocky fragments with a crystal-rich groundmass (Fig. 4-3a). The mineral assemblage contains leucite, pyroxene and sanidine. The interstitial glass composition is mainly foiditic to tephri-phonolitic when plotted on the total alkali-silica diagram (TAS, Le Bas et al., 1986; Fig. 4-4; Table 4-3). According to the  $^{14}\text{C}$  data (Table 4-2), lithology and

stratigraphic position, the OT0702-1 cryptotephra was deposited during the late Holocene (Table 4-2; Fig. 4-2). The only known source of undersaturated pyroclastic rocks in the central Mediterranean area during this period is the Somma-Vesuvius volcano (e.g. Ayuso et al. 1998; Santacroce et al. 2008). Foiditic magmas were erupted at Somma-Vesuvius in the period between AD 79 (Pompeii) and AD 1944 (Santacroce 1987;

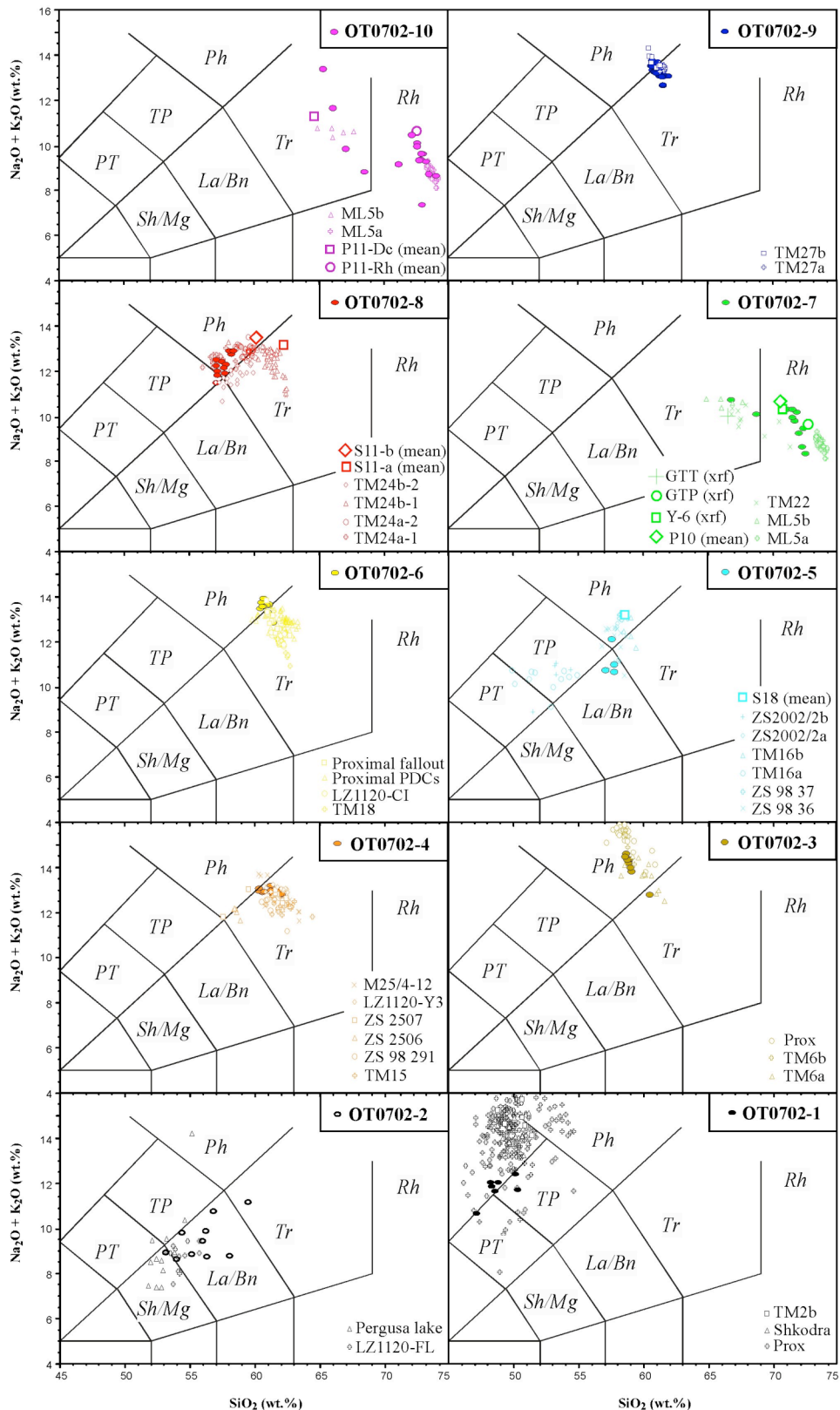


Fig. 4-4. Total alkali-silica diagram (TAS, Le Bas et al. 1986) used for the classification and correlation of tephra and cryptotephra identified in core Co1202 from Lake Ohrid. Raw data of tephra and cryptotephra layers found in core Co1202 is given in Table 3, mean values for the tephra layers used for the correlation are given in Table 4 and the full set of raw data available is documented in the Appendix.

Ayuso et al. 1998; Santacroce et al. 2008). Within this period, the composition of cryptotephra OT0702-1 matches those of AD 472 (1,478 cal yrs BP) and AD 512 (1,438 cal yrs BP) eruptions (Rosi and Santacroce 1983; Sulpizio et al. 2005; Santacroce et al. 2008). The composition of these two eruptions is relatively similar (Fig. 4-5), since they were erupted closely spaced in time from the same magma chamber (Santacroce et al. 2008). A careful inspection of the composition of cryptotephra OT0702-1 shows how it encompasses the less evolved composition of the AD 472 deposits and the AD 512 ones (Fig. 4-5), and thus cannot be unambiguously correlated with one of the two eruptions. However, it is

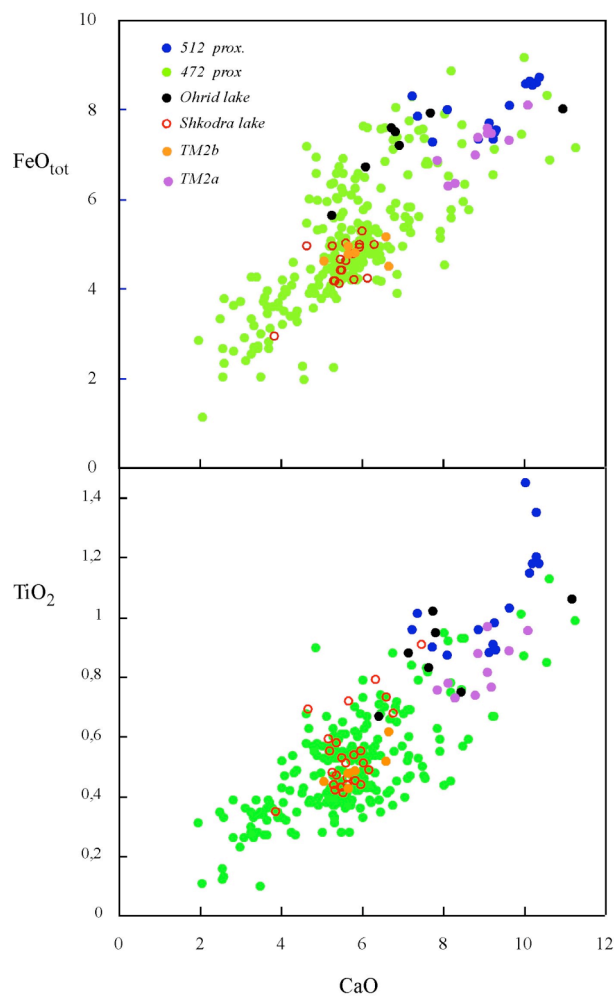


Fig. 4-5.  $\text{FeO}_{\text{tot}}$ – $\text{CaO}$  and  $\text{TiO}_2$ – $\text{CaO}$  diagram for geochemical discrimination between the AD 472 (Pollena) and AD 512 eruptions. Glass composition of proximal (prox) data from Santacroce et al. (2008). For comparison, data of AD 472 found at Lake Shkodra and of TM2a and TM2b from Lago Grande di Monticchio are also shown (Wulf et al. 2004; 2008; Sulpizio et al. 2009).

noteworthy that the composition of cryptotephra OT0702-1 is slightly different from the AD 472 tephra layer recognised in sediments from Lake Shkodra (border between Albania and Montenegro; Sulpizio et al. 2009; Table 4-4), and that it is straddling the composition of AD 472 and AD 512 tephra layers in the Lago Grande di Monticchio succession (layers TM2b and TM2a, respectively; Wulf et al. 2004; 2008; Fig. 4-5). This might suggest that the cryptotephra OT0702-1 comprises mixed populations from both eruptions, which were separated by only 40 years.

The OT0702-2 (145.5-144 cm) cryptotephra was identified from raised MS, K, and Sr values (Fig. 4-2). This cryptotephra consists of non-vesicular and blocky fragments with a porphyritic texture. Fragments exhibit mineral inclusions of plagioclase, clinopyroxene, and olivine up to some

plotting in the trachytic and mugearitic fields on the TAS diagram (Table 4-3; Fig. 4-4). The benmoreitic composition of the OT0702-2 cryptotephra constrains the source to the activity of Mt. Etna, which is the only known source of this magma type in the central Mediterranean area active during the Holocene (e.g. Kieffer 1979; Cristofolini and Romano 1982; Coltelli et al. 2000). According to its age (younger than  $8,260 \pm 50$  cal yrs BP; Table 4-2; Fig. 4-2), composition (Table 4-3; Fig. 4-4), and mineral assemblage, it can be correlated to a tephra layer already recognised in the Holocene sediments of Lake Ohrid (Wagner et al. 2008b) and Lago di Pergusa (central Sicily; Sadori and Narcisi 2001), which was correlated with the deposits of the FL eruption from Etna volcano ( $3,370 \pm 70$  cal yrs BP; Coltelli et al. 2000; Wagner et al. 2008b).

Cryptotephra OT0702-3 (277.5-269 cm) was identified from peaks in MS and Sr values (Fig. 4-2), and comprises mainly aphyric, vesicular micro-pumice. Bubbles of the micro-pumices are mainly circular with thick septa (Fig. 4-3c). The glass composition of the cryptotephra is a fairly homogeneous Na-rich phonolite (Table 4-3; Fig. 4-4). The peculiar composition and texture of OT0702-3 cryptotephra fragments indicates the Somma-Vesuvius volcano as the source and the Mercato eruption as proximal counterpart, since it is the only eruption during the Holocene and Late Pleistocene in the central Mediterranean area showing this particular composition (Santacroce et al. 2008; Di Vito et al. 2008). The correlation of OT0702-3 cryptotephra with the Mercato eruption of the Somma-Vesuvius volcano (dated at  $8,890 \pm 90$  cal. yrs. BP; Santacroce 1987; Rolandi et al. 1993; Santacroce et al. 2008) indicates that the radiocarbon age of bulk organic carbon samples at 242 cm (Table 4-2) is too old and probably contaminated by old material, as discussed in the preceding paragraph. The finding of the Mercato tephra in Lake Ohrid greatly enlarges its known dispersal area to the east and provides an important marker for the early Holocene on the Balkans.

The tephra layer OT0702-4 (620-617 cm) corresponds to peaks in MS, K, and Sr values (Fig. 4-2), is c. 3 cm thick, light-brown in colour, and is characterized by normally graded middle to fine sand. Glass shards are mixed with lacustrine sediment up to 2 cm above the tephra layer. The tephra comprises highly-vesicular, aphyric micro-pumice and cusped glass shards (Fig. 4-3d). Most of the glass shards show a trachytic composition with only few samples that plot close to the phonolitic field on the TAS diagram (Fig. 4-4). Bulk organic carbon dating from 617 cm depth (KIA35895) indicates an age of  $32,513 \pm 310$  cal yrs BP for the AR fraction and  $30,136 \pm 280$  cal yrs BP for the HA fraction (Table 4-2; Fig. 4-2), respectively. The composition, chronology and stratigraphic position suggest that this tephra layer correlates with the Y-3 tephra layer (Table 4-3; Fig. 4-4). The Y-3 tephra layer was already recognised in another core from Lake Ohrid (Wagner et al., 2008b) and represents one of the most important stratigraphic markers for the Upper Pleistocene all over

the central Mediterranean (Keller et al. 1978; Zanchetta et al. 2008). The Y-3 tephra corresponds to the proximal deposits of SMP1-e/VRa eruption from Campi Flegrei (Sulpizio et al. 2003; Di Vito et al. 2008), which is dated at  $30,670 \pm 230$  cal yrs BP (<sup>radiocarbon</sup> dating; Sulpizio et al. 2003). This age corresponds well with the <sup>40</sup>Ar/<sup>39</sup>Ar age of  $30,300 \pm 200$  yrs, obtained on sanidine crystals from the correlated proximal deposits (Pappalardo et al. 1999) and with the HA age (Table 4-2) in core Co1202. Zanchetta et al. (2008) discussed the age offset of the SMP1-e/Y-3 deposits with respect to the varve-supported age (23,930 yrs; Wulf et al. 2004) proposed for TM15 tephra layer in the Lago Grande di Monticchio succession, and proposed a best age of 31,000-30,000 yrs, which is in good agreement with the radiocarbon datings reported here. This may further suggest that hard water/reservoir effects changed in time, and possibly these effects were reduced during the Last Glacial.

Cryptotephra OT0702-5 (696-689 cm) was initially identified from high MS and Sr values (Fig. 4-2), and comprises tachilitic particles with a crystal-rich groundmass containing acicular clinopyroxene, plagioclase, and sanidine (Fig. 4-3e). The few glass compositions available range from latite to phonolite when plotted on the TAS diagram (Table 4-3; Fig. 4-4). The glass composition, the occurrence of clinopyroxene, plagioclase, and sanidine crystals, and the stratigraphic position downcore (older) from the Y-3 tephra layer suggests a correlation of cryptotephra OT0702-5 to the evolved composition of the Codola eruption (Sulpizio et al. 2003; Wulf et al. 2004; Giaccio et al. 2008b; Di Vito et al. 2008; Santacroce et al. 2008). The source of the Codola eruption is still under debate, and it has been attributed to either Somma-Vesuvius or Campi Flegrei volcanoes (e.g. Santacroce 1987; Sulpizio et al. 2003; Di Vito et al. 2008; Giaccio et al. 2008a; Santacroce et al. 2008). Giaccio et al. (2008b) suggested that the marine tephra layer C-10 (Paterne et al., 1988) is the distal counterpart of the Codola eruption. The age of the Codola eruption is poorly constrained. According to the most recent age model for records from Lago Grande di Monticchio, the Codola tephra (TM 16) has an age of 31,160 yrs (Brauer et al. 2007). Giaccio et al. (2008b), correlated the short-term climatic variations of the Monticchio paleoclimatic record to similar variations in the GRIP ice core and in marine records, and suggested a best age between 32,000 and 33,500 yrs for the Codola tephra. Radiocarbon dating of foraminifera directly below the Codola tephra in a marine core from the Tyrrhenian Sea yielded an age of  $34,270 \pm 870$  cal yrs BP (Paterne et al. 1999), which partially overlaps with the age window suggested by Giaccio et al. (2008b). The recognition of Codola deposits in Lake Ohrid sediments is the first in the Balkan area, and significantly enlarges its dispersal area to the east.

Table 4-3. Major elements glass chemistry of OT0702-1 to OT0702-10 tephras and cryptotephras recognised in core Co1202.

Sample	Depth (cm)	Shard	SiO <sub>2</sub>	TiO <sub>2</sub>	Al <sub>2</sub> O <sub>3</sub>	FeO <sub>tot</sub>	MnO	MgO	CaO	Na <sub>2</sub> O	K <sub>2</sub> O	P <sub>2</sub> O <sub>5</sub>	ClO	Total	Total alk	Alk. Ratio	
OT0702-1	74.5-77.5	1	47.15	1.06	18.95	7.62	0.34	2.08	11.16	6.34	4.35	0.04	0.92	100.01	10.69	0.69	
		2	48.32	0.75	20.29	7.56	0.13	1.49	8.45	5.64	6.24	0.09	1.04	100	11.88	1.11	
		3	48.28	0.95	21	7.07	0.33	1.39	7.81	5.68	6.39	0	0	1.09	99.99	12.07	1.13
		4	48.82	0.83	20.75	7.33	0.22	1.24	7.64	6.07	5.99	0.09	0	1.03	100.01	12.06	0.99
		5	48.61	1.02	20.79	7.28	0.4	1.35	7.72	6.4	5.29	0	0	1.15	100.01	11.69	0.83
		6	50.33	0.88	20.59	6.72	0.31	1.01	7.12	5.88	7.32	5.86	0.09	1.21	100	11.74	1.00
		7	50.21	0.67	21.69	5.96	0.17	1.19	6.41	7.32	5.13	0.09	0	1.14	99.98	12.45	0.70
		mean	<b>48.82</b>	<b>0.88</b>	<b>20.58</b>	<b>7.08</b>	<b>0.27</b>	<b>1.39</b>	<b>8.04</b>	<b>6.19</b>	<b>5.61</b>	<b>0.06</b>	<b>1.08</b>	-	-	-	
		sd	<b>1.12</b>	<b>0.14</b>	<b>0.84</b>	<b>0.58</b>	<b>0.10</b>	<b>0.34</b>	<b>1.51</b>	<b>0.58</b>	<b>0.72</b>	<b>0.04</b>	<b>0.10</b>	-	-	-	
OT0702-2	145.5-144	1	58.08	1.54	17.42	6.33	0.16	2.09	4.70	5.47	3.31	0.54	0.35	99.99	8.78	0.61	
		2	54.02	1.72	17.06	8.84	0.44	3.15	5.46	5.16	3.46	0.32	0.32	0.37	100.00	8.62	0.67
		3	56.01	1.80	18.89	5.28	0.12	1.65	6.25	6.58	2.85	2.85	0.36	0.21	100.00	9.43	0.43
		4	56.26	1.55	18.28	6.61	0.29	1.78	4.53	5.96	3.93	3.93	0.43	0.38	100.00	9.89	0.66
		5	55.13	1.74	17.20	8.10	0.13	2.40	5.61	5.42	3.44	3.44	0.50	0.32	99.99	8.86	0.63
		6	59.53	1.47	18.21	3.94	0.17	0.89	4.17	6.11	5.05	5.05	0.23	0.20	99.97	11.16	0.83
		7	53.15	1.99	17.27	8.81	0.35	2.80	5.87	5.32	3.60	3.60	0.53	0.31	100.00	8.92	0.68
		8	56.31	1.04	21.28	3.86	0.14	0.92	7.32	6.05	2.67	2.67	0.27	0.13	99.99	8.72	0.44
		9	56.87	1.58	18.59	5.45	0.00	1.32	4.67	6.42	4.33	4.33	0.37	0.41	100.01	10.75	0.67
		10	54.41	1.80	17.61	8.02	0.25	2.40	4.93	6.10	3.70	3.70	0.47	0.31	100.00	9.80	0.61
		mean	<b>55.98</b>	<b>1.62</b>	<b>18.18</b>	<b>6.52</b>	<b>0.21</b>	<b>1.94</b>	<b>5.35</b>	<b>5.86</b>	<b>3.63</b>	<b>0.40</b>	<b>0.30</b>	-	-	-	
		sd	<b>1.92</b>	<b>0.26</b>	<b>1.26</b>	<b>1.88</b>	<b>0.13</b>	<b>0.77</b>	<b>0.95</b>	<b>0.49</b>	<b>0.69</b>	<b>0.11</b>	<b>0.09</b>	-	-	-	
OT0702-3	269-277.5	1	58.94	0.30	21.45	1.89	0.21	0.04	1.86	7.84	6.98	0	0.50	100.01	14.82	0.89	
		2	58.79	0.00	21.50	2.02	0.00	0.10	1.93	7.65	7.52	0	0	0.49	100.00	15.17	0.98
		3	58.96	0.13	21.47	1.83	0.19	0.29	1.84	7.43	7.29	0	0	0.57	100.00	14.72	0.98
		4	60.50	0.24	21.77	2.00	0.22	0.25	1.66	6.13	6.70	0	0	0.53	100.00	12.83	1.09
		5	58.98	0.23	21.65	1.95	0.21	0.08	1.50	7.87	7.06	0	0	0.47	100.00	14.93	0.90
		6	58.82	0.19	21.69	1.83	0.17	0.07	1.78	7.70	7.17	0	0	0.57	99.99	14.87	0.93
		7	59.18	0.11	21.56	2.14	0.17	0.17	1.79	7.58	6.76	0	0	0.53	99.99	14.34	0.89
		8	58.68	0.17	21.42	2.08	0.15	0.16	1.82	8.04	6.97	0	0	0.51	100.00	15.01	0.87
		9	59.08	0.20	21.72	1.85	0.21	0.27	1.63	7.76	6.76	0	0	0.51	99.99	14.52	0.87
		mean	<b>59.10</b>	<b>0.17</b>	<b>21.58</b>	<b>1.95</b>	<b>0.17</b>	<b>0.16</b>	<b>1.76</b>	<b>7.56</b>	<b>7.02</b>	<b>0</b>	<b>0.52</b>	-	-	-	
		sd	<b>0.55</b>	<b>0.09</b>	<b>0.13</b>	<b>0.11</b>	<b>0.07</b>	<b>0.09</b>	<b>0.13</b>	<b>0.56</b>	<b>0.27</b>	<b>0</b>	<b>0.03</b>	-	-	-	

(Continues)

Table 4-3. (Continued)

Sample	Depth (cm)	Shard	SiO <sub>2</sub>	TiO <sub>2</sub>	Al <sub>2</sub> O <sub>3</sub>	FeO <sub>tot</sub>	MnO	MgO	CaO	Na <sub>2</sub> O	K <sub>2</sub> O	P <sub>2</sub> O <sub>5</sub>	ClO	Total	Total alk	Alk. Ratio		
OT0702-4	617-620	1	61.39	0.45	18.65	3.12	0.09	0.71	2.31	3.61	9.26	0	0.42	100.01	12.87	2.57		
		2	60.6	0.42	18.7	3.29	0.16	0.91	2.67	3.26	9.65	0	0.33	99.99	12.91	2.96		
		3	61.49	0.45	18.64	3.07	0.26	0.64	2.21	3.7	9.11	0	0.41	99.98	12.81	2.46		
		4	60.37	0.46	18.72	3.45	0	0.89	2.7	3.27	9.72	0	0.41	99.99	12.99	2.97		
		5	61.26	0.41	18.88	3.07	0.08	0.68	2.18	3.55	9.45	0	0.44	100	13	2.66		
		6	60.31	0.37	18.8	3.45	0.08	0.92	2.68	3.07	10.04	0	0.28	100	13.11	3.27		
		7	60.72	0.39	18.92	3.21	0.05	0.7	2.64	3.32	9.64	0	0.4	99.99	12.96	2.90		
		8	62.11	0.34	18.61	2.85	0.11	0.5	2.15	4.07	8.77	0	0.49	100	12.84	2.15		
		9	61.92	0.28	18.58	2.83	0.12	0.53	2.17	4.28	8.74	0	0.56	100.01	13.02	2.04		
		10	61.75	0.34	18.67	2.93	0.07	0.48	2.23	4.4	8.54	0	0.6	100.01	12.94	1.94		
		11	61.24	0.35	18.74	3.02	0.15	0.67	2.1	4.23	8.98	0	0.53	100.01	13.21	2.12		
		12	62.02	0.43	18.5	2.98	0.16	0.36	2.13	4.05	8.77	0	0.61	100.01	12.82	2.17		
		mean	<b>61.27</b>	<b>0.39</b>	<b>18.70</b>	<b>3.11</b>	<b>0.11</b>	<b>0.67</b>	<b>2.35</b>	<b>3.73</b>	<b>9.22</b>	<b>0</b>	<b>0.46</b>	-	-	-		
		sd	<b>0.64</b>	<b>0.06</b>	<b>0.12</b>	<b>0.21</b>	<b>0.18</b>	<b>0.18</b>	<b>0.25</b>	<b>0.46</b>	<b>0.48</b>	<b>0</b>	<b>0.10</b>	-	-	-		
OT0702-5	689-696	1	57.76	0.99	21.99	2.64	0.17	0.51	5.06	3.07	7.62	0	0.20	100.01	10.69	2.48		
		2	57.79	0.87	19.81	4.26	0.15	0.48	5.24	4.18	6.85	0	0.37	100.00	11.03	1.64		
		3	57.55	0.66	19.84	4.08	0.06	0.80	4.41	3.78	8.37	0	0.44	99.99	12.15	2.21		
		4	57.06	0.62	20.52	3.82	0.28	0.63	5.91	3.28	7.49	0	0.40	100.01	10.77	2.28		
				mean	<b>57.54</b>	<b>0.79</b>	<b>20.54</b>	<b>3.70</b>	<b>0.17</b>	<b>0.61</b>	<b>5.16</b>	<b>3.58</b>	<b>7.58</b>	<b>0</b>	<b>0.35</b>	-	-	-
				sd	<b>0.34</b>	<b>0.18</b>	<b>1.02</b>	<b>0.09</b>	<b>0.15</b>	<b>0.62</b>	<b>0.50</b>	<b>0.62</b>	<b>0</b>	<b>0.11</b>	-	-	-	-
		OT0702-6	743-752	1	60.67	0.43	19.02	2.98	0.13	0.42	1.8	6.45	7.4	0	0.69	99.99	13.85	1.15
				2	60.48	0.36	19.18	2.96	0.21	0.46	1.88	6.43	7.37	0	0.68	100.01	13.8	1.15
				3	61.12	0.38	19.2	2.86	0.13	0.4	1.58	6.36	7.3	0	0.67	100	13.66	1.15
				4	61.1	0.48	18.86	2.76	0.26	0.46	1.79	5.91	7.81	0	0.57	100	13.72	1.32
				5	60.69	0.29	19.06	2.84	0.1	0.48	1.82	6.66	7.32	0	0.73	99.99	13.98	1.10
				6	60.89	0.46	19.1	2.99	0.25	0.46	1.56	6.62	7.05	0	0.62	100	13.67	1.06
7	61.01			0.45	19.2	3.08	0.26	0.38	1.65	6.22	7.14	0	0.63	100.02	13.36	1.15		
8	61.43			0.14	19.16	3.02	0	0.69	2.3	5.08	7.81	0	0.37	100	12.89	1.54		
9	60.41			0.55	19.2	3	0.36	0.5	1.72	6.44	7.07	0	0.75	100	13.51	1.10		
10	60.65			0.42	19.24	3.06	0.15	0.57	1.6	6.45	7.16	0	0.7	100	13.61	1.11		
11	60.63			0.39	19.24	2.66	0.17	0.41	1.72	6.74	7.32	0	0.73	100.01	14.06	1.09		
12	60.57			0.42	19.21	3.03	0.31	0.45	1.67	6.53	7.07	0	0.73	99.99	13.6	1.08		
		mean	<b>60.80</b>	<b>0.40</b>	<b>19.14</b>	<b>2.94</b>	<b>0.19</b>	<b>0.47</b>	<b>1.76</b>	<b>6.32</b>	<b>7.32</b>	<b>0</b>	<b>0.66</b>	-	-	-		
		sd	<b>0.31</b>	<b>0.10</b>	<b>0.11</b>	<b>0.13</b>	<b>0.08</b>	<b>0.20</b>	<b>0.45</b>	<b>0.26</b>	<b>0</b>	<b>0</b>	<b>0.10</b>	-	-	-		

(Continues)

Table 4-3. (Continued)

Sample	Depth (cm)	Shard	SiO <sub>2</sub>	TiO <sub>2</sub>	Al <sub>2</sub> O <sub>3</sub>	FeO <sub>tot</sub>	MnO	MgO	CaO	Na <sub>2</sub> O	K <sub>2</sub> O	P <sub>2</sub> O <sub>5</sub>	ClO	Total	Total alk	Alk. Ratio	
OT0702-7	822-825	1	71.88	0.33	8.26	7.97	0.16	0	0.29	5.99	4.2	0	0.92	100	10.19	0.70	
		2	71.75	0.51	8.15	8.1	0.41	0	0.38	5.54	4.23	0	0.93	100	9.77	0.76	
		3	71.57	0.45	8.3	8.12	0.33	0.12	0.38	5.46	4.48	4.31	0	0.9	100.01	9.94	0.82
		4	72.06	0.6	8.28	8.02	0.46	0.06	0.36	4.92	4.31	4.45	0	0.92	99.99	9.23	0.88
		5	72.61	0.58	8.45	8.29	0.34	0.2	0.35	3.88	4.45	4.45	0	0.84	99.99	8.33	1.15
		6	71.13	0.51	8.07	8.15	0.39	0.12	0.35	6.04	4.26	4.26	0	0.98	100	10.3	0.71
		7	71.55	0.32	8.18	8	0.23	0.17	0.3	5.82	4.47	4.47	0	0.96	100	10.29	0.77
		8	72.44	0.44	8.36	7.86	0.31	0	0.29	5.05	4.4	4.4	0	0.83	99.98	9.45	0.87
		9	71.56	0.32	8.3	8.05	0.34	0.14	0.42	5.57	4.36	4.36	0	0.95	100.01	9.93	0.78
		10	72.31	0.48	8.76	8.1	0.38	0.08	0.34	4.15	4.48	4.48	0	0.92	100	8.63	1.08
		11	69.23	0.56	10.59	7.95	0.29	0.18	0.57	5.38	4.71	4.71	0	0.54	100	10.09	0.88
		12	66.84	0.61	12.15	7.56	0.41	0.35	0.85	6.06	4.66	4.66	0	0.5	99.99	10.72	0.77
		mean1	<b>71.89</b>	<b>0.45</b>	<b>8.31</b>	<b>8.07</b>	<b>0.34</b>	<b>0.09</b>	<b>0.34</b>	<b>5.24</b>	<b>4.36</b>	<b>0</b>	<b>0.92</b>	-	-	-	
		sd1	<b>0.47</b>	<b>0.10</b>	<b>0.19</b>	<b>0.12</b>	<b>0.09</b>	<b>0.07</b>	<b>0.05</b>	<b>0.74</b>	<b>0.11</b>	<b>0</b>	<b>0.05</b>	-	-	-	
		mean2	<b>68.04</b>	<b>0.59</b>	<b>11.37</b>	<b>7.76</b>	<b>0.35</b>	<b>0.27</b>	<b>0.71</b>	<b>5.72</b>	<b>4.69</b>	<b>0</b>	<b>0.52</b>	-	-	-	
		sd2	<b>1.64</b>	<b>0.11</b>	<b>1.25</b>	<b>0.18</b>	<b>0.08</b>	<b>0.10</b>	<b>0.16</b>	<b>0.71</b>	<b>0.16</b>	<b>0</b>	<b>0.16</b>	-	-	-	
OT0702-8	1140-1146.5	1	57.51	0.61	19.39	4.57	0.15	1.26	3.74	4.19	8.21	0	0.37	100	12.4	1.96	
		2	57.18	0.63	19.39	4.76	0.25	1.28	4.07	4.06	7.91	0	0.47	100	11.97	1.95	
		3	57.09	0.58	19.61	4.88	0.1	1.3	4.36	4.05	7.41	0.09	0.09	0.53	100	11.46	1.83
		4	58.27	0.52	19.32	4.11	0.19	1.01	3.43	3.92	8.83	0	0	0.39	99.99	12.75	2.25
		5	57.83	0.48	19.39	4.52	0.1	1.09	3.82	4.44	7.84	0	0	0.48	99.99	12.28	1.77
		6	57.69	0.43	19.48	4.39	0.16	1.25	4	4.31	4.31	7.82	0	0.47	100	12.13	1.81
		7	57.72	0.47	19.84	4.74	0.15	1.3	3.4	3.84	8.06	8.06	0	0.48	100	11.9	2.10
		8	58.05	0.56	19.37	4.01	0.13	1.07	3.48	4.38	8.5	8.5	0	0.45	100	12.88	1.94
		9	57.06	0.66	19.52	4.65	0.18	1.37	3.88	4.33	7.88	7.88	0	0.45	99.98	12.21	1.82
		10	57.21	0.58	19.46	4.75	0.22	1.51	4.07	4.31	7.48	7.48	0	0.41	100	11.79	1.74
		11	58.46	0.42	19.73	3.78	0	0.97	3.23	4.23	8.66	8.66	0	0.52	100	12.89	2.05
		12	57.12	0.62	19.38	4.62	0.23	1.24	3.77	4.05	8.46	8.46	0	0.52	100.01	12.51	2.09
		mean	<b>57.60</b>	<b>0.55</b>	<b>19.49</b>	<b>4.48</b>	<b>0.16</b>	<b>1.22</b>	<b>3.77</b>	<b>4.18</b>	<b>8.09</b>	<b>0.01</b>	<b>0.46</b>	-	-	-	
		sd	<b>0.48</b>	<b>0.08</b>	<b>0.16</b>	<b>0.34</b>	<b>0.07</b>	<b>0.16</b>	<b>0.33</b>	<b>0.19</b>	<b>0.45</b>	<b>0.03</b>	<b>0.05</b>	-	-	-	

(Continues)

Table 4-3. (Continued)

Sample	Depth (cm)	Shard	SiO <sub>2</sub>	TiO <sub>2</sub>	Al <sub>2</sub> O <sub>3</sub>	FeO <sub>tot</sub>	MnO	MgO	CaO	Na <sub>2</sub> O	K <sub>2</sub> O	P <sub>2</sub> O <sub>5</sub>	ClO	Total	Total alk	Alk. Ratio	
OT0702-9	1229-1232.5	1	61.45	0.45	18.91	3.07	0.16	0.49	1.75	5.37	7.93	0	0.42	100	13.3	1.48	
		2	61.7	0.38	18.85	2.86	0.18	0.51	1.72	5.86	7.28	0	0.66	100	13.14	1.24	
		3	61.15	0.59	18.89	3.1	0.23	0.23	0.57	1.73	5.38	7.84	0	0.51	99.99	13.22	1.46
		4	61.55	0.47	18.83	2.99	0.28	0.58	1.66	5.56	7.48	0	0.59	99.99	13.04	1.35	
		5	61.3	0.47	18.81	2.87	0.22	0.48	1.67	5.97	7.61	0	0.6	100	13.58	1.27	
		6	61.35	0.45	18.52	3.11	0.39	0.38	1.73	6.05	7.48	0	0.55	100.01	13.53	1.24	
		7	60.97	0.51	19.01	2.88	0.32	0.37	1.62	6.91	6.7	0	0.71	100	13.61	0.97	
		8	61.03	0.4	18.72	3.37	0.21	0.29	1.75	6.38	7.02	0	0.84	100.01	13.4	1.10	
		9	61.13	0.36	18.76	3.12	0.17	0.32	1.63	7.11	6.58	0	0.82	100	13.69	0.93	
		10	60.77	0.49	18.91	3.19	0.47	0.33	1.71	6.71	6.63	0	0.78	99.99	13.34	0.99	
		11	60.83	0.56	18.98	3.16	0.33	0.34	1.55	6.94	6.43	0	0.87	99.99	13.37	0.93	
		12	60.76	0.5	18.74	3.13	0.37	0.24	1.77	6.99	6.67	0	0.84	100.01	13.66	0.95	
		13	61.48	0.44	18.78	3.05	0.36	0.4	1.49	6.55	6.72	0	0.73	100	13.27	1.03	
		14	60.78	0.42	18.75	3.23	0.33	0.33	1.66	7.14	6.52	0	0.83	99.99	13.66	0.91	
		15	60.96	0.39	18.84	3.15	0.34	0.29	1.69	6.88	6.57	0	0.89	100	13.45	0.95	
mean			<b>61.15</b>	<b>0.46</b>	<b>18.82</b>	<b>3.09</b>	<b>0.29</b>	<b>0.39</b>	<b>1.68</b>	<b>6.39</b>	<b>7.03</b>	<b>0</b>	<b>0.71</b>	-	-	-	
sd			<b>0.31</b>	<b>0.07</b>	<b>0.12</b>	<b>0.14</b>	<b>0.09</b>	<b>0.11</b>	<b>0.08</b>	<b>0.64</b>	<b>0.52</b>	<b>0</b>	<b>0.15</b>	-	-	-	
OT0702-10	1440-1447	1	66.08	0.51	14.15	5.88	0.43	0.19	0.91	6.55	5.11	0	0.20	100.01	11.66	0.78	
		2	67.11	0.53	14.73	6.04	0.23	0.42	0.90	5.00	4.87	0	0.18	100.01	9.87	0.97	
		3	65.34	0.24	19.80	0.49	0.04	0.00	0.70	6.00	7.39	0	0.00	100.00	13.39	1.23	
		4	72.19	0.44	8.61	6.77	0.30	0.10	0.40	6.01	4.46	0	0.74	100.02	10.47	0.74	
		5	71.17	0.38	11.80	5.91	0.40	0.19	0.40	4.08	5.08	0	0.59	100.00	9.16	1.25	
		6	73.49	0.25	9.33	6.82	0.25	0.00	0.36	4.43	4.31	0	0.75	99.99	8.74	0.97	
		7	72.95	0.48	8.80	6.75	0.36	0.14	0.22	5.40	4.24	0	0.65	99.99	9.64	0.79	
		8	72.76	0.49	8.84	6.99	0.32	0.13	0.29	5.02	4.34	0	0.82	100.00	9.36	0.86	
		9	72.56	0.43	8.66	6.96	0.25	0.14	0.35	5.39	4.56	0	0.71	100.01	9.95	0.85	
		mean1			<b>66.18</b>	<b>0.43</b>	<b>16.23</b>	<b>4.14</b>	<b>0.23</b>	<b>0.20</b>	<b>5.85</b>	<b>5.79</b>	<b>0</b>	<b>0.13</b>	-	-	-
		sd1			<b>0.89</b>	<b>0.16</b>	<b>3.11</b>	<b>0.20</b>	<b>0.21</b>	<b>0.12</b>	<b>0.79</b>	<b>1.39</b>	<b>0</b>	<b>0.11</b>	-	-	-
		mean2			<b>72.52</b>	<b>0.41</b>	<b>9.34</b>	<b>6.70</b>	<b>0.31</b>	<b>0.34</b>	<b>5.06</b>	<b>4.50</b>	<b>0</b>	<b>0.71</b>	-	-	-
		sd2			<b>0.79</b>	<b>0.09</b>	<b>1.23</b>	<b>0.06</b>	<b>0.06</b>	<b>0.07</b>	<b>0.71</b>	<b>0.31</b>	<b>0</b>	<b>0.08</b>	-	-	-

Table 4-4. Selected analyses of tephra layers correlated to those found in core Co1202.

	SiO <sub>2</sub>	TiO <sub>2</sub>	Al <sub>2</sub> O <sub>3</sub>	FeO <sub>tot</sub>	MnO	MgO	CaO	Na <sub>2</sub> O	K <sub>2</sub> O	P <sub>2</sub> O <sub>5</sub>	ClO	Tot alk	K <sub>2</sub> O/Na <sub>2</sub> O
<b>AD 472 (Somma Vesuvius)</b>													
<b>Proximal deposit<sup>1</sup></b>													
mean	49.79	0.50	22.23	4.95	0.15	1.01	5.63	9.20	5.41	0.00	1.12	14.62	0.73
sd	1.65	0.16	0.92	1.38	0.07	0.47	1.51	2.35	2.29	0.00	0.53	1.87	0.82
<b>Shkodra<sup>2</sup></b>													
mean	50.28	0.55	22.64	4.91	0.17	0.65	5.69	8.32	5.82	0.02	0.97	14.36	0.72
sd	0.83	0.11	0.62	0.53	0.07	0.29	0.67	1.02	0.92	0.03	0.10	0.54	0.17
<b>Monticchio/TM2b<sup>3</sup></b>													
mean	50.18	0.50	21.61	4.79	0.20	0.64	5.89	7.90	6.92	0.29	1.07	14.82	0.88
sd	1.02	0.07	0.19	0.24	0.04	0.20	0.61	0.35	0.72	0.17	0.19	0.56	0.12
<b>AD 512 (Somma Vesuvius)</b>													
<b>Proximal deposit<sup>1</sup></b>													
mean	47.81	1.05	19.40	7.97	0.20	2.97	9.11	4.60	5.85	0.31	0.75	10.45	1.28
sd	0.98	0.17	0.61	0.53	0.13	0.80	1.05	0.53	0.58	0.15	0.14	0.85	0.18
<b>Monticchio/TM2a<sup>3,4</sup></b>													
mean	48.44	0.83	19.19	7.23	0.26	2.85	8.89	4.33	6.86	0.59	0.69	11.18	1.65
sd	0.69	0.09	0.48	0.56	0.31	0.69	0.68	0.68	1.04	0.13	0.10	0.85	0.51
<b>FL (Mt. Etna)</b>													
<b>Ohrid (core Lz1120)<sup>5</sup></b>													
mean	54.25	1.76	17.48	8.15	0.00	2.85	6.02	5.40	3.29	0.48	0.31	8.69	0.61
sd	0.73	0.22	0.51	0.53	0.00	0.33	0.50	0.41	0.34	0.10	0.06	0.56	0.07
<b>Pergusa<sup>6</sup></b>													
mean	53.02	1.90	17.27	8.93	0.22	2.98	5.94	5.09	3.95	0.43	0.27	9.03	0.76
sd	1.03	0.50	1.50	1.95	0.10	0.89	1.18	0.50	1.43	0.15	0.12	1.87	0.19
<b>Mercato (Somma Vesuvius)</b>													
<b>Monticchio/TM6b<sup>3,4</sup></b>													
mean	58.68	0.14	21.41	1.80	0.18	0.07	1.76	8.58	6.76	0.02	0.58	15.34	0.79
sd	0.30	0.03	0.21	0.13	0.03	0.01	0.25	0.18	0.54	0.02	0.04	0.55	0.07
<b>Monticchio/TM6a<sup>3,4</sup></b>													
mean	59.99	0.30	20.61	2.24	0.13	0.16	2.42	5.58	8.02	0.05	0.51	13.60	1.51
sd	0.97	0.10	0.53	0.47	0.04	0.07	0.41	1.07	0.85	0.03	0.15	0.60	0.39
<b>Proximal deposit<sup>1</sup></b>													
mean	58.51	0.13	21.70	1.76	0.14	0.09	1.66	8.56	6.93	0.00	0.52	15.49	0.82
sd	0.72	0.08	0.41	0.19	0.10	0.08	0.26	0.62	0.38	0.00	0.09	0.49	0.11

(Continues)

Table 4-4. (Continued)

	SiO <sub>2</sub>	TiO <sub>2</sub>	Al <sub>2</sub> O <sub>3</sub>	FeO <sub>tot</sub>	MnO	MgO	CaO	Na <sub>2</sub> O	K <sub>2</sub> O	P <sub>2</sub> O <sub>5</sub>	ClO	Tot alk	K <sub>2</sub> O/Na <sub>2</sub> O
<b>SMP1eY-3 (Campi Flegrei)</b>													
<b>Monticchio/TM15<sup>3</sup></b>													
mean	62.22	0.38	18.36	3.27	0.13	0.61	2.19	3.85	8.36	0.12	0.52	12.21	2.21
sd	0.78	0.03	0.21	0.29	0.04	0.15	0.22	0.44	0.55	0.06	0.11	0.22	0.37
<b>ZS 98 291<sup>7</sup></b>													
mean	61.47	0.39	18.44	3.27	0.11	0.70	2.55	3.46	9.03	0.15	0.44	12.48	2.67
sd	0.60	0.03	0.11	0.26	0.03	0.14	0.21	0.49	0.32	0.05	0.06	0.45	0.47
<b>ZS 2506a<sup>7</sup></b>													
mean	58.51	0.56	18.60	4.42	0.16	1.18	3.78	3.91	8.10	0.25	0.52	12.02	2.07
sd	0.19	0.02	0.14	0.03	0.02	0.02	0.11	0.10	0.13	0.05	0.02	0.23	0.03
<b>ZS 2506b<sup>7</sup></b>													
mean	62.33	0.43	18.74	2.80	0.12	0.44	2.27	3.87	8.34	0.05	0.60	12.21	2.16
sd	0.40	0.01	0.17	0.15	0.02	0.07	0.07	0.15	0.04	0.06	0.01	0.11	0.10
<b>ZS 2507a<sup>7</sup></b>													
mean	58.49	0.50	18.64	4.32	0.15	1.15	3.63	3.67	8.75	0.27	0.44	12.41	2.39
sd	1.38	0.11	0.10	0.86	0.02	0.39	0.82	0.13	0.99	0.09	0.04	0.86	0.36
<b>ZS 2507b<sup>7</sup></b>													
mean	61.80	0.47	18.68	2.81	0.14	0.46	2.21	4.41	8.34	0.07	0.62	12.75	1.90
sd	0.38	0.01	0.10	0.10	0.03	0.05	0.10	0.21	0.19	0.02	0.02	0.22	0.11
<b>M25/4-12<sup>8</sup></b>													
mean	61.79	0.40	18.57	3.29	0.14	0.64	2.52	3.69	8.96	0.00	0.00	12.65	2.49
sd	1.21	0.05	0.22	0.32	0.09	0.19	0.40	0.44	0.95	0.00	0.00	0.65	0.54
<b>Ohrid (core Lz1120)<sup>5</sup></b>													
mean	61.88	0.29	18.63	2.92	0.03	0.50	2.20	4.18	8.82	0.00	0.54	12.99	2.15
sd	0.52	0.08	0.19	0.23	0.06	0.15	0.19	0.47	0.51	0.00	0.14	0.09	0.39

(Continues)

Table 4-4. (Continued)

	SiO <sub>2</sub>	TiO <sub>2</sub>	Al <sub>2</sub> O <sub>3</sub>	FeO <sub>tot</sub>	MnO	MgO	CaO	Na <sub>2</sub> O	K <sub>2</sub> O	P <sub>2</sub> O <sub>5</sub>	ClO	Totalk	K <sub>2</sub> O/Na <sub>2</sub> O
<b>Codola</b>													
<b>ZS 98 37<sup>7</sup></b>													
mean	58.42	0.59	19.84	3.38	0.17	0.60	3.84	3.86	9.29	0.00	0.00	13.15	2.41
sd	0.22	0.08	0.15	0.09	0.09	0.11	0.11	0.17	0.18	0.00	0.00	0.11	0.15
<b>ZS 98 36<sup>7</sup></b>													
mean	57.76	0.56	19.66	4.03	0.13	0.68	4.59	3.86	8.08	0.11	0.54	11.94	2.14
sd	0.57	0.05	0.47	0.46	0.03	0.15	0.40	0.48	1.11	0.03	0.06	0.74	0.48
<b>ZS 2002/2a<sup>7</sup></b>													
mean	57.92	0.53	19.74	3.56	0.15	0.59	4.28	3.57	9.06	0.11	0.51	12.63	2.54
sd	0.07	0.03	0.13	0.17	0.01	0.05	0.06	0.05	0.14	0.02	0.05	0.11	0.07
<b>ZS 2002/2b<sup>7</sup></b>													
mean	53.18	0.78	18.60	7.12	0.17	1.87	6.85	3.09	7.31	0.47	0.58	10.40	2.37
sd	1.04	0.04	0.82	0.51	0.03	0.56	1.54	0.29	0.63	0.04	0.18	0.90	0.12
<b>Monticchio TM16a<sup>3</sup></b>													
mean	52.39	0.79	19.04	7.06	0.16	1.85	7.13	3.65	6.66	0.71	0.56	10.31	1.86
sd	1.69	0.09	0.86	0.60	0.03	0.31	1.24	0.43	0.62	1.05	0.11	0.47	0.31
<b>Monticchio TM16b<sup>3</sup></b>													
mean	58.58	0.50	19.70	3.66	0.12	0.55	4.30	3.40	8.58	0.10	0.50	11.98	2.56
sd	0.65	0.06	0.41	0.33	0.03	0.14	0.95	0.49	0.40	0.04	0.08	0.76	0.31
<b>CiY-5 (Campi Flegrei)</b>													
<b>Proximal PDCs<sup>9</sup></b>													
mean	61.90	0.40	18.35	3.09	0.21	0.47	2.03	5.15	7.74	0.09	0.59	12.89	1.54
sd	0.85	0.04	0.32	0.27	0.08	0.16	0.34	0.58	0.51	0.06	0.20	0.40	0.31
<b>Proximal fallout<sup>9</sup></b>													
mean	61.33	0.42	19.16	2.89	0.24	0.35	1.75	5.96	7.00	0.05	0.84	12.96	1.18
sd	0.50	0.02	0.22	0.12	0.03	0.02	0.06	0.33	0.19	0.02	0.08	0.43	0.06
<b>Monticchio/TM16<sup>3</sup></b>													
mean	61.69	0.42	19.11	2.93	0.24	0.35	1.73	5.66	6.83	0.05	0.78	12.49	1.22
sd	0.46	0.02	0.21	0.09	0.02	0.02	0.07	0.71	0.29	0.03	0.05	0.78	0.15
<b>Ohrid (core Lz1120)<sup>5</sup></b>													
mean	61.64	0.43	19.05	3.04	0.20	0.44	1.94	5.11	7.40	0.08	0.68	12.50	1.50
sd	0.48	0.03	0.17	0.08	0.05	0.12	0.28	0.85	0.59	0.05	0.17	0.57	0.37
<b>Green Tuff/Y-6 (Pantelleria)</b>													
<b>GT Pantellerite<sup>10</sup></b>													
XRF	72.53	0.4	8.42	8.26	0.37	0.01	0.38	4.97	4.66	-	-	9.63	1.07
<b>GT Trachyte<sup>10</sup></b>													
XRF	66.47	0.66	12.68	7.59	0.27	0.32	1.28	5.56	4.56	0.05	0.19	10.12	1.22

(Continues)

Table 4-4. (Continued)

	SiO <sub>2</sub>	TiO <sub>2</sub>	Al <sub>2</sub> O <sub>3</sub>	FeO <sub>tot</sub>	MnO	MgO	CaO	Na <sub>2</sub> O	K <sub>2</sub> O	P <sub>2</sub> O <sub>5</sub>	ClO	Tot alk	K <sub>2</sub> O/Na <sub>2</sub> O
<b>X-5</b>													
<b>Monticchio/TM24a-1<sup>3</sup></b>													
<i>mean</i>	57.23	0.51	19.00	4.46	0.14	1.20	4.21	4.23	8.23	0.26	0.52	12.46	1.95
<i>sd</i>	0.59	0.03	0.19	0.20	0.02	0.12	0.30	0.10	0.22	0.04	0.04	0.21	0.08
<b>Monticchio/TM24a-2<sup>3</sup></b>													
<i>mean</i>	59.48	0.41	19.14	3.60	0.14	0.73	2.94	4.26	8.62	0.13	0.55	12.88	2.03
<i>sd</i>	0.45	0.03	0.16	0.21	0.03	0.10	0.26	0.18	0.22	0.04	0.05	0.22	0.12
<b>Monticchio/TM24b-1<sup>3</sup></b>													
<i>mean</i>	61.25	0.38	18.86	3.22	0.14	0.60	2.51	4.10	8.32	0.10	0.51	12.41	2.04
<i>sd</i>	0.80	0.03	0.29	0.24	0.03	0.08	0.19	0.35	0.32	0.03	0.08	0.58	0.16
<b>Monticchio/TM24b-2<sup>3</sup></b>													
<i>mean</i>	58.39	0.53	18.77	4.60	0.15	1.29	3.90	3.87	7.82	0.26	0.42	11.69	2.02
<i>sd</i>	0.86	0.04	0.37	0.34	0.02	0.23	0.47	0.16	0.42	0.06	0.06	0.39	0.16
<b>X-6</b>													
<b>Monticchio/TM27a<sup>11</sup></b>													
<i>mean</i>	61.56	0.45	18.52	2.78	0.20	0.45	1.89	5.88	7.57	0.08	0.63	13.45	1.29
<i>sd</i>	0.18	0.02	0.07	0.08	0.02	0.05	0.08	0.19	0.18	0.04	0.07	0.11	0.07
<b>Monticchio/TM27b<sup>11</sup></b>													
<i>mean</i>	60.79	0.48	18.55	2.98	0.31	0.30	1.73	7.21	6.54	0.04	0.89	13.75	0.91
<i>sd</i>	0.33	0.03	0.10	0.11	0.03	0.01	0.06	0.28	0.16	0.03	0.08	0.31	0.05
<b>P-11 (Pantelleria)</b>													
<b>KET82-22a<sup>12</sup></b>													
<i>mean</i>	64.67	0.83	15.5	5.88	-	0.28	1.45	6.41	4.98	-	-	11.39	1.29
<i>sd</i>	0.68	0.1	0.71	0.19	-	0.14	0.2	0.27	0.19	-	-	-	-
<b>KET82-22b<sup>12</sup></b>													
<i>mean</i>	72.41	0.34	8.95	7.43	-	0.08	0.17	6.09	4.54	-	-	10.63	1.34
<i>sd</i>	0.38	0.08	0.09	0.24	-	0.1	0.08	0.33	0.12	-	-	-	-
<b>Lesvos/ML-5a<sup>13</sup></b>													
<i>mean</i>	73.73	0.43	8.31	7.14	0.32	0.08	0.31	4.3	4.44	0.01	0.84	8.74	1.04
<i>sd</i>	0.24	0.01	0.1	0.16	0.02	0.01	0.01	0.25	0.09	0.01	0.03	0.25	0.07
<b>Lesvos/ML-5b<sup>13</sup></b>													
<i>mean</i>	66.23	0.75	14.32	6.06	0.3	0.27	1.16	5.59	4.99	0.1	0.17	10.58	0.9
<i>sd</i>	1.04	0.06	1.1	0.48	0.02	0.1	0.27	0.28	0.14	0.04	0.06	0.17	0.07

<sup>1</sup>Santacroce et al. (2008); <sup>2</sup>Sulpizio et al. (2009); <sup>3</sup>Wulf et al. (2004); <sup>4</sup>Wulf et al. (2008); <sup>5</sup>Wagner et al. (2008b); <sup>6</sup>Zanchetta (unpublished data); <sup>7</sup>Di Vito et al. (2008); <sup>8</sup>Zanchetta et al. (2008); <sup>9</sup>Giaccio et al. (2008b); <sup>10</sup>Civetta et al. (1988); <sup>11</sup>Wulf et al. (1988); <sup>12</sup>Wulf et al. (2006); <sup>13</sup>Margari et al. (2007).

The tephra layer OT0702-6 (752-743 cm) contains almost 100% of volcanic glass shards; it is reddish-brown to light-brown in colour, and shows high MS, K, Zr, and Sr values (Fig. 4-2). The glass shards are mixed with lacustrine sediments in the overlying c. 10 cm. Volcanic particles mainly comprise aphyric, vesicular micro-pumices and aphyric glass-shards with thick septa (Fig. 4-3f). Glass composition ranges from trachyte to phono-trachyte (Table 4-3; Fig. 4-4). The composition and the stratigraphy within core Co1202 indicate that tephra OT0702-6 can be correlated with the Campanian Ignimbrite (CI) deposits (Civetta et al. 1997; Pappalardo et al. 2002; Orsi et al. 1996; Table 4-4) and the Y-5 tephra layer (Keller et al. 1978; Thunell et al. 1979; Wulf et al. 2004; Pyle et al. 2006; Margari et al. 2007; Giaccio et al. 2008b; Table 4-4). Characteristic for the CI products is the continuous variation in composition from trachyte to phono-trachyte (Civetta et al. 1997; Signorelli et al. 2001; Pappalardo et al. 2002), a compositional variability also found for the Y-5 tephra layer in many distal archives (e.g. Vezzoli 1991; Wulf et al. 2004; Pyle et al. 2006; Margari et al. 2007; Giaccio et al. 2008b). The best age of the Campanian Ignimbrite eruption is  $39,280 \pm 110$  yrs ( $^{40}\text{Ar}/^{39}\text{Ar}$  dating on sanidine crystals; De Vivo et al. 2001). The occurrence of CI/Y-5 deposits in Lake Ohrid sediments confirm earlier recognitions (Wagner et al. 2008b).

The cryptotephra OT0702-7 (825-822 cm), initially identified from raised Zr values (Fig. 4-2), comprises cusped glass-shards with thin septa (Fig. 4-3g). Glasses have a composition ranging from rhyolitic (main) to trachytic (Table 4-3; Fig. 4-4). When plotted on the  $\text{Fe}_{\text{tot}}$  vs  $\text{Al}_2\text{O}_3$  diagram the rhyolite plots into the field of pantellerites (Fig. 4-6), which suggests the peralkaline volcano of Pantelleria as its source (Fig. 4-1). The composition of cryptotephra OT0702-7 shows a good match with the Pantelleria Green Tuff eruption (Cornette et al. 1983; Orsi and Sheridan 1984), which corresponds to the distal marine tephra layer Y-6 (Keller et al. 1978; Narcisi and Vezzoli 1999; Table 4-4; Fig. 4-4). A peculiar characteristic of the Green Tuff composition is the compositional variability from pantelleritic to trachytic (Civetta et al. 1988; White et al. 2009; Fig. 4-4). Another possible correlation would be with TM22 tephra layer in the Monticchio succession (Wulf et al., 2004), correlated to the P-10 marine tephra layer (Paterne et al. 1988), or with the P-11 tephra layer, which shows a similar compositional variability from trachyte to rhyolite (Paterne et al. 2008). A useful geochemical discrimination among the three different candidates for correlation can be obtained by plotting the data on the  $\text{SiO}_2$  vs  $\text{FeO}_{\text{tot}}$  diagram (Fig. 4-7). The OT0702-7 tephra has the highest content in  $\text{FeO}_{\text{tot}}$  (Fig. 4-7), which is significantly different if compared to the TM22/P-10 and P-11 tephra layers (Fig. 4-7). The  $\text{FeO}_{\text{tot}}$  content of the OT0702-7 tephra layer is the closest to that of the Y-6 marine tephra layer (Keller et al. 1978), and fits well to the data of the Green Tuff from the proximal area (Civetta et al. 1988; Fig. 4-6). Therefore, we propose here the correlation of OT0702-7 tephra layer with the Green Tuff and Y-6 marine tephra layer. Margari et al. (2007) correlated a trachytic-pantelleritic tephra layer

(ML5) recognised in a core drilled on the island of Lesbos (Aegean Sea) with the Green Tuff/Y-6. When plotted on the  $\text{SiO}_2$  vs  $\text{FeO}_{\text{tot}}$  diagram of Fig. 4-7 the ML5 data do, however, not support a correlation to the Green Tuff/Y-6 deposits. The ML5 data show a similar trend if compared to the OT0702-7/Green Tuff/Y-6 products but also exhibit a significant shift towards lower contents in  $\text{SiO}_2$  and  $\text{FeO}_{\text{tot}}$  (Fig. 4-7), which would suggest a different eruption for the ML5 data. Several K/Ar datings ranging from  $50,800 \pm 3,600$  to  $46,900 \pm 2000$  yrs are reported for the Green Tuff on Pantelleria Island (e.g. Cornette et al. 1983; Civetta et al. 1988). A best age estimation of  $49,200 \pm 1100$  yrs is here proposed by averaging the available ages. The recognition of the Green Tuff/Y-6 tephra layer in Lake Ohrid is the first

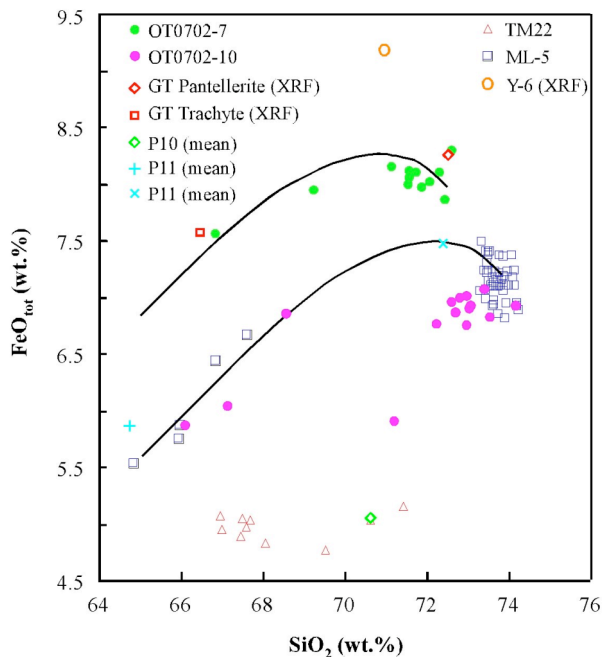


Fig. 4-7.  $\text{SiO}_2$  vs  $\text{FeO}_{\text{tot}}$  diagram showing compositional trends of OT0702-7 and OT0702-10 cryptotephra. For comparison data of TM22 from Lago Grande di Monticchio (Wulf et al., 2004) and ML5 from the island of Lesbos in the Aegean Sea (Margari et al. 2007) are also reported. EDS mean data of P-10 and P-11 tephra layers (Paterne et al. 2008), XRF data of Y-6 (Keller et al. 1978), and GT Pantellerite-Trachyte (Civetta et al. 1988) are also reported.

occurrence described in the Balkan area and extends the known dispersal area to the northeast.

The tephra layer OT0702-8 (1146.5-1140 cm) is rusty-red in colour and corresponds to peaks in MS, K, Zr, and Sr values (Fig. 4-2). This layer mainly comprises coarse ash and shows sharp basal and top contacts. Volcanic particles are aphyric micro-pumices and glass-shards (Fig. 4-3h). Glass composition is mainly phonolitic (Table 4-3; Fig. 4-4). Many tephra layers punctuate the central Mediterranean tephrostratigraphy during the period before 50 kyrs BP (Di Vito et al. 2008; Paterne et al. 1988; 2008), but in a reasonable time interval (i.e. between

50,000 and 150,000 yrs) the best match of the OT0702-8 glass composition is with the X-5 tephra layer (Table 4-3; Fig. 4-4), recognised in cores from the Ionian and Tyrrhenian Sea (Keller et al. 1978; Paterne et al. 2008), Lago Grande di Monticchio (Wulf et al. 2004), and San Gregorio Magno Basin (Munno and Petrosino 2007). In the Monticchio succession, X-5 deposits have been reported as two different tephra layers (Table 4-4), which comprise an upper fallout deposit (TM24a) and a lower co-ignimbrite deposit (TM24b; Wulf et al. 2004). The composition of the OT0702-8 tephra layer closely matches the composition of the TM24a-1 tephra layer (Table 4-4; Fig. 4-4), which has a varve-based age of 101,600 yrs (Wulf et al., 2006, Brauer et al., 2007). This age is in relatively good agreement with an

$^{40}\text{Ar}/^{39}\text{Ar}$  age of  $105,000 \pm 2,000$  yrs obtained on sanidine crystals from X-5 tephra layer recognised in a Ionian deep-sea core (Kraml 1997; Wulf et al. 2006). The source of the X-5 tephra layer is still unknown, although some mid-proximal exposures suggest a Campanian origin (Di Vito et al. 2008; Marciano et al. 2008). This finding is the first recognition of the X-5 tephra layer in the Balkans.

The tephra layer OT0702-9 (1232.5-1229 cm) is light brown in colour, corresponds to high MS, K, and Zr values (Fig. 4-2), and shows sharp basal and top boundaries. Grain-size mainly comprises fine to coarse ash. Volcanic particles are highly vesicular, aphyric micropumices and glass-shards with a large variability in shape and size (Fig. 4-3i). Glass composition is mainly trachytic, with few analyses that plot into phonolitic field on the TAS diagram (Table 4-3; Fig. 4-4). Due to the chemical composition and the stratigraphic position not far downcore of the OT0702-8 tephra layer, the OT0702-9 tephra layer can be correlated with the X-6 tephra layer (Table 4-4; Fig. 4-4), recognised in cores from the Ionian and Tyrrhenian Sea (Keller et al. 1978; Paterne et al. 2008), from Lago Grande di Monticchio (Wulf et al. 2006), and from the San Gregorio Magno basin (Munno and Petrosino 2007). Brauer et al. (2007) quoted an  $^{40}\text{Ar}/^{39}\text{Ar}$  age of  $107,000 \pm 2,000$  yrs for the X-6 tephra, which is in good agreement with the suggested age of 108,430 yrs obtained from the varve-supported chronology of the Lago Grande di Monticchio record.

The cryptotephra OT0702-10 (1447-1440 cm) has initially been identified from raised Zr intensities (Fig. 4-2) and comprises mainly aphyric cusped glass shards (Fig. 4-3k). When plotted on the TAS diagram the glass shards reveal a bimodal chemical composition, which comprises a trachyte and a rhyolite without any compositional trend between (Fig. 4-4). The peculiar chemical composition of the glass shards assigns them to the comendites and the pantellerites, respectively, when plotted on the  $\text{Fe}_{\text{tot}}$  vs  $\text{Al}_2\text{O}_3$  diagram (Fig. 4-6). The comenditic to pantelleritic composition indicate that the glass shards were generated by the explosive activity of the Pantelleria Island, since it represented the only source of magmas with this composition in the Mediterranean area during the late Quaternary (Peccerillo, 2005). Recently, Paterne et al. (2008) described a comenditic to pantelleritic tephra layer in a core from the Ionian Sea (P-11 tephra layer). Glass compositions of P-11 and OT0702-10 tephra layers show a good match (Table 4-3 and 4-4; Fig. 4-4 and 4-7), and thus a correlation between the two tephra layers is proposed here. Moreover, the OT0702-10 data show a good match with the ML5 tephra layer (Fig. 4-4 and 4-7) from Lesvos island (Margari et al., 2007), and here we propose the correlation of the ML5 tephra layer with the OT0702-10/P-11 ones. The estimated age of the P-11 tephra layer is c. 131,000 yrs (Paterne et al. 2008), and therefore provides a very important chronologic constrain for the lowest part of the retrieved Co1202 sediment succession from Lake Ohrid.

#### 4.4.5. Core chronology and interpretation

Based on the ten recognized tephra and cryptotephra layers (Fig. 4-2) and with contribution from radiocarbon ages obtained at seven different depths (Table 4-2), an age model can be established for core Co1202 from Lake Ohrid. The age-depth correlation is based on linear interpolation between chronological tie points, excluding the mass-wasting deposit at 1095.5-1064 cm and by subtracting the thicknesses of the distinct tephra layers at 1232.5-1229 cm (OT0702-9), 1146.5-1140 cm (OT0702-8), 752-743 cm (OT0702-6), and 620-617 cm (OT0702-4) from the composite depth (Fig. 4-2). The year of coring (2007) is used as time marker for the sediment/water interface and thus the top of core Co1202.

The age of Lithofacies 1 at the base of core Co1202 can be determined by the lowermost cryptotephra at 1,447-1,440 cm (OT0702-10; Fig. 4-2 and 4-8) with a proposed age of c. 131,000 yrs (Paterne et al., 2008). This suggests that Lithofacies 1 at the base of core Co1202, which is dominated by detrital clastic material and a significant occurrence of dropstones (Fig. 4-2) was deposited during the penultimate glacial period of marine isotopic stage (MIS) 6. Sedimentation of Lithofacies 1 under glacial conditions explains the occurrence of dropstones as an effect of ice floe transport, high amount of clastic matter due to enhanced surface runoff and lower carbonate and organic matter content as a result of cold climate conditions leading to lower productivity.

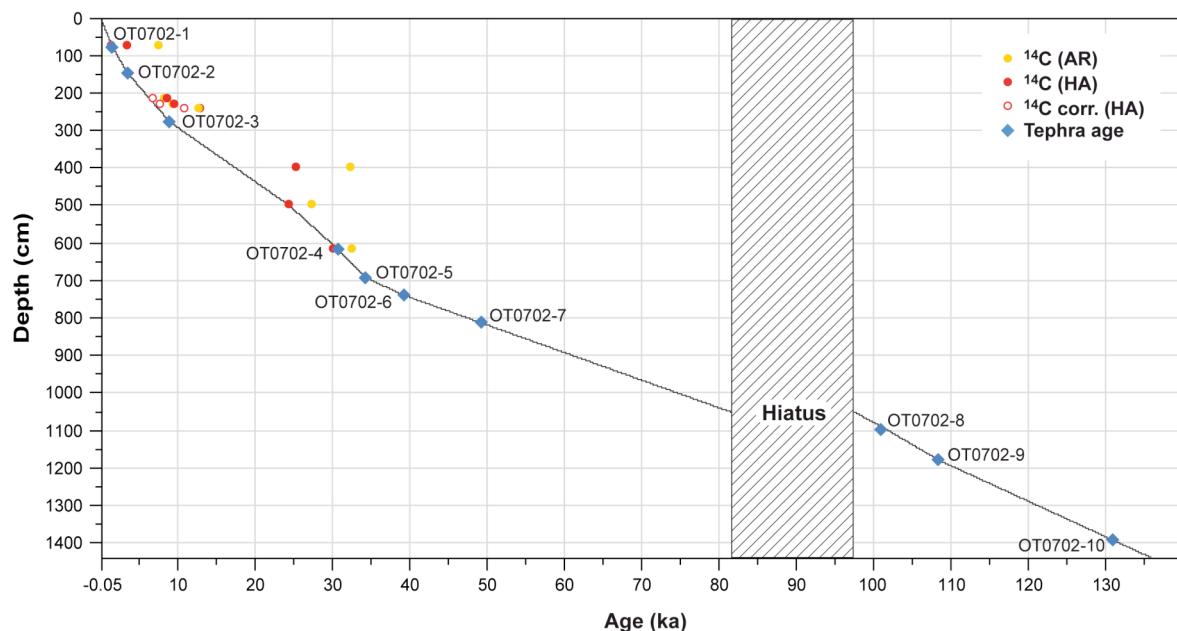


Fig. 4-8. Age-depth model and calculated sedimentation rates for the Co1202 sediment succession. Ages from tephras and cryptotephras are indicated by blue rhombs, calibrated radiocarbon ages of the AR fraction ( $^{14}\text{C}$  AR) are indicated by yellow dots, calibrated radiocarbon ages of the HA fraction ( $^{14}\text{C}$  HA) are indicated by red dots, and corrected, calibrated radiocarbon ages of the HA fraction ( $^{14}\text{C}$  corr. HA) are indicated by open red dots.

The age of Lithofacies 2 between 1,439 and 1,095.5 cm is derived from tephra OT0702-9 at 1,232.5-1,229.5 cm and OT0702-8 at 1,147-1,140 cm with ages of 108,430 and 101,600 yrs (Wulf et al. 2006, Brauer et al. 2007), respectively. The ages obtained from the two tephra layers, in combination with the high amounts of carbonates (Fig. 4-2), suggest that the interval between 1,440 cm to the base of the mass wasting deposit at 1,095.5 cm was deposited during MIS 5. Extrapolation of the sedimentation rate obtained for the interval between OT0702-9 and OT0702-8 yields an age of ca. 97,600 yrs for the upper limit of Lithofacies 2 at 1095.5 cm (Fig. 4-8). Sedimentation of Lithofacies 2 under warm climate conditions during MIS 5 would explain relatively high amounts of carbonate and organic matter.

Age control for Lithofacies 1 between 1,064 and 240 cm is given by five tephra and cryptotephra layers at 826-821.5 (OT0702-7), 752.5-743 (OT0702-6), 696-688.5 (OT0702-5), 620.5-616 (OT0702-4), and 277-268 cm (OT0702-3) and four radiocarbon datings obtained on bulk organic matter at 617, 500, 400, and 242 cm (Table 4-2, Fig. 4-2 and 4-8). Whilst the age of OT0702-7 is averaged to  $49,200 \pm 1100$  yrs, based on the existing age estimations (Cornette et al. 1983; Civetta et al. 1988), the age of OT0702-6 is relatively well determined to  $39,280 \pm 110$  yrs (De Vivo et al. 2001). The correlation of cryptotephra OT0702-5 to the Codola eruptions suggests an age between 31,000 and 34,000 yrs (Paterne et al. 1999, Wulf et al. 2004; Giaccio et al. 2008). Among these proposed ages the one quoted by Paterne et al. (1999) of  $34,270 \pm 870$  cal yrs BP would best match with relatively constant sedimentation rates between OT0702-6 (CI/Y-5) and OT0702-4 (Y-3; Fig. 4-8), which dates at  $30,670 \pm 230$  cal yrs BP (Zanchetta et al. 2008). The age of OT0702-4 is well constrained by the radiocarbon age obtained on the HA fraction of bulk organic carbon of sample KIA35895 from 617 cm depth (Table 4-2), indicating  $30,136 \pm 280$  cal yrs BP. Thus it can be assumed that no significant hard-water or reservoir effect biases the radiocarbon ages obtained on the HA fraction in Lithofacies 1, which indicates that these ages are more reliable if compared to the ages obtained on the AR fraction. Sample KIA36602 from 500 cm depth dates to  $24,358 \pm 337$  cal yrs BP (HA) and thus indicates that the sedimentation rates throughout the glacial period are relatively constant (Fig. 4-8). The radiocarbon ages of samples KIA36601 and KIA35894 (Table 4-2) from 400 and 242 cm depths, respectively, are likely affected by contamination of old carbon and therefore not included in the age-depth correlation. A more reliable age is given by tephra OT0702-3 from 277.5-269 cm depth, which has a proposed age being close to  $8,890 \pm 90$  cal yrs BP (Santacroce et al. 2008). Extrapolating the mean sedimentation rates downcore, the mass-wasting event at the base of Lithofacies 1 occurred around 81,700 yrs, and caused an erosional hiatus of c. 16,000 yrs in core Co1202. Hence, most of Lithofacies 1 is likely deposited during the last glacial including MIS 4, 3, and 2, which would explain the high amounts of detrital clastic material and dropstones. It seems,

however, that the topmost part of Lithofacies 1, from about 300 cm (Fig. 4-8) is deposited during the Holocene, and that the Pleistocene/Holocene transition in core Co1202 is not concomitant with a substantial change in lithofacies.

The age of Lithofacies 2 between 240 cm and the surface is derived from cryptotephra OT0702-2 at 145.5-144 and OT0702-1 at 77.5-74.5 cm (Fig. 4-2) and three radiocarbon ages (Table 4-2). Cryptotephra OT0702-2 gives a relatively well constrained age control point at 145.5-144 cm of  $3,370 \pm 70$  cal yrs BP (Coltelli et al. 2000; Wagner et al. 2008b). Cryptotephra OT0702-1 can, with very small error, be placed between 1,438 and 1,478 yrs (Rosi and Santacroce 1983; Sulpizio et al. 2005; Santacroce et al. 2008). For further discussions on the age-depth correlation we tend to place the age of OT0702-1 at 1,460 yrs. The bulk organic carbon samples from 230 (KIA35893), 217.5 (KIA36600), and 74 cm (KIA35892) indicate ages of  $8,645 \pm 45$ ,  $7,860 \pm 35$ , and  $3,145 \pm 35$   $^{14}\text{C}$  yrs BP for the HA fraction and  $6,730 \pm 50$ ,  $7,425 \pm 40$ , and  $8,370 \pm 30$   $^{14}\text{C}$  yrs BP for the AR fraction. The discrepancy between the age of OT0702-1 and the ages of the HA and AR fractions of sample KIA35892 from the same depth implies that significant hard water and/or reservoir effects bias the radiocarbon ages in Lithofacies 2. This is confirmed by the close agreement of the estimated modern hard water and reservoir effect quoted by Wagner et al. (2008a) of  $1,560 \pm 30$   $^{14}\text{C}$  yrs BP, which matches relatively well the difference of c. 1,564  $^{14}\text{C}$  yrs between OT0702-1 and the age of the HA fraction of sample KIA35892. Assuming a constant hard water and reservoir effect throughout Lithofacies 2 in the topmost 240 cm of core Co1202, corrected ages of  $7,910 \pm 40$  and  $7,225 \pm 35$  cal yrs BP for the samples KIA35893 and KIA36600 from 230 and 217.5 cm depth, respectively, show a good fit to a relatively constant sedimentation rate between OT0702-3 and OT0702-2 (Table 4-2, Fig. 4-2 and 4-8). The ages derived from cryptotephra OT0702-2, OT0702-1 and the three radiocarbon datings indicate a Holocene age of Lithofacies 2 in the upper part of core Co1202. Deposition during relatively warm periods would explain high contents of carbonate and increased amounts of organic matter, such as observed in another core from the south-eastern part of Lake Ohrid (Wagner et al. 2008b; 2009).

## 4.5. Conclusions

Sedimentological studies and chronostratigraphic work on core Co1202 from Lake Ohrid provided crucial information with respect to the dispersal of tephras originating from explosive eruptions of Italian volcanoes during the last climatic cycle. In addition to four macroscopically identified tephra layers (OT0702-4, OT0702-6, OT0702-8, OT0702-9), six cryptotephra layers (OT0702-1, OT0702-2, OT0702-3, OT0702-5, OT0702-7, OT0702-10), occurring finely dispersed and admixed with lacustrine sediment in core Co1202, have been identified from raised K, Zr, Sr element intensities and MS values using rapid and non-destructive techniques. The tephra and cryptotephra layers could be precisely correlated with known and relatively well dated explosive eruptions. Tephras OT0702-9, OT0702-8, OT0702-6, and OT0702-4 could be correlated to X-6, X-5, CI/Y-5, and SMP1-e/VRa/Y-3 tephra layers, respectively. Cryptotephras OT0702-10, OT0702-7, OT0702-5, OT0702-3, OT0702-2, and OT0702-1 were correlated to P-11, Green Tuff/Y-6, Codola, Mercato, FL (Mount Etna), and AD472/512 (Somma-Vesuvius) tephra layers, respectively. The finding of X-5, Green Tuff/Y-6, Codola, Mercato, and AD472/512 (Somma-Vesuvius) tephras and cryptotephras in Lake Ohrid sediments document the first occurrence of these important stratigraphical markers thus far east on the Balkans and greatly enlarge their area of dispersal. Given the high number of tephra and cryptotephra layers reported in this study in combination with an age of 5-2 Myrs Lake Ohrid provides an important archive to study the dispersal of volcanic material originating from Italian sources over long distances during the Quaternary. Based on an age-model derived from tephra and cryptotephra layers as well as from seven radiocarbon datings, sedimentation at coring location Co1202 was dominated by detrital clastic material and frequent occurrences of dropstones during glacial MIS 6, 4, 3, and 2. In contrast sediments deposited during interglacial climate conditions of MIS 5 and the Holocene are characterized by high amounts of carbonate, low amounts of clastic detritus and absence of dropstones. The large number of independent stratigraphical markers, in combination with the lithological and sedimentological peculiarities makes Lake Ohrid a valuable archive for paleoenvironmental and paleoclimatological studies.

# Chapter V

## **A paleoclimate record with tephrochronological age control for the last glacial-interglacial cycle from Lake Ohrid, Albania and Macedonia**

### **Abstract**

Lake Ohrid is likely of Pliocene age and thus commonly referred to as the oldest existing lake in Europe. In this study climatic and environmental changes in the course of the last glacial-interglacial cycle are assessed using lithological, sedimentological, geochemical and physical properties of a c. 15 m long sediment succession from Lake Ohrid. The chronological framework derives from tephrochronology and radiocarbon dating and yielded a basal age of c. 136 ka. The succession is, however, not continuous and exhibits a hiatus between c. 97.6 and 81.7 ka. Sedimentation in course of the last climatic cycle is controlled by a complex interaction of various climate-controlled factors and their impact on catchment dynamics, limnology, and hydrology of the lake. Warm interglacial and cold glacial climate conditions can clearly be distinguished from organic matter, calcite, and clastic detritus contents as well as lithological peculiarities. During interglacial periods short-term fluctuations are recorded by abrupt variations in organic matter and in particular calcite contents indicating climatic induced changes in lake productivity and hydrology. During glacial periods highly variable contents of aeolian transported clastic matter are likely due to climatic forcing on catchment dynamics. In some instances tephra layers provide potential stratigraphic markers for short-lived climate perturbations and given their widespread dispersal yield the potential to link climate and environmental changes and their local impact in different records of the Mediterranean.

## 5.1. Introduction

In the past decades large ancient lakes have come into focus as favourable archives of past climatic and environmental changes over long time scales within terrestrial settings. Globally distributed examples comprise the lakes Malawi (e.g. Johnson et al. 2002), Bosumtwi (e.g. Peck et al. 2002), Baikal (e.g. Colman et al. 1998), El'gygytgyn (e.g. Melles et al. 2007), and Laguna Potrok Aike (e.g. Zolitschka et al. 2006). Situated within an active subsidence zone Lake Ohrid located in the north-eastern Mediterranean (Fig. 5-1) potentially contains a continuous sediment record back into the Pliocene. Geological and biological age estimations yielded an approximate age between five to two million years (Cvijic 1911; Stankovic 1960; Albrecht et al. 2006; Albrecht and Wilke, 2008) making it the oldest existing lake in Europe.

Given its age and geographical position at the interface of the large-scale atmospheric Hadley and Mid-Latitude cells and with a climate strongly influenced by the westerlies as well as continental and maritime factors Lake Ohrid fulfils important prerequisites for paleoclimatic studies in a climate sensitive region. Although numerous terrestrial paleoclimate records already exist in the Mediterranean region only few continuously cover the last glacial-interglacial cycle or more (e.g. Bar-Matthews et al. 2000; Martrat et al. 2004; Brauer et al. 2007; Tzedakis et al. 2006). Most studies conducted on lacustrine records focus on palynological data and reconstruction of local vegetation patterns (e.g. Follieri et al. 1989; Tzedakis et al. 2006; Tinner et al. 2009; Allen and Huntley, 2009) often with little emphasis on the sedimentary record. The sedimentary record can, however, yield important additional information on catchment dynamics, hydrology, and limnological parameters and can therefore lead to a more comprehensive picture of the impact of climatic perturbations on the environment.

A crucial prerequisite to link the impact of climatic and environmental changes in different geographical settings and thus their spatial variability is precise and accurate dating. Age determinations of lacustrine sediment sequences beyond the limit of radiocarbon dating are, however, commonly hampered due to the lack of precise and "absolute" dating techniques. Due to their "fingerprint-like" geochemical composition, morphology and mineral phases tephra layers can provide independent stratigraphical tie points, which can be used for precise correlation of different records over wide areas. Ar/Ar and K/Ar dating on mineral phases occurring in volcanic glass shards can yield radiometric controlled ages and thus provide a chronological framework for sediment records beyond the limit of radiocarbon dating. The Mediterranean region is particularly dedicated for the application of tephra layers as independent time markers since intense and perpetual volcanic activity led to widespread dispersal of pyroclastic material (ash) in the course of the Quaternary (e.g. Giaccio et al.

2008). Although various marine records have intensively been studied with respect to the occurrence of tephra layers as independent time markers over long periods (e.g. Keller et al. 1978; Paterne et al. 2008; Siani et al. 2004), comparable lacustrine terrestrial sequences are commonly lacking this information. The only such records covering, the last climatic cycle, derive from Lago Grande di Monticchio (Wulf et al. 2004; 2006; 2008; Brauer et al. 2007). More recently, tephrostratigraphical studies on sedimentary records from Lake Ohrid revealed that also this lake acts as a detailed tephrostratigraphic archive (Wagner et al. 2008a; Vogel et al. 2009), where spatial diversity of climatic and environmental variability can potentially be linked to other Mediterranean paleoclimate records from the marine and terrestrial realm.

Studies focussing on the recent response of Lake Ohrid to climatic and environmental change and anthropogenic impact have shown that the limnological parameters react sensitively to subtle changes in temperature and nutrient supply (Matzinger et al. 2006a; 2007). So far four longer records have been recovered from different parts of the lake (Roelofs and Kilham, 1983; Wagner et al. 2009; Belmecheri et al. 2009; Vogel et al. 2009). A 8.85 m long core (Core 9) recovered by Roelofs and Kilham (1983) from the northern part of the lake reaches back to c. 30 ka, but due to few and controversial radiocarbon dates and probable erosional hiatus, the chronology lacked precision. A prominent increase in productivity within "Core 9" is indicated by a shift of calcite, organic matter contents and a change in diatom assemblages and thought to represent the transition from the last glacial to the Holocene. A 10.75 m long core (Lz1120) recovered by Wagner et al. (2008a; 2009) from the north-eastern part of the lake provides a chronology based on radiocarbon dating and tephrostratigraphy and shows a basal age of c. 40 ka. Physical, sedimentological, geochemical, and biological properties were investigated and revealed strikingly different limnological, biological, and vegetation characteristics during the last Glacial and Holocene as well as short-term climate fluctuations during these periods. Core Lz1120 is, however, not continuous and comprises a hiatus between c. 14.5 and 9.4 ka and thus lacks the transition from the last Glacial to the Holocene. A 10 m long core (JO2004-1) recovered by Belmecheri et al. (2009) from the south-eastern part of the lake provides a chronology based on a sedimentation based age-depth model with contribution of radiocarbon dating and tephrostratigraphy. It covers except for a hiatus between 102.75 and 89.9 ka the last glacial-interglacial cycle back to c. 140 ka. Analyses of the calcite content and ostracod assemblages revealed that both the occurrence and/or preservation of calcite and ostracod valves are primarily restricted to interglacials at Lake Ohrid. Until today a comprehensive highly resolved investigation of Lake Ohrids sediment record, focussing on limnological and hydrological variability and changes in catchment dynamics, is so far lacking for the last glacial-interglacial cycle.

In this study lithological, sedimentological, geochemical, and physical properties are used to assess climatic and environmental changes in the course of the last glacial-interglacial cycle and back to MIS 6 using a c. 15 m long sediment record (core Co1202) from the north-eastern part of Lake Ohrid. The chronological framework of the Co1202 record is primarily based upon ten tephra and cryptotephra layers, which have been correlated to prominent, well-dated proximal deposits (Vogel et al. 2009). Although core Co1202 comprises an erosional hiatus between c. 96 and 81 kyrs BP (Vogel et al. 2009) it seems to be complete for the remaining part of the succession namely the last interglacial, the Holocene and most of the last glacial. Due to the ubiquitous occurrence of independent time markers the spatial variability of climatic and environmental change deduced from core Co1202 is compared to other records from Lake Ohrid as well as the wider Mediterranean region.

## 5.2. Site description

Lake Ohrid (41°01'N, 20°43'E; Fig. 5-1, 5-2) a transboundary lake shared by the Republics of Albania and Macedonia is situated at 693 m above sea level (a.s.l.) and surrounded by high mountain ranges reaching heights of up to 2,300 m a.s.l. The lake is c. 30 km long, c. 15 km wide and covers an area of c. 358 km<sup>2</sup>. The lake basin shows a relatively simple tub-shaped morphology with a maximum water depth of 289 m (Fig. 5-2), an average water depth of 151 m, and a total volume of 50.7 km<sup>3</sup> (Popovska and Bonacci 2007).

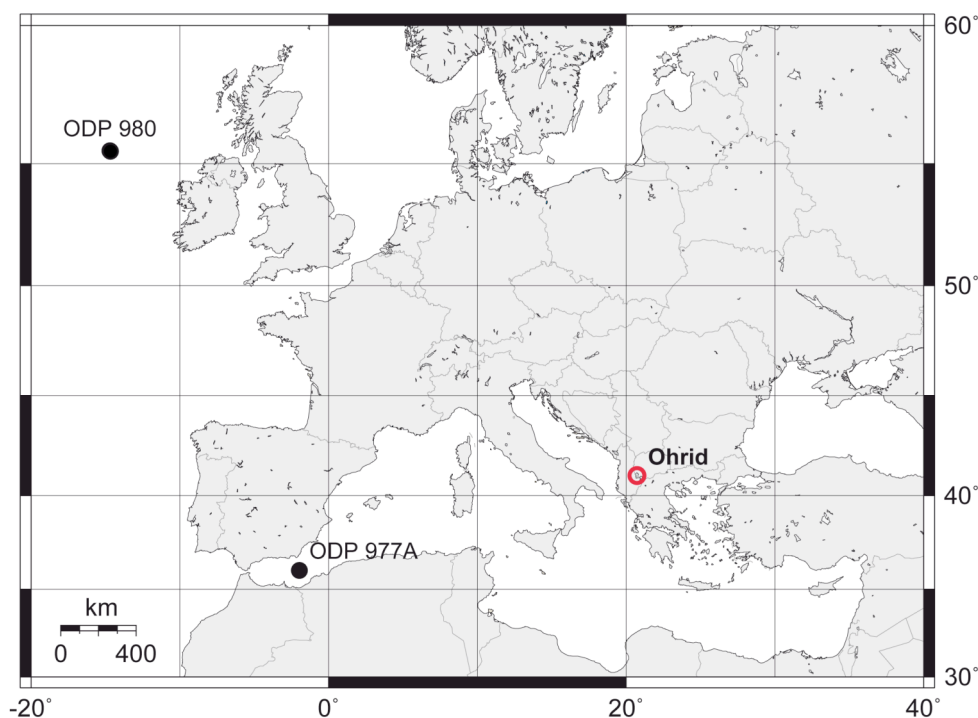


Fig. 5-1. Map showing the location of Lake Ohrid on the Balkan Peninsula in the central/northern Mediterranean. Locations of ODP sites 980 (McManus et al. 1999) and 977A (Martrat et al. 2004) referred to in the text and figures 6-8 are also shown.

The topographic watershed of Lake Ohrid comprises an area of 2,393 km<sup>2</sup> incorporating Lake Prespa, which is situated 10 km to the east of Lake Ohrid at an altitude of 848 m a.s.l.. Excluding Lake Prespa, the direct watershed of Lake Ohrid covers an area of 1,002 km<sup>2</sup> (Popovska and Bonacci 2007). Both lakes are connected via karst aquifers

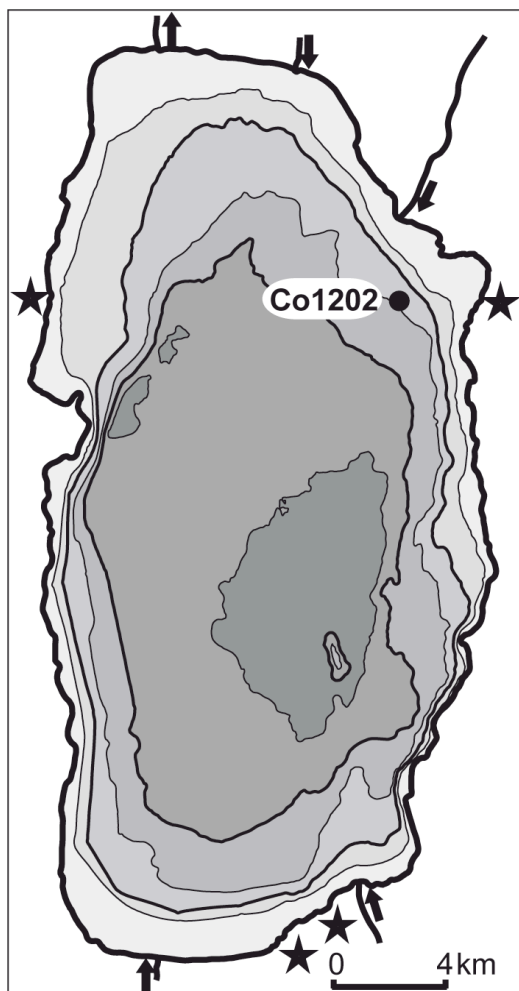


Fig. 5-2. Bathymetric map of Lake Ohrid and location of coring site Co1202. Main riverine inflows are indicated by arrows pointing towards the lake and the outlet is indicated by the arrow pointing away from it. Major subaerial spring areas are indicated by asterisks.

passing the Galicica and Suva Gora mountain range. Due to the altitudinal gradient of c. 155 m, water seeping into subaquatic sinkholes of Lake Prespa, travels through karst aquifers of the mountain range and emerges from karst springs along the eastern shore of Lake Ohrid. According to isotope and tracer investigations water emerging from these springs originates to approximately 50 % from Lake Prespa, and 50 % are charged from direct precipitation on the mountain range, which is seeping through crevasses in the karstified terrain (Anovski et al. 1992; Amataj et al. 2007; Matzinger et al. 2007). The water from these karst springs, is depleted in nutrients and minerogenic load, and contributes to c. 55 % to the net hydrologic input to Lake Ohrid. Direct precipitation on the lake surface, river- and direct surface runoff share the remaining 45 % of the hydrologic input. River Sateska, which has been diverted into Lake Ohrid in 1962, as well as the Çerava and the Koselska Rivers represent the largest riverine inflow on Macedonian territory. Riverine inflows, of notable size, on Albanian territory encompass

the rivers Pogradec and Verdova (Watzin et al. 2002). Surface outflow (60 %) through the river Crn Drim to the north and evaporation (40 %) are the main hydrologic outputs (Matzinger et al. 2006a).

Due to its sheltered position in a relatively deep valley surrounded by high mountain ranges and the proximity to the Adriatic Sea, the climate of the Lake Ohrid watershed shows both, Mediterranean and continental influences (Watzin et al. 2002). With its thermal capacity and ice-free conditions all year round Lake Ohrid serves as thermoregulating factor in the area, reducing temperature extremes. For the period between 1961-1990 an average annual air temperature of 11.1°C was registered at Ohrid meteorological station, situated close to

the north-eastern shore. Maximum temperatures never exceeded 31.5°C and minimum temperatures never fell below -5.7°C (Popovska and Bonacci 2007). In the course of the year, January is the coldest month with a mean temperature of 2.1°C and July is the warmest month with a mean temperature of 20.8°C (Watzin et al. 2002). Belonging to the Mediterranean pluviometric regime, the Lake Ohrid region shows a precipitation pattern with highest amount of precipitation during winter and lowest during summer. The average annual precipitation for the period between 1960 to 1990 on the Lake Ohrid watershed comprises 900 mm and 800 mm on the Lake Prespa watershed (Popovska and Bonacci 2007). Prevailing wind directions follow the N-S axis of the Ohrid valley.

Complete convective mixing of the water column of Lake Ohrid only takes place irregularly every seven years during severe winters when homothermy of the water body is established (Stankovic 1960; Hadzisce 1966; Matzinger et al. 2006a). Wind driven convective mixing of the superficial 150 – 200 m of the water column throughout the year is, however, supported by a lack of stratification as common for deep, temperate lakes. Despite the irregular pattern of complete overturn, it is observed that dissolved oxygen (DO) concentrations remain above 6 mg/l below 200 m water depth throughout every year (Stankovic 1960; Matzinger et al. 2007). Due to the overall low nutrient load of the hydrologic inputs, inhibited resuspension of nutrients from the sediment-water interface by incomplete and irregular mixing of the water body, and its large volume, Lake Ohrid has an oligotrophic state.

The Ohrid valley is located within an active tectonic graben system emplaced in the Western Macedonian geotectonic zone, which is part of the interior Dinaric Alps. Extensional tectonic movements during the Pliocene lead to the subsidence of the Ohrid graben zone (Aliaj et al. 2001). The beginning of lacustrine sedimentation is believed to have evolved in the early to late Pliocene 5 – 2 Ma ago (Stankovic 1960; Watzin et al. 2002). Metamorphic and magmatic rocks of Paleozoic age are exposed to the north and north-east of the valley. Strongly karstified limestones and clastic sedimentary rocks of Triassic age are exposed along the north-western, eastern, and south-eastern shorelines (Watzin et al. 2002). Ultramafic rocks and associated weathering crusts of Jurassic-Cretaceous age crop out along the south-western and western shorelines (Dilek et al. 2007). These peridotites contain chromium and iron-nickel ore deposits which have been subject to intensive mining activities (Spirkovski et al. 2001). Alluvial sediments of Pliocene age are exposed to the south and east of the lake. Quarternary lacustrine and fluvial deposits occupy the Struga and Ohrid plain to the north and the plain near Pogradec to the south (Watzin et al. 2002).

## 5.3. Materials and methods

### 5.3.1. Core recovery

Core Co1202 was recovered from the north-eastern part of the lake basin, where a hydro-acoustic survey indicated a water depth of 145 m (Fig. 5-2) and a widely undisturbed sediment succession with planar bedding and parallel reflectors. Coring was carried out from a floating platform in autumn 2007. The surface sediments and deeper sediments were collected using a 0.6 m gravity corer and a 3 m long percussion piston corer, respectively (both UWITEC Co.). The overlapping 3 m long core segments were subdivided into 1 m long segments in the field. In the laboratory the 1 m long core segments were split in two halves.

### 5.3.2. Analytical work

One of the core halves was used for high-resolution X-ray fluorescence (XRF) and magnetic susceptibility (MS) measurements. XRF-analysis was carried out using an ITRAX core scanner (COX Ltd.), equipped with a Mo-tube set to 30 kV and 30 mA and a Si-drift chamber detector. Scanning was performed at 1 mm resolution and an analysis time of 20 s per measurement. Data were smoothed using a 5 pt running mean to reduce noise. The obtained count rates for Ti, Zr, Cr, Fe, and Mn, can be used as estimates of the relative concentrations for these elements (Croudace et al. 2006). MS measurements were performed at 1 mm resolution using a Bartington system equipped with a high-resolution MS2E sensor.

The other core halve was subsampled continuously at 2 cm intervals. Aliquots of the freeze-dried subsamples were ground to a particle size below 63  $\mu\text{m}$  using a planetary mill for subsequent biogeochemical analyses. Concentrations of total carbon (TC), total nitrogen (TN), and total sulphur (TS) were measured with a Vario Micro Cube combustion CNS elemental analyzer (VARIO Co.). Samples for total organic carbon (TOC) analysis were pre-treated with HCl (10%) at a temperature of 80°C to remove carbonates and then analyzed using a Leco CS-225 carbon-sulfur detector (LECO Corp.). The amount of total inorganic carbon (TIC) was determined from the difference between TC and TOC. The calcite ( $\text{CaCO}_3$ ) content was calculated from TIC under the assumption that TIC solely originates from  $\text{CaCO}_3$ . Biogenic silica (BSi) concentrations were assessed using Fourier transform infrared spectroscopy (FTIRS) and a partial least square calibration model build upon 119 samples of core Lz1120 from the south-eastern part of the lake (Vogel et al. 2008). For a detailed description of the method and sample pre-treatment prior to analysis see Vogel et al. (2008) and Rosén et al. (2009).

Grain-size analyzes were carried out on clastic detritus. For this purpose carbonates, finely dispersed iron sulphides, organic matter, and biogenic silica were removed from the subsamples. Depending on the carbonate content of the samples 0.5 - 1 g of sediment was placed into a 100 ml centrifuge vial. Carbonates and iron sulphides were removed by adding 10% HCl to each vial, heated in a water bath to 80°C. HCl was added until the reaction was completed and samples were rinsed with deionised water (DI) to remove excess HCl and residual sulphur. Organic matter was removed by adding 30% H<sub>2</sub>O<sub>2</sub> to each vial placed in a water bath at 80°C. After 12 h samples were resuspended and H<sub>2</sub>O<sub>2</sub> was added until the reaction was completed. Subsequently samples were rinsed with DI to remove excess H<sub>2</sub>O<sub>2</sub>. Biogenic silica was removed by adding 20 ml of a 1 M NaOH solution to each vial. The suspended solution was heated to 80-85°C and shaken every 5 minutes to prevent settling of the sample. After 30 minutes the supernatant solution was removed and replaced by 20 ml of fresh 1 M NaOH. Samples were resuspended and the solution was again heated to 80-85°C and shaken every 5 minutes for 30 minutes. The supernatant solution was removed and samples were rinsed 2 times with DI to remove excess NaOH and residues. Treated samples were transferred into screw cap plastic bottles, resuspended using 20 ml of a 40 g/l Na<sub>2</sub>PO<sub>4</sub> and 7 g/l Na<sub>2</sub>CO<sub>3</sub> solution as dispersing agent, and shaken for 12 h to obtain well-dispersed clastic sediments. Subsequently the samples were placed into open beakers and 80 ml of DI and degassed water was added to reduce the relative amount of air bubbles in the suspension. Grain size distributions were measured using a Micromeritics Saturn Digisizer 5200 laser particle analyzer equipped with a Master Tech 52 multisampler. A flow rate of 10 l/min and 10 s of ultrasonic treatment resuspended the sediments and removed gas bubbles prior to detection. The laser particle analyzer uses a 1,280 x 1,024 pixel CCD detector, which enables grain-size diameter determination at c. 1 µm resolution between 0.1 – 1,000 µm. Grain size distributions are calculated from the average values of 3 runs and given as volume percentages (vol %) of the individual grain-size fractions.

The chronology of core Co1202 is based on tephrochronology (Table 5-1) and radiocarbon dating (Table 5-2) and discussed in detail in Vogel et al. (2009). The tephrochronology is based on ten encountered tephra and cryptotephra layers and their correlation to eruptions with known ages. Radiocarbon dating was performed by accelerator mass spectrometry (AMS) at the Leibniz Laboratory for Radiometric Dating and Isotope Research in Kiel, Germany. Radiocarbon measurements were conducted on bulk organic matter carbon on seven samples throughout core Co1202 (Table 5-2). According to Vogel et al. (2009) radiocarbon measurements obtained on the humic acid (HA) fraction yielded the most reliable ages and were thus used as support for the age-depth model. Radiocarbon ages for the HA of all samples were calibrated into calendar years before present (cal yrs

BP) using CalPal-2007<sup>online</sup> and the CalPal2007\_HULU calibration curve (Danzeglocke et al. 2008).

Table 5-1. Correlated depth, chemical characteristics, source, eruption and assigned ages of the ten recognized tephra and cryptotephra layers in core Co1202.

Tephra	Depth (cm)	Chemistry	Source	Eruption	Assigned age (cal. years BP)
OT0702-1	77.5-74.5	Foiditic, tephri-phonolitic	Somma-Vesuvius	AD 472, AD 512	1,460
OT0702-2	145.5-144	Benmoreitic	Etna	FL	3370 ± 70
OT0702-3	277.5-269	phonolitic	Somma-Vesuvius	Mercato	8890 ± 90
OT0702-4	620-617	Trachytic	Campi Flegrei-	SMP1-e/VRa/Y-3	30,670 ± 230
OT0702-5	696-689	Latitic, phonolitic	Somma-Vesuvius or Campi Flegrei -	Codola	34,270 ± 870
OT0702-6	752-743	trachytic to phono-trachytic	Campi Flegrei	CI/Y5	39,280 ± 110
OT0702-7	825-822	Rhyolitic to trachytic (pantelleritic)	Pantelleria	Green tuff/Y-6	49,200 ± 1100
OT0702-8	1146.5-1140	Mainly phonolitic	Unknown	X-5	101,600
OT0702-9	1232.5-1229	Mainly trachytic	Unknown	X-6	108,430
OT0702-10	1447-1440	Rhyolitic and Trachytic (comenditic, pantelleritic)	Pantelleria	P-11	131,000

Table 5-2. Radiocarbon measurements of bulk organic carbon collected at seven different depths along core Co1202. Radiocarbon ages and calendar ages inferred using CalPal-2007<sup>online</sup> (Danzeglocke et al. 2008) are given for the humic acid fraction (HA), and/or the reservoir effect corrected HA fraction.

Sample	Depth (cm)	<sup>14</sup> C age (year BP)	Corrected <sup>14</sup> C age (year BP)	Calendar age (cal. years BP)
KIA35892	74	3,145 ± 35	1,581 ± 35	1,470 ± 45
KIA36600	217.5	7,860 ± 35	6,296 ± 35	7,225 ± 35
KIA35893	230	8,645 ± 45	7,081 ± 45	7,910 ± 40
KIA35894	242	10,880 ± 60	-	12,845 ± 85
KIA36601	400	21,170 ± 200	-	25,330 ± 400
KIA36602	500	20,420 +170/-160	-	24,360 ± 340

## 5.4. Results and discussion

### 5.4.1. Lithology and lithofacies classification

Individual core segments were correlated using magnetic susceptibility (MS), x-ray fluorescence (XRF) data, and lithological core descriptions, thus leading to a composite core of 14.94 m length. The succession comprises two distinctly different Lithofacies, which can further be subdivided into sublithofacies (1a, b, c & 2a, b; Fig 5-3). In addition, ten layers comprising glass shards and micropumices of volcanic origin were identified as tephra and cryptotephra layers (OT0702-1 – 10; Vogel et al. 2009; Table 5-1; Fig. 5-3;).

Lithofacies 1 (1,494-1439, 1,064-246 cm; Fig. 5-3) appears light-grey to dark-grey and black and is mainly composed of clastic clayey-sandy silts. Frequent occurrences of coarse sand and gravel grains are interpreted as ice rafted detritus (IRD). The significant amount of clastic material is well correlated to high Ti and MS values (Fig. 5-3). MS values exhibit some lower scale fluctuations throughout Lithofacies 1 with extraordinary high MS

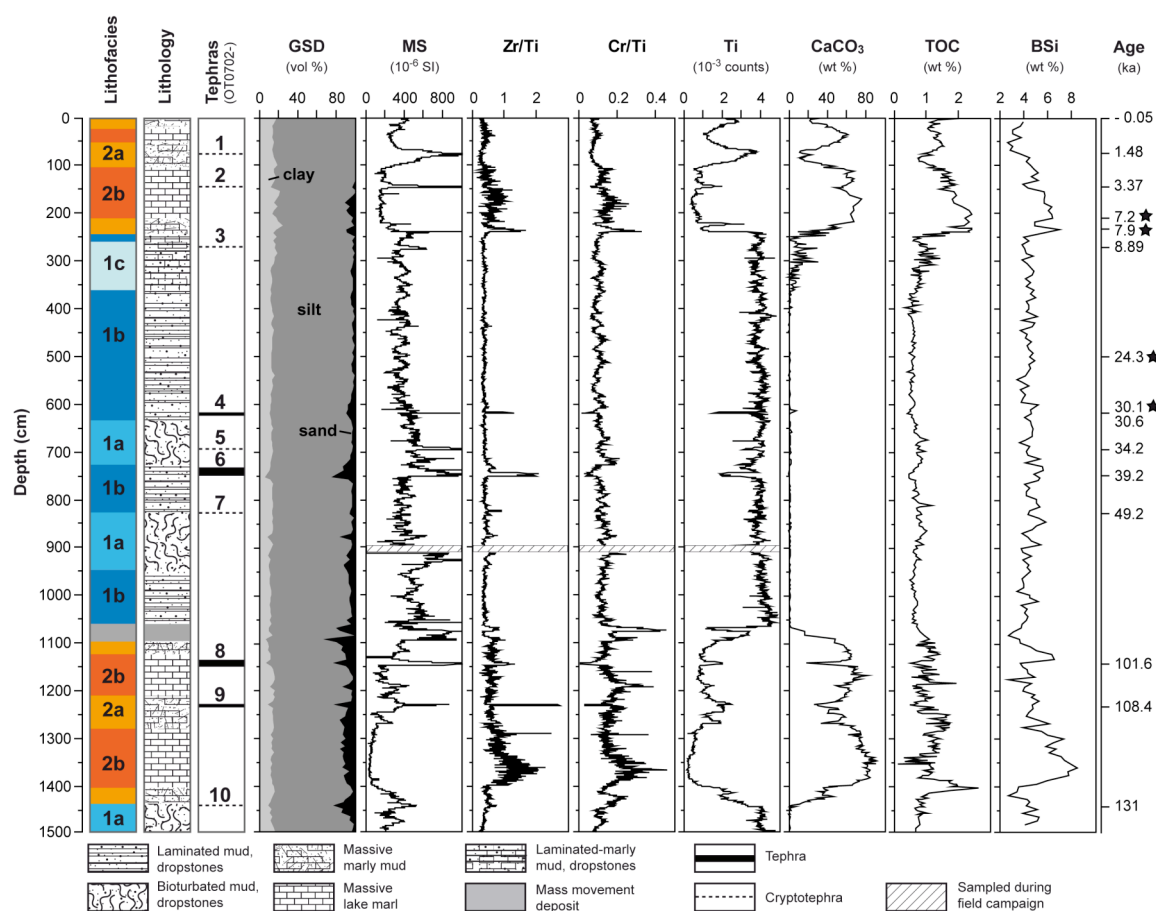


Fig. 5-3. Lithofacies, lithology, position of tephra and cryptotephra layers, grain-size distribution (GSD), magnetic susceptibility (MS), Zr/Ti, Cr/Ti ratios, Ti intensities, calcite (CaCO<sub>3</sub>), TOC, and biogenic silica (BSi) contents of core Co1202. Ages to the right of the figure are derived from correlations of tephra and cryptotephra horizons (ka) and radiocarbon dating (asterisks; cal ka BP).

values centred around 927 cm, 746 cm, 693 cm, 619 cm, and 275 cm. Ti values also show some minor fluctuations and distinct minima centred at 746, 693, and 619 cm. MS maxima at 746, 693, 619, and 275 cm as well as Ti minima at 746, 693, and 619 cm correspond to tephra (OT0702-6, 752-743 cm; OT0702-4, 620-617 cm) and cryptotephra (OT0702-5, 696-689 cm; OT0702-3, 277.5-269 cm) layers (Table 5-1; Fig. 5-3). Despite these tephra and cryptotephra layers corresponding to high MS and low Ti values, cryptotephra OT0702-10 and OT0702-7 were identified at 1,447-1,440 and 825-822 cm, respectively (Vogel et al. 2009; Table 5-1; Fig. 5-3). Carbonates are widely absent throughout Lithofacies 1 except for the section between 362 and 264 cm. The amount of finely dispersed organic matter, as also indicated by the TOC content, is relatively low throughout Lithofacies 1 but shows some lower scale variations (Fig. 5-3). Terrestrial and subaquatic plant macrofossils are absent. Poorly preserved diatom frustules occur in relatively low abundance as also indicated by low BSi concentrations (Fig. 5-3). Based on more subtle changes in sediment structure and composition Lithofacies 1 can further be divided into three sublithofacies (1a, b, c). Lithofacies 1a (1,494-1,439, 949-825, 727-634 cm; Fig. 5-3) appears dark-grey to black, massive, exhibits clear signs of bioturbation, and intermediate amounts of finely dispersed OM within Lithofacies 1. Lithofacies 1b (1,064-949, 825-727, 634-362, 264-246 cm; Fig. 5-3) appears light grey, shows irregular laminations, concretionary horizons, and the lowest amounts of OM within Lithofacies 1. Laminations show varying thicknesses of 0.5-2 mm, dark grey to dark green colours, and often occur as stacked sequences composed of several individual layers. Concretionary horizons show thicknesses of up to 2 cm, dark grey colours and often contain vivianite crystals. Lithofacies 1c (362-264 cm) appears light grey, shows irregular laminations, features highest OM contents within Lithofacies 1, and contains finely dispersed carbonates.

Lithofacies 2 (1,439 – 1,097, 246 – 0 cm; Fig. 5-3) appears either light-brown to light-grey or dark-brown to black and contains significant amounts of clay to fine-silt sized carbonates and generally low but varying amounts of clay to fine-sand sized detrital clastic material. Coarse sand and gravel is absent throughout Lithofacies 2. The significant amount of carbonates and consecutive low amounts of detrital clastic material is well documented by low Ti and MS values (Fig. 5-3). Peak MS values centred around 1,229, 1,143, 145, 76 cm correspond to tephra (OT0702-9, 1,232.5-1,229 cm; OT0702-8, 1,146.5-1,140 cm) and cryptotephra (OT0702-2, 146-144 cm; OT0702-1, 77.5-74.5 cm) (Vogel et al. 2009). Well-preserved carbonate microfossils (ostracods) are abundant, while terrestrial and subaquatic plant macrofossils are absent. The content of OM is higher if compared to Lithofacies 1 as is the amount and preservation of diatom frustules. A subdivision of Lithofacies 2 into two sublithofacies is based on colour variations along with changes of the carbonate and clastic matter content. Lithofacies 2a (1,439-1,402, 1,271-1,209, 1,122-1,095.5, 246-222, 106-52,

25 – 0 cm; Fig. 5-3) appears dark-brown to black and features lowest carbonate contents and highest amounts of clastic detritus within Lithofacies 2. Lithofacies 2b (1,402-1,271, 1,209-1,122, 222-106, 52-25 cm; Fig. 5-3) appears light brown to light-grey and features highest carbonate and lowest detrital clastic material contents within the entire sediment sequence. Despite these visible features, the amount and preservation of diatom frustules as revealed by SEM investigations and BSi values is generally higher and better, respectively, in sub-lithofacies 2b compared to sub-lithofacies 2a.

At 1,095.5-1,064 cm Lithofacies 1 and 2 are separated by a graded sandy horizon with an apparent erosive base (Fig. 5-3), such as it is characteristic for a mass-wasting deposit. Mass wasting deposits are common especially in the lateral part of the lake basin (Wagner et al. 2008b) and also might have affected core Co1202, which was recovered from a slightly inclined slope approximately 2.5 km offshore. Possible triggers for these events are either earthquakes or lake level changes or a combination of both. Thus it seems that the event, which led to the deposition of this deposit likely caused an erosional hiatus in core Co1202.

### 5.4.2. Chronology of core Co1202

The chronology of core Co1202 is based on ten tephrostratigraphic time markers (Table 5-1; Fig. 5-3, 5-4) and seven radiocarbon dates (Table 5-2; Fig. 5-3, 5-4). The year of the coring campaign (2007) was used as date for the sediment-water interface. After removal of event layers, such as discrete tephra layers at 1,232.5-1,229 cm (OT0702-9), 1,146.5-1,140 cm (OT0702-8), 752-743 cm (OT0702-6), 620-617 cm (OT0702-4), and the mass-wasting deposit at 1,095.5-1064 cm (Fig. 5-3), chronological tie points were interpolated linearly and yielded a basal age of c. 136 ka for core Co1202 (Vogel et al. 2009). Due to the erosive base of the mass movement deposit at 1,095.5-1,064 cm and unusually low sedimentation rates indicated by interpolation between OT0702-8 and OT0702-7, Vogel et al. (2009) proposed a hiatus of c. 16 kyrs between c. 97,6 - 81,7 ka (Fig. 5-3, 5-4). That assumes constant sedimentation rates below and above the event layer.

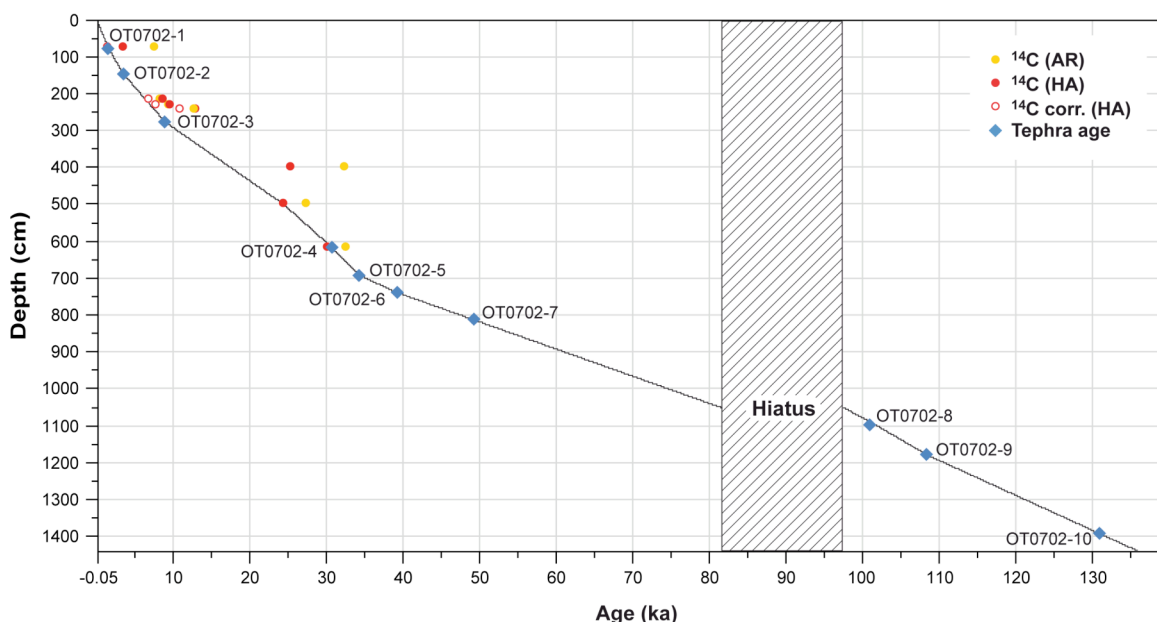


Fig. 5-4. Age-depth model for core Co1202. Ages from tephtras and cryptotephtras are indicated by blue rhombs, calibrated radiocarbon ages of the AR fraction ( $^{14}\text{C}$  AR) by yellow dots, calibrated radiocarbon ages of the HA fraction ( $^{14}\text{C}$  HA) by red dots, and reservoir effect corrected, calibrated radiocarbon ages of the HA fraction ( $^{14}\text{C}$  corr. HA) by open red dots. Evidence for the hiatus between 97.6 and 81.7 ka comes from a sandy layer with erosional base at 1,095.5 cm depth and presumed constant sedimentation rates below and above the layer.

### 5.4.3. Indicators for environmental and climatic change

#### TOC content

The TOC content represents the amount of finely dispersed OM and closely resembles the subdivision of core Co1202 into lithofacies and sublithofacies. Lithofacies 1 sediments are generally characterized by low (0.3 - 1.5 %) TOC contents (Fig. 5-3). Lowest TOC concentrations (0.3 – 0.7 %) occur in Lithofacies 1b, intermediate (0.5 - 1.2 %) in Lithofacies 1a and highest (up to 1.5%) in Lithofacies 1c (Fig. 5-3). Lithofacies 2 sediments show generally high but strongly variable (0.1 – 2.6 %) TOC contents throughout the whole Co1202 succession (Fig. 5-3).

OM found in Lake Ohrid sediments is mainly of autochthonous origin with only minor contribution from allochthonous sources (Matzinger et al. 2007; Wagner et al. 2008b; 2009) and thus strongly controlled by primary productivity in the lake. Water temperature, light availability, and nutrient supply/replenishment are the principal factors controlling productivity in Lake Ohrid today (Matzinger et al. 2006a; b; Wagner et al. 2008b; 2009). The photic zone in Lake Ohrid extends down to 40-50 m water depth, which is due to its oligotrophic state and the low amount of detrital material brought in by its tributaries (Matzinger et al. 2007). The highest quantity of nutrients delivered to Lake Ohrid today originates from its riverine inflows, which pass agricultural and/or densely populated areas (Matzinger et al. 2007). A lower but still significant quantity of nutrients is delivered by karst springs, being strongly controlled by the trophic state and water level of Lake Prespa. Modelling results have shown that nutrient input from Lake Prespa via karst aquifers is enhanced when its water level drops by 10-15 m compared to its present water level, which is due to the higher concentration of nutrients in the water body if compared to a situation when lake levels are higher (Matzinger et al. 2006b). However, a complete dessication or a significantly lowered lake level at Lake Prespa would lead to a considerably lower supply of nutrients to Lake Ohrid. Recycling of nutrients from the sediment-water interface in Lake Ohrid also contributes to the productivity.

Not only the rate of productivity but also the degree of decomposition, controlled by the concentration and replenishment of oxygen in the water column and sediments, determines the concentration of OM recorded in lake sediments. The concentration of oxygen in the water column and sediment is dependant on the mixes of the water body as well as on the uptake of oxygen during aerobic decomposition of OM. Today, the upper part of Lake Ohrid's water column down to 150 m water depth and site Co1202 is well ventilated and oxygen is continuously replenished (Matzinger et al. 2006a). Therefore, it can be assumed that the higher the flux of OM the lower the oxygen content in the water column and surface sediments and the better the preservation of OM.

### Calcite content (CaCO<sub>3</sub>)

The majority of CaCO<sub>3</sub> in Lake Ohrid sediments can be attributed to photosynthesis induced inorganic calcite precipitation (Wagner et al. 2008b; 2009; Belmecheri et al. 2009), with only minor contribution from biogenic sources such as ostracod valves (Belmecheri et al. 2009; Viehberg pers. comm.). Calcite contents match well with the subdivision of core Co1202 into two lithofacies and sublithofacies (Fig. 5-3). Sediments assigned to Lithofacies 1, with the exception of Lithofacies 1c, are characterized by negligible calcite contents (< 3%). Lithofacies 1c sediments are characterized by strongly variable calcite contents with concentrations ranging from 1 – 30 %. Lithofacies 2 sediments exhibit highest but also strongly variable calcite contents. The strong variability closely matches the subdivision of Lithofacies 2 into sublithofacies where Lithofacies 2b sediments can contain up to 90 % and Lithofacies 2a sediments as little as 10 % calcite.

Precipitation and preservation/dissolution of calcite is dependant on various physico-chemical and biogenic factors (Stumm and Morgan 1970; Wetzel 2001; Müller et al. 2006). Calcite precipitation in hard water lakes such as Lake Ohrid primarily occurs during spring-summer in the epilimnion where CO<sub>2</sub> is assimilated by photoautotrophic organisms (Gruber et al. 2000; Wetzel 2001; Matzinger et al. 2007). The rate of assimilation of CO<sub>2</sub> by photoautotrophic organisms is dependant on light availability, nutrient supply and temperature. While light availability and the supply of nutrients only influences productivity, higher temperatures lead to higher productivity as well as lower solubility of CO<sub>2</sub> in water. The removal of CO<sub>2</sub> by these mechanisms increases the pH, shifts the HCO<sub>3</sub><sup>-</sup>/CO<sub>3</sub><sup>2-</sup> equilibrium and causes calcite supersaturation, which consequently leads to precipitation of calcite as long as supply of Ca<sup>2+</sup> and HCO<sub>3</sub><sup>-</sup> ions maintains. Thus a vital factor necessary to sustain calcite supersaturation is not only the removal of CO<sub>2</sub> but also the supply of Ca<sup>2+</sup> and HCO<sub>3</sub><sup>-</sup> ions to the lake. Ca<sup>2+</sup> and HCO<sub>3</sub><sup>-</sup> ions are mainly delivered to Lake Ohrid by karstic inflows, which account for about 50% of the net hydrologic inputs today. Surface runoff and direct precipitation on the lake surface depleted in Ca<sup>2+</sup> and HCO<sub>3</sub><sup>-</sup> ions complete the hydrologic inputs to Lake Ohrid (Matzinger et al. 2006b) and dilute the lake water with respect to Ca<sup>2+</sup> and HCO<sub>3</sub><sup>-</sup> ion concentrations (Belmecheri et al. 2009). The concentration of Ca<sup>2+</sup> and HCO<sub>3</sub><sup>-</sup> ions is also modified by the rate of evaporation, which is primarily controlled by temperature and wind intensity. Concentration of the water body with respect to Ca<sup>2+</sup> and HCO<sub>3</sub><sup>-</sup> ions and thus enhanced calcite precipitation and preservation occurs when the input from karstic inflows is higher compared to the combined inputs from surface runoff and direct precipitation on the lake surface and when evaporation is strong.

Dissolution of calcite in the water column and in surface sediments is triggered by aerobic decomposition of OM. Aerobic decomposition of OM produces CO<sub>2</sub>, which is partly

converted to carbonic acid ( $\text{H}_2\text{CO}_3$ ), leading to a decrease in pH and thus dissolution of calcite. Anaerobic decomposition produces less  $\text{H}_2\text{CO}_3$  compared to aerobic decomposition of OM and thus rather promotes calcite preservation (Müller et al. 2006). The persistence of aerobic decomposition of OM is controlled by the availability and replenishment of  $\text{O}_2$  in the water column and surface sediments, which is closely linked to wind and density driven mixes of the water column as well as OM fluxes. Since Lake Ohrids water column is well ventilated throughout the year it can be assumed that most of the calcite dissolution takes place in the surface sediments, where the persistence of aerobic over anaerobic decomposition of OM is principally controlled by the accumulation rate and flux of OM.

### Grain-size distribution (GSD)

The grain-size distribution of clastic detritus in core Co1202 serves as an indicator for transport processes and energies. Fine to medium-sized silts with lower but variable contents of coarse silt represent the majority (60 - 85 vol %) within the clastic fraction. The proportion of clay (5 - 23 vol %) and sand (0 - 37 %) form the major variations in the GSD throughout core Co1202 (Fig. 5-3). Most of the sand sized clastics are fine sands (0 - 35 vol %) with only minor contribution from medium sands (< 3 vol %). Highest sand contents at 1,438, 1,229, 1,140, 752, and 617 cm correspond to tephra or cryptotephra layers, while those between 1,095.5-1,064 cm are related to a mass movement deposit (Vogel et al. 2009; Fig. 5-3). The sand content within Lithofacies 1 sediments is with some exceptions generally lower if compared to Lithofacies 2 but exhibits some low-scale fluctuations. Coarse sand and gravel, have not been quantitatively assessed, but are restricted to Lithofacies 1 sediments.

Clay and silt sized clastics in lakes can easily be transported over long distances by wind-induced or riverine currents. The transport of fine to medium-sized sand requires a different transport mechanism and/or higher transport energies. Since coring site Co1202 is situated c. 2.5 km from the nearest shore and not in close proximity to any major riverine inflow (Fig. 5-2) it can be assumed that sedimentation of fine to medium-sized sand at site Co1202 requires aeolian transport and/or significantly stronger wind-induced surface currents. Within Lithofacies 1, however, transport and deposition of coarser sand- to gravel-sized material can also derive from ice floe transport.

### Titanium (Ti)

Ti can occur in a wide range of relatively insoluble mineral phases and is therefore commonly applied as indicator for aeolian (Yancheva et al. 2007) or fluvial clastic input in lacustrine systems (Minyuk et al. 2007; Haberzettl et al. 2007). The highest Ti intensities occur within

Lithofacies 1 sediments. Within Lithofacies 2 sediments assigned to Lithofacies 2a exhibit highest and sediments assigned to Lithofacies 2b lowest Ti intensities (Fig. 5-3).

Since the majority of clastic detritus in core Co1202 are fine to medium-sized silts, and a negative correlation between the sand content and Ti intensities is indicated it can be speculated that Ti intensities in Lake Ohrid sediments are principally associated to fine-grained, clay to silt-sized clastic material and thus mainly derive from fluvial input.

#### Zirconium (Zr) and Zr/Ti ratio

Zr is regarded as relatively immobile element primarily originating from the mineral zircon, which has a high density ( $4.7 \text{ g/cm}^3$ ) and resistivity against chemical and physical weathering and thus is likely transported along with coarser grain-size fractions. To account for dilution mainly by authigenic calcite in Lithofacies 2 and 1c, Zr was normalized against Ti. Highest Zr/Ti ratios generally occur in Lithofacies 2b and in particular between 1,390-1,330 cm. Despite this general pattern peak Zr/Ti ratios at 1,230, 1,144, 825, 746, and 618 cm are related to tephra or cryptotephra layers (Vogel et al. 2009; Fig. 5-3). Lower but highly variable Zr/Ti ratios are documented for Lithofacies 1.

In previous studies Zr contents have been applied as a proxy for wind intensities and aeolian transported clastic material (Müller et al. 2001). Support for an origin mainly associated to aeolian activity of Zr in sediments of Lake Ohrid comes from the relatively close correlation of the Zr/Ti ratio with the sand content in core Co1202.

#### Chromium (Cr) and Cr/Ti ratio

Cr in sediments of Lake Ohrid likely derives from Cr ore bearing ultramafites and associated weathering profiles situated along its south-western and western shore line (Albanian geological survey 1999; Spirkovski et al. 2001). Cr intensities were normalized against Ti to account for dilution mainly by authigenic calcite (Fig. 5-3) and thus define variations of the Cr content within the clastic fraction of the sediments. Highest Cr/Ti ratios generally occur in Lithofacies 2b sediments and in particular between 1,390-1,330 cm. Lower but strongly variable Cr/Ti ratios are documented for Lithofacies 1 sediments. A relatively strong correlation with the sand content and the Zr/Ti ratio in core Co1202 implies that the Cr/Ti ratio reflects local or internal-lake variations in transport processes or energies likely related to aeolian activity rather than different redox conditions or variations in OM content, which are also known to influence Cr concentrations in lake sediment (Schaller et al. 1997; Cohen, 2003).

### Concretionary Fe/Mn horizons (Fe/Mn redox fronts)

Clearly visible concretionary horizons occurring in Lithofacies 1b (Fig. 5-3) correspond well to peak Fe and Mn intensities in core Co1202 (Fig. 5-5). Similar horizons enriched in Fe and Mn have previously been described for sites with high (up to 0.8 mm/yr) or extremely low

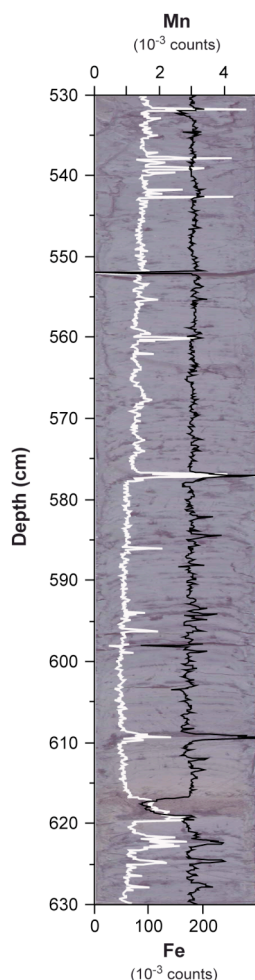


Fig. 5-5. Core photograph of the section between 630 – 530 cm showing the correlation of peak Mn (white line) and Fe (black line) intensities with concretionary horizons and laminations in core Co1202. The light red horizon between 620 – 617 cm represents tephra layer OT0702-4.

(0.02 – 0.14 mm/yr) sedimentation rates in Lake Baikal (Granina et al. 2004; Fagel et al. 2005). Since sedimentation rates during deposition of Lithofacies 1b (0.08 – 0.18 mm/yr; Fig. 5-4) are comparable to sites with low sedimentation rates at Lake Baikal, it can be assumed that concretionary horizons occurring in Lithofacies 1b at Lake Ohrid formed under similar conditions. At sites with low sedimentation rates in Lake Baikal Fe/Mn horizons today form at redox fronts 15 to 25 cm below the sediment-water interface (Granina et al. 2004; Fagel et al. 2005), hence the depth of oxygen penetration generally marks the upper boundary of the redox front (Wetzel 2001). Slow dissolution and reprecipitation causes a continuous upward movement of these concretionary horizons as long as the sedimentation regime remains constant (Granina et al. 2004). Changes in the sedimentation regime can lead to burial and preservation of these Fe/Mn horizons (Deike et al. 1997; Granina et al. 2004; Demory et al. 2005). Therefore, Fe/Mn concretionary horizons found in Lithofacies 1b sediments in core Co1202 likely represent buried paleo redox fronts and can be used as indicators for low sedimentation rates, well-oxygenated water and upper sediment column, and rapid and recurrent changes in sedimentation regime.

## 5.5. Interpretation

### 5.5.1. The penultimate glacial and transition II (c. 135.9 – 127.3 ka)

Lithofacies 1a sediments (1,494-1,439 cm; c. 135.9 -130.3 ka) denote environmental and climatic conditions of MIS 6 in core Co1202. Marginal variations in sediment composition, which is dominated by clastic detritus and only low amounts of biogenic and authigenic material (Fig. 5-6) imply a relatively stable low productivity environment between c. 135.9 and 130.3 ka.

Occurrences of coarse-grained detritus (Fig. 5-6) in sediments at site Co1202 (Fig. 5-2) require transport by ice floes. This implies that Lake Ohrid was at least partly ice covered during winter between c. 135.9 – 130.3 ka. Given that Lake Ohrid today only rarely freezes (Stankovic 1960) it can be assumed that winter temperatures have been significantly lower during the end of MIS 6, which is well supported by pollen based temperature reconstructions in the region (Allen and Huntley 2009).

The stable low productivity environment is likely a result of persisting cold climate conditions in the Mediterranean (e.g. Martrat et al. 2004; Sprovieri et al. 2006; Allen and Huntley 2009) and further implies that surface waters during spring and summer were

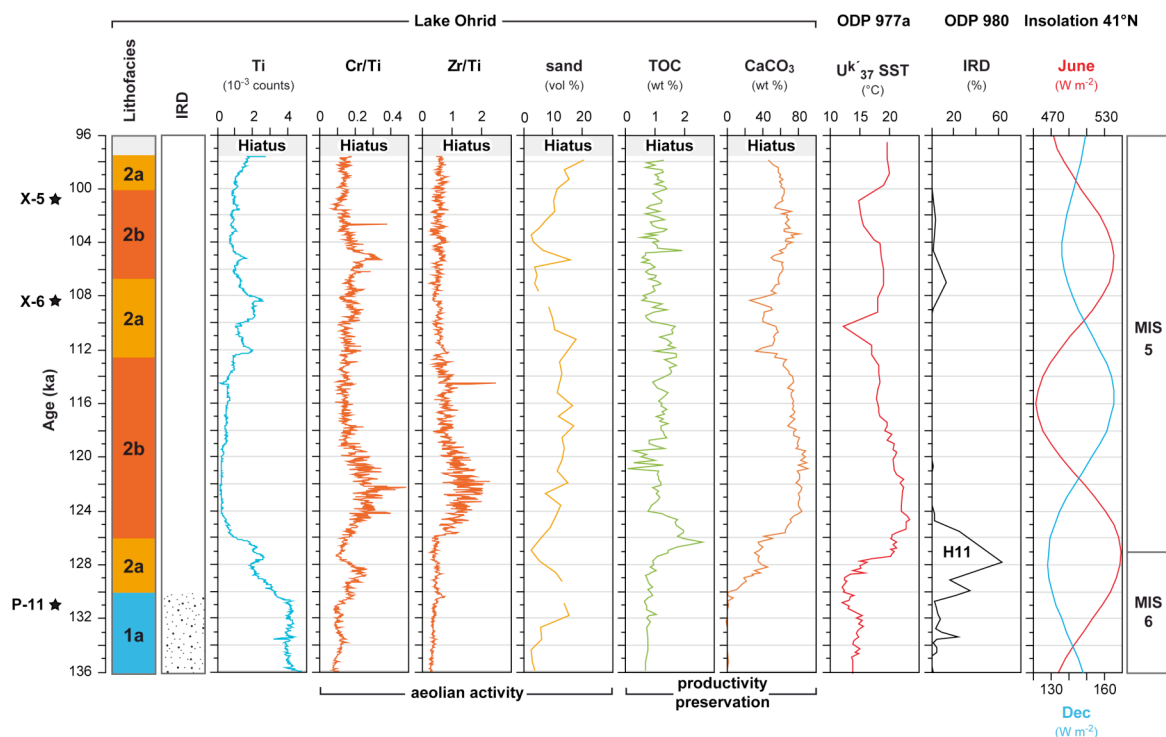


Fig. 5-6. Lithofacies, IRD occurrences, Ti intensities, Cr/Ti, Zr/Ti ratios, sand, TOC, CaCO<sub>3</sub> contents, and tephrochronological age control points (asterisks) of core Co1202 between c. 136 and 97.6 ka. Also shown are U<sup>k</sup><sub>37</sub> derived sea surface temperatures from ODP site 977a (Martrat et al., 2004), IRD contents from ODP site 980 (McManus et al., 1999), the local June and December (Dec) insolation (Berger and Loutre, 1991), and marine isotope stages (MIS; Bassinot et al., 1994). H11 = Heinrich event 11.

significantly lower. Other effects interfering productivity and preservation of OM and precipitation/dissolution of calcite are reduced supply and replenishment of nutrients, enhanced mixes of the water column, low  $\text{Ca}^{2+}$  and  $\text{HCO}_3^-$  ion concentrations and reduced water transparency. The supply of nutrients by surface runoff, rivers and via karst aquifers from Lake Prespa remains elusive for the penultimate glacial. It can, however, be speculated that nutrient supply by surface runoff and rivers was reduced due to a relatively sparse steppe-like vegetation cover in the region (e.g. Follieri et al. 1989; Tzedakis et al. 2003; Tzedakis et al. 2006; Allen and Huntley 2009), which likely resulted in poorly developed soils at Lake Ohrid. Complete mixis once or twice a year promoted by low winter temperatures would have resulted in a well-oxygenated water column and surface sediment. Enduring oxic conditions as result of a well ventilated water column and low fluxes of OM likely restricted the release of nutrients from the sediment surface (Wetzel 2001 and references therein; Wagner et al. 2009), and facilitated decomposition of OM and dissolution of calcite (Müller et al. 2006). Reduced  $\text{Ca}^{2+}$  and  $\text{HCO}_3^-$  ion concentrations can probably be explained by a combination of different interlocked processes. Sparse vegetation coverage likely suppressed the formation of soils and concomitantly the generation of humic and carbonic acids from organic litter, a necessity for the dissolution of the calcareous bedrock. Local ice caps and frozen surfaces on the surrounding mountain ranges (Belmecheri et al. 2009) probably reduced the amount of water percolating through crevasses and promoted surface runoff and erosion particularly due to pulsed spring-summer melt water discharges. Additionally, lower temperatures and a semipermanent ice cover restricted evaporation, thus leading to relatively low ion concentrations in the water column. Hence, Lake Ohrid was likely primarily fed by surface runoff and direct precipitation on its surface with only minor contribution of karst springs between c. 135.9 – 130.3 ka. This together with restricted productivity due to reduced temperatures and nutrient supply explains the relatively high amounts of clastic detritus.

An increase in the amount of fine-sand along with concomitant increases of Cr/Ti and Zr/Ti ratios between c. 134 – 127.8 ka with maximum values at c. 129 ka (Fig. 5-6) implies stronger supply of aeolian transported material and/or stronger wind induced surface currents. The timing of this increase in aeolian activity at Lake Ohrid may correspond to the interruption of North Atlantic deep-water formation associated with Heinrich Event 11 (e.g. McManus et al. 1999; Lototskaya and Ganssen 1999; Skinner and Shackleton 2006; Fig. 5-6). These Heinrich events are likely to promote a cold and dry climate in the wider region including mid-latitude Western Europe (Genty et al. 2003), the Mediterranean (Wohlfahrt et al. 2008), and northern Africa (Tjallingii et al. 2008). The cold and dry climate between c. 134 – 127.8 ka therefore may have led to sparsely vegetated soils and increased deflation at Lake Ohrid.

The transition from a stable low productivity to a more productive and unstable environment is confined within a relatively short period and represented by Lithofacies 2a sediments between 1,439-1,402 cm (Figs. 5-3, 5-6; c. 130.3 - 126.3 ka). Raising calcite contents and the absence of ice-rafted detritus (IRD) from c. 130 ka (Fig. 5-6) are indicators for the transition from cold glacial to warmer interstadial climate conditions at Lake Ohrid and seem to be roughly isochronous with other paleoclimate records in the Mediterranean (e.g. Frogley et al. 1999; Martrat et al. 2004; Drysdale et al. 2005; Brauer et al. 2007; Allen and Huntley 2009; Fig. 5-6). After a plateau-like transitional phase, which lasted until c. 127.3 ka, a rapid increase in OM content contemporaneous with a stepwise increase in calcite contents probably marks the onset of stronger productivity and Last Interglacial (LI) climate conditions at Lake Ohrid (Fig. 5-6).

### **5.5.2. The last interglacial complex (c. 127.3 – 97.6 ka)**

Sedimentation under environmental and climatic conditions of the last interglacial complex including MIS 5.5, 5.4, and 5.3 between 127.3 – 97.6 ka is characterized by Lithofacies 2 sediments (1,402 – 1,095.5 cm) with generally high contents of authigenic calcite, low amounts of clastic detritus and absence of dropstones (Fig. 5-3, 5-6). The sediment composition during MIS 5 exhibits distinct variations in clastic detritus contents, grain-size distribution, OM, and in particular calcite contents (Fig. 5-6). The distinct variability of these proxies suggests rather unstable climatic and environmental conditions.

The lack of IRD between c. 127.3 – 97.6 ka (Fig. 5-6) implies that winter temperatures were high enough to inhibit the formation of an ice-cover at Lake Ohrid. High contents of OM and in particular calcite (Fig. 5-6) indicate enhanced productivity due to increased spring-summer temperatures and/or relatively low decomposition of OM and dissolution of calcite. Decreased decomposition of OM and dissolution of calcite is likely a result of a reduced mixing and increased fluxes of OM to the sediment. Hydrological changes may have added up on the effect of a generally stronger productivity in facilitating precipitation and preservation of calcite. A denser vegetation cover in the region (Tzedakis et al. 2003) likely led to a decrease in surface runoff and erosion and promoted the formation of well-developed soils in the catchment. The decrease in surface runoff, in combination with a stronger production of humic and carbonic acid from the soils in the catchment, stronger evaporation, and increased supply of spring water probably led to higher proportions of  $\text{Ca}^{2+}$  and  $\text{HCO}_3^-$  ions contributing to the hydrological budget of Lake Ohrid during MIS 5. Overall, the calcite content during MIS 5 at Lake Ohrid primarily seems to reflect changes in temperature either through direct or indirect mechanisms and can thus tentatively be applied as temperature proxy. This is supported by a relatively close correlation of the calcite content in core Co1202 between

127.3 – 97.6 ka to the alkenone based ( $U^{K}_{37}$ ) sea surface temperature record from ODP site 977a in the western Mediterranean Sea (Martrat et al. 2004; Fig. 5-6) as well as pollen based temperature reconstructions from Lago Grande di Monticchio (Allen and Huntley 2009).

Despite the general climatic and environmental information indicating relatively warm summers and mild winters throughout the period between c. 127.3 – 97.6 ka at Lake Ohrid, variations in the calcite content point to climatic and environmental diversity. Maximum calcite contents between c. 124 – 120 ka likely represent maximum temperatures during the LI, which closely coincides with temperature reconstructions from the Western Mediterranean (Martrat et al. 2004), the Iberian margin (Martrat et al. 2007) and hydrological changes reconstructed from speleothems from central Italy (Drysdale et al. 2005), and Israel (Bar-Matthews et al. 2000; 2003). This period is furthermore characterized by high fine sand contents and maximum Cr/Ti and Zr/Ti values indicating strong supply of aeolian transported clastic detritus. Since the LI in the Mediterranean in general is supposed to be a period with warm and wet conditions (Drysdale et al. 2005; Bar-Matthews et al. 2000; 2003), with a dense vegetation cover (Frogley et al. 1999; Tzedakis et al. 2003), deflation in the catchment of Lake Ohrid is rather unlikely to explain the relatively high amounts of aeolian material. More likely, higher wind speeds promoted stronger surface currents in Lake Ohrid and thus explain the increased Cr/Ti and Zr/Ti ratios.

According to the gradually decreasing calcite contents temperatures probably decreased from c. 120 ka on at Lake Ohrid (Fig. 5-6). This pattern matches well with the gradual temperature decrease reconstructed in the Western Mediterranean (Martrat et al. 2004; Fig. 5-6), on the Iberian margin (Martrat et al. 2007), at Lago Grande di Monticchio (Allen and Huntley 2009) as well as a phase of forest opening at Ioannina (Frogley et al. 1999; Tzedakis et al. 2003) and Tenaghi Philippon (Tzedakis et al. 2003). Following this rather gradual cooling trend is a more rapid, stepwise decrease in calcite contents commencing at 114.4 ka and lasting until c. 112 ka, where a minimum (33 %) in calcite concentrations probably marks the end of LI climate conditions at lake Ohrid (Fig. 5-6).

Although the general pattern with a rapid stepwise cooling at the end of the LI corresponds well to other paleoclimate reconstructions in the Mediterranean (e.g. Tzedakis et al. 2003; Martrat et al. 2004) the timing seems to be problematic. Based on the general pattern of this period at Lake Ohrid a correlation of the abrupt cooling centred at c. 112 ka (Fig. 5-6) to Greenland stadial (GS) 25 recorded in the NGRIP ice core record (NGRIP members, 2004) and cold event C24 recorded in North Atlantic (e.g. McManus et al. 1994; Shackleton et al. 2002) and Mediterranean sediment (e.g. Martrat et al. 2004; Sprovieri et al. 2006) and speleothem (Drysdale et al. 2007) records seems feasible. The most precise age estimation for this cooling event at the end of the LI derives from U/Th dating performed on a speleothem from Antro del Corchia, northern Italy, which indicates an age of c.  $112 \pm 0.8$  for

its onset and c.  $108.8 \pm 1.0$  ka for its end (Drysdale et al. 2007). Both the general character and duration of the event recorded in the Lake Ohrid calcite record seem to correspond relatively well to GS25 and C24, the timing, but is about of c. 2 kyrs too early, which might be explained by age uncertainties in core Co1202 for this period (Vogel et al. 2009).

Between c. 111.6 – 110.2 ka increased calcite contents (>50 %) probably indicate a period of warmer climate conditions followed by another rapid stepwise cooling beginning at c. 110.2 and its minimum centred at c. 108.4 ka (Fig. 5-6). A period of warmer climate conditions following the cold event tentatively correlated to GS25 and C24 at Lake Ohrid corresponds well to a similar pattern in many other paleoclimate records in the northern Hemisphere (e.g. McManus et al. 1994; Shackleton et al. 2002; NGRIP members 2004; Sprovieri et al. 2006; Drysdale et al. 2007). The minimum in calcite content at c. 108.4 ka is relatively well constrained by the occurrence of tephra layer OT0702-9, which correlates with the marine X-6 tephra layer (Vogel et al. 2009). The age of c. 108.4 ka assigned to the OT0702-9/X-6 tephra layer derives from the varve-supported age-model from Lago Grande di Monticchio (Brauer et al. 2007). At Lago Grande di Monticchio Brauer et al. (2007) correlated a distinct decrease in arboreal pollen percentage centred around the occurrence of the X-6 tephra layer to the C24 cold event. However, Ar/Ar dating obtained on sanidine crystals of the X-6 tephra layer suggests a slightly younger age of c.  $107 \pm 2$  ka. An age of c.  $107 \pm 2$  ka for the calcite minimum at Lake Ohrid would suggest a relatively close correlation to cold events recorded in Greenland ice cores (GS24; NGRIP members, 2004), North Atlantic sediments (C23; e.g. McManus et al. 1994; Shackleton et al. 2002), and the Antro del Corchia speleothem record (Drysdale et al. 2007). The most precise age estimation for this cold event again originates from the Antro del Corchia speleothem record, where U/Th dating yielded an age of  $105.1 \pm 0.9$  ka for the onset and  $102.6 \pm 0.8$  ka for the end of the cold event. These ages are within the error of the Ar/Ar age of the X-6 tephra layer and would suggest a tentative correlation of the cooling event recorded at Lake Ohrid to GS24 and C23.

From c. 108.4 ka a rapid warming followed by a more gradual warming is indicated by raising calcite contents until c. 103.3 ka, with calcite contents reaching comparable values (>80 %) as in sediments from the LI at Lake Ohrid (Fig. 5-6). This indicates comparable climatic conditions during interstadial 5.3 and the LI at Lake Ohrid. Support for comparable climatic and environmental conditions during MIS 5.3 and the LI comes from the Lago Grande di Monticchio record where the vegetation pattern of MIS 5.3 also closely matches that of the LI (Brauer et al. 2007). From c. 103.3 ka temperatures gradually decreased again at Lake Ohrid, with calcite values falling below 50 % at c. 98 ka (Fig. 5-6). The period between c. 97.6 and 81.7 ka is due to the hiatus not documented in core Co1202 (Fig. 5-4).

### 5.5.3. The last glacial (c. 81.7 – 15 ka)

The last glacial climatic and environmental conditions between c. 81.7 and 15 ka, including MIS 4, 3, and 2, are represented by Lithofacies 1a and b sediments, which are dominated by clastic fine to medium sized silts, frequent occurrences of dropstones, low amounts of organic matter, and negligible calcite contents (Fig. 5-3, 5-7). Marginal variation in sedimentary composition indicates a relatively stable low productivity environment.

Overall, climatic and environmental conditions between c. 81.7 and 15 ka seem to have been comparable to MIS 6 at Lake Ohrid (Fig. 5-3, 5-6, 5-7). This is indicated by the occurrence of IRD throughout this succession (Fig. 5-7), indicating that the lake was at least partly ice covered during winter. Low amounts of OM and authigenic calcite (Fig. 5-7) indicate a low productivity, likely related to low spring-summer surface temperatures, reduced supply and replenishment of nutrients and  $\text{Ca}^{2+}$  and  $\text{HCO}_3^-$  ions, and facilitated decomposition of OM and dissolution of calcite by a well oxygenated water column and surface sediment. This general picture of persisting cold climate conditions at Lake Ohrid during the last glacial corresponds well to other paleoclimate reconstructions in the Mediterranean (e.g. Allen et al. 1999; Cacho et al. 1999; Bar-Matthews et al. 1999; Martrat et al. 2004; 2007).

Based on the co-occurrence of changes in the lithology and the OM contents (Fig. 5-7) low amplitude climatic and environmental variations can be inferred from the Co1202 sediment sequence. The occurrence of Fe/Mn redox fronts in combination with lowest amounts of OM in Lithofacies 1b between c. 81.6 – 66.1, c. 46.7 – 38.2, and c. 31.7 – 15 ka (Fig. 5-7) point to enhanced mixes of the water column and significantly reduced OM fluxes. Although a well-oxygenated upper sediment column can explain the formation of redox fronts in sediments of Lake Ohrid, the preservation of these fronts requires abrupt and recurrent changes of the sedimentation regime (Deike et al. 1997). Processes, which could explain these rapid changes in sedimentation regime, are probably related to variable catchment dynamics. For instance, melt water pulses originating from local snowfields and ice caps in the Lake Ohrid catchment (Belmecheri et al. 2009) could have led to abrupt and recurrent changes in sedimentation regime. Other explanations are variations in vegetation coverage and moisture supply, which are known to have been highly variable during this period in the Mediterranean (Allen et al. 1999). In contrast to Lithofacies 1b, Lithofacies 1a sediments between c. 66.1 – 46.7 and c. 38.2 – 31.7 ka are characterized by moderately increased amounts of OM and the absence of Fe/Mn redox fronts (Fig. 5-7), which suggests slightly enhanced productivity and a more stable catchment during these periods. Thus, it can be assumed that Lithofacies 1a sediments represent slightly warmer conditions with enhanced productivity and a more stable catchment. The general pattern recorded at Lake Ohrid only

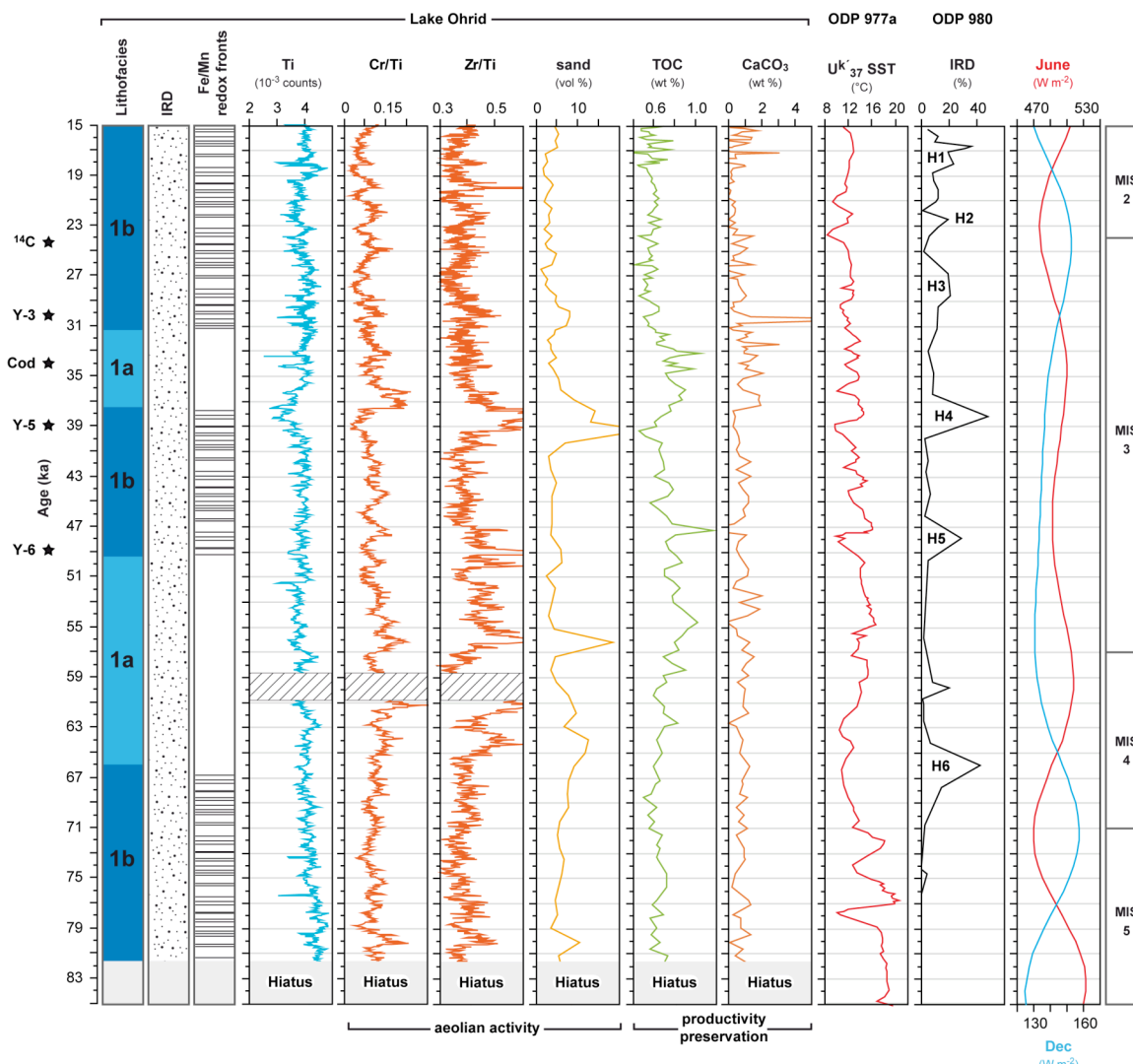


Fig. 5-7. Lithofacies, IRD occurrences, Fe/Mn redox front occurrences, Ti intensities, Cr/Ti, Zr/Ti ratios, sand, TOC, CaCO<sub>3</sub> contents, and tephrochronological age control points (asterisks) of core Co1202 between c. 81.7 and 15 ka. Also shown are  $U^k_{37}$  derived sea surface temperatures from ODP site 977a (Martrat et al., 2004), IRD contents from ODP site 980 (McManus et al., 1999), the local June and December (Dec) insolation (Berger and Loutre, 1991), and marine isotope stages (MIS; Bassinot et al., 1994). H6 – H1 = Heinrich events 6 – 1.

partly matches with coldest climate conditions during peak glacials of MIS 4 (c. 71 – 57 ka) and 2 (c. 24 – 11 ka) and slightly warmer conditions during the MIS 3 interstadial (c. 57 – 24 ka) (Bassinot et al. 1994; Fig. 5-7). It resembles, however, more closely the local summer insolation pattern (Berger and Loutre 1991) with phases of high OM contents and lacking paleo-redox fronts correlated to highest summer insolation (Fig. 5-7).

Despite these rather moderate long term climatic induced changes in productivity and catchment dynamics, short term climatic variability and its imprint on the environment at Lake Ohrid is indicated by quasi-cyclic changes in the amount of fine-sand and Cr/Ti and Zr/Ti ratios. Corresponding fine-sand and Cr/Ti, Zr/Ti maxima are centred at c. 80, 64, 62, 56, 50, 38, and 30 ka (Fig. 5-7), with the timing of the latter two periods being relatively well defined by tephra layers OT0702-6/Y-5 and OT0702-4/Y-3 (Vogel et al. 2009). These increases in

supply of coarse-grained material to site Co1202 points to stronger aeolian activity and/or enhanced deflation of dry, sparsely vegetated soils. A cold and dry climate with relatively sparse vegetation coverage in the Lake Ohrid catchment is confirmed for periods around 38 and 30 ka by a multiproxy study on core Lz1120 from the south-eastern part of the lake (Wagner et al. 2009). Wagner et al. (2009) tentatively correlated these periods of cold and dry climate conditions to Heinrich events 4 and 3. Concomitant decreases in arboreal pollen in core Lz1120 support the assumption that the increase in fine-sand sized material in core Co1202 during these periods is likely related to enhanced deflation of dry and sparsely vegetated soils. Moreover, the timing of maxima in fine-sand sized material in core Co1202 at c. 64 and 50 ka corresponds relatively well with Heinrich events 6 and 5 at c. 66 and 48 ka, respectively (e.g. McManus et al. 1999; Lototskaya and Ganssen 1999; Skinner and Shackleton 2006; Fig. 5-7). Maxima in aeolian clastic detritus occurring at c. 80, 62, and 54 ka (Fig. 5-7) indicate that cold and dry climate conditions persisted also during periods with less severe changes in Northern Hemisphere atmospheric circulation than those correlated to Heinrich events. More subtle quasi-cyclic fluctuations in the highly-resolved Cr/Ti and Zr/Ti ratios between c. 81.7 and 15 ka (Fig. 5-7) imply that climatic and environmental conditions were subject to recurrent changes throughout the last glacial at Lake Ohrid. A pattern of cyclic and recurrent changes in dust flux is also recorded in ice core records from Greenland and has been assigned to perturbations of the atmospheric circulation (e.g. Mayewski et al. 1997). Direct linkage of the pattern observed at Lake Ohrid to the pattern found in Greenland ice cores is, however, hampered by chronological uncertainties in both records.

#### **5.5.4. Transition I and the Holocene (c. 15 ka – present)**

Climatic and environmental conditions for the period from c. 15 ka to the present at Lake Ohrid are indicated by the occurrences of sediments assigned to Lithofacies 1c (362-264 cm) and b (264-246 cm) and 2a (246-222, 106-52, 25-0 cm) and b (222-106, 52-25 cm; Fig. 5-8). Based on distinct differences in sediment characteristics varying from clastic dominated sediments of Lithofacies 1b to calcite dominated sediments of Lithofacies 2b it can be assumed that climatic and concomitant environmental changes varied significantly during this period. Climatically induced variations of catchment dynamics, limnology, productivity and hydrology are expressed by changes in the grain-size distribution and in particular by strongly variable amounts of OM and calcite (Fig. 5-8).

The period from c. 14.7 to 11 ka is characterized by abundance of IRD (Fig. 5-8) indicating cold winters with at least partly ice coverage of the lake. A modest increase of OM and calcite contents from c. 14.7 ka (Fig. 5-8) implies that fluxes and preservation of OM and calcite were likely facilitated by stronger productivity due to higher spring-summer

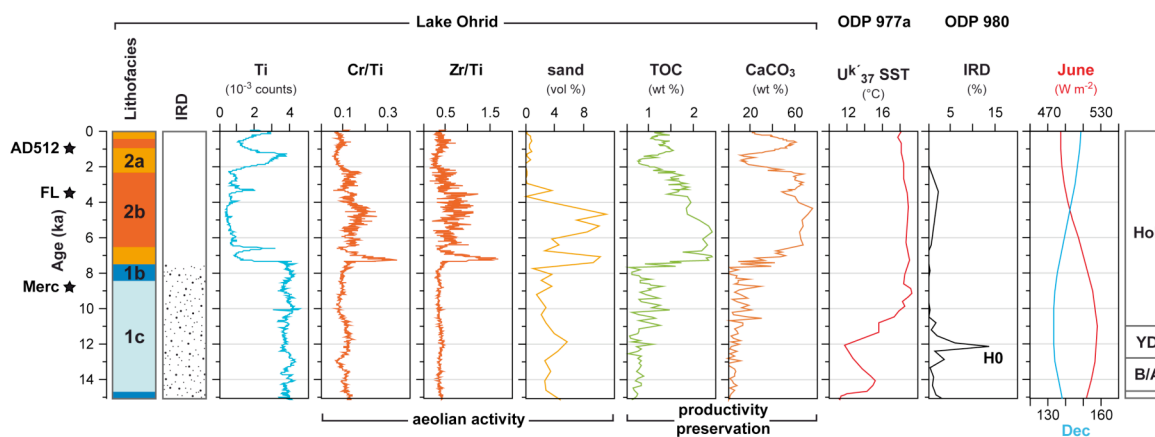


Fig. 5-8. Lithofacies, IRD occurrences, Ti intensities, Cr/Ti, Zr/Ti ratios, sand, TOC, CaCO<sub>3</sub> contents, and tephrochronological age control points (asterisks) of core Co1202 between c. 15 ka and the present. Also shown are U<sup>k</sup><sub>37</sub> derived sea surface temperatures from ODP site 977a (Martrat et al., 2004), IRD contents from ODP site 980 (McManus et al., 1999), the local June and December (Dec) insolation (Berger and Loutre, 1991), and marine isotope stages (MIS; Bassinot et al., 1994). H0 = Heinrich event 0, B/A = Bölling/Alleröd, YD = Younger Dryas, Hol. = Holocene.

temperatures. Increasing spring-summer temperatures are supported by the onset of warmer climate conditions in the Mediterranean during the Bölling/Alleröd interstadial complex (e.g. Rossignol-Strick 1995; Allen et al. 1999; Martrat et al. 2004; Bordon et al. 2008), which commenced at the same time. The subsequent cool Younger Dryas interval between c. 12.7 and 11.6 ka (e.g. Rossignol-Strick 1995; Allen et al. 1999; Martrat et al. 2004; Bordon et al. 2008), cannot be inferred with confidence from OM and calcite contents at Lake Ohrid (Fig. 5-8). However the fine-sand and Cr/Ti, Zr/Ti maxima in core Co1202 centred at c. 11.8 ka (Fig. 5-8) might be an expression of a cold but in particular dry climate at Lake Ohrid, which promoted a stronger deflation of dry and sparsely vegetated soils (Denèfle et al. 2000; Bordon et al. 2008) and aeolian supply of clastic material during the Younger Dryas.

From c. 11 ka a stepwise increase in OM and calcite contents (Fig. 5-8) probably marks the beginning of warm Holocene climate conditions at Lake Ohrid consistent with other paleoclimate reconstructions in the region (e.g. Allen et al. 1999; Sadori and Narcisi 2001; Martrat et al. 2004; Lawson et al. 2004; 2005; Bordon et al. 2008; Kotthoff et al. 2008; 2008b). It is, however, not until c. 7.5 ka that IRD disappears from the sediments of Lake Ohrid and that OM and in particular calcite contents rise to levels comparable to the LI (Fig. 5-8). Occurrences of IRD unequivocally indicate that winter temperatures were low enough to promote the formation of an ice cover at least along the shore of Lake Ohrid until c. 7.5 ka. This is in contrary to most other paleoclimate reconstructions in the region, which indicate rather mild winters during the early Holocene (e.g. Lawson et al. 2004; 2005; Bordon et al. 2008). One exception is the Lago Grande di Monticchio record where slightly colder winter temperatures are indicated for the early Holocene compared to the middle and late Holocene (Allen et al. 2002). Chronological uncertainties for the discrepancy to most other records can

be ruled out due to the occurrence of the OT0702-3 cryptotephra layer at 277.5-269 cm (Table 5-1; Fig. 5-3, 5-4, 5-8), which was unambiguously correlated to the Mercato eruption of Somma-Vesuvius (Vogel et al. 2009) dated to c. 8.9 ka (Rolandi et al. 1993; Santacroce et al. 2008). Hence, a possible explanation might be a stronger influence of cold polar air outbreaks influencing winter temperatures at Lake Ohrid between c. 11-7.5 ka. The Lake Ohrid region might have particularly been affected by these polar air masses due to its relatively northward location and the N-S trending Ohrid valley. Cold winters promoted mixing of the water column and thus facilitated decomposition of OM and dissolution of calcite as recorded by relatively low OM and calcite contents (Fig. 5-8). An additional explanation for low calcite concentrations between c. 11-7.5 ka could be a water column depleted in  $\text{Ca}^{2+}$  and  $\text{HCO}_3^-$  ions. Stronger precipitation during the early Holocene is reported by other paleoclimate studies from the northern-central and eastern Mediterranean (e.g. Aksu et al. 1999; Aritztegui et al. 2000; Sadori and Narcisi 2001; Zanchetta et al. 2007; Roberts et al. 2008; Wilson et al. 2008) and likely caused enhanced surface runoff and direct precipitation and thus led to waters depleted in  $\text{Ca}^{2+}$  and  $\text{HCO}_3^-$  ions in Lake Ohrid. A stronger contribution of surface runoff to the hydrological budget of Lake Ohrid would also explain higher amounts of clastic detritus. Based on these assumptions it can be speculated that lower OM and calcite contents in combination with IRD during the early Holocene at Lake Ohrid are an expression of cold winters, relatively warm summers, and enhanced humidity. This general climate pattern for the early Holocene at Lake Ohrid is interrupted between c. 8.3 and 7.5 ka, when OM and calcite contents drop to values comparable to the glacial period (Fig. 5-8). Whilst no differences in winter temperatures can be inferred with confidence from these proxies it seems likely that a reduction in OM and calcite contents are a result of lowered spring-summer temperatures between c. 8.3 and 7.5 ka. This phase of inferred lower spring-summer temperatures at Lake Ohrid partly overlaps with the 8.2 ka event recognized as climate deterioration in several paleoclimate records of the northern Hemisphere (e.g. Alley et al. 1997; Alley and Águstdóttir 2005) and the Mediterranean (e.g. Bordon et al. 2008; Kotthoff et al. 2008). A drop in OM and calcite concentrations concomitant with a decrease in arboreal pollen percentages occurring around 8.2 ka has also been recognized in core Lz1120 from the south-eastern part of the lake and was tentatively correlated to the 8.2 ka event (Wagner et al. 2009).

The following rapid increase in OM and calcite contents and absence of IRD from c. 7.5 ka (Fig. 5-8) indicate that spring-summer temperatures likely increased and that the lake remained ice-free during winter. A contemporaneous increase in fine sand content commencing between c. 7.3 ka and c. 6.9 ka (Fig. 5-8) indicates increasing aeolian activity. Since clearance of the local vegetation cover is not documented in the pollen record for this period from Lake Ohrid (Wagner et al. 2009) and the closer region (Bordon et al. 2008) it can

be speculated that higher wind speeds promoted stronger surface currents in Lake Ohrid. Calcite contents reach maximum concentrations comparable to the LI at c. 6.4 ka (Fig. 5-8). Since reconstructed temperatures (e.g. Martrat et al. 2004; Allen et al. 1999; Bordon et al. 2008) do not exhibit major fluctuations from c. 7.5 ka to the present it can be assumed that highest contents of calcite in Lake Ohrid between c. 6.4 and 2.4 ka are due to a generally warm but also due to drier climate conditions as also suggested by other paleoclimate reconstructions in the region (e.g. Roberts et al. 2001; 2008; Kotthoff et al. 2008). Warm and dry climate conditions would have favoured a stronger evaporation and reduced contribution of surface runoff and direct precipitation relative to the amount of water enriched in  $\text{Ca}^{2+}$  and  $\text{HCO}_3^-$  ions from karst springs. The persisting negative hydrological budget could have led to a gradual lake-level lowering and probably explains the increased amounts of fine sand between c. 5.8 to 4.3 ka (Fig. 5-8) in consequence of erosion of exposed shorelines.

A decrease in OM and calcite concentrations between c. 4.3 and 3.0 ka (Fig. 5-8), coincident with a similar decrease in core Lz1120 from the south-eastern part of the lake (Wagner et al. 2008), might indicate reduced primary productivity due to lower temperatures and/or slightly wetter climate conditions. Wetter climate conditions are, however, rather unlikely since most paleoclimate records indicate increased aridity during this period (e.g. Bar-Matthews et al. 1999; Cullen et al. 2000; Sadori and Narcisi 2001; Drysdale et al. 2006). A reduced primary productivity as a result of lower temperatures is supported by temperature reconstructions from marine records from the surrounding Adriatic (Sangiorgi et al. 2003) and Aegean Seas (Rohling et al. 2002). This cooling event is relatively well constrained at Lake Ohrid by the occurrence of the OT0702-2/FL cryptotephra (Table 5-1; Fig. 5-3, 5-4, 5-8) found in both cores Co1202 (Vogel et al. 2009) and Lz1120 (Wagner et al. 2008a) and dated to c.  $3.37 \pm 0.7$  ka (Coltelli et al. 2000).

Between c. 3.0 and 2.4 ka calcite contents rise again to levels comparable to the preceding period while OM contents remain relatively low (Fig. 5-8). Low OM contents during this period could be due to enhanced mixis as also indicated for the same period in core Lz1120 from the south-eastern part of the lake (Wagner et al. 2009) rather than reduced productivity, which would have also strongly affected calcite precipitation. A rapid decrease in both OM and calcite contents commencing at c. 2.4 ka (Fig. 5-8) is coeval with anthropogenic deforestation in the catchment of Lake Ohrid (Wagner et al. 2008). Deforestation likely led to stronger contribution of  $\text{Ca}^{2+}$  and  $\text{HCO}_3^-$  depleted surface runoff to the hydrological budget and promoted enhanced erosion in the catchment. This might explain lower calcite concentrations and higher amounts of clastic detritus between c. 2.4 and 1.0 ka in the Co1202 sediment succession. Lower amounts of OM might be due to enhanced mixis and decomposition (Wagner et al. 2009) and/or lower productivity. A combination of low  $\text{Ca}^{2+}$  and  $\text{HCO}_3^-$  ion concentrations, enhanced decomposition, and lower

productivity may also explain lower calcite concentrations in the sediment. Adding up on the effects of anthropogenic induced catchment erosion could be a generally wetter climate during this period in the Mediterranean such as suggested by climate reconstructions from Greece (Frogley et al. 2001) and Spain (Martín-Puertas et al. 2009). The late Holocene OM and calcite minimum is relatively well constrained by the OT0702-1 cryptotephra (Table 5-1; Fig. 5-3, 5-4, 5-8;), which comprises a mixed population of the AD 472 and AD 512 eruptions of Somma-Vesuvius (Vogel et al. 2009).

OM and calcite contents rise again from c. 1,000 yrs and drop again until c. 100 yrs (Fig. 5-8). The peak in OM and calcite contents centred at 800 yrs (Fig. 5-8) might result from enhanced productivity forced by increased nutrient input from Lake Prespa (Wagner et al. 2009). This increase of nutrient supply via karst aquifers from Lake Prespa is likely to have occurred when historical settlements from the 11<sup>th</sup> and 12<sup>th</sup> century AD indicate a 6 m lower lake-level of Lake Prespa than today (Matzinger et al. 2006b). The lake-level lowering of Lake Prespa further implies a more arid climate after c. 1,000 yrs. Hence, the relatively high amounts of calcite between c. 1,000 and 300 yrs (Fig. 5-8) in core Co1202 could additionally be a result of stronger evaporation and lower contribution of surface runoff and direct precipitation to the hydrological budget of Lake Ohrid. Rapid environmental changes for the period from c. 1,000 yrs to the present might be the expression of climate and concomitant environmental changes of the “Medieval Warm Period” and the following “Little Ice Age” (Wagner et al. 2009). However, it cannot be excluded that the anthropogenic activities during the late Holocene (Wagner et al. 2009) overprinted the natural climate variability.

## 5.6. Conclusions

Based on sedimentological and geochemical studies on sediment core Co1202 from the north-eastern part of Lake Ohrid climatic variability and their imprint on the local hydrology, limnology, and catchment dynamics were reconstructed qualitatively for the last climatic cycle and back to MIS 6. The chronology is based on tephrostratigraphy and radiocarbon dating. One hiatus recorded between c. 96 and 81 ka is most likely due to a mass-wasting event. Sedimentary characteristics differ significantly between glacial and interglacial stages at Lake Ohrid during the last c. 136 kyrs. In particular climatic control on the hydrological budget, catchment dynamics, and limnology seem to primarily control sedimentation and support the outcome of earlier studies, which indicated that Lake Ohrid is a relatively complex system.

Penultimate (MIS 6, c. 136-127.3 ka) and last glacial (MIS 4, 3, 2; c. 81-11 ka) settings at Lake Ohrid, seem to have been relatively similar and were characterized by cold climate conditions and a relatively stable low productivity environment. Low winter temperatures with at least seasonal ice coverage of the lake are confined by occurrences of IRD. An extremely low productivity environment and relatively stable ultraoligotrophic conditions within the lake during glacial periods are evidenced through persisting low OM and negligible calcite contents and a sediment composition dominated by clastic detritus. Despite this general pattern subtle long-term, climatic induced environmental changes are indicated through the appearance and disappearance of Fe/Mn redox fronts, in combination with concomitant shifts of the OM content. Based on these proxies coldest conditions are inferred for the periods between c. 81.6 – 66.1, 46.7 – 38.2, and 31.7 – 15 ka and slightly warmer conditions for the periods between c. 66.1 – 46.7 and 38.2 – 31.7 ka at Lake Ohrid. Quasi-cyclic fluctuations in fine-sand contents and Cr/Ti and Zr/Ti ratios were assigned to variations in the supply of aeolian transported material to the lake. Increased influx of aeolian material was likely a result of particularly cold and dry climate conditions, which led to increased erosion of dry and sparsely vegetated soils around c. 129, 64, 50, 38, 30, and 11.8 ka. These periods can tentatively be correlated to Heinrich events 11, 6, 5, 4, 3, and 0, respectively.

Climatic and environmental conditions of the last interglacial complex (MIS 5.5, 5.4, 5.3; c. 127.3 – 96 ka) and Holocene (c. 11 ka – present) at Lake Ohrid are characterised by elevated OM and calcite contents, thus indicating enhanced productivity and preservation primarily due to elevated spring-summer temperatures, strong input of water from karst springs, and relatively strong supply and replenishment of nutrients. Winter temperatures, however, seem to have been relatively low during the early Holocene (c. 11-7.5 ka) such as indicated by the occurrence of IRD. It is suggested that the early Holocene between c. 11 to

6.5 ka was characterized by relatively humid climate conditions at Lake Ohrid. Several short-termed events during the interglacials seem to be recorded in the proxies. Distinct drops in calcite contents indicate cooling events during the last interglacial complex centred at c. 112 and c. 108.4 ka and were tentatively correlated to North Atlantic cooling events C24 and C23, respectively. Distinct drops in OM and calcite during the Holocene point to short-term cooling events around c. 8.0 and c. 3.8 ka. Climatic and environmental variability is probably blurred by significant anthropogenic impact on the catchment at Lake Ohrid from c. 2.4 ka to the present.

Overall, it can be concluded that Lake Ohrids sediments sensitively record long and short termed climatic and environmental changes and that variations in sediment composition are generally isochronous at different locations within the lake basin. Therefore, the sediment record of Lake Ohrid provides an excellent archive of climatic and environmental variability in the northern Mediterranean. Climatic and environmental changes deduced from the Co1202 sediment record are in general well correlated to other records in the Mediterranean and the northern Hemisphere but owing to the spatial variability of this climatically complex region also exhibits some local peculiarities.

# **Chapter VI**

**Summary, critical review, and outlook**

## 6.1. Part I: Fourier transform infrared spectroscopy (FTIRS)

The first part of the thesis work dealt with the application of FTIRS as potential analytical alternative for quantitative inference of biogeochemical properties in lacustrine sediment. Applications of FTIRS were tested on several lacustrine sediment successions originating from a wide diversity of localities. The results clearly demonstrate that FTIRS is an analytical tool capable of enabling rapid and cost-efficient analysis of biogeochemical properties from lacustrine sediment using only small samples (Vogel et al. 2008; Rosén et al. 2009). Comparison with conventionally measured concentrations yielded good reproducibility with respect to general trends and absolute values for both, site-specific calibrations (Lakes Ohrid and El'gygytgyn; Vogel et al. 2008) and calibrations made using a 94 lake surface sediment sample dataset from northernmost Sweden (Rosén et al. 2009). FTIRS can therefore represent a powerful analytical alternative for the quantitative inference of biogeochemical properties in lacustrine sediment, particularly when large numbers of samples need to be analysed.

Although the results presented by Vogel et al. (2008) and Rosén et al. (2009) are promising, the method needs further development to overcome some critical limitations. One major limitation of the FTIRS technique is due to complications caused by overlapping absorption bands that can result from the mixture of a large number of components. As a consequence, probably only major sediment components or those with narrow absorption bands can be assessed quantitatively using FTIRS. Quantitative inference of certain sediment components might be confounded by other components, such as carbonates, showing strong absorption bands in various parts of the mid infrared region (Vogel et al. 2008). This problem can in some cases be dealt with if only compound specific wavenumbers are selected for the calibration model (Rosén et al. 2009). Another option could be additional sample pretreatment prior to FTIRS analyses, which might give the opportunity to also infer concentrations of minor sediment components. Additional sample pretreatment could, however, cancel out important advantages of FTIRS over conventional analytical techniques.

Even though the FTIRS calibrations on a surface sediment set yielded reasonable estimates for biogeochemical property concentrations (Rosén et al. 2009), site-specific calibrations might be more appropriate in some instances. Site-specific calibration models are more likely to cover the full range of the property concentrations of interest within that particular site, which might not be the case if a calibration from another site or region is applied. Therefore for longer sediment records, originating for instance from ICDP deep drilling projects, with cores exceeding several hundred meters in length to be analyzed, the creation of a site-specific "internal calibration" (Vogel et al. 2008) is recommended. Since

FTIRS has only been applied to a relatively small number of lakes so far, it might still be prudent to crosscheck the accuracy of the FTIRS results by using conventional methods.

A site-specific, internal FTIRS calibration has successfully been applied to infer BSi concentrations on >1,600 samples from a c. 16 m long sediment succession from Lake El'gygytyn, NE Siberia (core Lz1024; Melles et al. submitted; Cunningham et al. in preparation a; b). The Lz1024 record spans the last 340 kyrs and thus represents the longest terrestrial paleoclimate record from the Arctic. Of the proxies investigated, BSi, primarily originating from well-preserved diatom frustules in Lake El'gygytyn sediments, represents one of the most promising indicators for past climatic and environmental change (Melles et al. submitted). This is because diatoms are the main primary producers in Lake El'gygytyn and diatom productivity at high latitudes is strongly controlled by factors directly or indirectly related to temperature. FTIRS inferred BSi already contributed significantly to the outcome of three studies, which emphasize the uniqueness of Lake El'gygytyn as paleoclimate archive and provide important new insights on climate variability over the past 340 kyrs in the Arctic, one of the key regions of the global climate system (Melles et al. submitted; Cunningham et al. in preparation a; b; Fig. 6-1).

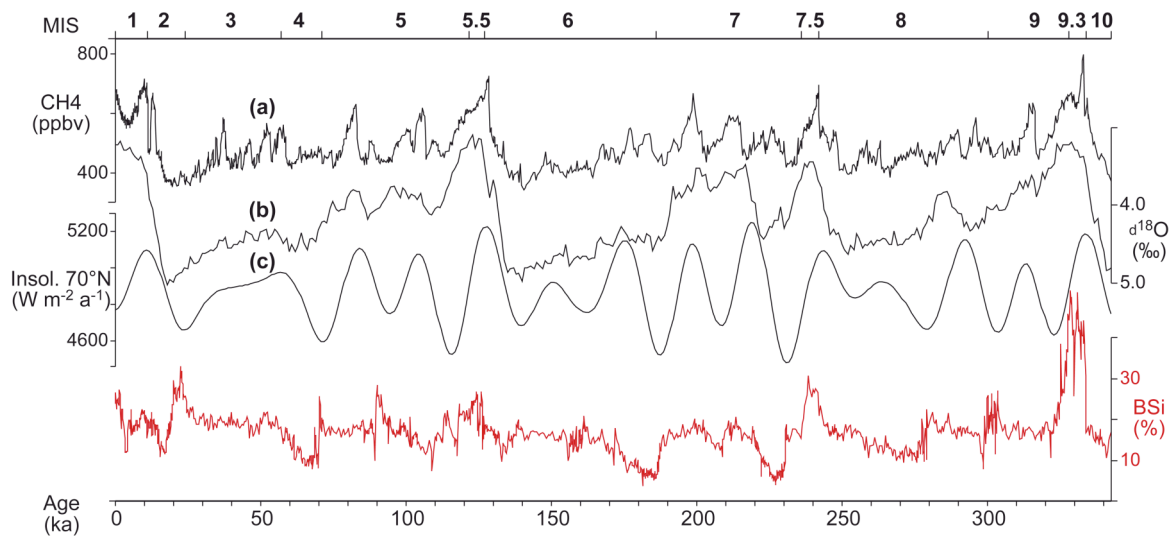


Fig. 6-1. Modified after Melles et al. (submitted). Comparison of FTIRS inferred BSi (red) from Lake El'gygytyn, NE Siberia, for the past 340 kyrs, with published paleoclimate data: (a) Methane (CH<sub>4</sub>) concentrations in the EPICA Ice Core, Antarctica (Loulergue et al. 2008); (b) Stable oxygen isotope stack LR04 from benthic marine foraminifera (Lisiecki and Raymo 2005); (c) Annual insolation pattern for 70°N (Berger and Loutre 1991). MIS = marine isotope stages.

FTIRS has further been applied to a long sediment record from Lake Pingualuit (N Canada), spanning the past 250 kyrs (Cunningham et al. unpublished data). FTIRS is currently being applied to assess concentrations of biogeochemical properties on sediment cores from successfully completed ICDP deep drilling campaigns at Laguna Potrok Aike (S Argentina) and Lake El'gygytyn, which led to the recovery of sediment successions reaching back c. 80 (B. Zolitschka, personal communication) and c. 3,600 kyrs (M. Melles,

personal communication), respectively. The technique is also likely to be applied to long sediment records recovered during the envisaged ICDP campaign at Lake Ohrid. Biogeochemical data assessed using FTIRS in combination with other techniques will therefore help to enable decipherment of climatic and environmental information contained in these valuable paleoclimate archives.

In addition to the FTIRS applications presented by Vogel et al. (2008) and Rosén et al. (2009), it might be possible to further refine the method so that additional sediment components can be identified qualitatively and perhaps also assessed quantitatively. In previous studies it has been shown that quantitative information on mineral phases, such as quartz, feldspar, and kaolinite can potentially be inferred from FTIR spectra (Bertaux et al. 1998; Wirmann and Bertaux 2001). Moreover, qualitative identification of humic materials in sediment is possible from FTIR spectra (Braguglia et al. 1995; Belzile et al. 1997; Calace et al. 1999). Thus future developments of FTIRS in paleolimnology could aim on the development of quantitative inferences of these minerogenic and organic sediment components using FTIR spectral information.

More work is required to establish FTIRS as a stand-alone analytical technique in paleolimnology. For instance, there is a need to develop independent calibration models, as current FTIRS calibrations are limited by the precision of conventional analytical methods. This strong dependence of current FTIRS models (Vogel et al. 2008, Rosén et al. 2009) on conventional methods for calibration causes the accuracy of FTIRS to be reduced relative to conventional methods. One approach to overcome this predicament might be the establishment of FTIRS calibrations based on synthetic sediment mixtures. This approach could potentially lead to an increase in accuracy of FTIRS calibrations for major sediment components such as BSi and calcite but most importantly it would make FTIRS applications more independent from conventional methods.

## **6.2. Part II: Lake Ohrid's sediment record**

The primary focus of the second part of this thesis was the evaluation of Lake Ohrid's sediment record as an archive for the dispersal of tephra and climatic and environmental changes over the last glacial-interglacial cycle. A sediment succession covering the last glacial-interglacial cycle was not, however, available at the University of Cologne and partner institutions at the beginning of the project. Therefore the planning and execution of a field campaign to recover new sediment successions from Lake Ohrid formed an important component of the thesis work. Investigations conducted on the new material successfully recovered in 2007 (core Co1202), in combination with data gathered from earlier studies, clearly highlight Lake Ohrid's potential as important and valuable archive for tephra dispersal

(Wagner et al. 2008b; Vogel et al. 2009) and climatic and environmental change (Wagner et al. 2009; Vogel et al. submitted) over longer time scales in the northern Mediterranean region.

An important prerequisite necessary for the interpretation of information contained in lacustrine sediment archives is a thorough understanding of recent processes controlling sedimentation. Sedimentation in the Lake Ohrid basin is controlled by a complex interaction of multiple processes, which consequently result in a distinct spatial heterogeneity in the composition of surface sediments (Fig. 6-2). This spatial heterogeneity is associated with differences in catchment configuration, inflow from karst springs, and anthropogenic influences. Despite distinct spatial differences, Lake Ohrid appears to have reacted uniformly to climatic forcing on changes in catchment configuration, limnology and hydrology over the past 40 ka as evidenced by contemporaneous changes in sediment composition in cores Lz1120 and Co1202 (Vogel et al. submitted; Fig. 1-4, 6-3). Although both sites differ with respect to the surrounding catchment characteristics, water depth, and sediment accumulation rate (Wagner et al. 2009; Vogel et al. submitted), patterns of important sediment components (TOC,  $\text{CaCO}_3$ ) over the past 40 ka are remarkably similar (Fig. 6-3). Minor discrepancies between cores Lz1120 and Co1202 with respect to TOC and  $\text{CaCO}_3$  concentrations, in particular during the early Holocene, can potentially be explained by differential chronologies for cores Lz1120 and Co1202, mass wasting events, and slightly different hydrological and limnological boundary conditions. Some of these factors might have been amplified by significant environmental change during the early Holocene (Wagner et al. 2009, Vogel et al. submitted).

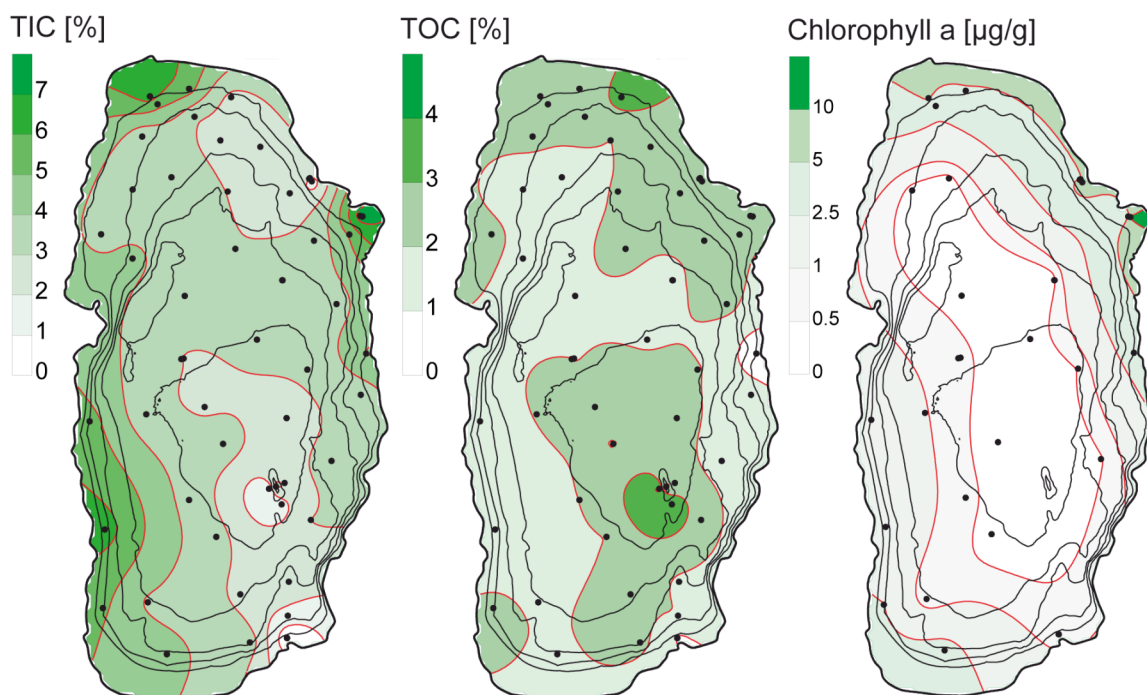


Fig. 6-2. Bathymetric map of Lake Ohrid showing the spatial heterogeneity of TIC, TOC, and chlorophyll a concentrations in surface sediments (uppermost 2 cm). Black dots indicate sampling sites.

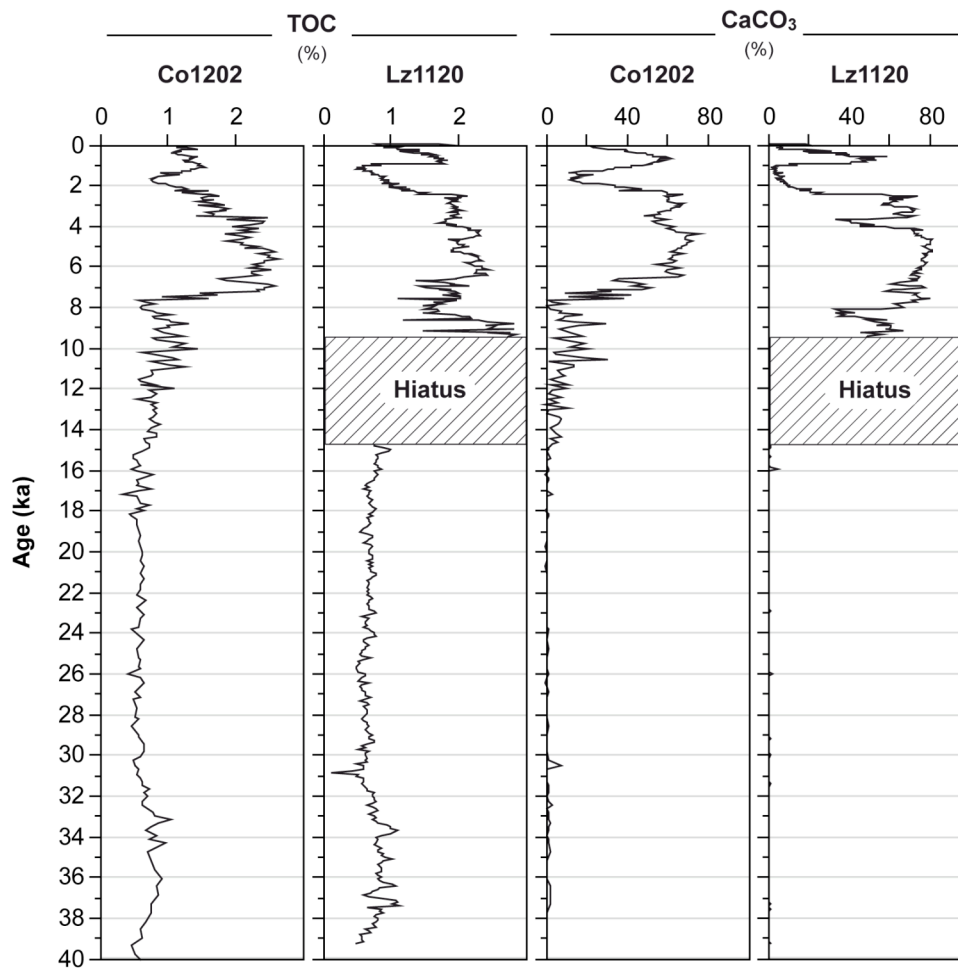


Fig. 6-3. Comparison of TOC and  $\text{CaCO}_3$  concentrations in cores Co1202 (Vogel et al. 2009; submitted) and Lz1120 (Wagner et al. 2008b; 2009) for the past 40 ka. The period between 14.6-9.4 ka is due to a Hiatus not documented in core Lz1120. Coring sites Co1202 and Lz1120 are shown in Fig. 1-4.

The finding of ten tephra and cryptotephra layers in Lake Ohrid sediments of the last glacial-interglacial cycle and their successful correlation to eruptions of Italian volcanoes provided important new data on the area of dispersal of these volcanic products (Vogel et al. 2009). Volcanic material is easily detectable in sediments of Lake Ohrid either through macroscopic inspection or by application of XRF scanning techniques (Vogel et al. 2009). This, in combination with the fact that tephra and cryptotephra layers ubiquitously occur in its sediments, proves that Lake Ohrid can become the “Rosetta Stone” in Mediterranean tephrostratigraphy. Since the age of tephra and cryptotephra layers can be determined using radiometric methods, such as Ar/Ar and K/Ar dating, they provide important independent chronological tie points essential for the establishment of a age-depth relationship for sediments of Lake Ohrid. This is particularly crucial since radiocarbon dating is limited to the past c. 50 ka and has proven to be a rather inadequate method for the establishment of a reliable chronological framework for sediments in the deeper parts of the basin (Vogel et al. 2009). Other dating approaches to be tested in cooperation with partner institutions include paleomagnetism (N. Nowaczyk, GFZ Potsdam, Germany), ESR, IRSL (A. Hilgers, University of Cologne, Germany), and U/Th (N.N.).

Based on the tephrochronological framework of core Co1202 (Vogel et al. 2009) and various analyses conducted on this sediment succession, conclusions on climatic and environmental change and their impact on catchment dynamics, limnology, and hydrology of the lake have been drawn. The interplay of climatic forced factors has varied significantly in the course of the last glacial-interglacial cycle and led to distinctly different sediment characteristics during glacial and interglacial phases at Lake Ohrid. Interglacial sediments commonly appear as calcareous mud and glacial sediments are dominated by clastic material. Despite this general pattern tied to high amplitude climate fluctuations, short-term climatic fluctuations of reduced amplitude are also recorded in the sediment succession (Vogel et al. submitted). A quantitative inference of climate fluctuations in terms of absolute temperatures, precipitation, and changes of the vegetation in the region has not yet been possible using the proxies investigated (Wagner et al. 2009; Vogel et al. submitted). However, based on the detection of subaquatic terrace levels it seems likely that pronounced climate fluctuations in the past had substantial impact on the hydrological budget of the lake and led to significant lake level lowering (Fig. 6-4). Ongoing analyses and dating of the sediments recovered from these subaquatic terrace levels (cores Co1200 and Co1201; Fig. 1-4, 6-4) may thus provide a more quantitative estimate on the magnitude of past climatic change. In addition, analysis of supplemental proxies allowing a more quantitative estimate on past climatic and environmental change is desirable and currently under way.

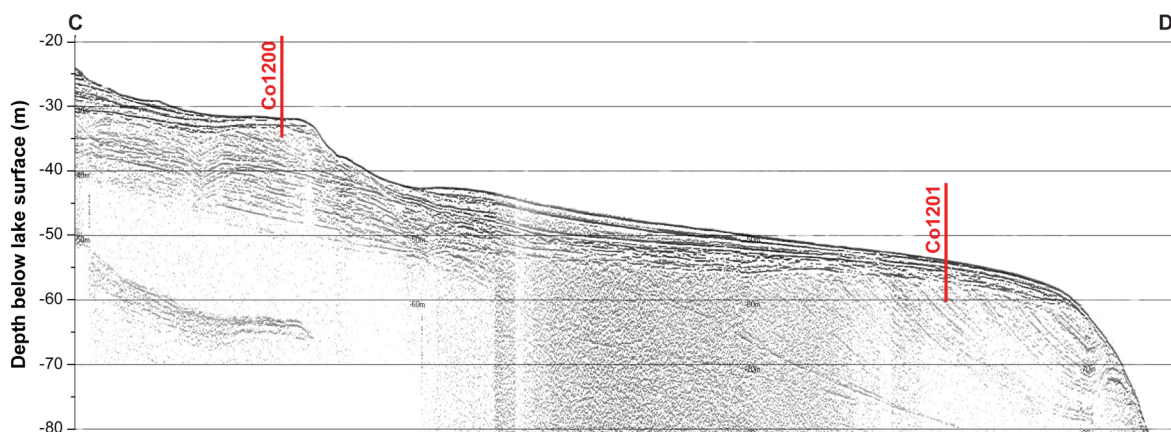


Fig. 6-4. NE-SW trending hydroacoustic profile from the Bay of Ohrid showing two subaquatic terrace levels. The location and penetration depths of cores Co1200 and Co1201 are also indicated. Letters (C) and (D) refer to the beginning and end of the profile indicated in Fig. 1-4.

Ongoing proxy analyses of sediments from core Co1202 focus on pollen (A. Lotter, University of Utrecht, The Netherlands), diatoms (J. Reed, University of Hull, UK), ostracods (A. Schwalb et al., University of Braunschweig, Germany), stable isotopes (M.J. Leng, NERC, UK), and a variety of organic geochemical proxies (H. Vogel, University of Cologne, Germany; S. Schouten, NIOZ, The Netherlands; T. Wagner, University of Newcastle, UK; J. Holtvoeth, University of Liverpool, UK). Despite the common difficulties, which also accompany interpretation of these proxies, a more comprehensive picture of the magnitude

of past climatic fluctuations in the Lake Ohrid region can be expected. Diatom and ostracod transfer functions might for instance yield information on the trophic state, water temperature, pH, and salinity of Lake Ohrid in the past. Pollen and pollen based transfer functions may provide a tool for the reconstruction of the local vegetation as well as temperatures and precipitation. Stable isotope ( $\Delta^{18}\text{O}$ ,  $\Delta^{13}\text{C}$ ) measurements on authigenic calcite might help to infer past variations of the influence of the karst springs and hydrological balance of the lake. Organic geochemical proxies provide a wide array of applications. One of the most promising applications is the analysis of fossil membrane lipids biosynthesized by crenarchaeota for the reconstruction of past lake surface temperatures (Schouten et al. 2002). Laboratory studies have shown that the number of cyclopentane rings in these membrane lipids, the glycerol dialkyl glycerol tetraethers (GDGTs), is strongly dependant on water temperature, whilst other factors, such as nutrients and salinity, are found to be negligible (Wuchter et al. 2004). An index derived from tetraethers consisting of 86 carbon atoms ( $\text{TEX}_{86}$ ) has been proposed as means to quantify the relative abundance of GDGTs and hence can be used as a surface water paleotemperature proxy (Schouten et al. 2002; Powers et al. 2004; Kim et al. 2008).

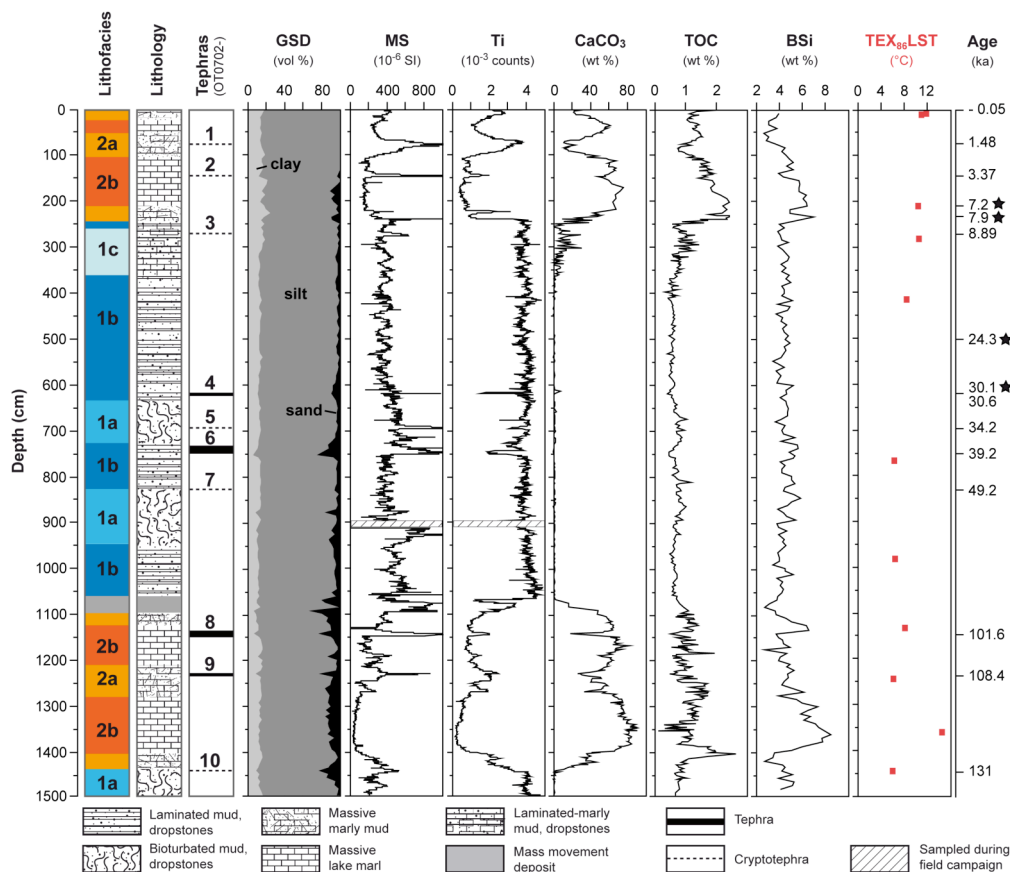


Fig. 6-5. Modified after Vogel et al. (submitted). Lithofacies, lithology, occurrence of tephras, and selected physical and geochemical properties of core Co1202.  $\text{TEX}_{86}$  test measurements reveal a temperature anomaly of ca. 5-6 $^{\circ}\text{C}$  between glacial and interglacial periods. The warmest temperature is reconstructed for the last interglacial. Ages are based on radiocarbon dating (asterisks) and on tephrostratigraphy.

With a water depth of 289 m and a relatively small amount of water supply from the catchment, Lake Ohrid has revealed to be an ideal target for the application of the TEX<sub>86</sub> paleothermometer (Blaga et al. 2008). This is supported by initial TEX<sub>86</sub> test measurements carried out on 11 samples from core Co1202, which yielded very promising results, with c. 5-6°C lower temperatures in the glacial compared with the interglacial periods (Fig. 6-5). The reconstructed glacial and interglacial temperatures from Lake Ohrid correspond relatively well with temperature anomalies derived from sea surface temperature reconstructions in the marine (-4°C) and pollen-based temperature reconstructions in the terrestrial (-9°C) vicinity (Fig. 6-6). Currently ongoing TEX<sub>86</sub> analysis on >190 additional samples will complement the initial data set and will thus yield a high-resolution inference of absolute temperature variations in course of the last glacial-interglacial cycle at Lake Ohrid. In lacustrine systems the origin of the TEX<sub>86</sub> signature is, however, not completely decoded. Therefore a thorough study of the parameters influencing the temperature signal at Lake Ohrid will substantially improve the worldwide applicability of this proxy in lacustrine environments and will significantly contribute to establish Lake Ohrid as reference site for paleoclimatic reconstructions in the northern Mediterranean region. Such a study is planned and funded for the coming two years and commences in autumn 2009.

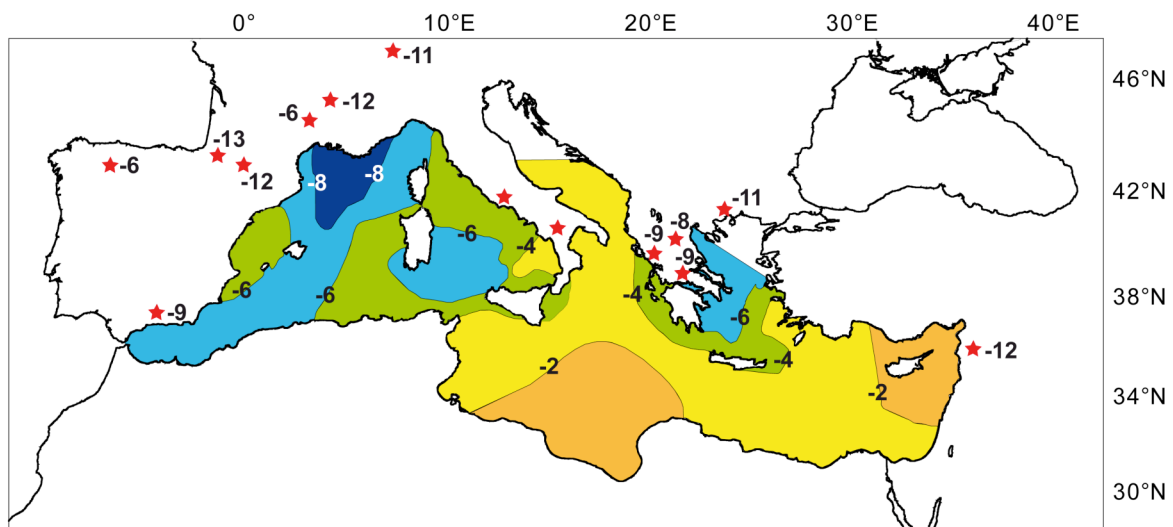


Fig. 6-6. Reconstructed temperature anomalies in the Mediterranean region between the Last Glacial Maximum (LGM) and today. Annual summer sea surface temperature anomalies are based on foraminiferal transfer functions (Hayes et al. 2005). Asterisks indicate sites of pollen-based temperature estimations (Peyron et al. 1998).

## References

- Aksu AE, Abrajano T, Mudie PJ, Yasar D (1999) Organic geochemical and palynological evidence for terrigenous origin of the organic matter in Aegean Sea sapropel S1. *Marine Geology* 153:303-318
- Albanian geological survey (1999) Geological and mineral deposit map of Albania 1:200,000.
- Albrecht C, Trajanovski S., Kuhn K, Streit B, Wilke T (2006) Rapid evolution of an ancient lake species flock: Freshwater limpets (Gastropoda: Ancyliidae) in the Balkan Lake Ohrid. *Organisms Diversity & Evolution* 6:294-307
- Albrecht C, Wilke T (2008) Ancient Lake Ohrid: biodiversity and evolution. *Hydrobiologia* 615:103-140
- Allen JRM, Brandt U, Brauer A, Hubberten H-W, Huntley B, Keller J, Kraml M, Mackensen A, Mingram J, Negendank JFW, Nowaczyk NR, Oberhänsli H, Watts WA, Wulf S, Zolitschka B (1999) Rapid environmental changes in southern Europe during the last glacial period. *Nature* 400:740-743
- Allen JRM, Watts WA, McGee E, Huntley B (2002) Holocene environmental variability – the record from Lago Grande di Monticchio, Italy. *Quaternary International* 88:69-80
- Allen JRM, Huntley B (2009) Last Interglacial palaeovegetation, palaeoenvironments and chronology: a new record from Lago Grande di Monticchio, southern Italy. *Quaternary Science Reviews* 28:1521-1538
- Alley RB, Ágústsdóttir AM (2005) The 8k event: cause and consequences of a major Holocene abrupt climate change. *Quaternary Science Reviews* 24:1123-1149
- Alley RB, Mayewski PA, Sowers T, Stuiver M, Taylor KC, Clark PU (1997) Holocene climatic instability: a prominent, widespread event 8200 yr ago. *Geology* 25:483-486
- Aliaj S, Baldassarre G, Shkupi D (2001) Quaternary subsidence zones in Albania: some case studies. *Bulletin of Engineering Geology and the Environment*, 59:313-318
- Amataj S, Anovski T, Benischke R, Eftimi R, Gourcy LL, Kola L, Leontiadis I, Micevski E, Stamos A, Zoto J, (2007) Tracer methods used to verify the hypothesis of Cvijic about the underground connection between Prespa and Ohrid Lakes. *Environmental Geology* 51, 749-753
- Anovski T, Andonovski B, Minceva B (1992) Study of the hydrological relationship between Lake Ohrid and Prespa. *Proceedings of Symposium on Isotope Techniques in Water Resources Development*. IAEA, Vienna, Austria, March 1991
- An Zhisheng, Ai Li, Song Yougui, Colman SM (2006) Lake Qinghai Scientific Drilling Project. *Scientific Drilling* 2:20-22

- Aritztegui D, Asioli A, Lowe JJ, Trincardi F, Vigliotti L, Tamburini F (2000) Palaeoclimate and the formation of Sapropel S1: inferences from Late Quaternary lacustrine and marine sequences in the central Mediterranean region. *Palaeogeography, Palaeoclimatology, Palaeoecology* 158:215-240
- Asikainen CA, Francus P, Brigham-Grette J (2007) Sedimentology, clay mineralogy and grain-size as indicators of 65 ka of climate change from El'gygytgyn Crater Lake, Northeastern Siberia. *Journal of Paleolimnology* 37:105-122
- Ayuso RA, De Vivo B, Rolandi G, Seal RR, Paone A (1998) Geochemical and isotopic (Nd–Pb–Sr–O) variations bearing on the genesis of volcanic rocks from Vesuvius, Italy. *Journal of Volcanology and Geothermal Research* 82:53-78
- Bar-Matthews M, Ayalon A, Kaufman A, Wasserburg G (1999) The eastern Mediterranean paleoclimate as a reflection of regional events: Soreq Cave, Israel. *Earth and Planetary Science Letters* 166:85-95
- Bar-Matthews M, Ayalon A, Kaufmann A (2000) Timing and hydrological conditions of Sapropel events in the Eastern Mediterranean, as evident from speleothems, Soreq cave, Israel. *Chemical Geology* 169:145-156
- Bar-Matthews M, Ayalon A, Gilmour M, Matthews A, Hawkesworth CJ (2003) Sea-land oxygen isotopic relationships from planktonic foraminifera and speleothems in the eastern Mediterranean region and their implication for paleorainfall during interglacial intervals. *Geochimica et Cosmochimica Acta* 67:3181-3199
- Bard E, Delaygue G, Rostek F, Antonioli F, Silenzi S, Schrag D (2002) Hydrological conditions over the western Mediterranean basin during the deposition of the cold Sapropel 6 (ca 175 kyr BP). *Earth and Planetary Science Letters* 202:481-494
- Barnekow L (2000) Holocene regional and local vegetation history and lake-level changes in the Torneträsk area, northern Sweden. *Journal of Paleolimnology* 23:399-420
- Bassinot FC, Labeyrie LD, Vincent E, Quidelleur X, Shackleton NJ, Lancelot Y (1994) The astronomical theory of climate and the age of the Brunhes-Matuyama magnetic reversal. *Earth and Planetary Science Letters* 126:91-108
- Battarbee RW (2000) Palaeolimnological approaches to climate change with special regard to the biological record. *Quaternary Science Reviews* 19:107-124
- Belmecheri S, Namiotko T, Robert C, von Grafenstein U, Danielopol DL (2009) Climate controlled ostracod preservation in Lake Ohrid (Albania, Macedonia). *Palaeogeography, Palaeoclimatology, Palaeoecology* 277:236-245
- Belzile N, Joly HA, Li H (1997) Characterization of humic substances extracted from Canadian lake sediments. *Canadian Journal of Chemistry* 75:14-27

- Ben Tiba B, Reille M (1982) Recherches pollenanalytiques dans les montagnes de Kroumirie (Tunisie septentrionale), premières résultats. *Ecologia Mediterranea* 7:75-86
- Bengtsson L, Enell M (1986) Chemical analysis. In Berglund, B. E. (ed.), *Handbook of Holocene Palaeoecology and Palaeohydrology*. John Wiley & Sons Ltd., Chichester, 423–451
- Berger A, Loutre MF (1991) Insolation values for the climate of the last 10 million years. *Quaternary Science Reviews* 10:297-317
- Bertaux J, Ledru M-P, Soubié F, Sondag F (1996) The use of quantitative mineralogy linked to palynological studies in paleoenvironmental reconstruction: the case study of the “Lagoa Campestre” lake, Salitre, Minas Gerais, Brazil. *C.R. Académie Scientifique Paris*, 323 (Series II):65-71
- Bertaux J, Fröhlich F, Ildefonse P (1998) Multicomponent analysis of FTIR spectra: Quantification of amorphous and crystallized mineral phases in synthetic and natural sediments. *Journal of Sedimentary Research* 68:440-447
- Bigler C, Hall, RI (2002). Diatoms as indicators of climatic and limnological change in Swedish Lapland: A 100-lake calibration set and its validation for paleoecological reconstructions. *Journal of Paleolimnology* 27:97-115
- Birks HJB (1998) Numerical tools in palaeolimnology - Progress, potentialities, and problems. D.G. Frey and E.S. Deevey Review #1. *Journal of Paleolimnology* 20:307-332
- Blaga CI, Reichert G-J, Heiri O, Sinnighe Damsté JS (2008) Tetraether membrane lipid distributions in water-column particulate matter and sediments: a study of 47 European lakes along a north–south transect. *Journal of Paleolimnology* 41:523–540
- Bordon A, Peyron O, Lézine A-M, Brewer S, Fouache E (2009) Pollen-inferred Late-Glacial and Holocene climate in southern Balkans (Lake Maliq). *Quaternary International* 200:19-30
- Bottema S, Sarpaki A (2003) Environmental change in Crete, a 9000-year record of Holocene vegetation history and the effect of the Santorini eruption. *The Holocene* 13:733-749
- Braguglia CM, Campanella L, Petronio BM, Scerbo R (1995) Sedimentary humic acids in the continental margin of the Ross Sea (Antarctica). *International Journal of Environmental Analytical Chemistry* 60:61-70
- Brauer A, Endres C, Günter C, Litt T, Stebich M, Negendank JFW (1999) High resolution sediment and vegetation responses to Younger Dryas climate change in varved lake sediments from Meerfelder Maar, Germany. *Quaternary Science Reviews* 18:321-329
- Brauer A, Mingram J, Frank U, Günter C, Schettler G, Wulf S, Zolitschka B, Negendank JFW (2000) Abrupt environmental oscillations during the Early Weichselian recorded at Lago Grande di Monticchio, southern Italy. *Quaternary International* 73/74:79-90

- Brauer A, Allen JRM, Mingram J, Dulski P, Wulf S, Huntley B (2007) Evidence for last interglacial chronology and environmental change from Southern Europe. *Proceedings of the National Academy of Sciences* 104:450-455
- Brigham-Grette J, Melles M, Minyuk P (2007) Overview and significance of a 250 ka paleoclimate record from El'gygytyn Crater Lake, NE Russia. *Journal of Paleolimnology* 37:1-16
- Brigham-Grette J, Melles M, Minyuk P, Koeberl C, Science Party (2009) Lake El'gygytyn's emerging IPY record of Pliocene to recent Arctic change. *PAGES* 1:19-21
- Buttner R, Dellino P, Raue H, Sonder I, Zimanowski B (2006) Stress-induced brittle fragmentation of magmatic melts: Theory and experiments. *Journal of Geophysical Research* 111:B08204
- Cacho I, Grimalt JO, Pelejero C, Canals M, Sierro FJ, Flores JA, Shackleton N (1999) Dansgaard-Oeschger and Heinrich Event Imprints in Alboran Sea Paleotemperatures. *Paleoceanography* 14:698-705
- Calace N, Capolei M, Lucchese M, Petronio BM (1999) The structural composition of humic compounds as indicator of organic carbon sources. *Talanta* 49:277-284
- Calace N, Cardellicchio N, Petronio BM, Pietrantonio M, Pietroletti M (2006) Sedimentary humic substances in the northern Adriatic sea (Mediterranean sea). *Marine Environmental Research* 61:40-58
- Calanchi N, Cattaneo A, Dinelli E, Gasparotto G, Lucchini F (1998) Tephra layers in Late Quaternary sediments of the Central Adriatic Sea. *Marine Geology* 149:191-209
- Chang C-W, You C-F, Huang C-Y, Lee T-Q (2005) Rapid determination of chemical and physical properties in marine sediments using a near-infrared reflectance spectroscopic technique. *Applied Geochemistry* 20:1637-1647
- Cioni R, Marianelli P, Santacroce R. (1997) Thermal and compositional evolution of the shallow magma chambers of Vesuvius: evidence from pyroxene phenocrysts and melt inclusions. *Journal of Geophysical Research* 103:18277-18294
- Civetta L, Cornette Y, Gillot PY, Orsi G (1988) The eruptive history of Pantelleria (Sicily Channel) in the last 50 ka. *Bulletin of Volcanology* 50:47-57
- Civetta L, Orsi G, Pappalardo L, Fisher RV, Heiken G, Ort M (1997) Geochemical zoning, mingling, eruptive dynamics and depositional processes - the Campanian Ignimbrite, Campi Flegrei caldera, Italy. *Journal of Volcanology and Geothermal Research* 75:183-219
- Cohen AS, Soreghan MJ, Scholz CA (1993) Estimating the age of formation of lakes; an example from Lake Tanganyika East African Rift system. *Geology* 21:511-514
- Cohen, AS (2003) *Paleolimnology. The history and evolution of lake systems.* Oxford University Press, New York. 500 pp

- Colman SM, Peck JA, Karabanov EB, Carter SJ, Bradbury JP, King JW, Williams DF (1995) Continental climate response to orbital forcing from biogenic silica records in Lake Baikal. *Nature* 378:769-771
- Coltelli M, Del Carlo P, Vezzoli L (2000) Stratigraphic constraints for explosive activity in the past 100 ka at Etna volcano, Italy. *International Journal of Earth Sciences* 89:665-677
- Colthup NB, Daly LH, Wiberley SE (1990) *Introduction to Infrared and Raman spectroscopy*. Academic Press, San Diego
- Comas MC, Zahn R, Klaus A, et al. (1996) ODP Proceedings, Initial Reports 161. College Station, Texas, USA (Ocean Drilling Program).
- Conley DJ (1998) An interlaboratory comparison of the measurement of biogenic silica in sediments. *Marine Chemistry* 63:39-48
- Conley DJ, Schelske CL (2001) Biogenic silica. In: Smol JP, Birks HJB, Last WM (eds). *Tracking environmental change using lake sediments*. Volume 3: Terrestrial, algal, and siliceous indicators. Kluwer Academic Publishers, Dordrecht, pp 281-293
- Cornette Y, Crisci GM, Gillot PY, Orsi G (1983) Recent volcanic history of Pantelleria: a new interpretation. *Journal of Volcanology and Geothermal Research* 17:361-373
- Croudace IW, Rindby A, Rothwell RG (2006) ITRAX: description and evaluation of a new multi-function X-ray core scanner. In: Rothwell, R.G. *New Techniques in Sediment Core Analysis*. Geological Society, London, Special Publications, 267:51-63
- Cullen HM, de Menocal PB, Hemming S, Hemming G, Brown FH, Guilderson T (2000) Climate change and the collapse of the Akkadian empire: evidence from the deep sea. *Geology* 28:379-382
- Cunningham L, Vogel H, Persson P, Rosén P (in preparation a) Climatic warming during Transition 4 may be greater than previously thought: evidence from the biogenic silica record of Lake El'gygytgyn.
- Cunningham L, Vogel H, Persson P, Rosén P (in preparation b) Paleoclimate records from Lake El'gygytgyn supports climatic variability during the last interglacial.
- Cvijic J (1911) L'ancien Lac Égéen. *Ann Geogr* 20:233-259
- Danzeglocke U, Jöris O, Weninger B (2008) CalPal-2007online. <http://www.calpal-online.de/>, accessed 2008-07-21
- De Beaulieu J-L, Andrieu-Ponel V, Reille M, Grüger E, Tzedakis C, Svoboda H (2001) An attempt at correlation between the Velay pollen sequence and the Middle Pleistocene stratigraphy from central Europe. *Quaternary Science Reviews* 20:1593-1602
- Dehnert A (2004) Rezente Sedimentation im El'gygytgyn See, NO-Sibirien, abgeleitet aus der Zusammensetzung von Oberflächensedimenten [recent sedimentation in Lake El'gygytgyn, NE-Siberia, inferred from the composition of surface sediments].

- Diploma Thesis (Diplomarbeit). Leipzig, Germany: Institute for Geophysics and Geology, University of Leipzig
- Deike RG, Granina L, Callender E, McGee JJ (1997) Formation of ferric iron crusts in Quaternary sediments of Lake Baikal, Russia, and implications for paleoclimate. *Marine Geology* 139:21-46
- DeMaster DJ (1981) The supply and accumulation of silica in the marine environment. *Geochimica et Cosmochimica Acta* 45:1715-1732
- Demory F, Oberhänsli H, Nowaczyk NR, Gottschalk M, Wirth R, Naumann R (2005) Detrital input and early diagenesis in sediments from Lake Baikal revealed by rock magnetism. *Global and Planetary Change* 46:145-166
- Denèfle M, Lézine AM, Fouache E, Dufaure JJ (2000) A 12,000 year pollen record from Lake Maliq, Albania. *Quaternary Research* 54:423-432
- De Vivo B, Rolandi G, Gans PB, Calvert A, Bohrsen WA Spera FJ, Belkin HE (2001) New constraints on the pyroclastic eruptive history of the Campanian volcanic Plain (Italy). *Contributions to Mineralogy and Petrology* 73:47-65
- Digerfeldt G, Olson S, Sandgren P (2000) Reconstruction of lake-level changes in Lake Xinias, central Greece, during the last 40,000 years. *Palaeogeography, Palaeoclimatology, Palaeoecology* 158:65-82
- Dilek Y, Furnes H, Shallo M (2007) Suprasubduction zone ophiolite formation along the periphery of Mesozoic Gondwana. *Gondwana Research* 11:453-475
- Di Vito M, Sulpizio R, Zanchetta R, D'Orazio M (2008) The late Pleistocene pyroclastic deposits of the Campanian Plain: new insights on the explosive activity of Neapolitan volcanoes. *Journal of Volcanology and Geothermal Research* 177:19-48
- Drysdale R, Zanchetta G, Hellstrom JC, Fallick A, Zhao J-X (2005) Stalagmite evidence for the onset of the Last Interglacial in southern Europe at  $129 \pm 1$  ka. *Geophysical Research Letters* 32
- Drysdale R, Zanchetta G, Hellstrom J, Maas R, Fallick A, Pickett M (2006) Late Holocene drought responsible for the collapse of old world civilizations is recorded in an Italian cave flowstone. *Geology* 34:101-104
- Drysdale RN, Zanchetta G, Hellstrom JC, Fallick AE, McDonald J, Cartwright I (2007) Stalagmite evidence for the precise timing of North Atlantic cold events during the early last glacial. *Geology* 35:77-80
- Dumurdzanov N, Serafimovski T, Burchfiel BC (2004) Evolution of the Neogene-Pleistocene basins of Macedonia: Geological Society of America. Digital Map and Chart Series 1 (accompanying notes), 20 p. <http://gsamaps.gsjournals.org/gsamaps/toc>

- Ehrmann W, Schmiedl G, Hamann Y, Kuhnt T, Hemleben C, Siebel W (2007) Clay minerals in late and Holocene sediments of the northern and southern Aegean Sea. *Palaeogeography, Palaeoclimatology, Palaeoecology* 249:36-57
- Fagel N, Alleman LY, Granina L, Hatert F, Thamo-Bozso E, Cloots R, André L (2005) Vivianite formation and distribution in Lake Baikal sediments. *Global and Planetary Change* 46:315-336
- Farmer VC (1974) *The infrared spectra of minerals*. Mineralogical Society Monograph 4, London
- Follieri M, Magri D, Sadori L (1989). Pollen stratigraphical synthesis from Valle di Castiglione (Roma). *Quaternary International* 3/4:81-84
- Fuji N (1988) Palaeovegetation and palaeoclimate changes around Lake Biwa, Japan during the last ca. 3 million years. *Quaternary Science Reviews* 7:21-28
- Franz SO, Schwark L, Brüchmann C, Scharf B, Klingel R, Van Alstine JD, Çagatay N, Ülgen UB (2006) Results from a multi-disciplinary sedimentary pilot study of tectonic Lake Iznik (NW Turkey) – geochemistry and paleolimnology of the recent past. *Journal of Paleolimnology* 35:715-736
- Fritz SC, Baker PA, Seltzer GO, Ballantyne A, Tapia P, Cheng H, Edwards RL (2007) Quaternary glaciation and hydrologic variation in the South American tropics as reconstructed from the Lake Titicaca drilling project. *Quaternary Research* 68:410-420
- Frogley MR, Tzedakis PC, Heaton THE (1999) Climate variability in Northwest Greece during the Last Interglacial. *Science* 285:1886-1889
- Frogley MR, Griffiths HI, Heaton THE (2001) Historical biogeography and Late Quaternary environmental change of Lake Pamvotis, Ioannina (north-western Greece): evidence from ostracods. *Journal of Biogeography* 28:745-756
- Gaffey SJ (1986) Spectral reflectance of carbonate minerals in the visible and near infrared (0.35-2.55  $\mu\text{m}$ ): calcite, aragonite, and dolomite. *American Mineralogist* 71:151-162
- Gebhardt AC, Niessen F, Kopsch C (2006) Central ring structure identified in one of the world's best-preserved impact craters. *Geology* 34:145-148
- Geladi P, MacDougall D, Martens H (1985) Linearization and Scatter-Correction for Near-Infrared Reflectance Spectra of Meat. *Applied Spectroscopy* 39:491-500
- Geladi P, Dåbakk E (1999) Computational methods and chemometrics in near-ir spectroscopy. In: Tranter E. et al. (ed) *Encyclopedia of spectroscopy and spectrometry*. Elsevier Academic Press, Amsterdam, pp. 343-349
- Gendron-Badou A, Coradin T, Maquet J, Fröhlich F, Livage J (2003) Spectroscopic characterization of biogenic silica. *Journal of Non-Crystalline Solids* 316:331-337

- Genty D, Blamart D, Ouahdi R, Gilmour M, Baker A, Jouzel J, Van-Exter S (2003) Precise dating of Dansgaard-Oeschger climate oscillations in western Europe from stalagmite data. *Nature* 421:833-837
- Giaccio B, Isaia R, Sulpizio R, Zanchetta G (2008a) Explosive volcanism in the central Mediterranean area during the late Quaternary: linking sources and distal archives. Editorial, *Journal of Volcanology and Geothermal Research* 177, v-vii
- Giaccio B, Isaia R, Fedele FG, Di Canzio E, Hoffecker J, Ronchitelli A, Sinitsyn A, Anikovich M, Lisitsyn SN (2008b) The Campanian Ignimbrite and Codola tephra layers: two temporal/stratigraphic markers for the Early Upper Palaeolithic in southern Italy and eastern Europe. *Journal of Volcanology and Geothermal Research* 177:208-226
- Glushkova OYu, Smirnov VN (2007) Pliocene to Holocene geomorphic evolution and paleogeography of the El'gygytgyn Lake region, NE Russia. *J Paleolimnol* 37:37-47
- Granina L, Müller B, Wehrli B (2004) Origin and dynamics of Fe and Mn sedimentary layers in Lake Baikal. *Chemical Geology* 205:55-72
- Grieve RAF, Rupert J, Smith J, Thierrault A (1995) The record of terrestrial impact cratering. *Geological Society of America Today* 5:189-196
- Griffiths PR, De Haseth JA (1986) *Fourier Transform Infrared Spectrometry*. John Wiley & Sons, New York
- Gruber N, Wehrli B, Wüest A (2000) The role of biogeochemical cycling for the formation and preservation of varved sediments in Soppensee (Switzerland). *Journal of Paleolimnology* 24:277-291
- Haberzettl T, Corbella H, Fey M, Janssen S, Lücke A, Mayr C, Ohlendorf C, Schäbitz F, Schleser GH, Wille M, Wulf S, Zolitschka B (2007) Lateglacial and Holocene wet-dry cycles in southern Patagonia: chronology, sedimentology and geochemistry of a lacustrine record from Laguna Potrok Aike, Argentina. *The Holocene* 17:297-310
- Hadzisce SD (1966) The mixo-phenomenon of Lake Ohrid in the course of the years 1941/42 – 1964/65 (in German). *Proceedings of the International Association of Theoretical Applied Limnology* 16:134-138
- Hajdas I, Zolitschka B, Ivy-Ochs SD, Beer J, Bonani G, Leroy SAG, Negendank JW, Ramrath M, Suter M (1995) AMS radiocarbon dating of annually laminated sediments from lake Holzmaar, Germany. *Quaternary Science Reviews* 14:137-143
- Harris DC (1998) *Quantitative chemical analysis*. W.H. Freeman and Company, New York
- Heiri O, Lotter AF, Lemcke G (2001) Loss on ignition as a method for estimating organic and carbonate content in sediments: reproducibility and comparability of results. *Journal of Paleolimnology* 25:101–110

- Herbert TD, Brian AT, Burnett C (1992) Precise major component determination in deep-sea sediments using Fourier Transform Infrared Spectroscopy. *Geochimica et Cosmochimica Acta* 56:1759-1763
- Hodell D, Anselmetti F, Brenner M, Ariztegui D, and the PISDP Science Party. (2006) The Lake Petén Itzá Scientific Drilling Project. *Scientific Drilling* 3:25-29.
- Hoffmann N (in preparation) Sedimentary and neotectonic history of Lake Ohrid (Macedonia/Albania): acquisition and interpretation of new geophysical and geological data. Dissertation, RWTH Aachen, Germany
- Ispolatov VO, Tikhomirov P, Heizler M, Cherepanova IYu (2004) New  $^{40}\text{Ar}/^{39}\text{Ar}$  Ages of Cretaceous Continental Volcanics from Central Chukotka: Implications for Initiation and Duration of Volcanism within the Northern Part of the Okhotsk-Chukotka Volcanic Belt (Northeastern Eurasia). *Journal of Geology* 112:369-377
- Jarrard RD, Vanden Berg MD (2006) Sediment Mineralogy based on visible and near-infrared reflectance spectroscopy. In: Rothwell RG (ed) *New Techniques in Sediment Core Analysis*. Geological Society Special Publications 267, London, pp. 129-140
- Johnson TC, Brown ET, McManus J, Barry S, Barker P, Gasse F (2002) A high-resolution paleoclimate record spanning the past 25,000 years in southern East Africa. *Science* 296:113-132
- Jones MD, Roberts CN, Leng MJ, Türkeş M (2006) A high-resolution Late Holocene lake isotope record from Turkey and links to North Atlantic and monsoon climate. *Geology* 34:361-364
- Keller J, Ryan WBF, Ninkovich D, Altherr R (1978) Explosive volcanic activity in the Mediterranean over the past 200,000 years as recorded in deep-sea sediments. *Geological Society of America Bulletin* 89:591-604
- Kellner R, Mermet J-M, Otto M, Widmer HM (1998) *Analytical chemistry*. Wiley-VCH, Weinheim, Berlin, New York, Chichester, Brisbane, Singapore, Toronto
- Kim J-H, Schouten S, Hopmans EC, Doner B, Sinninghe Damsté JS (2008) Global sediment core-top calibration of the  $\text{TEX}_{86}$  paleothermometer in the ocean. *Geochimica et Cosmochimica Acta* 72:1154-1173
- Koeberl C, Peck JA, King JW, Milkereit B, Overpeck JT, Scholz CA (2005) The ICDP Lake Bosumtwi Drilling Project: A First Report. *Scientific Drilling* 1:23-27.
- Korsman T, Renberg I, Dåbakk E, Nilsson MB (2001) Near-Infrared Spectrometry (NIRS) In Palaeolimnology. In: Last WM, Smol JP (eds), *Tracking Environmental Change Using Lake Sediments*. Vol. 2: Physical and Geochemical Methods. Kluwer Academic Publishers, Dordrecht, The Netherlands, pp. 299-317
- Kossmat F (1924) *Geologie der zentralen Balkanhalbinsel*. Borntraeger: Berlin

- Kotthoff U, Müller UC, Pross J, Schmiedl G, Lawson IT, van de Schootbrugge B, Schulz H (2008) Lateglacial and Holocene vegetation dynamics in the Aegean region: an integrated view based on pollen data from marine and terrestrial archives. *The Holocene* 18:1019-1032
- Kraml M (1997) Laser-40Ar/39Ar-Datierungen an distalen marinen Tephren des Jungquartären mediterranen Vulkanismus (Ionisches Meer, METEOR-Fahrt 25/4). Ph.D. Thesis: Albert-Ludwigs-Universität Freiburg i.Br., 216 pp
- Lawson IT, Frogley M, Bryant C, Preece R, Tzedakis P (2004) The Lateglacial and Holocene environmental history of the Ioannina basin, north-west Greece. *Quaternary Science Reviews* 23:1599-1625
- Lawson IT, Al-Omari S, Tzedakis PC, Bryant CL, Christanis K (2005) Lateglacial and Holocene vegetation history at Nisi Fen and the Boras mountains, northern Greece. *The Holocene* 15:873-887
- Layer P (2000) Argon-40/argon-39 age of the El'gygytgyn impact event, Chukotka, Russia. *Meteoritics & Planetary Science* 35:591-599
- Lindhorst K (in preparation) Sedimentary and neotectonic history of Lake Ohrid (Macedonia/Albania): acquisition and interpretation of new geophysical and geological data. Dissertation, University of Kiel, Germany
- Lisiecki LE, Raymo ME (2005) A Pliocene-Pleistocene stack of 57 globally distributed benthic  $\Delta^{18}\text{O}$  records. *Paleoceanography* 20:PA1003
- Litt T, Krastel S, Sturm M, Kipfer R, Örcen S, Heumann G, Franz SO, Ülgen UB, Niessen F (2009) 'PALEOVAN', International Continental Scientific Drilling Program (ICDP): site survey results and perspectives. *Quaternary Science Reviews* 28: 1555-1567.
- Louergue L, Schilt A, Spahni R, Masson-Delmotte V, Blunier T, Lemieux B, Barnola J-M, Raynaud D, Stocker TF, Chappellaz J (2008) Orbital and millennial-scale features of atmospheric  $\text{CH}_4$  over the past 800,000 years. *Nature* 453:383-386
- Lozhkin AV, Anderson PM, Matrosova TV, Minyuk PS (2007) Vegetation and Climate Histories of El'gygytgyn Lake, Northeast Siberia. *Journal of Paleolimnology* 37:135-153
- Magny M, Vannièrè B, Zanchetta G, Fouache E, Touchais G, Petrika L, Coussot C, Walter-Simmonet A-M, Arnaud F (2009) Possible complexity of the climatic event around 4300-3800 cal. BP in the central and western Mediterranean. *The Holocene* 19:1-11
- Malley DF, Williams PC 1997 Use of Near-Infrared Reflectance Spectroscopy in prediction of heavy metals in freshwater sediment by their association with organic matter *Environmental Science and Technology* 31:3461-3467

- Malley DF, Röncke H, Findlay DL, Zippel B (1999) Feasibility of using near-infrared reflectance spectroscopy for the analysis of C, N, P, and diatoms in lake sediments. *Journal of Paleolimnology* 21:295-306
- Malley DF, Lockhardt L, Wilkinson P, Hauser B (2000) Determination of carbon, carbonate, nitrogen, and phosphorus in freshwater sediments by near-infrared reflectance spectroscopy: rapid analysis and a check on conventional analytical methods. *Journal of Paleolimnology* 24: 415-425
- Marciano R, Munno R, Petrosino P, Santangelo N, Santo A, Villa I (2008) Late quaternary tephra layers along the Cilento coastline (southern Italy). *Journal of Volcanology and Geothermal Research* 177:227-243
- Marianelli P, Sbrana A (1998) Risultati di misure di standard di minerali e di vetri naturali in microanalisi a dispersione di energia. *Atti Soc Tosc Nat Mem, Serie A* 105:57-63
- Margari V, Pyle DM, Bryant C, Gibbard PL (2007) Mediterranean tephra stratigraphy revisited: Results from a long terrestrial sequence on Lesvos Island, Greece. *Journal of Volcanology and Geothermal Research* 163:34-54
- Martens H, Næs T (1989) *Multivariate Calibration*. John Wiley & Sons, New York
- Martín-Puertas C, Valero-Garcés BL, Brauer A, Pilar-Mata M, Delgado-Huertas A, Dulski P (2009) The Iberian-Roman Humid Period (2600-1600 cal yr BP) in the Zoñar Lake varve record (Andalucía, southern Spain). *Quaternary Research* 71:108-120
- Martrat B, Grimalt JO, Lopez-Martinez C, Cacho I, Sierro FJ, Flores, JA, Zahn R, Canals M, Curtis JH, Hodell DA (2004) Abrupt temperature changes in the Western Mediterranean over the past 250,000 years. *Science* 306:1762-1765
- Martrat B, Grimalt JO, Shackleton NJ, de Abreu L, Hutterli MA, Stocker TF (2007) Four climate cycles of recurring deep and surface water destabilizations on the Iberian margin. *Science* 317:502-507
- Matzinger A, Spirkovski Z, Patceva S, Wüest A (2006a) Sensitivity of ancient Lake Ohrid to local anthropogenic impacts and global warming. *Journal of Great Lakes Research* 32:158-179
- Matzinger A, Jordanoski M, Veljanoska-Sarafiloska E, Sturm M, Müller B, Wüest A (2006b) Is Lake Prespa jeopardizing the ecosystem of ancient Lake Ohrid? *Hydrobiologica* 553:89-109
- Matzinger A, Schmid M, Veljanoska-Sarafiloska E, Patceva S, Guseska D, Wagner B, Müller B, Sturm M, Wüest A (2007) Eutrophication of ancient Lake Ohrid: Global warming amplifies detrimental effects of increased nutrient inputs. *Limnology and Oceanography* 52:338-353
- Mayewski PA, Meeker LD, Twickler MS, Whitlow S, Yang Q, Lyons WB, Prentice M (1997) Major features and forcing of high-latitude northern hemisphere atmospheric

- circulation using a 100,000-year-long glaciochemical series. *Journal of Geophysical Research* 102:345-366
- McCoy F, Cornell W (1990) Volcaniclastic sediments in the Thyrrenian basin. In *Proceedings of ODP Scientific Results* 107:291-305, Kastens KA, Mascle J, et al. (eds). College Station, TX Ocean Drilling Program
- McManus JF, Bond G, Broecker W, Johnsen S, Labeyrie L, Higgins S (1994) High-resolution climate records from the North Atlantic during the Last Interglacial. *Nature* 371:326-329
- McManus JF, Oppo DW, Cullen JL (1999) A 0.5-million-year record of millennial-scale climate variability in the North Atlantic. *Science* 283:971-975
- Meadows J (2005) The Younger Dryas episode and the radiocarbon chronologies of the Lake Huleh and Ghab Valley pollen diagrams, Israel and Syria. *The Holocene* 15:631-636
- Mecozzi M, Pietrantonio E, Amici M, Romanelli G (2001) Determination of carbonate in marine solid samples by FTIR-ATR spectroscopy. *Analyst* 126:144-146
- Mecozzi M, Pietrantonio E (2006) Carbohydrates proteins and lipids in fulvic and humic acids of sediments and its relationships with mucilaginous aggregates in the Italian seas. *Marine Chemistry* 101:27–39
- Melles M, Juschus O, Nowaczyk N, Vogel H, Wennrich V, Brigham-Grette J, Minyuk P, Rosén P, Wagner B (submitted) Highly variable interglacial climates in the Siberian Arctic during the past 340,000 years. *Science*
- Melles M, Brigham-Grette J, Glushkova OY, Minyuk PS, Nowaczyk NR, Hubberten H-W (2007) Sedimentary geochemistry of core PG1351 from Lake El'gygytgyn – a sensitive record of climate variability in the East Siberian Arctic during the past three glacial-interglacial cycles. *Journal of Paleolimnology* 37:89-104
- Meyers PA, Ishiwatari R (1993) Lacustrine organic geochemistry- an overview of indicators of organic-matter sources and diagenesis in lake-sediments. *Organic Geochemistry* 20:867-900
- Minyuk PS, Brigham-Grette J, Melles M, Borkhodoev BY, Glushkova OY (2007) Inorganic geochemistry of El'gygytgyn Lake sediments (northeastern Russia) as an indicator of paleoclimatic change for the last 250 kyr. *Journal of Paleolimnology* 37:123-133
- Moenke HHW (1974) Silica, the three-dimensional silicates, borosilicates and beryllium silicates. In: Farmer VC (ed), *The infrared spectra of minerals*. Mineralogical Society Monograph 4, London, pp. 365-379
- Munno R, Petrosino P (2007) The late Quaternary tephrostratigraphical record of the San Gregorio Magno basin (southern Italy). *Journal of Quaternary Science* 22:247–266

- Müller PJ, Schneider J (1993) An automated leaching method for the determination of opal in sediments and particulate matter. *Deep-Sea Research* 40:425-444
- Müller J, Oberhänsli H, Melles M, Schwab M, Rachold V, Hubberten H-W (2001) Late Pliocene sedimentation in Lake Baikal: implications for climatic and tectonic change in SE Siberia. *Palaeogeography, Palaeoclimatology, Palaeoecology* 174:305-326
- Müller B, Wang Y, Wehrli B (2006) Cycling of calcite in hard water lakes of different trophic states. *Limnology and Oceanography* 51:1678-1688
- Narcisi B, Anselmi B, Catalano F, Dai Pra G, Magri G (1992) Lithostratigraphy of the 250,000 year record of lacustrine sediments from the Valle di Castiglione crater, Roma. *Quaternary Science Reviews* 11:353-362
- Narcisi B, Vezzoli L (1999) Quaternary stratigraphy of distal tephra layers in the Mediterranean - an overview. *Global and Planetary Change* 21:31-50
- Niessen F, Gebhardt AC, Kopsch C, Wagner B (2007) Seismic investigation of the El'gygytyn impact crater lake (Central Chukotka, NE Siberia): preliminary results. *Journal of Paleolimnology* 37:49-63
- NGRIP members (2004) High-resolution record of Northern Hemisphere climate extending into the last interglacial period. *Nature* 431:147-151
- Nolan M, Brigham-Grette J (2007) Basic hydrology, limnology, and meteorology of modern Lake El'gygytyn, Siberia. *Journal of Paleolimnology* 37:17-35
- Nowack E (1929) Übersicht über die tektonische Entwicklung Albaniens. *International Journal of Earth Sciences* 20:96-107
- Nowaczyk N, Minyuk P, Melles M, Brigham-Grette J, Glushkova O, Nolan M, Lozhkin AV, Stetsenko TV, Andersen PM, Forman SL (2002) Magnetostratigraphic results from impact crater Lake El'gygytyn, northeastern Siberia: a 300 kyr long high-resolution terrestrial palaeoclimatic record from the Arctic. *Geophysical Journal International* 150:109-126
- Nowaczyk N, Melles M, Minyuk P (2007) A revised age model for core PG1351 from Lake El'gygytyn, Chukotka, based on magnetic susceptibility variations tuned to northern hemisphere insolation variations. *Journal of Paleolimnology* 37:65-76
- Orsi G, Sheridan G (1984) The Green Tuff of Pantelleria: Rheoignimbrite or Rheomorphic Fall? *Bulletin of Volcanology* 47:611-626
- Orsi G, De Vita S, Di Vito MA (1996) The restless, resurgent Campi Flegrei nested caldera (Italy): constraints on its evolution and configuration. *Journal of Volcanology and Geothermal Research* 74:179-214
- Pantaléon-Cano J, Yll E-I, Perez-Obiol R, Roure JM (2003) Palynological evidence for vegetational history in semi-arid areas of the western Mediterranean (Almería, Spain). *The Holocene* 13:109-119

- Pappalardo L, Civetta L, D'Antonio M, Deino A, Di Vito MA, Orsi G, Carandente A, De Vita S, Isaia R, Piochi M (1999) Chemical and Sr-isotopic evolution of the Phlegraen magmatic system before the Campanian Ignimbrite and the Neapolitan Yellow Tuff eruptions. *Journal of Volcanology and Geothermal Research* 91:141-166
- Pappalardo L, Civetta L, De Vita S, Di Vito MA, Orsi G, Carandente A, Fisher RV (2002) Timing of magma extraction during the Campanian Ignimbrite eruption (Campi Flegrei caldera). *Journal of Volcanology and Geothermal Research* 114:479-497
- Paterne M, Guichard F, Labeyrie J, Gillot PY, Duplessy JC (1986) Tyrrhenian Sea tephrochronology of the oxygen isotope record for the past 60 000 years. *Marine Geology* 72:259-285
- Paterne M, Guichard F, Labeyrie J (1988) Explosive activity of the south Italian volcanoes during the past 80,000 years as determined by marine tephrochronology. *Journal of Volcanology and Geothermal Research* 34:153-172
- Paterne M, Labeyrie J, Guichard F, Mazaud A, Maitre F (1990) Fluctuations of the Campanian explosive volcanic activity (south Italy) during the past 190,000 years as determined by marine tephrochronology. *Earth and Planetary Science Letters* 98:166-174
- Paterne M, Kallel N, Labeyrie L, Vautravers M, Duplessy JC, Rossignol-Strick M, Cortijo E, Arnold M, Fontugne M (1999) Hydrological relationship between the North Atlantic Ocean and the Mediterranean Sea during the past 15–75 kyr. *Paleoceanography* 14:626-638
- Paterne M, Guichard F, Duplessy JC, Siani G, Sulpizio R, Labeyrie J. (2007) A 90,000-200,000 yrs marine tephra record of Italian volcanic activity in the Central Mediterranean Sea. *Journal of Volcanology and Geothermal Research* 177:187-196
- Peck JA, King JW, Colman SM, Kravchinsky VA (1994) A rock-magnetic record from Lake Baikal, Siberia: Evidence for Late Quaternary climate change. *Earth and Planetary Science Letters* 122:221-238
- Peck JA, Green RR, Shanahan T, King JW, Overpeck JT, Scholz CA (2004) A magnetic mineral record of Late Quaternary tropical climate variability from Lake Bosumtwi, Ghana. *Palaeogeography, Palaeoclimatology, Palaeoecology* 215:37-57
- Poli S, Chiesa S, Gillot PY, Guichard F (1987) Chemistry versus time in the volcanic complex of Ischia (Gulf of Naples, Italy): evidence of successive magmatic cycles. *Contributions to Mineralogy and Petrology* 95:322-335
- Pons A, Reille M (1988) The Holocene- and Upper Pleistocene pollen record from Padul (Granada, Spain), a new study. *Palaeogeography, Palaeoclimatology, Palaeoecology* 66:243-263

- Popovska C, Bonacci O (2007) Basic data on the hydrology of Lakes Ohrid and Prespa. *Hydrological Processes* 21:658-664
- Powers LA, Werne JP, Johnson TC, Hopmans EC, Sinninghe Damsté JS, Schouten S (2004) Crenarcheotal membrane lipids in lake sediments: A new paleotemperature proxy for continental paleoclimate reconstruction? *Geology* 32:613-616
- Prokopenko AA, Hinnov LA, Williams DF, Kuzmin MI (2006) Orbital forcing of continental climate during the Pleistocene: a complete astronomically tuned climatic record from Lake Baikal, SE Siberia. *Quaternary Science Reviews* 25:3431-3457
- Pyle DM, Ricketts GD, Margari V, van Andel TH, Sinitsyn AA, Praslov N, Lisitsyn S (2006) Wide dispersal and deposition of distal tephra during the Pleistocene “Campanian Ignimbrite/Y5” eruption, Italy. *Quaternary Science Reviews* 25:2713-2728
- Radoman P (1985) Hydrobioidea, a Superfamily of Prosobranchia (Gastropoda), II: Origin, Zoogeography, Evolution in the Balkans and Asia Minor. *Monographs of the Institute of Zoology*, vol. 1: Beograd.
- Ravazzi C, Rossignol-Strick M (1995) Vegetation change in a climatic cycle of Early Pleistocene age in the Lefte Basin (Northern Italy). *Palaeogeography, Palaeoclimatology, Palaeoecology* 117:105-122
- Reille M, Andrieu V, de Beaulieu J-L, Guenet P, Goeury C (1998) A long pollen record from Lac du Bouchet, Massif Central, France for the period 325-100 ka (OIS 9c to OIS 5e). *Quaternary Science Reviews* 17:1107-1123
- Renberg I (1991) The HON-Kajak sediment corer. *Journal of Paleolimnology* 6:167-170
- Rickert D, Schlüter M, Wallmann K (2002) Dissolution kinetics of biogenic silica from the water column to the sediments. *Geochimica et Cosmochimica Acta* 66:439-455
- Roberts N, Black S, Boyer P, Eastwood EJ, Griffiths HI, Lamb HF, Leng MJ, Parish R, Reed JM, Twigg D, Yigitbasioglu H (1999) Chronology and stratigraphy of Late Quaternary sediments in the Konya basin, Turkey: results from the KOPAL project. *Quaternary Science Reviews* 18:611-630
- Roberts N, Reed J, Leng MJ, Kuzucuoğlu C, Fontugne M, Bertaux J, Woldring H, Bottema S, Black S, Hunt E, Karabıyıkoglu M (2001) The tempo of Holocene climatic change in the eastern Mediterranean region: new high-resolution crater-lake sediment data from central Turkey. *The Holocene* 11:721-736
- Roberts N, Jones MD, Benkaddour A, Eastwood WJ, Filippi ML, Frogley M.R, Lamb HF, Leng MJ, Reed JM, Stein M, Stevens L, Valero-Garcés B, Zanchetta G (2008) Stable isotope records of Late Quaternary climate and hydrology from Mediterranean lakes: the ISOMED synthesis. *Quaternary Science Reviews* 27:2426-2441
- Robertson A, Shallo M (2000) Mesozoic-Tertiary tectonic evolution of Albania in its regional Eastern Mediterranean context. *Tectonophysics* 316:197-254

- Roelofs AK, Kilham P (1983) The diatom stratigraphy and paleoecology of Lake Ohrid, Yugoslavia. *Palaeogeography, Palaeoclimatology, Palaeoecology* 42:225-245
- Rohling EJ, Mayewski PA, Abu-Zied RH, Casford JSL, Hayes A (2002) Holocene atmosphere-ocean interactions: records from Greenland and the Aegean Sea. *Climate Dynamics* 18:587-593
- Rolandi G, Mastrolorenzo G, Barrella AM, Borrelli A (1993) The Avellino Plinian eruption of Somma-Vesuvius (3760 y BP): the progressive evolution from magmatic to hydromagmatic style. *Journal of Volcanology and Geothermal Research* 58:67–88
- Rosén P, Dábakk E, Renberg I, Nilsson M, Hall R (2000) Near-infrared spectrometry (NIRS): a new tool to infer past climatic changes from lake sediments. *The Holocene* 10:161-166
- Rosén P (2005) Total organic carbon (TOC) of lake water during the Holocene inferred from lake sediments and near-infrared spectroscopy (NIRS) in eight lakes from northern Sweden. *Biogeochemistry* 76:503-516
- Rosén P, Persson P (2006) Fourier-transform infrared spectroscopy (FTIRS), a new method to infer past changes in tree line position and TOC using lake sediment. *Journal of Paleolimnology* 35: 913-923
- Rosén P, Hammarlund D (2007) Effects of climate, fire and vegetation development on Holocene changes in total organic carbon concentration in three boreal forest lakes in northern Sweden. *Biogeosciences* 4:975-984
- Rosén P, Vogel H, Cunningham L, Reuss N, Conley D, Persson P (2009) Fourier transform infrared spectroscopy, a new method for rapid determination of total organic carbon and inorganic carbon and opal concentrations in lake sediments. *Journal of Paleolimnology*. DOI: 10.1007/s10933-009-9329-4
- Rosi M, Santacroce R. (1983) The A.D. 472 “Pollena” eruption: volcanological and petrological data for this poorly-known, Plinian-type event at Vesuvius. *Journal of Volcanology and Geothermal Research* 17:249-271
- Rosi M, Sbrana A (1987) The Phlegraean Fields, Quaderni de ‘La ricerca Scientifica’ 114. Consiglio Nazionale delle Ricerche: Rome
- Rossignol-Strick M (1995) Sea-land correlation of pollen records in the eastern Mediterranean for the glacial-interglacial transition: Biostratigraphy versus radiometric time-scale. *Quaternary Science Reviews* 14:893-915
- Saccone L, Conley DJ, Koning E, Sauer D, Sommer M, Kaczorek D, Blecker SW, Kelly EF (2007) Assessing the extraction and quantification of amorphous silica in soils of forest and grassland ecosystems. *European Journal of Soil Sciences* 58:1446-1459
- Sadori L, Narcisi B (2001) The postglacial record of environmental history from Lago di Pergusa, Sicily. *The Holocene* 11:655-670

- Salamani M (1993) Premières données paléophytogéographiques du Cèdre de l'Atlas (*Cedrus atlantica*) dans la région de Grand Kabylie (NE Algérie). *Palynosciences* 2:147-155
- Sangiorgi F, Capotondi L, Combourieu Nebout N, Vigliotti L, Brinkhuis H, Giunta S, Lotter AF, Morigi C, Negri A, Reichert G-J (2003) Holocene seasonal sea-surface temperature variations in the southern Adriatic Sea inferred from a multiproxy approach. *Journal of Quaternary Science* 18:723-732
- Santacroce R. (ed) (1987) *Somma-Vesuvius*. Quaderni de la Ricerca Scientifica, CNR, 114. Progetto Finalizzato Geodinamica, Monografie Finali, 8. CNR: Rome
- Santacroce R, Cioni R, Marianelli P, Sbrana A, Sulpizio R, Zanchetta G, Donahue DJ, Joron JL (2008) Age and whole rock-glass compositions of proximal pyroclastics from the major explosive eruptions of Somma-Vesuvius: a review as a tool for distal tephrostratigraphy. *Journal of Volcanology Geothermal Research* 177:1-18
- Santacroce R, Cioni R, Marianelli P, Sbrana A, Sulpizio R, Zanchetta G, Donahue DJ, Joron JL (2008) Age and whole rock-glass compositions of proximal pyroclastics from the major explosive eruptions of Somma-Vesuvius: a review as a tool for distal tephrostratigraphy. *Journal of Volcanology Geothermal Research* 177:1-18
- Schaller T, Moor HC, Wehrli B (1997) Sedimentary profiles of Fe, Mn, V, Cr, As and Mo as indicators of benthic redox conditions in Baldeggersee. *Aquatic Sciences* 59:345-361
- Schmiedl G, Hemleben C, Keller J, Segl M (1998) Impact of climatic changes on the benthic foraminiferal fauna in the Ionian Sea during the past 330,000 years. *Paleoceanography* 13:447-458
- Schouten S, Hopmans EC, Schefuß E, Sinninghe Damsté JS (2002) Distributional variations in marine crenarchaeotal membrane lipids: a new organic proxy for reconstructing ancient sea water temperatures? *Earth and Planetary Science Letters* 204:265-274
- Shackleton N, Chapman M, Sánchez Gōni M, Pailler D, Lancelot Y (2002) The classic Marine Isotope Substage 5e. *Quaternary Research* 58:14-16
- Siani G, Sulpizio R, Paterne M, Sbrana A (2004) Tephrostratigraphy study for the last 18,000 14C years in a deep-sea sediment sequence for the South Adriatic. *Quaternary Science Reviews* 23:2485-2500
- Sifeddine A, Fröhlich F, Fournier M, Martin L, Servant M, Soudies F, Turcq B, Suguio K, Volkmer-Rubeiro C (1994) La sédimentation lacustre indicateur de changements de paléoenvironnements au cours des 30 000 dernières années (Carajas, Amazonie, Brésil) [Lacustrine sedimentation as indicator of environmental change during the past 30 000 years (Carajas, Amazon, Brazil)]. *C.R. Académie Scientifique Paris*, 318 (Series II):1645-1652

- Signorelli S, Vaggelli G, Romano C, Carroll MR (2001) Volatile element zonation in Campanian Ignimbrite magmas (Phlegrean Fields, Italy): evidence from the study of glass inclusions and matrix glasses. *Contributions to Mineralogy and Petrology* 140:543-553
- Schmidt M, Bottz R, Rickert D, Bohrmann G, Hall SR, Mann S (2001) Oxygen isotopes of marine diatoms and relations to opal-A maturation. *Geochimica et Cosmochimica Acta* 65:201–211
- Scholz CA, Cohen AS, Johnson TC, King JW, Moran K (2006) The 2005 Lake Malawi Scientific Drilling Project. *Scientific Drilling* 2:17-19
- Skinner LC, Shackleton NJ (2006) Deconstructing Terminations I and II: revisiting the glacioeustatic paradigm based on deep-water temperature estimates. *Quaternary Science Reviews* 25:3312-3321
- Spirkovski Z, Avramovski O, Kodzoman A (2001) Case Report: Watershed management in the Lake Ohrid region of Albania and Macedonia. *Lakes & Reservoirs: Research and Management* 6:237-242
- Sprovieri R, Di Stefano E, Incarbona A, Oppo DW (2006) Suborbital climate variability during Marine Isotopic Stage 5 in the central Mediterranean basin: evidence from calcareous plankton record. *Quaternary Science Reviews* 25:2332-2342
- Stankovic S (1960) The Balkan Lake Ohrid and its living world. *Monographiae Biologicae IX*: Dr. W. Junk, Den Haag, The Netherlands
- Stehfest K, Toepel J, Wilhelm C (2005) The application of micro-FTIR spectroscopy to analyze nutrient stress-related changes in biomass composition of phytoplankton algae. *Plant Physiology and Biochemistry* 43:717–726
- Stumm W, Morgan JJ (1970) *Aquatic Chemistry*. John Wiley & Sons Inc., New York. 583 pp
- Sulpizio R, Zanchetta G, Paterne M, Siani G (2003) A review of tephrostratigraphy in central and southern Italy during the last 65 ka. *Il Quaternario* 16(1):91-108
- Sulpizio R (2005) Three empirical methods for the calculation of distal volume of tephra-fall deposits. *Journal of Volcanology and Geothermal Research* 145: 315-336
- Sulpizio R, Mele D, Dellino P, La Volpe L (2005) A complex, Subplinian-type eruption from low-viscosity, phonolitic to tephri-phonolitic magma: the AD 472 (Pollena) eruption of Somma-Vesuvius, Italy. *Bulletin of Volcanology* 67:743-767
- Thunell R, Federman A, Sparks S, Williams D (1979) The age, origin and volcanological significance of the Y-5 ash layer in the Mediterranean. *Quaternary Research* 12:241-253
- Tiercelin JJ, Lezzar KE (2002) A 300 million years history of rift lakes in Central and East Africa: An updated broad review. In: Odada EO, Olago DO (eds) *The East African*

- great lakes: Limnology, palaeolimnology and biodiversity. Kluwer Academic Publishers, Dordrecht, The Netherlands, pp. 3-60
- Tinner W, van Leeuwen JFN, Colombaroli D, Vescovi E, van der Knaap WO, Henne PD, Pasta S, D'Angelo S, La Mantia T (2009) Holocene environmental and climatic changes at Gorgo Basso, a coastal lake in southern Italy. *Quaternary Science Reviews* 28:1498-1510
- Tjallingii R, Claussen M, Stuut J-BW, Fohlmeister J, Jahn A, Bickert T, Lamy F, Röhl U (2008) Coherent high- and low-latitude control of the northwest African hydrological balance. *Nature Geoscience* 1:670-675
- Tzedakis PC (1999) The last climatic cycle at Kopais, central Greece. *Journal of the Geological Society* 156:425-434
- Tzedakis PC, Lawson IT, Frogley MR, Hewitt GM, Preece RC (2002) Buffered tree population changes in a Quaternary refugium: Evolutionary implications. *Science* 297:2044-2047
- Tzedakis PC, McManus JF, Hooghiemstra H, Oppo DW, Wijmstra TA (2003) Comparison of changes in vegetation in northeast Greece with records of climate variability on orbital and suborbital frequencies over the last 450 000 years. *Earth and Planetary Science Letters* 212:197-212
- Tzedakis PC, Frogley MR, Heaton THE (2003) Last Interglacial conditions in southern Europe: evidence from Ioannina, northwest Greece. *Global and Planetary Change* 36:157-170.
- Tzedakis PC, Hooghiemstra H, Pälike H (2006) The last 1.35 million years at Tenaghi Philippon: revised chronostratigraphy and long-term vegetation trends. *Quaternary Science Reviews* 25:3416-3430
- Van Welden A, Beck C, Reyss J-R, Bushati R, Koci R, Juane F, Mugnier J-L (2007) The last 500 year of sedimentation in Shkodra Lake (Albania/Montenegro): paleoenvironmental evolution and potential for paleoseismicity studies. *Journal of Paleolimnology* 40:619-633
- Vezzoli L (1991) Tephra layers in the Bannock Basin (Eastern Mediterranean). *Marine Geology* 100:21-34
- Vogel H, Rosén P, Wagner B, Melles M, Persson P (2008) Fourier transform infrared spectroscopy, a new cost-effective tool for quantitative analysis of biogeochemical properties in long sediment records. *Journal of Paleolimnology* 40:689-702
- Vogel H, Zanchetta G, Sulpizio R, Wagner B, Nowaczyk N (2009) A tephrostratigraphic record for the last glacial-interglacial cycle from Lake Ohrid, Albania and Macedonia. *Journal of Quaternary Science*. DOI: 10.1002/jqs.1311

- Vogel H, Wagner B, Zanchetta G, Sulpizio R, Rosén P (submitted) A paleoclimate record with tephrochronological age control for the last glacial-interglacial cycle from Lake Ohrid, Albania and Macedonia. *Journal of Paleolimnology*
- Wagner B, Sulpizio R, Zanchetta G, Wulf S, Wessels M, Daut G, Nowaczyk N (2008a) The last 40 ka tephrostratigraphic record of Lake Ohrid, Albania and Macedonia: a very distal archive for ash dispersal from Italian volcanoes. *Journal of Volcanology and Geothermal Research* 177:71-80
- Wagner B, Reicherter K, Daut G, Wessels M, Matzinger A, Schwalb A, Spirkovski Z, Sanxhaku M (2008b) The potential of Lake Ohrid for long-term palaeoenvironmental reconstructions. *Palaeogeography, Palaeoclimatology, Palaeoecology* 259:341-356
- Wagner B, Lotter AF, Nowaczyk N, Reed JM, Schwalb A, Sulpizio R, Valsecchi V, Wessels M, Zanchetta G (2008c) A 40,000-year record of environmental change from ancient Lake Ohrid (Albania and Macedonia). *Journal of Paleolimnology* 41:407-430
- Watzin MC, Puka V, Naumoski TB (2002) Lake Ohrid and its Watershed, State of the Environment Report. Lake Ohrid Conservation Project. Tirana, Albania and Ohrid, Macedonia
- Wetzel, R.G., 2001. *Limnology*. Academic Press, San Diego, London. 1006 pp.
- White WB (1974) The carbonate minerals. In: Farmer VC (ed), *The infrared spectra of minerals*. Mineralogical Society Monograph 4, London, pp. 227-242
- Wick L, Lemcke G, Sturm M (2003) Evidence of Lateglacial and Holocene climatic change and human impact in eastern Anatolia, high resolution pollen, charcoal, isotopic and geochemical records from the laminated sediments of Lake Van, Turkey. *The Holocene* 13:665-675
- Williams DF, Peck J, Karabanov EB, Prokopenko AA, Kravchinsky V, King J, Kuzmin MI (1997) Lake Baikal record of continental climate response to orbital insolation during the past 5 million years. *Science* 278:1114-1117
- Wilson GP, Reed JM, Lawson IT, Frogley MR, Preece RC, Tzedakis PC (2008) Diatom response to the last glacial-interglacial transition in the Ioannina basin, northwest Greece: implications for Mediterranean palaeoclimate reconstruction. *Quaternary Science Reviews* 27:428-440
- Wirrman H, Bertaux J, Kossoni A (2001) Late Holocene paleoclimatic changes in western central Africa inferred from mineral abundances in dated sediments from Lake Ossa (southwestern Cameroon). *Quaternary Research* 56:275-287
- Wohlfarth B, Veres D, Ampel L, Lacourse T, Blaauw M, Preusser F, Andrieu-Ponel V, Kéravis D, Lallier-Vergès E, Björk S, Davies SM, de Beaulieu J-L, Risberg J, Hormes A, Kasper HU, Possnert G, Reille M, Thouveny N, Zander A (2008) Rapid ecosystem

- response to abrupt climate changes during the last glacial period in western Europe, 40-16 ka. *Geology* 36:407-410
- Wuchter C, Schouten S, Coolen MJL, Sinninghe Damsté JS (2004) Temperature-dependent variation in the distribution of tetraether membrane lipids of marine Crenarcheota: Implications for TEX<sub>86</sub> paleothermometry. *Paleoceanography* 19:PA 4028
- Wulf S, Kraml M, Brauer A, Keller J, Negendank JFW (2004) Tephrochronology of the 100 ka lacustrine sediment record of Lago Grande di Monticchio (southern Italy). *Quaternary International* 122:7-30
- Wulf S, Brauer A, Mingram J, Zolitschka B, Negendank JFW (2006) Distal tephras in the sediments of Monticchio maar lakes. In *La geologia del Monte Vulture. Regione Basilicata*, Principe C (ed). Consiglio Nazionale delle Ricerche: Roma; 105-122
- Wulf S, Kraml M, Keller J (2008) Towards a detailed distal tephrostratigraphy in the central Mediterranean: the last 20,000 yrs record of Lago Grande di Monticchio. *Journal of Volcanology and Geothermal Research* 177:118-132
- Yancheva G, Nowaczyk NR, Mingram J, Dulski P, Schettler G, Negendank JFW, Liu J, Sigman DM, Peterson LC, Haug GH (2007) Influence of the intertropical convergence zone on the East Asian monsoon. *Nature* 445:74-77
- Zanchetta G, Bonadonna FP, Leone G (1999) A37-meter record of paleoclimatological events from stable isotope data on continental molluscs in Valle di Castiglione, near Rome, Italy. *Quaternary Research* 52:293-299
- Zanchetta G, Drysdale RN, Hellstrom JC, Fallick AE, Isola I, Gagan, MK (2007) Enhanced rainfall in the Western Mediterranean during deposition of sapropel S1: stalagmite evidence from Corchia Cave (central Italy). *Quaternary Science Reviews* 26:279-286
- Zanchetta G, Sulpizio R, Giaccio B, Siani G, Paterne M, Wulf S, D'Orazio M (2008) The Y-3 Tephra: a Last Glacial stratigraphic marker for the central Mediterranean basin. *Journal of Volcanology and Geothermal Research* 177:145-154
- Zolitschka B, Corbella H, Maidana N, Ohlendorf C (2006) Investigating Maar Formation and the Climate History of Southern Argentina - the Potrok Aike Maar Lake Sediment Archive Drilling Project (PASADO). *Scientific Drilling* 3: 54-55

# Erklärung

Ich versichere, dass ich die von mir vorgelegte Dissertation selbstständig angefertigt, die benutzten Quellen und Hilfsmittel vollständig angegeben und die Stellen der Arbeit – einschließlich Tabellen, Karten und Abbildungen-, die anderen Werken im Wortlaut oder dem Sinn nach entnommen sind, in jedem Einzelfall als Entlehnung kenntlich gemacht habe; dass diese Dissertation noch keiner anderen Fakultät oder Universität zur Prüfung vorgelegen hat; dass sie – abgesehen von unten angegebenen Teilpublikationen – noch nicht veröffentlicht worden ist sowie, dass ich eine solche Veröffentlichung vor Abschluss des Promotionsverfahrens nicht vornehmen werde.

Die Bestimmungen dieser Promotionsordnung sind mir bekannt. Die von mir vorgelegte Dissertation ist von Prof. Dr. Martin Melles betreut worden.

Nachfolgend genannte Teilpublikationen liegen vor:

- (1) Vogel H, Rosén P, Wagner B, Melles M, Persson P (2008) Fourier transform infrared spectroscopy, a new cost-effective tool for quantitative analysis of biogeochemical properties in long sediment records. *Journal of Paleolimnology* 40:689-702
- (2) Rosén P, Vogel H, Cunningham L, Reuss N, Conley D, Persson P (2009) Fourier transform infrared spectroscopy, a new method for rapid determination of total organic carbon and inorganic carbon and opal concentrations in lake sediments. *Journal of Paleolimnology*. DOI: 10.1007/s10933-009-9329-4
- (3) Vogel H, Zanchetta G, Sulpizio R, Wagner B, Nowaczyk N (2009) A tephrostratigraphic record for the last glacial-interglacial cycle from Lake Ohrid, Albania and Macedonia. *Journal of Quaternary Science*. DOI: 10.1002/jqs.1311
- (4) Vogel H, Wagner B, Zanchetta G, Sulpizio R, Rosén P (eingereicht) A paleoclimate record with tephrochronological age control for the last glacial-interglacial cycle from Lake Ohrid, Albania and Macedonia. *Journal of Paleolimnology*

Köln den 14. August 2009